In-vitro Studies of Photodynamic Mechanisms Induced by Hypericin and meso-Tetrahydroxyphenyl Chlorin

---

Dissertation

zur

Erlangung der naturwissenschaftlichen Doktorwürde

(Dr. sc. nat.)

vorgelegt der

Mathematisch-naturwissenschaftlichen Fakultät

der

Universität Zürich

von

Emina Besic Gyenge

aus

Zürich, ZH

Promotionskomitee

Prof. Dr. Esther Stöckli (Vorsitz)

Prof. Dr. Caroline Maake (Leitung der Dissertation)

Prof. Dr. Heinrich Walt

Zürich, 2012

To my family, Bešićs and Gyenges

Omnia mea mecum porto.
Bias di Priene

Acknowledgments

I am definitely indebted to many people for their long-lasting support, encouragement and their patience during my PhD. In the following lines I will try to express my gratitude and respect I feel for all of those important people.

First of all, I would like to thank my family, especially mom and dad for supporting me in my intentions to study (even though they did not always understand why I am so passionate about science AND despite my age).

From my whole heart, I would like to thank to my husband (my love, my best friend and critic) Michael for his great support, his admiration, selfless love, for always finding the right words, for making me delicious suppers ("Schlund" is awesome), for making me smile and for being my oasis of peace and silence. Without you, this would not have been possible.

Many thanks also go to my brother Elmin and his wife Mimoza for reminding me to do my hair (Brothers and sisters in science: you need a hairdresser in the family! No wonder that almost all PhDs look like they are from the planet of the apes during their final work stage…).

I would like to express my special thanks to my uncle Redžep and aunt Sebiha for being so proud of what I'm doing, and their daughter, and my true sister, Ćera, for her help, pure heart and for her huge love (to the moon and back).

Furthermore I would like to thank the rest of my family for their mental support: my grandmother (I know nana, you would rather see me having a child than a PhD title…), my lovely parents-in-law Mumin and Pupin, my "godparents" Götti-May and Götti and all other close relatives.

My gratitude also goes to my (not-genetic) sisters and brother for being part of my life for such a long time (in alphabetical order!): Nicole, Stefan, Tu-My and Vicky. Thank you for your kind sixth sense, chats, chocolate, music, love and good food. I cherish your support and hope that we will be able to stay in touch despite the long distances between us.

I would like to thank many other friends such as super-Claudia, my sunshine-Dana, my Austrian "Schatzerl" Doris, my usz "mom" Doris, the dream-team Georg, calmly problems solver Gery, IT- and culinary god Hoai, my incredible Jay (-zilla), our medical encyclopaedia Katja, lovely and so helpful Marianne "Frau Ott", my personal running trainer Marion, art connoisseur and so lovely Miriam, incredible Martin, unperturbed Seeli, my university "mom" Sonja, angel-Stefi, adorable and so smart Susann (Su), skilful and green thumbed Svantje, sweet-tempered Swantje, angelic brave Theresa, always helpful and

marvellously scented Therese, my Tschiggiman Andres (with “streichel-koma Spike”), my local honey dealer Txema and high-spirited Maestro Urs and alongside many other colleagues from the Institute of Anatomy, especially those from the H-floor for supporting me mentally, technically and making this PhD time more bearable.

Sincere thanks to all my medical and biology students that I supervised during their doctoral or bachelor and master thesis: Andrea, Angelica, Anina, Daniel, Dominik, Marco E., Marco C., Martin, Martina, Martha, Mathias, Nicola M., Nicola S., Patrick, Sybille, Tobias, Xenia. It was not always easy, but now I am happy to have so many clinicians as friends covering all-important clinical areas: dentists, psychologists, cardiologists, internal specialist and many, many others… I still need one plastic surgeon! Guys, I’m not getting younger!

My very special gratitude goes to Gesine - pardon me… Dr. Bradacs - who always supported me with her excellent scientific know-how (not only on plants), for proof reading much of my (sometimes horrible) writings, for sharing my happiness and sadness and for being such a pleasant office neighbour. I miss you.

Firstly, let me thank my impressive power-PhD-mom Prof. Dr. Esther Stöckli for taking care of me and guiding me through the endless bureaucratic PhD jungle.

There are also two people from University Hospital of Zurich who deserve my deepest gratitude: Prof. Dr. med., Dr. med. dent. Klaus Grätz and Dr. med. dent. Marius Bredell. Thank you for the financial support and your indispensable clinical point of view.

I would like to thank Prof. Dr. Heinrich Walt for opening the doors to the fascinating field of photodynamic therapy (PDT), for initiating my PhD project and for letting me be part of the worldwide PDT-network. Thank you for your extraordinarily good ideas, for enabling the connection to like-minded people and for creating interdisciplinary projects.

Finally, I would like to express my deepest gratitude to my PhD supervisor Prof. Dr. med. Caroline Maake. Thank you for your intellectual and financial support. You gave me space to develop my own ideas and you always supported me. Discussions with you were always fruitful and very inspiring. You taught me how to control my florid/ extravagant writing style (which does not belong in grants and papers... I know… now…). I adore your scepticism, pragmatism and envy your calmness and coolness**.** You made a substantial contribution to the kind of scientist I am today and will be in the future. Thank you for everything, my mentor.

Table of Contents

List of Abbreviations

$^1O_2$	-	singlet oxygen
$^3O_2$	-	oxygen in ground state
$^1P_{sen}$	-	singlet photosensitizer in ground state
$^1P_{sen}^*$	-	singlet excited photosensitizer
$^1P_{sen}^{*-}$	-	photosensitizer radical anion
$^3P_{sen}^*$	-	triplet excited photosensitizer
ALA	-	aminolevulinic acid
BSA	-	bovine serum albumin
CM-H_2DCFDA	-	chloromethyl derivative of 2',7'-dichlorodihydrofluorescein diacetate
DNA	-	deoxyribonucleic acid
DPPC	-	dipalmitoyl-phosphatidylcholine
DPPG	-	dipalmitoyl-phospatidylglycerol
DLS	-	dynamic light scattering
e^-	-	electron
Φ_Δ	-	singlet oxygen yield
FDA	-	food and drug administration
FITC	-	fluorescein isothiocyanate
FLICA	-	fluorochrome labelled inhibitors of caspases
HNSCC	-	head and neck squamous cell carcinoma
HpD	-	hematoporphyrin
HPV	-	human papillomavirus
HSA	-	human serum albumin
hν	-	electromagnetic energy
IC	-	internal conversion
ISC	-	intersystem crossing
mTHPC	-	meso tetrahydroxyphenyl chlorin
MTT	-	3-(4,5-dimethylthiazol-2-yl)-2,5-diphenyltetrazolim bromide
M_w	-	molecular weight
PBS	-	phosphate buffered saline
PC-3	-	prostate carcinoma cell line
PDD	-	photodynamic diagnosis
PDT	-	photodynamic therapy

PEG	-	polyethylene glycol
PS	-	photosensitizer
PpIX	-	protoporphyrin IX
RBA	-	rose Bengal acetate
RNA	-	ribonucleic acid
ROS	-	reactive oxygen species
rtPCR	-	real time polymerase chain reaction
SEM	-	scanning electron microscopy
S_0	-	ground state
S_n	-	excited states with different vibrational sub-levels S'_n
SOSG	-	singlet oxygen sensor green
substrate^{*+}	-	substrate radical cations
TEM	-	transmission electron microscopy
TGA	-	thioglycolic acid
TNM	-	classification of malignant tumours (T: tumour, N: nodes; M.metastatis)
TSP- 1	-	thrombospondin- 1
VEGF-A	-	vascular endothelial growth factor– A
WHO	-	world health organisation

Summary

INTRODUCTION: The conventional treatment of cancer includes surgery, radiotherapy and chemotherapy alone or in combination. These treatment modalities are often accompanied with severe side effects and repeated treatments may significantly reduce quality of life. Photodynamic therapy (PDT) is commonly known as a treatment modality for skin disorders. Today, PDT has been approved for a broad spectrum of applications, such as the diagnosis of neoplastic lesions during surgery, the treatment of age related wet macular degeneration, as well as the treatment of various superficial cancer types.
In this present work PDT effects mediated by two very potent photosensitizers, a liposomal mTHPC derivative (Foslipos®), the most powerful natural occurring photosensitizer hypericin and especially their 1:1 mixture *in-vitro* were examined. Different cell models were used to elucidate the photosensitizers- and PDT-mediated cellular effects.

MATERIALS AND METHODS: Three different cell lines were used for this study: prostate carcinoma cell line PC-3, and the two head and neck squamous cell carcinoma cell lines UMB-SCC 745 and UMB-SCC 969. The physico-chemical properties of photosensitizers alone, and particularly in the mixture, were examined with different approaches. Furthermore uptake, distribution and intracellular localization of photosensitizers were examined with help of confocal microscopy. Photosensitizer-mediated cell viability in the dark and after illumination was monitored with cell viability assays. Morphological changes and death pathways were monitored with wide-field and confocal microscopy. In addition, DNA- and RNA damage was examined. Gene expression changes after PDT were followed by rtPCR (array systems or specific gene observations).

RESULTS: The examination of photosensitizer physico-chemical properties correlated to the values found in the literature except for the singlet oxygen yield for hypericin which was found to be slightly lower as previously reported. Their combination in solution does not show any interaction effects aside from some prolonged photobleaching kinetics. ROS measurements after PDT indicated that hypericin and photosensitizer mixture treated cells accumulated the fluorescent CM-H_2DCFDA dye while Foslipos® treated cells displayed some fluorescence, but only in the beginning. The observations made on photosensitizer uptake, distribution and localization showed that Foslipos® intracellular accumulation was continuous over 24 hours and was localised mainly in the cell cytoplasm, while hypericin achieved its

maximum after five hours of incubation with localization preferably in cellular membranes and perinuclearly. Total clearance of Foslipos® was not reached after 24 hours while intracellular hypericin remains after 24 hours were minimal. Photosensitizer mixture showed similar results as reported for single photosensitizer applications. The cell viability in the dark in photosensitizer mixture treated cells was not affected while Foslipos® and hypericin treated cells showed some dark toxicity for certain concentrations. Cell viability after illumination was highly decreased for all three cell lines and all applied photosensitizer applications. PDT induced processes had different kinetics and cell death outcomes dependent on cell lines and treatment protocols. Foslipos® treated cells displayed a necrotic, hypericin treated cells more apoptotic death outcome while photosensitizer mixture displayed features of both. Photosensitizer influence on molecular mechanisms showed DNA- and RNA damage in the dark and after illumination depending on cell line and applied photosensitizer. Changes in gene expression patterns in particular a high up-regulation of heat shock genes were detected for all cell lines used.

CONCLUSIONS: Our study documents a highly responsiveness of the cell models used on PDT and it indicates an improvement of PDT effects if photosensitizer mixtures are applied. These results are the first emphasizing advantages of this simple but innovative PDT approach.

Zusammenfassung

EINLEITUNG: Die konventionelle Krebstherapie umfasst Chirurgie, Radio- und Chemotherapie. Diese Behandlungsmethoden sind sehr oft von schwerwiegenden Nebenwirkungen begleitet, welche grossen Einfluss auf die Lebensqualität der behandelten Personen ausüben können. Die photodynamische Therapie (PDT) ist seit geraumer Zeit als Therapie für Hauterkrankungen bekannt. Sie ist heutzutage für ein breites Spektrum von medizinischen Anwendungen zugelassen, wie beispielsweise für die Diagnose von neoplastischen Läsionen während chirurgischen Eingriffen, Behandlung altersbedingter Makuladegeneration, sowie die Behandlung verschiedener oberflächlicher Krebsarten.
In der vorliegenden Arbeit wurden *in-vitro* PDT Effekte untersucht, induziert durch zwei sehr starke Photosensitizer, zum Einen durch das liposomale mTHPC Derivat Foslipos®, zum Anderen den stärksten natürlich vorkommenden Photosensitizer Hypericin – jeweils einzeln und in einer 1:1-Kombination. Wir haben verschiedene Zellmodelle verwendet, um die Photosensitizer sowie der PDT induzierten Zelleffekte zu analysieren.

MATERIALIEN AND METHODEN: In unserer Studie wurden drei verschiedene Zelllinien verwendet: die Prostatakarzinom Zelllinie PC-3 sowie zwei Plattenepithelkarzinom Zelllinien aus dem Kopf- und Halsbereich (UMB-SCC 745 und UMB-SCC 969). Die physikalisch-chemischen Eigenschaften der Photosensitizer wurden mit unterschiedlichen Methoden untersucht. Insbesondere die Eigenschaften betreffend ihrer Kombination waren von grossem Interesse. Zusätzlich haben wir die intrazelluläre Aufnahme, Distribution und die Lokalisation der jeweiligen Photosensitizer mittels konfokaler Mikroskopie untersucht. Die Zellviabilität wurde in Dunkelheit und nach Beleuchtung untersucht. Ebenso die morphologischen Veränderungen und der damit verbundene Zelltod wurden eingehend erläutert. Die DNA- und RNA-Schädigung sowie die Veränderung der Genexpression wurden mittels Arraysystemen oder durch die Untersuchung spezifischer Gene analysiert.

RESULTATE: Die Untersuchungsresultate der physikalisch-chemischen Eigenschaften der Photosensitizer entsprachen den in der Fachliteratur aufgeführten Werten. Einzig die Ausbeute des Singulett-Sauerstoffs für Hypericin war etwas tiefer als von anderen Forschungsgruppen berichtet. Die beiden Photosensitizer in Kombination zeigten, ausser der etwas verlangsamten Photobleaching Kinetik, keine auffälligen Wechselwirkungen. ROS Messungen nach PDT zeigten, dass die Zellen, die mit Hypericin und Photosensitizer in

Kombination behandelt wurden, die fluoreszente Form des CM-H_2DCFDA akkumulierten, während Foslipos® kein solches Verhalten aufzeigte. Die Studien betreffend Aufnahme, Verteilung und Lokalisation der Photosensitizer zeigten, dass die intrazelluläre Akkumulation mit Foslipos® über 24 Stunden kontinuierlich war und dessen Lokalisation sich auf das Zellzytoplasma beschränkte, ohne eine eindeutige Kolokalisation mit Zellorganellen aufzuweisen. Hypericin dagegen erreichte sein Akkumulationsmaximum nach 5 Stunden und wurde in Membransystemen, wie auch peri-nuklear aufgefunden. Die gesamte Beseitigung des Foslipos® wurde nicht nach 24 Sunden erreicht, während interzelluläre Hypericin-Rückstände auf ein Minimum reduziert wurden. Die Photosensitizer in Kombination zeigten ähnliche Resultate wie die Einzelsubstanzen. Die Behandlung mit Photosensitizer in Kombination ohne Beleuchtung hatte keinen Einfluss auf die Zellviabilität, während mit Foslipos® und Hypericin behandelte Zellen eine Toxizität für gewisse Konzentrationen aufwiesen. Die Beleuchtung der Zellen in Abhängigkeit der angewendeten Photosensitizer führte zu einer signifikant tieferen Zellviabilität. Die PDT-induzierten Prozesse wiesen verschiedene Kinetiken und Zelltodwege auf, welche stark mit Zellmodellen und Behandlungsprotokollen zusammenhängen. Mit Foslipos® behandelte Zellen hatten nekrotische Eigenschaften, mit Hypericin behandelte Zellen die eines apoptotischen Zelltods. Die Behandlung mit den Photosensitizern in Kombination wiesen die Eigenschaften der Nekrose und Apoptose auf. Einfluss der Photosensitizer auf die molekularen Mechanismen zeigten DNA- und RNA- Schädigung auch ohne Beleuchtung auf. Auch hier war das Ausmass abhängig vom Zellmodell und der verwendeten Photosensitizer. Der Effekt war stärker und ausgeprägter nach der Photodynamischen Therapie. Veränderungen in Genexpressionen, insbesondere heat shock Gene, konnten für alle Zellmodelle nachgewiesen werden.

SCHLUSSFOLGERUNGEN: Unsere Studie belegt eine signifikante Empfindlichkeit verschiedener Zellmodelle auf PDT und deutet auf verbesserte PDT-Effekte bei der Anwendung der Photosensitizer in Kombination hin. Diese Resultate sind die Ersten, welche die Vorteile dieser simplen aber innovativen Behandlungsmethode hervorheben.

Aims and rational of the thesis

Photodynamic therapy (PDT) is a recognised therapeutic strategy known for over a hundred years. It is used in different medical areas and it is well suitable for superficial skin disorders and age related macular degeneration. The modern age of PDT treatment has begun in 1903 with the first clinical application on basal cell carcinoma. Since then many studies on PDT-mediated cancer treatment have been performed. Additionally, new potent photosensitizers and optimised light devices have been developed. The relatively simple mode of PDT action - a short administration of photoactive substance, illumination with the appropriate wavelength and singlet oxygen and reactive oxygen species – mediated tumour destruction - makes this treatment very attractive for therapy of any cancer type, as long as the tumour does not exceed a certain size and has good accessibility. Tumour cells, when compared to normal cells, display higher photosensitizer uptake rates and, with illumination restricted to the desired area, tumour destruction with low side effects is achievable.

The aim of this thesis was to test the applicability of Foslipos® and later hypericin and a 1:1 mixture of both photosensitizers on three different cancer cell lines (see chapters 2-4).

In the initial study (see chapter 2) the effects of novel second generation photosensitizer Foslipos® on prostate carcinoma cell line PC-3 were explored. The focus was on uptake kinetics and subsequent changes on DNA and RNA levels after PDT treatment.

When studying the PC-3 cell line, further questions were raised, leading to the inclusion of two different HNSCC cell lines into the study. Additionally, the study of Schneider-Yin showed very interesting and promising results in optimization of PDT. The PDT effects resulted from treatment with combined photosensitizers. In the case of the above mentioned study, hypericin and 5-ALA showed a higher protoporphyrin IX (PpIX) production when compared to treatment with 5-ALA alone. Based on this knowledge, the questions of Foslipos®, hypericin and their 1:1 mixture uptake as well as distribution kinetics, localization and influence of photosensitizing agents in the dark were explored, as is shown in chapter 3. Chapter 4 is devoted to the prosecution of the study of HNSCC. In this chapter the focus is on PDT effects of applied photosensitizers and their mixture. The questions were related to singlet oxygen production, cell death mechanisms and PDT efficiency. In the chapter 5 the most important results were discussed.

In chapter 6 the establishment of three dimensional HNSCC cell culture protocols is described. This is the basis for further PDT investigations in multi-cellular and more complex systems which are closer to the morphological situation *in vivo*.

Close collaboration with clinicians from the Cranio-Maxillo-Facial and the Oral surgery department of the University Hospital of Zurich encouraged us to expand PDT treatment on oral pathogens to treat local infections in oral region. Thus, in chapter 7 additional published studies performed as a part of the above mentioned work, including not only treatment of oral pathogens but also the development of novel silica carrier systems for photosensitizer encapsulation, are described.

1

GENERAL INTRODUCTION

1. General Introduction

1.1 Photodynamic Therapy

General information: Photodynamic therapy (PDT) was already known to the ancient Indians, Greeks, Incas, Mayas and Egyptians as a medication for skin disorders [1, 2]. This so called heliotherapy was used to treat psoriasis and vitiligo with psoralen-containing plant extracts [3]. Rebirth of modern PDT begun last century with Oscar Raab, one of the von Tappeiner's medical students who observed that acridines showed toxic properties towards the protozoan paramecium if combined with illumination [4]. However, the first clinical PDT application was described by von Tappeiner and Jesionek in 1903 [5]. They applied eosin topically as a remedy for basal cell carcinoma. They were the first explaining dynamic interactions between light, photosensitizing agent and molecular oxygen which resulted in tissue destruction [6]. A few years later in 1913, Friedrich Meyer-Betz conducted a self-experiment and adminstred 200 mg of hematoporphyrin (HpD) intravenously [7]. More than two months he suffered from extreme photosensitivity (fig. 1).

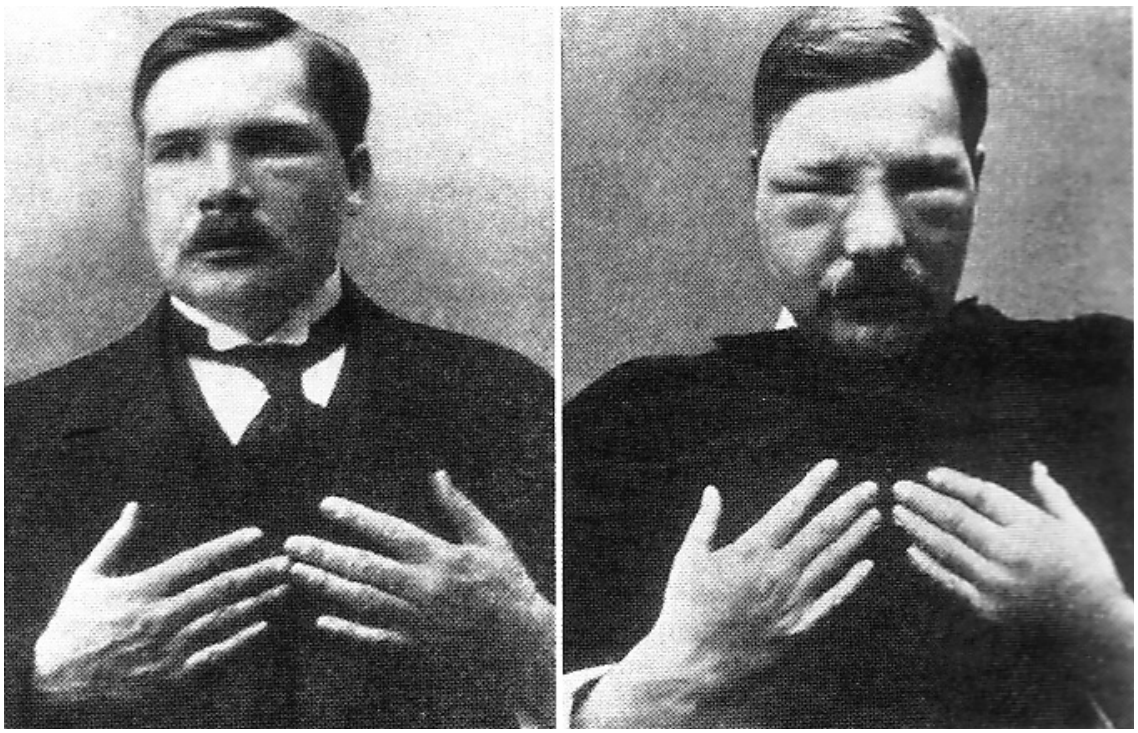

Figure 1: Friedrich Meyer-Betz after intravenous injection of 200 mg of hematophophyrin and light exposure [8].

Sixty years later Dougherty et al. used HpD derivatives to treat different cutaneous diseases. HpD was chromatographically purified by Dougherty's group to Photofrin, which is still the most widely used clinical PDT photosensitizer. For more information on detailed historical data refer to the table below from the review of Allison et al [9].

Ancient history	''Sun Worship'' practiced by Egyptians, Indians and Chinese Heliotherapy by Greeks
1400 B.C.	Ayurvedic system uses naturally occurring psoralens as salves to treat skin problems in India
1820s	Porphyrias clinically described with light photosensitivity
1841	Hematoporphyrin synthesised
1840s–1870s	Hematoporphyrin fluorescence discovered
1896	Finsen Light Institute founded to treat disease
1900	Oscar Raab, medical student, described fluorescence and PDT using dyes, Prime, described sunlight photosensitivity due to orally administered eosin dye
1900-1905	Tappeiner and Jesionek successfully treated human tumors with topical eosin and light
1904	Von Tappeiner and Jodlbauer report oxygen is needed for photosensittzation
1907	Von Tappeiner publishes first text and coins term Photodynamic Therapy
1908	Hausmann reports on fluorescence and cell destruction with hematoporphyrin
1912	Fisher describes porphyrin chemistry with emphasis on porphyrias
1913	Myer-Betz injects self with hematoporphyrin and conducts PDT on himself
1942	Auler and Banzer describes hematoporphyrin accumulation in human tumors, fluorescence and PDT
1950s	Rasmussen's group describe hematoporphyrin tumor localization and excess skin photo sensitivity
1955	Schwartz develops hematoporphyrin-derivative (HpD) from hematoporphyrin
1960	Lipson, Baldes, Schwartz show HpD localtzation for PD in human tumors
1966	Lipson treats a recurrent breast mass with HpD
1976	Kelly and Snell achieve successful PD/PDT in patients with bladder cancer
1978	Dougherty reports on PDT success on multiple patients with cutaneous diseases using HpD
1980s	Clinical Photofrin® PDT success on multiple sites: bladder, lung, esophagus, head and neck, eye, brain
1993	Bladder cancer Photofrin® PDT receives governmental approval in Canada
1995	Lightdale reports positive results on a randomized Photofrin® PDT esophageal trial, FDA and Canadian government approves esophageal treatment for obstructing lesions with Photofrin® PDT
1998	FDA approval for early and late stage lung cancer with Photofrin® PDT
1999	Multicenter randomtzed trial reports positive results for wet macular degeneration treatment with Visudyne™ PDT; FDA approves Visudyne™ PDT for wet macular degeneration treatments
2000	Multicenter trials show positive results for ALA (Levulan®) PDT in actinic keratoses (AK); FDA approves ALA (Levulan®) PDT for AK with DUSA Blu-U® Light System
2004	FDA approves Photofrin® PDT for Barrett's Esophagus

Table 1: A short overview of milestones in the development of PDT and photodiagnosis (PD). Table from [9].

Nowadays, there are many PDT application areas with novel photosensitizers and light sources being developed. Some of the photosensitizers are already clinically approved, others are still under investigation. Currently, PDT is food and drug administration (FDA) approved for treatment of different skin disorders such as actinic keratosis or acne vulgaris [10]. Further, one of the largest patient cohort belongs to treatment of age related wet macular degeneration [11]. Additionally, PDT is used for pre-cancerous diseases such as "Barrett's Esophagus" and various cancer types e.g. advanced stage esophageal tumours, bladder cancer, prostate cancer, lung cancer or palliative treatment of head and neck cancers or as adjuvant

therapy for brain tumours [12-14]. In addition to skin disorders and cancer treatments PDT has shown very promising results in treatment of microorganisms such as antibiotic-resistant strains of methicillin-resistant *Staphylococcus aureus* (*MRSA*) [15] or oral pathogens such as *Candida albicans* or *Streptotcoccus mutans* and *S. sobrinus* [16].

Mechanisms of Action: PDT involves three per se non toxic key components: a photosensitizer, light (visible light or light with an appropriate wavelength) and molecular oxygen. In a simplified scheme (fig. 2) after photosensitizer administration, followed by its distribution and photosensitizer accumulation in the tumour, the desired area is illuminated with light of the appropriate wavelength resulting in production of singlet oxygen and other reactive oxygen species (ROS) subsequently leading to cellular and vascular damage and cell death.

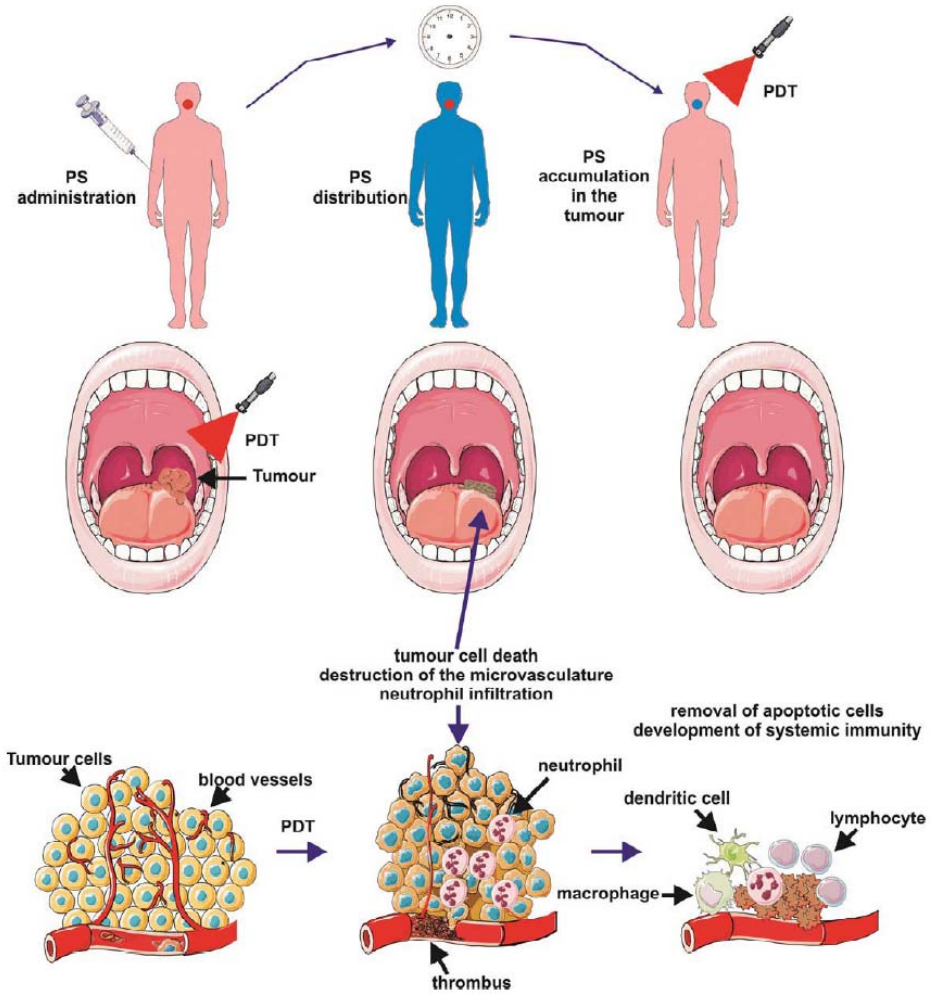

Figure 2: Schematic view of principles of PDT in cancer treatment. Photosensitizer administration occurs systemically or topically. After a period of the time systemic photosensitizer is distributed in the whole body with selective accumulation in dysplasia or tumours. Irradiation triggers a photochemical reaction resulting in production of singlet oxygen and other reactive species leading to irreparable cellular damage and cell death [14].

The processes behind PDT are called photochemical reactions or photosensitizations. Generally, the photosensitization is divided in to two major pathways: Type I and Type II reactions (fig.3).

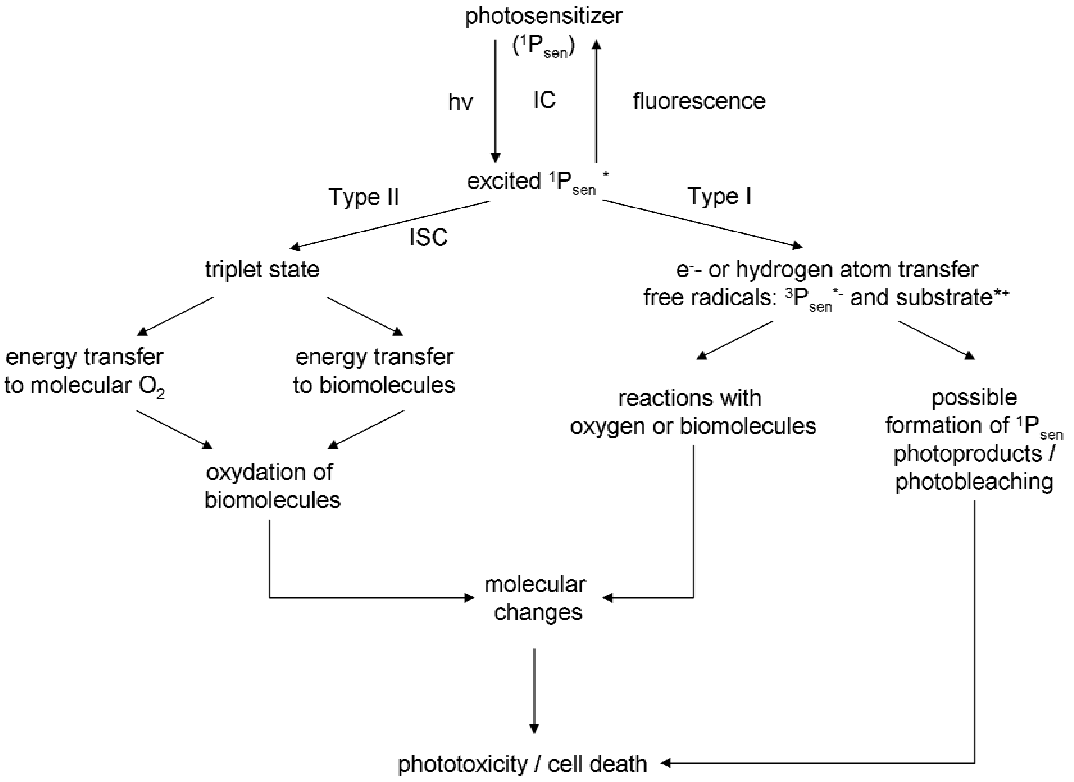

Figure 3: Schematic overview of photosensitization. IC: internal conversion, ISC: intersystem crossing, hv: electromagnetic energy, $^1P_{sen}$: singlet photosensitizer in ground state, $^1P_{sen}{}^*$: singlet excited photosensitizer, $^1P_{sen}{}^{*-}$: photosensitizer radical anion, substrate^{*+}: substrate radical cations.

The Type I reaction is characterised by the production of two types radicals, photosensitizer and substrate radicals. The substrate can transfer either an electron or a hydrogen atom to the excited state of the photosensitizer producing a photosensitizer$^{\circ-}$ radical anion and substrate$^{\circ+}$ cations or free radicals (photosensitizer° and substrate°). Further, the radicals can react with oxygen or biomolecules generating a complex mixture of intermediates, which can be cytotoxic but which also can initiate a cascade of cytotoxic free processes as well. Type I reactions can additionally lead to formation of photosensitizer photoproducts (true photobleaching) which can be cytotoxic [17]. In Type II reactions excited photosensitizers transfer their energy via intersystem crossing (ISC) to long living triplet state photosensitizers and finally to molecular oxygen or other biomolecules such as electron-rich compounds, e.g. unsaturated fatty acids. Photochemical mechanisms are explained in a modified Jablonski

energy diagram depicted in figure 4 [18]. These energy transfers result in oxidation of biomolecules and in generation of singlet oxygen ($^1O_2$) and other ROSs leading to cell death.

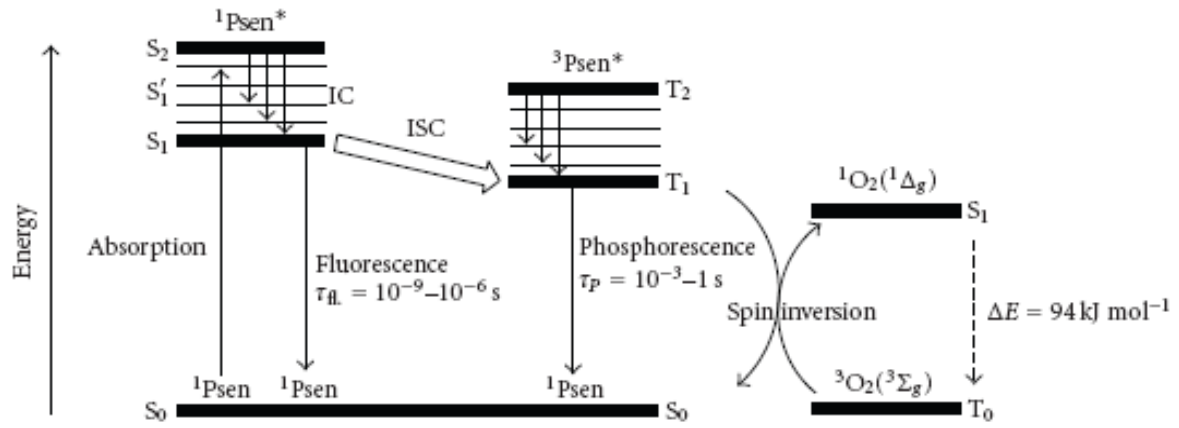

Figure 4: Modified Jablonski energy diagram [18] explaining photochemical mechanisms from photon absorption by photosensitizer to energy transfer and generation of singlet oxygen. $^1P_{sen}$: singlet photosensitizer in ground state; $^1P_{sen}{}^*$: singlet excited photosensitizer; IC: internal conversion; ISC: intersystem crossing; $^3P_{sen}{}^*$: triplet excited photosensitizer; $^3O_2$: oxygen in ground state; $^1O_2$: singlet oxygen; S_0: ground state; S_n: excited states with different vibrational sub-levels S'_n.

Absorption of light by $^1P_{sen}$ elevates an electron (e^-) from the photosensitizer ground singlet state (S_0) into an excited vibronic sub-levels S'_n without changing the e^- spin direction. The excited photosensitizer ($^1P_{sen}{}^*$) can lose its energy by decaying (vibrational relaxation → energy dissipated as heat) through these sub-levels via IC to populate the first excited singlet state S_1 (fluorescent state). The relaxation from S_1 to S_0 results in fluorescence. Alternatively, e^- from excited fluorescent state (S_1) may undergo spin inversion and populate lower – energy excited triplet state T_1 via ISC. The decay processes from T_1 to S_0 have a longer lifetime and are called phosphorescence. Due to the longer lifetime and presence of unpaired valence e^-, photosensitisation may be initiated.

Photobleaching: Singlet oxygen and ROS production by photosensitizer have not only influence on cellular damage but also on the photodegradation of the photosensitizer itself. The degradation of the dye is called photobleaching and is defined as the loss of absorption or emission intensity caused by light [19]. In general, there are two different types of irreversible photosensitizer degradation:

i) *Photomodification:* Here, a photosensitizer or chromophore is retained in a modified form but there is a loss of absorbance or fluorescence at some wavelengths.

ii) *True photobleaching:* In this case, chemically changed photosensitizer leads to molecular degradation, resulting in small fragments which have no absorption in visible light region.

The pathways of photobleaching may have oxidative or reductive nature. Involvement of singlet oxygen enhances the photobleaching processes.

Advantages and Disadvantages of PDT: Clinical application of PDT is nowadays considered to be a new and very promising treatment [20] but its full potential has not been exploited yet. PDT treatment is still restricted to dermatological oncology and ophthalomology. Despite many advantages [21] of PDT, such as low side effects, no further cell mutations as observed in radiation therapy, no cellular resistance as well as high treatment repeatability or activation of immune response [22] in contrast to chemotherapy and noteworthy possible combination with other conventional treatments [23, 24] there is resistance from the clinical side to this new approach. The costs for the establishment of PDT centres and lack of convenient and inexpensive light sources are major resistance reasons. Nevertheless, progress is slow but steady. Unfortunately, there are only randomised clinical trials at the moment and the PDT treatments do not outperform conventional therapies yet.

Besides general scepticism there are three major drawbacks in PDT: prolonged skin photosensitivity, low tumor selectivity and limited tissue penetration which restrict this therapy to superficial treatment modality only. However, the success of PDT is unstoppable and new photosensitizers with higher tumor selectivity and cheaper light delivery sources are under development.

1.2 Photosensitizers

PDT efficacy is mainly dependent on the photosensitizing agent and applied light dose. An ideal photosensitizer should be a pure compound with minimal systemic toxicity, high singlet and/ or ROS quantum yield, high tumour selectivity, an absorption wavelength > 650 nm and low manufacturing costs [21]. So far, there are many different photosensitizers which are clinically approved and widely used such as Photofrin (porphyrin sodium) or under current investigations such as different formulations of mTHPC (Foslip®, Fospeg®). In general, photosensitizers can be classified in to porphyrin and non-porphyrin photosensitizers [13]. Furthermore, porphyrin-derived photosensitizers are classified in first, second or third generation (conjugations with antibodies) of photosensitizers (fig. 5).

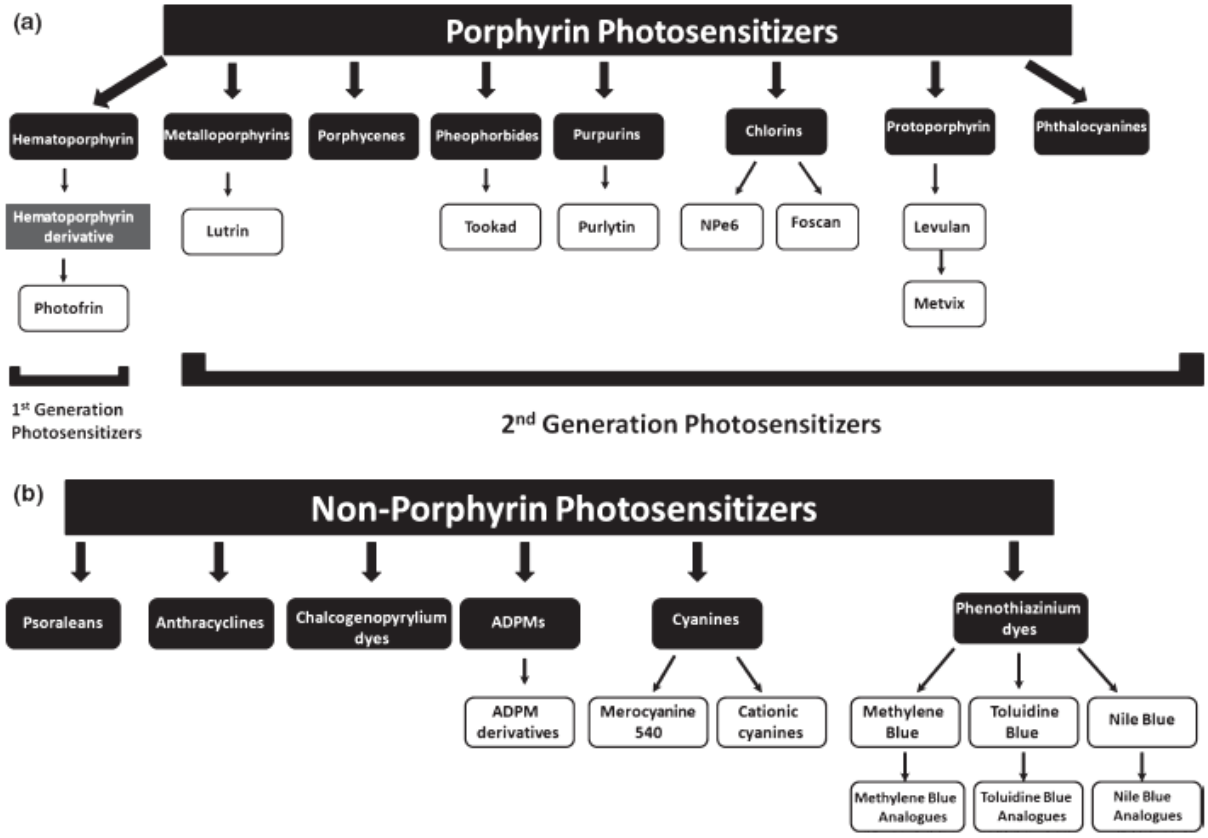

Figure 5: Classification of photosensitizers a) porphyrins-derived and b) non-porphyrin derived photosensitizers [13].

Taken together, development of photosensitizers is focusing on increasing PDT efficacy and tumour selectivity while minimizing systemic toxicity. This work is ongoing in many research groups around the globe [25].

1.2.1 Hypericin

General Information: Common St. John's Wort is a perennial plant with golden yellow flowers (fig. 6 A and B) that can be found in sunny and dry places all over Europe, Western Asia, Northern Africa and America. This plant has been known since ancient time and has a long history. It was used as a analgesic in wound healing or against mild depressions [26, 27]. The use of the plant originates in Greece in the 1st century A.C. described by the herbologists Dioscorides and Plenius but its therapeutic potential was already mentioned in the 5th century B.C. by the father of Medicine, Hippocrates.

Figure 6: Showed in A is *Hypericum perforatum* flower with typical golden yellow blossom (found on University of Zurich campus, Irchel). Hypericin (10, 11-dimethyl -1, 3, 4, 6, 8, 13-hexahydroxynaphtho-dianthrone) and his congener pseudo-hypericin are located in dark granulates on the leafs and plant buds (B). In C is depicted chemical structure of hypericin.

Hypericin is a major active constituent of the plants of the genus *Hypericum*. This substance is known for its strong photo-activity and - if taken in larger amounts - it can cause serious non pigmented skin burnings associated with oedema (hypericism). In contrast to the light exposition hypericin shows very low cell toxicity if applied in the dark. Sanochemia Pharmazeutica AG has applied PVP-hypericin with the trade name Vidon® for diagnostic purposes in superficial bladder cancer. Currently they are in phase IIb clinical trials and ongoing results are outstanding but compared to Hexvex (hexaminolevulinate), the only clinical approved photosensitizer for photodynamic diagnosis (PDD), they seem to be much more advantageous for patients.

Physicochemical properties: Hypericin [28] (10,11-dimethyl-1, 3, 4, 6, 8, 13 – hexahydroxynaphthodianthrone, M_w = 504.45 g/ mol) (fig. 6 C) is a red, non planar aromatic polycyclic substance belonging to the chemical class of antraquinones. It shows low solubility

in water or organic solvents, but is well soluble in polar organic solvents such as dimethyl sulfoxid, tetrahydrofurane and ethanol with a pH ranging between 4 and 11. In physiological conditions hypericin is present as monosodium salt. In water, these monosodium salts form non-fluorescent aggregates (stacked and planar associations) [29]. Hypericin salts produce wine-red coloured solutions with a maximal absorption wavelength at 548 nm and 593 nm. Emitted fluorescence has its maxima at 594 nm and 642 nm. A very high triplet quantum yield and a high yield of singlet oxygen (Φ_t= 0.7; Φ_s= 0.7) as well as other reactive oxygen species (ROS) [30-32] characterise hypericin as a very promising photosensitizer. Besides the photoactive features, Kubin et al. [28] reported antineoplastic, antitumor and antiviral activities.

Tumorotropic properties: Kamuhabwa et al. [33] have shown that *in vitro* uptake behaviour of hypericin in malignant and healthy cells is very similar to each other and no significant difference could be proven. Many *in vitro* studies showed that cellular hypericin uptake relies mainly on passive processes (diffusion) [34] and its preferential incorporation involves cellular membranous systems (cell and nuclear membranes, mitochondria, golgi apparatus, endoplasmatic reticulum and lysosomes) [35]. In contrast, *in vivo* studies showed that hypericin preferentially accumulates in tumour tissue. This tumorotropic behaviour can be explained by hypericin's preferable lipoprotein interactions (low und high density lipoproteins) [36, 37]. This is not only an important carrier system *in vivo* but it is also responsible for receptor-mediated internalisation. The uptake could also be supported by the enhanced permeability and retention (EPR) effect in tumor tissues. Van de Putte et al. [38] elaborated the tumoritropic principle of hypericin in subcutaneously growing mouse tumours. They found up to 16-fold higher concentration in tumour tissue compared to surrounding healthy tissue. This study suggested that the accumulation of hypericin is highly dependent on the extent of local blood perfusion and on the tumour size. Smaller tumours display a more homogeneous and functional vessel distribution lacking necrotic areas if compared to larger tumours. The permeability of the tumour vessels has as well an important influence on intra-tumoural accumulation [39].

1.2.2 Foslipos®

General information: Meso-tetrahydroxyphenyl chlorin (mTHPC or temoporfin, M_w = 680.75 g/ mol) is a chemically derived substance and one of the most potent second generation photosensitizer [40, 41]. Based on clinical results it is 100-200 times more potent than Photofrin [42]. Nowadays, mTHPC is known under the trade name Foscan® (Biolitec AG, Jena, Germany). Foscan® is a non-aqueous formulation containing mTHPC in ethanol as a solvent and propylene glycol as a co-solvent. This mTHPC formulation is approved for palliative treatment of advanced head and neck cancer in Europe [43]. In order to enhance solubility and PDT efficacy of mTHPC Biolitec AG developed different liposomal formulations. The mTHPC loaded liposomes are based on dipalmitoyl-phosphatidylcholine (DPPC) with a small amount of dipalmitoylphosphatidylglycerol (DPPG) as physical liposome stabiliser (fig. 7 A and 7 B) [44].

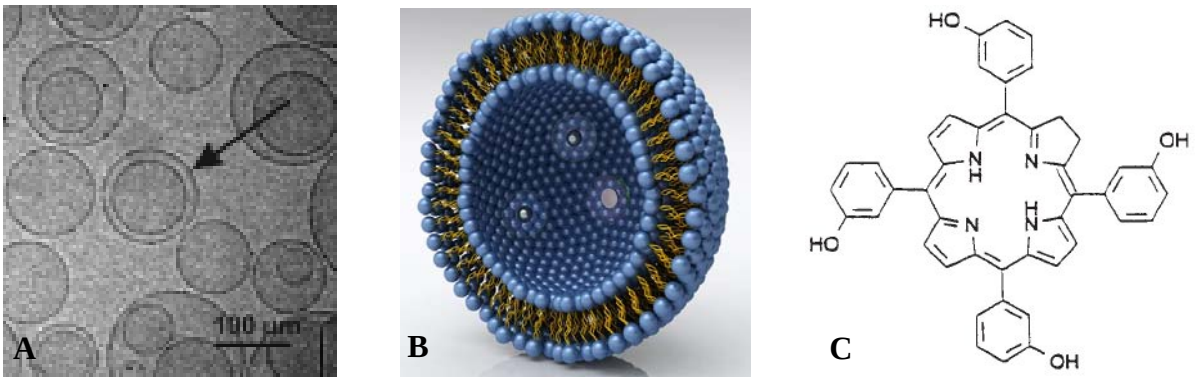

Figur 7: Liposomal mTHPC (5,10,15,20-Tetra(meso-hydroxyphenyl)chlorin) cryo electron microscopy pictures are shown In A [45] and in B schematic picture of a liposome [46]. mTHPC molecules are located between lipid bilayers. The chemical structure of mTHPC is shown in C.

The chemically flexible and biotolerable DPPC/ DPPG liposomes are very useful carrier systems for substances which are normally not soluble or toxic in a biological environment. This flexibility of DPPC/ DPPG liposomes was used to produce different mTHPC formulations such as Foslip® or Foslipos®, which only differs in additional 5% glucose in the Foslip® solution. Another promising DPPC/ DPPG-based mTHPC formulation is Fospeg®. The liposomal surface modifications with PEG were shown to have much longer systemic persistence *in vivo* [47, 48]. All these novel formulations are improving PDT treatments and outcomes in patients. On one side photosensitivity could be minimized but at the same time

bio-distribution and its systemic clearance as well as tumor selectivity could be enormously enhanced.

Physicochemical properties: Generally, mTHPC is a strongly hydrophobic substance and has low solubility in aqueous solvents. Additionally, it tends to aggregate in physiological solutions, leading to drastic decrease of fluorescence, limited photosensitizer transport, low uptake in tumours and extremely low PDT effects. Solubility of mTHPC is achieved in alcohol, acetone or in ethyl acetate. When dissolved, it displays a brown-reddish solution with maximal absorption wavelength at 417 nm and 651 nm. The emitted fluorescence has its maximum at 653 nm. The singlet oxygen yield is very high ($\Phi_t = 0.89$; $\Phi_s = 0.59$) if compared to other photosensitizers [49]. The size of liposomal formulations of mTHPC (in particular Foslip® and Foslipos®) measured by dynamic light scattering (DLS) in water was ~ 140 nm. The current drug loading (mTHPC) in DPPC/ DPPG liposomes is 8 mol%.

Tumourotropic properties: Foscan® has been evaluated as a phototherapeutic agent against early head and neck cancer or as an adjuvant therapy in advanced head and neck cancer when conventional treatments (surgery, chemo- and radiation therapy) have failed. Dougherty et al. [12] reported that this chlorin photosensitizer appears to be one of the most potent photosensitizer to date requiring very low drug and light doses. Unfortunately Foscan® can render patients photosensitive up to 20 days after initial illumination [50]. Lassalle et al. [51] studied correlations between pharmacokinetics, intra-tumoural distribution and PDT efficiency of Foslip® in EMT6 xenografted nude mice. Time dependent observations showed that after a short time post incubation fluorescence was found in vessels, tumour and endothelial cells. 15 h post injection the fluorescence was predominately localised in the cytoplasm of tumour cells. Kiesslich and colleagues reported that Foscan® has enhanced light tissue penetration in treatment of cholangiocarcinoma and that Foscan®-mediated PDT cause tumour necrosis and has higher tumouricidal depth (>7-8 mm) than Photofrin. Further *in vitro* studies were performed on two different biliary tract cancers [52]. The results of these studies indicated that less differentiated cell lines tend to be more sensitive to mTHPC-mediated PDT. Based on these investigations cellular uptake, phototoxicity and photosensitizer release were performed on a large set of cell lines [53]. Localisation of mTHPC was found partly in mitochondria, lysosomes or perinuclearly but in general it was difficult to provide evidence for an organelle specific localization. Uptake and the related phototoxicity correlated directly. Our study with the prostate carcinoma cell line (PC-3) displayed increasing accumulation of Foslip® in the cytoplasm, especially in the vicinity of the nucleus [54].

1.3 Cancer

General Information: According to the World Health Organisation (WHO) cancer is the leading cause of death worldwide (7.6 million deaths in 2008) [55, 56]. About 70 % of all cancer deaths occurred in developing countries and it is expected to rise to 11 million per annum in 2030. Table 2 illustrates worldwide statistics on cancer incidence and mortality.

WORLD	**Male**	**Female**	**Both sexes**
Population (thousands)	3'402'841	3'347'220	6'750'061
Number of new cancer cases (thousands)	6'617.8	6'044.7	12'662.6
Age-standardised rate (W)	203.8	165.1	181.6
Risk of getting cancer before age 75 (%)	21.2	16.5	18.7
Number of cancer deaths (thousands)	4'219.6	3'345.2	7'564.8
Age-standardised rate	128.6	87.6	106.1
Risk of dying from cancer before age 75 (%)	13.4	9.1	11.2
5 most frequent cancers	Lung Prostate Colorectum Stomach Liver	Breast Colorectum Cervix uteri Lung Stomach	Lung Breast Colorectum Stomach Prostate

Table 2: Worldwide statistics summary on cancer incidence and mortality (GLOBOCAN 2008) [57]. **Glossary:** Age-standardised rate (W): A rate is the number of new cases or deaths per 100'000 persons per year. An age-standardised rate is the rate that a population would have if it had a standard age structure. Standardization is necessary when comparing several populations that differ with respect to age because age has a powerful influence on the risk of cancer.
Risk of getting or dying from the disease before age 75 (%): The probability or risk of individuals getting/ dying from cancer. It is expressed as the number of newborn children (out of 100) who would be expected to develop/ die from cancer before the age of 75 if they had cancer rates (in the absence of other causes of death).

The cancer incidence is increasing as a result of population's aging and growth, cancer associated lifestyle such as smoking, alcohol consumption, physical inactivity, environmental conditions and nutrition. WHO advises that modifying and avoiding of risk factors may prevent more than 30 % of cancers. Additionally, evidence-based strategies for cancer prevention, early detection and management of patients with cancer can reduce the cancer mortality. Therefore, knowledge about cancer causes, which is molecularly seen as a multistep process is the first step in treating this complex disease. Hanahan and Weinberg [58] proposed six hallmarks (fig. 8) of cancer which are involved in transformation of normal to neoplastic and lastly to malignant cell state.

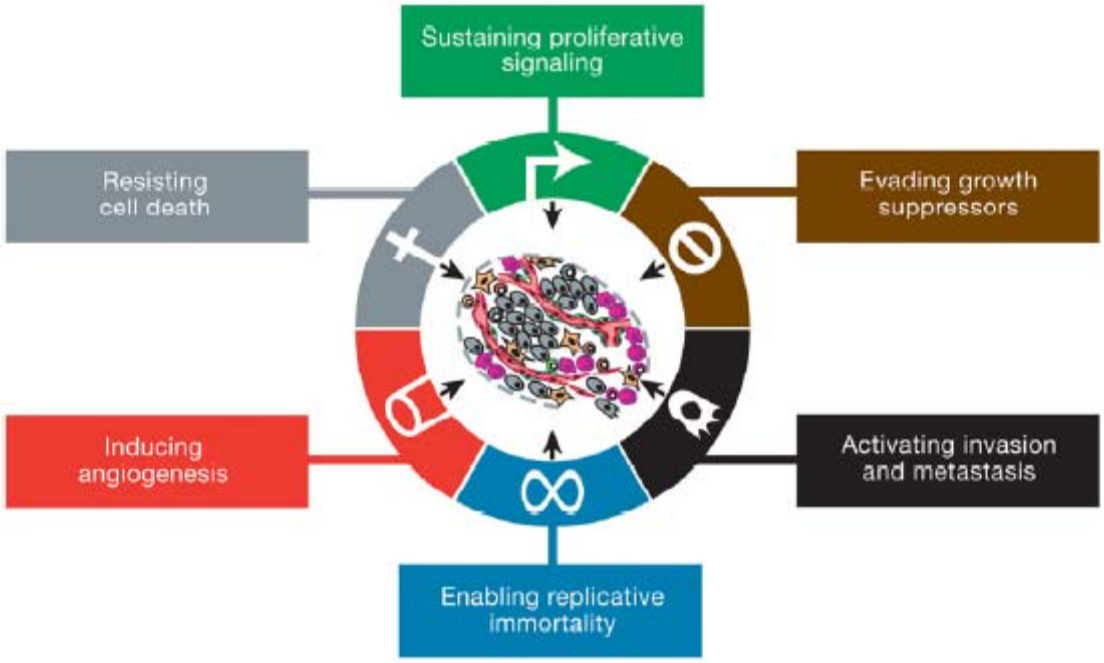

Figur 8: Illustration of the six hallmark capabilities proposed by Hanahan and Weinberg 2011 [58] (originally proposed in 2000).

They included the following biological capabilities:

i) Sustained proliferative signalling – this fundamental trait of cancer cells involves deregulation of homeostasis of cell growth-promoting signals. Cancer cells become masters of their own destinies. The regulation mechanisms are still not understood in detail.

ii) Evading growth suppressors – inactivation of dozens of tumour suppressor genes leads to deregulation of cell proliferation. Inactivation of cell-to-cell contacts

enables construction and maintenance of architecturally complex cancerogenous tissues.

iii) Resisting cell death – programmed cell death by apoptosis as a natural barrier for cancer development is disturbed by the loss of tumour suppressor functions such as TP53 or by suppressing pro-apoptotic factors. The diversity of cell death avoiding mechanisms is enormous and it is dependent on the cancer cell as well as their evolution to the malignant state.

iv) Enabling replicative immortality – Telomerase over-expression in cancer cells and therewith connected resistance to induction of cellular senescence and apoptosis.

v) Inducing angiogenesis – Starting with a certain tumour volume the induction of neo-vascularization is inevitable for further tumour survival. The "angiogenic switch" involves up-regulation of signalling proteins such as vascular endothelial growth factor– A (VEGF-A) and thrombospondin- 1 (TSP- 1).

vi) Activating Invasion and Metastasis – the responsible mechanisms were not known in 2000. This multistep process is termed the invasion-metastasis cascade and includes cell-biologic changes, local invasion, intravasation, transit of cancer cells to lymphatic and hematogenous systems, extravasation and colonisation.

Development of cancer and the complex biology behind its pathogenesis provide a huge challenge in treating this disease. The six acquired capabilities are integral components of most cancer types and their better understanding is from immense importance in creating personalised treatment methods. Additionally, the complex morphology of cancer and microenvironments demand different treatment approaches. Hanahan and Weinberg described illustrative samples for treatment of each proposed cancer hallmark (fig. 9). In particular, they state that selective co-targeting of multiple pathways will result in more effective and durable therapies for cancer.

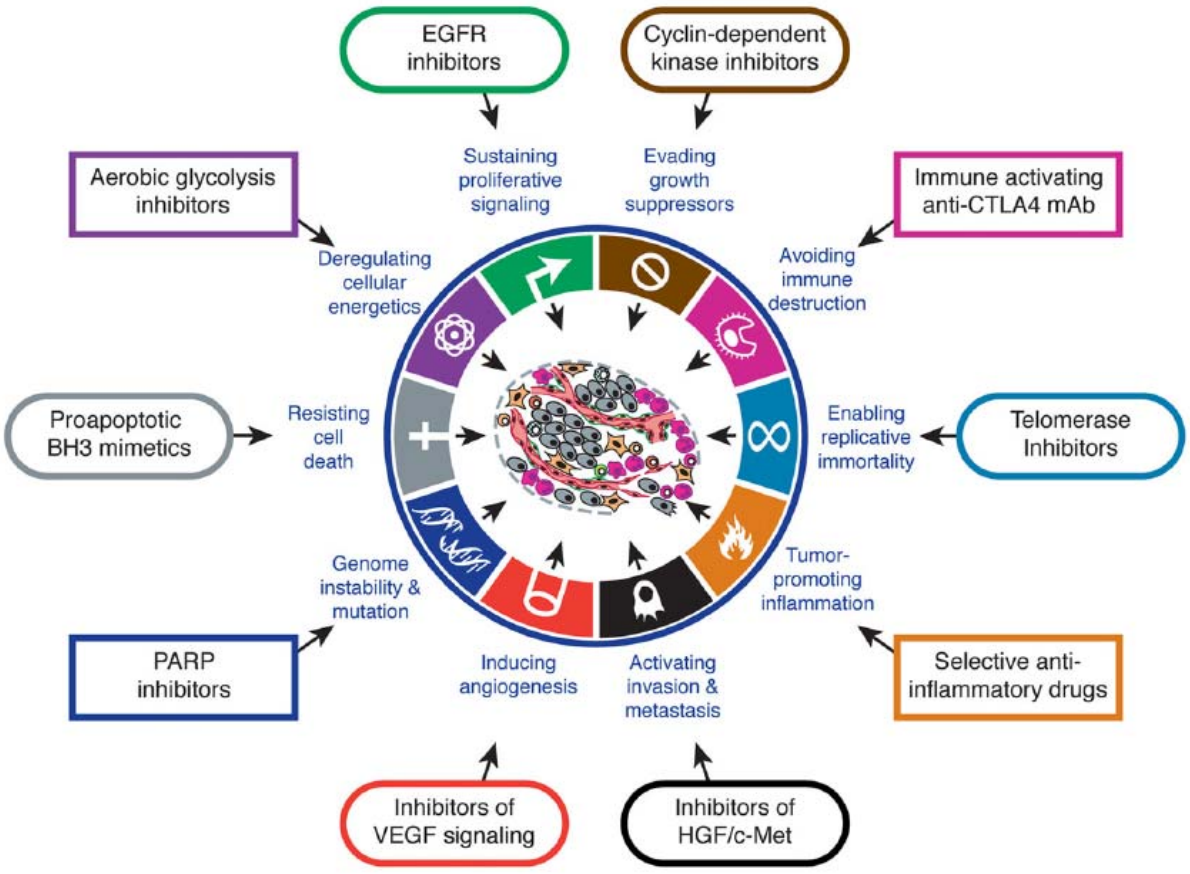

Figur 9: Illustrative examples of therapeutic targeting of the hallmarks of cancer used in clinics or in clinical trials [58].

The cancer treatment has to be a multiple step approach as it is its development. Introducing PDT as a supporting co-therapy can be very advantageous since the PDT mode of action is universal and independent from any hallmark of cancers. In the review of Firczuk et al. [21] was reported that combination of PDT with different established treatment modalities such as surgery, radiotherapy or chemotherapy provides significant improvement of treatment outcome.

1.3.1 Prostate Carcinoma

Background: Prostate cancer is the second most frequent cancer type and sixth leading cause of cancer death in male (app. 900'000 new cases per year worldwide) [56]. More than 70 % of cases are diagnosed in elderly men (prevalence rate in men ages 70-90 is 90 %) [59]. The

major risk factor for developing prostate cancer is age, followed by race, family history and high fat diet. The exact role of race remains unclear [60]. The autopsy data suggest that more man will die *with* than *from* prostate cancer. The early stage of this disease is asymptomatic and therefore is recommended to make a preventive prostate cancer screening (PSA screening, considered to be imperfect due to the non cancerous elevation of serum PSA or digital rectal exam) if one of the following statements are true: men with low risk from the age of 50 or men with high risk (relatives which have been diagnosed for prostate carcinoma) from the age of 40.

The treatment options for prostate cancer are based on the cancer staging and include localized prostate cancer active surveillance, radical prostatectomy, external beam radiation therapy, brachytherapy and cryotherapy. The treatments for advanced prostate cancer are hormone and chemotherapy as well as some newly emerging therapies. Incidence of prostate cancer will continue to rise therefore new therapies and nursing research are necessary.

1.3.2 Head and Neck Cancer

Background: Head and neck squamous cell carcinoma (HNSCC) comprises a group of epithelial cancers that arises from e.g. the lips, the oral or nasal cavity, salivary glands, paranasal sinuses, pharynx or larynx [61]. With a worldwide incidence of more than 600'000 new cases per year, HNSCC accounts for about 6 % of all malignant diseases diagnosed (http://globocan.iarc.fr). Almost 75 % are in men. Main risk factors for head and neck malignancies are tobacco and alcohol consumption but also low consumption of fruits and vegetables. If detected early, patients have cure rates of about 90 %. However, 60 % of patients present with advanced disease or loco-regional lymph node metastasis at the time of diagnosis and have a poor prognosis [62, 63]. Another reason for the poor prognosis is substantial risk of a second primary cancer which is higher at younger ages [64]. Differences in survival depend on sex, age and on socioeconomic status as well as on the site of origin of the cancer invasion [65]. It has also been shown that patients suffering from an infection with human papillomavirus (HPV) may have a different prognosis from those of non-HPV-related cancers [66].

Currently, treatment options for HNSCC patients include surgery, radiotherapy, chemotherapy or a combination of them [67, 68]. Due to the distinct localization of these tumours in regions with anatomic structures important to e.g. breathing, mastication, swallowing or phonation, invasive treatment regimes frequently leading to severe functional

impairments, - often accompanied by unfavorable cosmetic outcomes. This is true despite significant advancements made in the reconstructive abilities over the past two decades. Moreover, radiation may have long-term effects on surrounding healthy tissue structures such as parts of the brain, the spinal cord or salivary glands. However, while surgery or radiation therapy is local, chemotherapy is applied systemically and may thus result in severe adverse effects e.g. on blood cell production (anaemia, neutropenia or thrombopenia), the mucosa (mucositis), the auditory and vestibular system (ototoxicity) or the kidneys (nephrotoxicity). Despite this aggressive therapeutic regime, to date many patients with advanced disease cannot be cured and more then half of them die within five years [69-71]. HNSCC is thus currently the eighth leading cause of cancer death worldwide.

1.4 Cell Models

Research on two dimensional cell cultures has been routinely performed within the last sixty years. Drug screenings and developmental biology rely on the cell culture systems. In the following we used three different cell lines in culture to test the applicability of PDT *in vitro*.

1.4.1 Prostate Carcinoma Cell Line (PC-3)

The PC-3 [72] cell line was isolated from a 62-year-old Caucasian (from lumbar vertebra) originally presented with urinary retention, weight loss and anemia. His prostate was small and hard but mobile, four months after diagnosis the symptoms worsened and despite cryotherapy the patient died. Autopsy revealed tumour metastasis in the bone marrow and in the adrenal glands. The established cells show a population doubling time of approximately 33 hours. PC-3 cell line is aneuploid and tumourigenic. Colony forming in soft agar has an efficiency of 0.15 %.

1.4.2 Head and Neck Squamous Cell Carcinoma Cell Lines (UMB-SCC 745 and UMB-SCC 969)

The squamous cell carcinoma cell lines were isolated from oropharynx (UMB-SCC 745) and tonsil (UMB-SCC 969) [73]. Isolation of UMB-SCC 745 resulted from the primary tumour site ($T_4N_2M_0$, grading G_2) of a 48-year-old male patient. UMB-SCC 969 cells were also isolated from the primary tumour site ($T_4N_2M_1$, grading G_2) of a 67-year-old male patient. Both cell lines have p53 mutations. The cells have a population doubling time of approximately 36h. No colony forming was observable.

1.5 References

1. Nayak, C.S., *Photodynamic therapy in dermatology.* Indian J Dermatol Venereol Leprol, 2005. **71**(3): p. 155-60.
2. Pervaiz, S. and M. Olivo, *Art and science of photodynamic therapy.* Clin Exp Pharmacol Physiol, 2006. **33**(5-6): p. 551-6.
3. Luksiene, Z., *Photodynamic therapy: mechanism of action and ways to improve the efficiency of treatment.* Medicina (Kaunas), 2003. **39**(12): p. 1137-50.
4. Raab, O., *Über die Wirkung Fluoreszierender Stoffen auf Infusoira* Z. Biol., 1900. **39**: p. 612-617.
5. von Tappeiner, H., Jesionek H., , *Therapeutische versuche mit fluoreszierenden Stoffen.* Münch. Med. Wochenschr., 1903. **47**: p. 2042-2044.
6. Von Tappeiner, H., Jesionek H.,, *Die Sensibilisierende Wirkung Fluorescierender Substanzen: Gesammelte Untersuchungen über die Photodynamische Erscheinungen.* F.C.W. Vögel, 1907: p. 1-210.
7. Meyer-Betz, F., *Untersuchungen über die Biologische (photodynamische) Wirkung des hamatoporphyrins und anderer Derivative des Blut-und Gallenfarbstoffs.* Dtsch. Arch. Klin. Med., 1913. **112**: p. 476-503.
8. Calzavara-Pinton, P., R.M. Szeimies, and B.l. Orte, *Photodynamic therapy and fluorescence diagnosis in dermatology*. Comprehensive Series in Photosciences ed. J. Häder. Vol. 2. 2001, Amsterdam: Elsevier Science B.V. 11.
9. Allison, R., H Mota, C H Sibata *Clinical PD/PDT in North America: An historical review.* Photodiagnosis and Photodynamic Therapy 2004. **1**(4): p. 263-277.
10. Babilas, P., et al., *Photodynamic therapy in dermatology: state-of-the-art.* Photodermatol Photoimmunol Photomed, 2010. **26**(3): p. 118-32.
11. Couch, S.M. and S.J. Bakri, *Review of combination therapies for neovascular age-related macular degeneration.* Semin Ophthalmol, 2011. **26**(3): p. 114-20.
12. Dougherty, T.J., et al., *Photodynamic therapy.* J Natl Cancer Inst, 1998. **90**(12): p. 889-905.
13. O'Connor, A.E., W.M. Gallagher, and A.T. Byrne, *Porphyrin and nonporphyrin photosensitizers in oncology: preclinical and clinical advances in photodynamic therapy.* Photochem Photobiol, 2009. **85**(5): p. 1053-74.
14. Agostinis, P., et al., *Photodynamic therapy of cancer: an update.* CA Cancer J Clin, 2011. **61**(4): p. 250-81.
15. Maisch, T., *Anti-microbial photodynamic therapy: useful in the future?* Lasers Med Sci, 2007. **22**(2): p. 83-91.
16. Lüthi M., E.B.G., Mathias Engström, Marius Bredell, Klaus Grätz, Heinrich Walt, Rudolf Gmür and Caroline Maake, *Hypericin- and mTHPC-mediated photodynamic therapy for the treatment of cariogenic bacteria.* Med. Laser App., 2009. **24**(4): p. 227-236.
17. Bonnett, R., Martinez G., *Photobleaching of sensitisers used in photodynamic therapy.* Tetrahedron, 2001. **57**: p. 9513-9547.
18. Josefsen, L.B. and R.W. Boyle, *Photodynamic therapy and the development of metal-based photosensitisers.* Met Based Drugs, 2008. **2008**: p. 276109.
19. Verhoeven, J.W., *Glossary of terms used in photochemistry* Pure and Appl. Chem., 1996. **68**(12): p. 2223-2286.
20. Triesscheijn, M., et al., *Photodynamic therapy in oncology.* Oncologist, 2006. **11**(9): p. 1034-44.
21. Firczuk, M., et al., *Approaches to improve photodynamic therapy of cancer.* Front Biosci, 2011. **16**: p. 208-24.

22. Kammerer, R., et al., *Induction of immune mediators in glioma and prostate cancer cells by non-lethal photodynamic therapy.* PLoS One, 2011. **6**(6): p. e21834.
23. Zuluaga, M.F. and N. Lange, *Combination of photodynamic therapy with anti-cancer agents.* Curr Med Chem, 2008. **15**(17): p. 1655-73.
24. Bhuvaneswari, R., et al., *Antiangiogenesis agents avastin and erbitux enhance the efficacy of photodynamic therapy in a murine bladder tumor model.* Lasers Surg Med, 2011. **43**(7): p. 651-62.
25. Allison, R., Gordon H Downie, , X.-H.H. Rosa Cuenca, Carter JH Childs, , and C.H. Sibata, *Photosensitizers in clinical PDT.* Photodiagnosis and Photodynamic Therapy, 2004. **1**: p. 27-42.
26. Baruch, Y., *[Hypericum extract for treatment of depression: what's new?].* Harefuah, 2009. **148**(3): p. 183-5, 210, 209.
27. Istikoglou, C.I., V. Mavreas, and G. Geroulanos, *History and therapeutic properties of Hypericum Perforatum from antiquity until today.* Psychiatrike, 2010. **21**(4): p. 332-8.
28. Kubin, A., et al., *Hypericin--the facts about a controversial agent.* Curr Pharm Des, 2005. **11**(2): p. 233-53.
29. Bano, G., et al., *On the diffusion of hypericin in dimethylsulfoxide/water mixtures-the effect of aggregation.* J Phys Chem B, 2011. **115**(10): p. 2417-23.
30. Diwu, Z. and J.W. Lown, *Photosensitization with anticancer agents. 17. EPR studies of photodynamic action of hypericin: formation of semiquinone radical and activated oxygen species on illumination.* Free Radic Biol Med, 1993. **14**(2): p. 209-15.
31. Jardon, N.L.a.R.G., *Formation d'oxygène singulet 1Δg photosensibilisée par l'hypéricine, caractérisation et étude du mécanisme par spectroscopie laser.* J. Chim. Phys., 1987. **84**: p. 1141-1145.
32. Michaeli, A., Ayelet Regev, Yehuda Mazur, Jehuda Feitelson, Haim Levanon, *Triplet-state reactions of hypericin: time-resolved laser photolysis and electron paramagnetic resonance spectroscopy.* J. Phys. Chem., 1993. **97** (36): p. 9154-9160.
33. Kamuhabwa, A.R., et al., *Photodynamic activity of hypericin in human urinary bladder carcinoma cells.* Anticancer Res, 2000. **20**(4): p. 2579-84.
34. Siboni, G., et al., *The correlation between hydrophilicity of hypericins and helianthrone: internalization mechanisms, subcellular distribution and photodynamic action in colon carcinoma cells.* Photochem Photobiol Sci, 2002. **1**(7): p. 483-91.
35. Ho, Y.F., et al., *Lipid-mediated preferential localization of hypericin in lipid membranes.* Biochim Biophys Acta, 2009. **1788**(6): p. 1287-95.
36. Buriankova, L., et al., *Kinetics of hypericin association with low-density lipoproteins.* Photochem Photobiol, 2011. **87**(1): p. 56-63.
37. Mukherjee, P., et al., *Accumulation and interaction of hypericin in low-density lipoprotein--a photophysical study.* Photochem Photobiol, 2008. **84**(3): p. 706-12.
38. Van de Putte, M., et al., *Elucidation of the tumoritropic principle of hypericin.* Br J Cancer, 2005. **92**(8): p. 1406-13.
39. Roberts, W.G. and T. Hasan, *Tumor-secreted vascular permeability factor/vascular endothelial growth factor influences photosensitizer uptake.* Cancer Res, 1993. **53**(1): p. 153-7.
40. Senge, M.O. and J.C. Brandt, *Temoporfin (Foscan((R)) , 5,10,15,20-Tetra(m-hydroxyphenyl)chlorin)-A Second-generation Photosensitizer(dagger,double dagger).* Photochem Photobiol, 2011. **87**(6): p. 1240-96.
41. Mitra, S. and T.H. Foster, *Photophysical parameters, photosensitizer retention and tissue optical properties completely account for the higher photodynamic efficacy of meso-tetra-hydroxyphenyl-chlorin vs Photofrin.* Photochem Photobiol, 2005. **81**(4): p. 849-59.

42. Ball, D.J., D.I. Vernon, and S.B. Brown, *The high photoactivity of m-THPC in photodynamic therapy. Unusually strong retention of m-THPC by RIF-1 cells in culture.* Photochem Photobiol, 1999. **69**(3): p. 360-3.
43. EMEA, *www.emea.europa.eu/humandocs/Humans/EPAR/foscan/foscan.htm,* . European Public Assessment Report (EPAR) for Foscan;, 2009.
44. Kachatkou, D., et al., *Unusual photoinduced response of mTHPC liposomal formulation (Foslip).* Photochem Photobiol, 2009. **85**(3): p. 719-24.
45. Kuntsche, J., et al., *Temoporfin-loaded liposomes: physicochemical characterization.* Eur J Pharm Sci, 2010. **40**(4): p. 305-15.
46. Nutrients, L.-s., *Liposomal Nano-Spheres™.* 2011.
47. Buchholz, J., et al., *Optimizing photodynamic therapy: in vivo pharmacokinetics of liposomal meta-(tetrahydroxyphenyl)chlorin in feline squamous cell carcinoma.* Clin Cancer Res, 2005. **11**(20): p. 7538-44.
48. Bovis, M.J., et al., *Improved in vivo delivery of m-THPC via pegylated liposomes for use in photodynamic therapy.* J Control Release, 2011.
49. Bonnett, R., Paul Charlesworth, Birgul D. Djelal, Sarah Foley, D. J. McGarvey and T. George Truscott *Photophysical properties of 5,10,15,20-tetrakis(m-hydroxyphenyl)porphyrin (m-THPP), 5,10,15,20-tetrakis(m-hydroxyphenyl)chlorin (m-THPC) and 5,10,15,20-tetrakis(m-hydroxyphenyl)bacteriochlorin (m-THPBC): a comparative study.* J. Chem. Soc., , 1998. **Perkin Trans. 2,** : p. 325-328.
50. Kubler, A.C., et al., *Photodynamic therapy of primary nonmelanomatous skin tumours of the head and neck.* Lasers Surg Med, 1999. **25**(1): p. 60-8.
51. Lassalle, H.P., et al., *Correlation between in vivo pharmacokinetics, intratumoral distribution and photodynamic efficiency of liposomal mTHPC.* J Control Release, 2009. **134**(2): p. 118-24.
52. Kiesslich, T., et al., *Comparative characterization of the efficiency and cellular pharmacokinetics of Foscan- and Foslip-based photodynamic treatment in human biliary tract cancer cell lines.* Photochem Photobiol Sci, 2007. **6**(6): p. 619-27.
53. Kiesslich, T., et al., *Uptake and phototoxicity of meso-tetrahydroxyphenyl chlorine are highly variable in human biliary tract cancer cell lines and correlate with markers of differentiation and proliferation.* Photochem Photobiol Sci, 2010. **9**(5): p. 734-43.
54. Gyenge, E.B., et al., *Cellular and molecular effects of the liposomal mTHPC derivative Foslipos in prostate carcinoma cells in vitro.* Photodiagnosis Photodyn Ther, 2011. **8**(2): p. 86-96.
55. WHO, *Cancer.* WHO, 2011.
56. Jemal, A., et al., *Global cancer statistics.* CA Cancer J Clin, 2011. **61**(2): p. 69-90.
57. GLOBOCAN, *GLOBOCAN 2008 World.* 2011.
58. Hanahan, D. and R.A. Weinberg, *Hallmarks of cancer: the next generation.* Cell, 2011. **144**(5): p. 646-74.
59. Haas, G.P. and W.A. Sakr, *Epidemiology of prostate cancer.* CA Cancer J Clin, 1997. **47**(5): p. 273-87.
60. Dunn, M.W. and M.W. Kazer, *Prostate cancer overview.* Semin Oncol Nurs, 2011. **27**(4): p. 241-50.
61. Tobias, J.S., *Cancer of the head and neck.* Bmj, 1994. **308**(6934): p. 961-6.
62. Amir, Z., et al., *Diagnostic delays in head and neck cancers.* Eur J Cancer Care (Engl), 1999. **8**(4): p. 198-203.
63. Hunter, K.D., E.K. Parkinson, and P.R. Harrison, *Profiling early head and neck cancer.* Nat Rev Cancer, 2005. **5**(2): p. 127-35.
64. Bosetti, C., et al., *High constant incidence rates of second primary cancers of the head and neck: a pooled analysis of 13 cancer registries.* Int J Cancer, 2010. **129**(1): p. 173-9.

65. Zigon, G., et al., *Prognoses for head and neck cancers in Europe diagnosed in 1995-1999: a population-based study.* Ann Oncol, 2010. **22**(1): p. 165-74.
66. Licitra, L., et al., *Human papillomavirus in HNSCC: a European epidemiologic perspective.* Hematol Oncol Clin North Am, 2008. **22**(6): p. 1143-53, vii-viii.
67. Marur, S. and A.A. Forastiere, *Head and neck cancer: changing epidemiology, diagnosis, and treatment.* Mayo Clin Proc, 2008. **83**(4): p. 489-501.
68. Vermorken, J.B. and P. Specenier, *Optimal treatment for recurrent/metastatic head and neck cancer.* Ann Oncol, 2010. **21 Suppl 7**: p. vii252-61.
69. Berrino, F. and G. Gatta, *Variation in survival of patients with head and neck cancer in Europe by the site of origin of the tumours. EUROCARE Working Group.* Eur J Cancer, 1998. **34**(14 Spec No): p. 2154-61.
70. Conway, D.I., et al., *Socioeconomic factors associated with risk of upper aerodigestive tract cancer in Europe.* Eur J Cancer, 2009. **46**(3): p. 588-98.
71. Conway, D.I., et al., *Components of socioeconomic risk associated with head and neck cancer: a population-based case-control study in Scotland.* Br J Oral Maxillofac Surg. **48**(1): p. 11-7.
72. Kaighn, M.E., et al., *Establishment and characterization of a human prostatic carcinoma cell line (PC-3).* Invest Urol, 1979. **17**(1): p. 16-23.
73. Mandic, R., et al., *Reduced cisplatin sensitivity of head and neck squamous cell carcinoma cell lines correlates with mutations affecting the COOH-terminal nuclear localization signal of p53.* Clin Cancer Res, 2005. **11**(19 Pt 1): p. 6845-52.

2

PDT EFFECTS ON PC-3 CELL LINE

2. Cellular and molecular effect of the liposomal mTHPC derivate Foslipos in prostate carcinoma cells in vitro

The contributions of Emina Besic Gyenge to the study: „Cellular and molecular effect of the liposomal mTHPC derivate Foslipos® in prostate carcinoma cells in vitro" were the following:

1. Cell culturing

2. Time dependent uptake of Foslipos® experiment and collection of microscopic data, in particular **figure 2**

3. Cell treatments with Foslipos® and subsequent RNA and DNA extractions

4. Measurements of RNA quantity and quality, in particular **figure 5** (RNA content in µg per 100'00 cells after incubation) and **figure 6** (RNA integrity measurements)

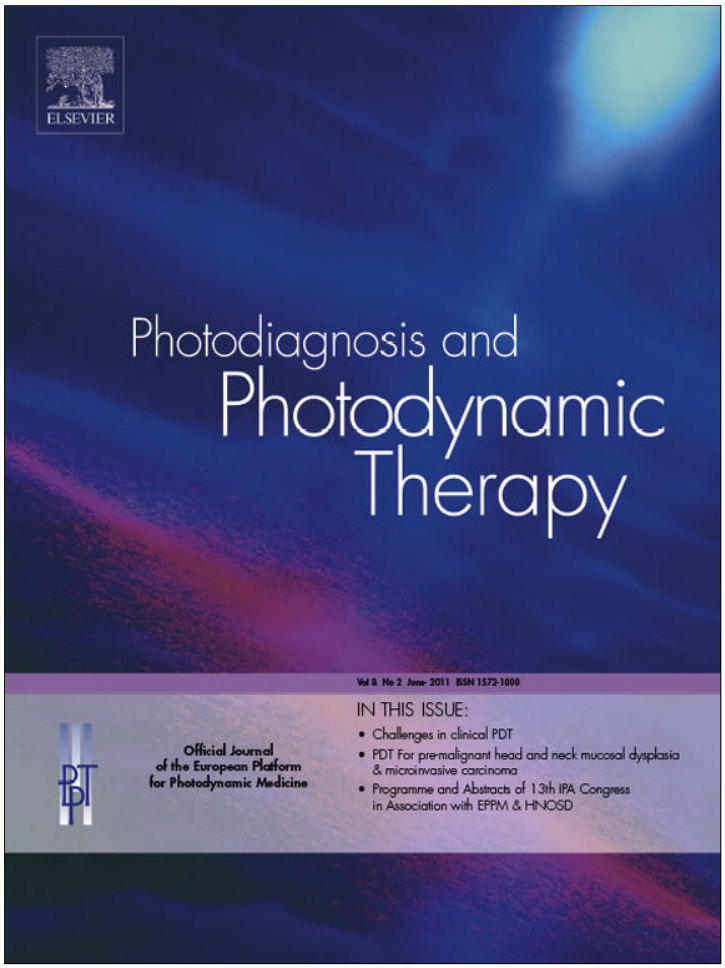

Photodiagnosis and Photodynamic Therapy (2011) 8, 86—96

available at www.sciencedirect.com

ScienceDirect

journal homepage: www.elsevier.com/locate/pdpdt

Cellular and molecular effects of the liposomal mTHPC derivative Foslipos in prostate carcinoma cells in vitro

Emina Besic Gyenge[a,1], Seraina Hiestand[a,1], Susanna Graefe[b], Heinrich Walt[c], Caroline Maake[a,*]

[a] *Institute of Anatomy, University of Zurich, Winterthurerstr. 190, 8057 Zurich, Switzerland*
[b] *biolitec AG, Otto-Schott-Straße 15, 07745 Jena, Germany*
[c] *Department of Cranio-Maxillo-Facial Surgery, University Hospital Zurich, Frauenklinikstr. 24, 8091 Zurich, Switzerland*

KEYWORDS
Photodynamic therapy;
Photosensitizer;
Cell line;
Prostate cancer;
Nucleic acids

Summary
Background: Meso-tetra-hydroxyphenyl-chlorine (mTHPC) is among the most powerful photosensitizers available for photodynamic therapy (PDT). However, the mechanisms leading to cell death are poorly understood. We here focused on changes at DNA and RNA levels after treatment with the liposomal mTHPC derivative Foslipos in vitro.
Methods: After determination of darktoxicity, laser conditions and uptake kinetics, PC-3 prostate carcinoma cells were subjected to PDT with Foslipos, followed by assessment of cell numbers directly (TP0) or 1 h (TP1), 2 h (TP2), 5 h (TP5) and 24 h (TP24) after illumination. Nucleic acids had been extracted for evaluation of RNA amounts and integrity as well as for estimation of abasic sites as a measure for DNA damage. Furthermore, expression changes of 84 genes related to oxidative stress were investigated by quantitative polymerase chain reaction.
Results: Already at TP0, the number of dead cells was significantly higher after PDT versus controls and at TP24 more than 90% of cells had been destroyed. PDT resulted in a severe damage of both RNA and DNA. Gene expression analyses revealed an impact of PDT on pathways for oxidative and metabolic stress, heat shock, proliferation and carcinogenesis, growth arrest, inflammation, DNA repair and apoptosis signaling.
Conclusions: Mechanisms of Foslipos-mediated PDT comprise a combination of acute and delayed lethal effects in PC-3 cells. The latter may include death processes initiated by nucleic acid damage, activation of stress and growth arrest genes in combination with a reduced capability to adequately cope with oxidative toxicity. Our results will help to better understand molecular photodynamic effects.

Introduction

Currently, one of the most powerful second-generation photosensitizers available for photodynamic therapy (PDT) is meso-tetra-hydroxyphenyl-chlorine (mTHPC, Temoporfin), a

* Corresponding author. Tel.: +41 44 6355338; fax: +41 44 6355702.
E-mail address: cmaake@anatom.uzh.ch (C. Maake).
[1] These authors contributed equally to this work.

1572-1000/$ — see front matter © 2011 Elsevier B.V. All rights reserved.
doi:10.1016/j.pdpdt.2011.02.001

member of the chlorine family of photosensitizers. The commercial product Foscan gained approval in the EC for palliative PDT treatment of patients with recurrent or refractory head and neck cancers, but it is also under investigation as a promising therapeutic modality for early cancers of the head and neck region, colon adenocarcinoma, non-melanotic skin tumors, pleural mesothelioma, pancreas cancer, hepatoma, carcinoma in situ of the vulva, malignant brain tumors, ovarian neoplasms, and organ confined prostate cancer [1,2].

However, Foscan is highly hydrophobic and thus requires the use of organic solvents like alcohols, acetone or ethyl acetate. After intravenous injection in patients, mTHPC molecules tend to aggregate and display very complex biokinetics, such as, e.g. a series of subsequent concentration maxima in plasma or limitations in transportation and tumor-uptake [3,4]. In recent years, these clinically unfavorable characteristics prompted the development of new derivatives of Temoporfin, including the liposomal formulations Foslip and Fospeg (the latter being PEGylated). In addition to the advantage of solvency in hydrophilic media, in first in vivo and in vitro studies liposome-incorporated mTHPC had been shown to accumulate faster, selectively and with higher fluorescence in tumor tissues [5—8].

The cell death pathways evoked by oxidative damage in mTHPC-mediated PDT are far from being clear and appear to depend not only on cell type investigated but also on PDT protocol. It had been reported that apoptotic pathways may be initiated [9—12], however, autophagy or necrosis [13] may prevail — especially if high PDT doses are applied [14]. To date only a limited number of studies are available that focus on the spectrum of signaling pathways affected in the course of mTHPC-mediated PDT. Apparently, effects may not only include activation of caspase cascades [10,11] but also acute-phase response processes [15], and expression changes of heat-shock proteins [16], hypoxia-markers [17], matrix metalloproteinases [18] or cytokines [19]. Since some of these cellular responses may modify, delay or even counteract cell death mechanisms, detailed analyses are highly needed.

With the aim to elucidate pathways leading to and/or interfering with cell death in PDT procedures with liposomal mTHPC we here focus on changes at the DNA and RNA level, as well as on gene expression profiles, using the established prostate carcinoma cell line PC-3 as model system.

Material and methods

Cell line and reagents

The androgen-independent human prostate carcinoma cell line PC-3 was obtained from the European Collection of Cell Cultures (ECACC). Cells were grown in DMEM+ (1:1 mixture of DMEM and Ham's F-12, without phenol red indicator and pyridoxal HCl, supplemented with 10% fetal calf serum and 1% Penicillin-Streptomycin, 10,000 UI/ml, all purchased from Gibco, Basel, Switzerland) at 37 °C and 5% CO_2 in a humid environment. Cells were passaged by trypsinization using 1× trypsin/EDTA (Invitrogen, Basel, Switzerland). As photosensitizer, we used mTHPC encapsulated into dipalmitoylphosphatidylcholine/dipalmitoylphosphatidylglycerol (DPPC/DPPG) liposomes (Foslipos, Biolitec AG, Jena, Germany). Concentration of mTHPC in liposomes was 1.5 mg/ml. Unless otherwise stated, chemicals were purchased from Sigma, Buchs, Switzerland.

Dark toxicity assay

PC-3 cells were plated at a density of 1000 cells per 60 mm Petri dish and allowed to attach for 24 h. Thereafter, Foslipos was added to end concentrations of 0.1, 0.5, 1.0, 5.0, and 10.0 μg/ml, respectively, and incubated for 5 h. Then a colony forming assay was performed as described earlier [20]. Briefly, after treatment, cells were washed with PBS and fresh DMEM+ was added. Cells were cultured for another 10 days and colonies were fixed, stained with azur-methylenblue-Giemsa and counted, whereby only colonies containing ≥50 cells were considered. Controls were run under the same conditions, while Foslipos was omitted.

Selection of laser intensity

PC-3 cells were processed as for the dark toxicity assay described above with the exception that cells were exposed to laser light after the 5 h incubation period with Foslipos. Laser intensities of 1, 3, and 5 J/cm^2, respectively, were applied, using a diode laser (Applied Optronics Corporation, USA) at 652 nm and a powermeter (Lightwave OMM6810B, GMP, Renens, Switzerland). After irradiation, colony forming assays were carried out as described above.

Confocal laser scanning microscopy

PC-3 cells grown on cover slips were incubated with 5 μg/ml Foslipos for 15 min, and 1, 2, 3, 4, and 5 h, respectively. After a buffer wash, cells were fixed with 4% buffered paraformaldehyde, again washed, coverslipped with Glycergel (Dako, Baar, Switzerland) and analyzed with a confocal laser scanning microscope (SP2, Leica Microsystems, Heerbrugg, Switzerland), using an excitation wavelength of 488 nm and detection wavelengths of 580—660 nm.

Cell culture treatment

PC-3 cells were plated on 60 mm Petri dishes at a density of 1×10^6, allowed to recover for 24 h and treated with Foslipos for 5 h at an end concentration of 5 μg/ml. Cells were then exposed to 652 nm laser light reaching a dose of 1 J/cm^2. This experimental setting was termed PDT. Three series of controls were included: (1) omission of the photosensitizer, i.e. replacement of the photosensitizer by buffer, but inclusion of irradiation (IRR), (2) omission of the irradiation and treatment with Foslipos (FOS) and (3) omission of both photosensitizer and irradiation (CO).

After washing all samples with PBS, fresh DMEM+ medium was added and the dishes were placed back in the incubator. Experiments were stopped immediately (i.e. after about 3—4 min) or after 1, 2, 5, and 24 h, respectively, by 2 × 3 min washing and 5 min trypsinization. These five time points are referred to as TP0, TP1, TP2, TP5 and TP24. After centrifu-

gation at 1000 rpm for 5 min, cell pellets were resuspended in 1 ml PBS and either directly used for cell counting or frozen for later nucleic acid analyses.

Cell survival test

Resuspended cells (10 μl) from experimental settings described in ''cell culture treatment'' were mixed with equal volumes of trypan blue solution (0.5%, Serva, Buchs, Switzerland) and cells (dead and alive) were immediately counted in a Neubauer chamber.

Nucleic acid extractions and quality analyses

From the remainder of resuspended cells (i.e. 990 μl), genomic DNA and total RNA was extracted with the NucleoSpin RNA II kit in conjunction with the NucleoSpin RNA/DNA buffer set (Macherey-Nagel, Oensingen, Switzerland), following the protocol of the manufacturer. The kit allows for a sequential elution of DNA and RNA from the same cell lysate using a silica membrane filter column and a set of predesigned buffers. Final elution volumes per sample for genomic DNA and total RNA were 100 μl and 60 μl, respectively. Nucleic acid concentrations were determined with a Nanodrop spectrophotometer (ND-1000, Wilmington, DE).

RNA quality was assessed by means of the Agilent 2100 Bioanalyzer equipped with the RNA integrity number (RIN) software algorithm (Agilent, Waldbronn, Germany). For this purpose, total RNA was assayed with the Eukaryote total RNA Nano LabChip kit (Agilent) according to the manufacturer's instructions.

DNA quality was determined with the DNA Damage Quantification kit (MBL, Woburn, MA) that measures the number of apurinic/apyrimidinic sites in DNA lesions. Following the recommendations of the manufacturer, genomic DNA was diluted to 100 μg/ml and labelled with the biotinylated aldehyde reactive probe provided with the kit. Tagged DNA and a tagged standard (provided with the kit) were then bound to a 96-well microplate, followed by an avidin—biotin assay and colorimetric detection at $O.D_{460\,nm}$. The number of abasic sites within the genomic DNA was determined by comparison with the standard curve.

Gene expression analyses

For gene expression analyses, the PAHS-003 RT^2 Profiler PCR array system was performed according to instructions of the manufacturer (Human stress and toxicity pathways finder array, SuperArray, Frederick, MD). Briefly, 0.5 μg total RNA each from samples TP1 (PDT and CO) and TP5 (PDT and CO) were reverse transcribed with the RT^2 First Strand kit (SuperArray). Resulting cDNA was subjected to quantitative PCR (qPCR) on an ABI 7500 sequence detection system (Applied Biosystems, Rotkreuz, Switzerland) using the supplied 96-well plate format with pre-dispensed specific primer sets and the RT^2 SYBR green/ROX qPCR master mix (SuperArray). Cycling parameters were as follows: 1 cycle for 10 min at 95 °C and 40 cycles of 15 sec at 95 °C and 1 min at 60 °C. Both threshold and baseline values were automatically obtained by the SDS software (Applied Biosystems) and CTs for all wells were exported to the company's data analysis web tool (www. superarray.com).

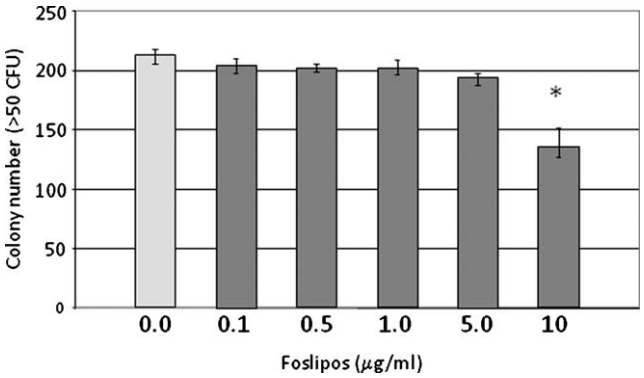

Figure 1 Dark toxicity in PC-3 cells: results of colony forming assays after incubation without or with 0.1—10 mg/ml Foslipos. * $p > 0.05\%$.

Statistical analyses

All experiments were carried out in triplicate. Statistical analyses were performed with the StatView software (www.statview.com). All possible pairwise differences between time points as well as between experimental conditions were examined by Fisher's Protected Least Significant Difference (PLSD) tests. *p*-Values less than 0.05 were considered significant.

Results

Experimental conditions

With the aim to establish the appropriate experimental conditions, we first determined the maximal non-dark-toxic concentration of Foslipos. We found that colony numbers after treatment with 10 μg/ml Foslipos were significantly lower compared to untreated controls ($p < 0.0001$), while all other concentrations of Foslipos used showed no statistically significant effects compared to controls (Fig. 1). We thus decided to perform further experiments with 5 μg/ml Foslipos end concentration in the medium. We next investigated the conditions of light exposure with minimal lethal effect at 5 μg/ml Foslipos. 1 J/cm^2 showed the lowest phototoxic effect (data not shown) and was thus choosen for our further study.

Microscopy

Cellular uptake kinetics of Foslipos in PC-3 cells were evaluated on the basis of its intracellular fluorescence (Fig. 2). Already after 15 min, a weak signal was detectable within cells. The fluorescence intensity increased steadily over time, reaching a maximum at 4 h. It was always diffusely distributed throughout the cytoplasm, with a tendency for a higher signal accumulation in the vicinity of the nucleus. However, the nuclear compartment itself always remained non-fluorescent (Fig. 2).

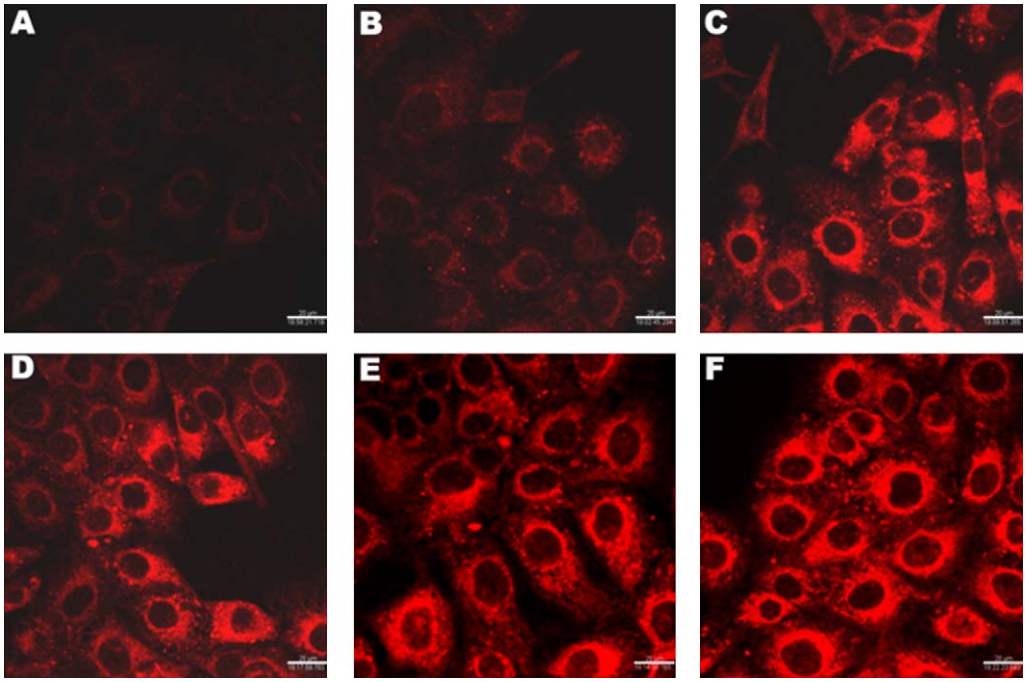

Figure 2 Uptake of Foslipos into PC-3 cells after (A) 15 min, (B) 1 h, (C) 2 h, (D) 3 h, (E) 4 h, and (F) 5 h incubation with photosensitizer. Confocal laser scanning microscopy, bar denotes 20 μm.

PDT-effects on cell death

As shown in Fig. 3, up from the earliest time point investigated (TP0), PDT samples contained statistically significant more dead cells than untreated controls ($p = 0.0002$), with a death of about 43% of cells compared to CO. The number of dead cells in PDT samples, however, remained constant up to TP5, while in the TP24-samples this parameter significantly rose ($p < 0.0001$) compared to time points before. At TP24, PDT samples contained only 9% of living cells found in CO. The number of dead cells in IRR and FOS was uniformly low and not statistically different from CO at all time points investigated.

Effects on nucleic acid quantity and integrity

Genomic DNA damage was estimated by measuring the amount of apurinic/apyrimidinic sites — a marker for oxidative stress (Fig. 4). We found that at all time points measured (TP0, TP1, TP24), the degree of oxidative DNA damage was significantly higher in PDT-treated cells compared to CO samples (TP0, $p < 0.0001$; TP1, $p < 0.0001$; TP24, $p < 0.0001$). DNA quality was also impaired in FOS and IRR samples (compared to CO), however, the difference between PDT and FOS or IRR was still statistically significant at all time points measured (in all cases: $p < 0.0001$). Generally, DNA damage of PDT-treated cells was always high, corresponding to an average of 22 abasic sites per 10^5 base pairs at TP0, 18 sites per 10^5 base pairs at TP1 and 16 sites per 10^5 base pairs at TP24.

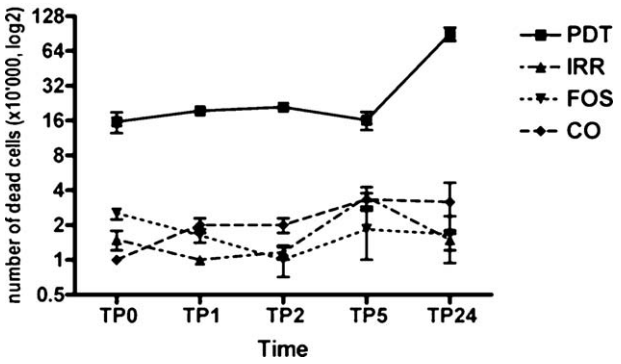

Figure 3 Effect of PDT with Foslipos on cell death: direct counts after trypan blue staining directly (TP0) and 1 h (TP1), 2 h (TP2), 5 h (TP5) and 24 h (TP24) after light application. CO: no treatment, IRR: with light application, FOS: with incubation of Foslipos.

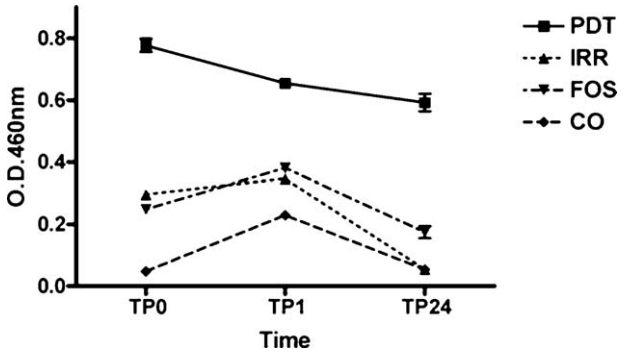

Figure 4 Estimation of DNA lesions: binding of an aldehyde reactive probe to DNA after PDT with Foslipos directly (TP0), 1 h (TP1) and 24 h (TP24) after light application. CO: no treatment, IRR: with light application, FOS: with incubation of Foslipos. Measurements in arbitrary units at $O.D_{460\,nm}$

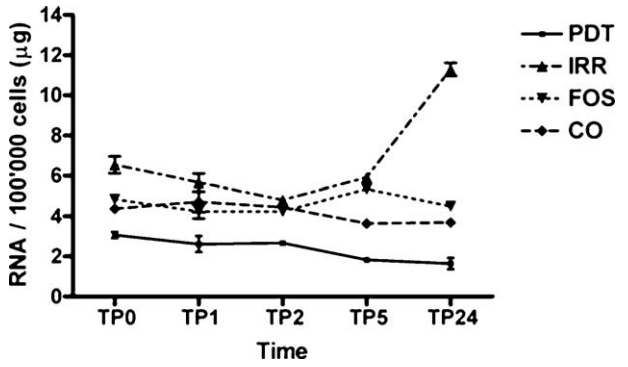

Figure 5 RNA content in µg per 100,000 cells after incubation with Foslipos directly (TP0) and 1 h (TP1), 2 h (TP2), 5 h (TP5) and 24 h (TP24) after light application (PDT). CO: no treatment, IRR: with light application, FOS: with incubation of Foslipos.

At all time points investigated, absolute amounts of total RNA in PDT samples were significantly lower than in CO samples. Being stable until (and including) TP2, RNA amounts in PDT samples significantly decreased at TP5, followed by an additional drop at TP24 ($p = 0.0009$ and 0.0097, respectively). FOS samples contained RNA amounts comparable to those of CO samples, while IRR samples had a significantly higher RNA content up from TP1 compared to CO. In all control reactions, significant increases in total RNA amounts were found between TP5 and TP24 (IRR: $p < 0.0001$; FOS: $p = 0.009$; CO: $p = 0.0065$). When expressed as a ratio of RNA per (living) cell, RNA content per PDT-treated cell was significantly lower compared to CO from TP0 on ($p = 0.0248$), but then remained unchanged over all time points investigated (Fig. 5). In CO and FOS the ratio of RNA per cell was comparable and remained constant over time, while IRR samples had significantly more RNA per cell at TP5 compared to CO ($p < 0.0001$, Fig. 5).

In contrast to all controls, RNA quality was clearly affected by PDT treatment. A small, but statistically significant RNA degradation was already seen at TP0, while RNA integrity was completely maintained under all control conditions (RNA integrity number, RIN, of CO versus PDT: $p = 0.0022$; IRR versus PDT: $p = 0.001$; FOS versus PDT: $p = 0.001$). In plus, RNA continued to significantly deteriorate over time after PDT, being significantly worse compared to controls at all time points measured (Fig. 6).

Effects on gene expression profiles

With the aim to further characterize the effects of Foslipos-mediated PDT, we investigated the expression of 84 genes involved in stress and toxicity pathways by qPCR at TP1 and TP5. Taken together, we found that roughly 57% of all genes investigated changed at least two-fold in expression after PDT. Of these, the majority showed reduced transcript numbers at TP1 (about 83%). Over time, most of the regulated genes (about 54%) maintained their initially changed expression levels. However, at TP5 versus TP1, about 23% had been further downregulated (HSPA4, CCNC, CCND1, E2F1, NFKB1, ATM, DDB1, BCL2L1, CASP8, CASP10, FASLG), about 12% displayed an further upregulation (CRYAB, DNAJB4, HSPA1A, HSPA1L, HSPA6), and about 10% showed

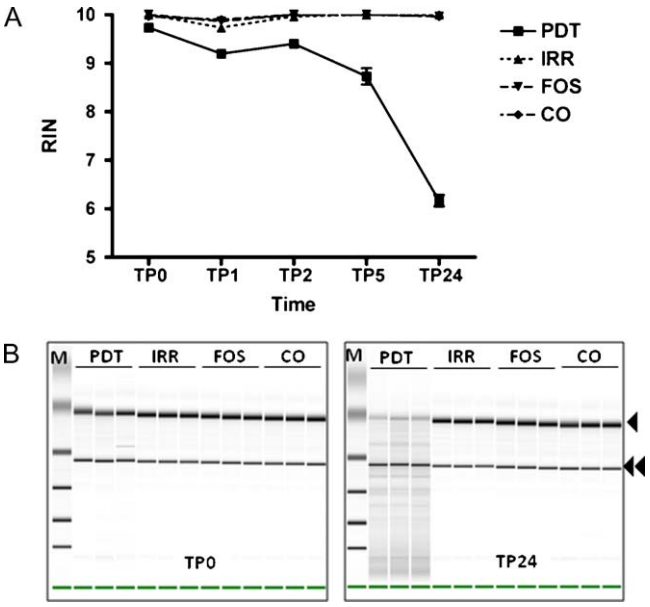

Figure 6 (A) Effect of Foslipos-mediated PDT on RNA integrity directly (TP0) and 1 h (TP1), 2 h (TP2), 5 h (TP5) and 24 h (TP24) after light application (PDT). CO: no treatment, IRR: with light application, FOS: with incubation of Foslipos. Calculation of the RNA integrity number (RIN), where 10 is intact and 1 is disintegrated. (B) Virtual electrophoresis of total RNA after PDT with Foslipos directly after illumination (TP0) and 24 h after light application (TP24). CO: no treatment, IRR: with light application, FOS: with incubation of Foslipos, M: molecular weight marker. Arrow and double arrow denote 28S rRNA and 18S rRNA, respectively.

signs of recovery (GSTM3, HSPA2, ERCC3, RAD50, TNFRSF1A, TNFSF10). Tables 1—7 summarize those genes whose expression changed more than twofold between CO versus PDT and/or over time.

In addition, we found that the following genes are expressed in PC-3 but do not appear to be regulated after PDT: CYP2E1, GPX1, MT2A, PRDX1, DNAJA1, HSF1, HSPA8, HSPB1, HSP90AA2, HSPH1, MIF, GADD45A, GDF15, TP53, CSF2, IL1A, IL6, SERPINE1, CHEK2, ANXA5, and NFKBIA. Genes not expressed in PC-3 cells (neither CO nor PDT) comprise: CRP1A1, CYP7A1, EGR1, EPHX2, FMO1, PTGS1, CCL3, CCL4, CCL21, CXCL10, NOS2A, UGT1A4, CASP1, LTA, and TNF. All gene names are designated according to the HUGO gene name nomenclature (www.genenames.org).

Discussion

Several new strategies are currently under development aiming to improve the efficiency and specificity of PDT. In this context, liposomal photosensitizer preparations are of interest mainly for two reasons: on the one hand they may serve as useful carriers for hydrophobic photoactive molecules in biosystems and on the other hand, they may possess a high payload for targeting molecules. Among others, the photosensitizer mTHPC had been incorporated into different types of liposomes and successfully applied in PDT protocols in vitro and in vivo [5,6,8,21—24]. However, the lack of information on molecular effects prompted us to

Table 1 List of genes involved in oxidative or metabolic stress with expression levels altered at least 2-fold in samples subjected to Foslipos-mediated PDT versus untreated controls. TP1: 1 h after illumination, TP5: 5 h after illumination.

Gene symbol	Description	Pathway	Fold change TP1	Fold change TP5
CAT	Catalase	Oxidative or metabolic stress	−3.3	−3.5
CRYAB	Crystallin, alpha B	Oxidative or metabolic stress	+6.8	+42.8
FMO5	Flavin containing monooxygenase 5	Oxidative or metabolic stress	−5.5	−4.7
GSR	Glutathione reductase	Oxidative or metabolic stress	−4.8	−4.5
GSTM3	Glutathione S-transferase mu 3	Oxidative or metabolic stress	−3.0	−1.6
HMOX1	Heme oxygenase (decycling) 1	Oxidative or metabolic stress	+4.6	+3.2
POR	P450 (cytochrome) oxidoreductase	Oxidative or metabolic stress	−3.8	−4.7
PRDX2	Peroxiredoxin 2	Oxidative or metabolic stress	−2.6	−3.3
SOD1	Superoxide dismutase 1, soluble	Oxidative or metabolic stress	−2.2	−2.2
SOD2	Superoxide dismutase 2, mitochondrial	Oxidative or metabolic stress	−2.7	−3.4

Table 2 List of heat shock genes with expression levels altered at least 2-fold in samples subjected to Foslipos-mediated PDT versus untreated controls. TP1: 1 h after illumination, TP5: 5 h after illumination.

Gene symbol	Description	Pathway	Fold change TP1	Fold change TP5
DNAJB4	DnaJ (Hsp40) homolog, subfamily B, member 4	Heat shock	−1.4	+3.3
HSPA1A	Heat shock 70 kDa protein 1A	Heat shock	+6.5	+11.1
HSPA1L	Heat shock 70 kDa protein 1-like	Heat shock	−1.2	+7.2
HSPA2	Heat shock 70 kDa protein 2	Heat shock	−2.2	+1.3
HSPA4	Heat shock 70 kDa protein 4	Heat shock	−5.4	−7.5
HSPA5	Heat shock 70 kDa protein 5 (glucose-regulated protein, 78 kDa)	Heat shock	−5.6	−5.5
HSPA6	Heat shock 70 kDa protein 6 (HSP70B′)	Heat shock	+282.1	+1112.8
HSP90AB1	Heat shock protein 90 kDa alpha (cytosolic), class B member 1	Heat shock	−1.8	−2.2
HSPD1	Heat shock 60 kDa protein 1 (chaperonin)	Heat shock	−2.3	−1.7
HSPE1	Heat shock 10 kDa protein 1 (chaperonin 10)	Heat shock	−2.4	−2.1

Table 3 List of genes involved in proliferation and carcinogenesis with expression levels altered at least 2-fold in samples subjected to Foslipos-mediated PDT versus untreated controls. TP1: 1 h after illumination, TP5: 5 h after illumination.

Gene symbol	Description	Pathway	Fold change TP1	Fold change TP5
CCNC	Cyclin C	Proliferation and carcinogenesis	−3.0	−5.2
CCND1	Cyclin D1	Proliferation and carcinogenesis	−8.6	−15.0
CCNG1	Cyclin G1	Proliferation and carcinogenesis	−4.0	−5.1
E2F1	E2F transcription factor 1	Proliferation and carcinogenesis	−2.6	−6.6
PCNA	Proliferating cell nuclear antigen	Proliferation and carcinogenesis	−4.3	−6.1

Table 4 List of genes involved in growth arrest and senescence with expression levels altered at least 2-fold in samples subjected to Foslipos-mediated PDT versus untreated controls. TP1: 1 h after illumination, TP5: 5 h after illumination.

Gene symbol	Description	Pathway	Fold change TP1	Fold change TP5
CDKN1A	Cyclin-dependent kinase inhibitor 1A (p21, Cip1)	Growth arrest and senescence	−2.0	−2.1
DDIT3	DNA-damage-inducible transcript 3	Growth arrest and senescence	+10.3	+6.5
IGFBP6	Insulin-like growth factor binding protein 6	Growth arrest and senescence	−8.5	−7.6
MDM2	Mdm2 p53 binding protein homolog (mouse)	Growth arrest and senescence	−5.3	−3.5

Table 5 List of genes involved in inflammation with expression levels altered at least 2-fold in samples subjected to Foslipos-mediated PDT versus untreated controls. TP1: 1 h after illumination, TP5: 5 h after illumination.

Gene symbol	Description	Pathway	Fold change TP1	Fold change TP5
IL1B	Interleukin 1, beta	Inflammation	−2.1	−3.1
IL18	Interleukin 18 (interferon-gamma-inducing factor)	Inflammation	−3.0	−3.5
NFKB1	Nuclear factor of kappa light polypeptide gene enhancer in B-cells 1	Inflammation	−2.1	−3.6

Table 6 List of genes involved in DNA damage and repair with expression levels altered at least 2-fold in samples subjected to Foslipos-mediated PDT versus untreated controls. TP1: 1 h after illumination, TP5: 5 h after illumination.

Gene symbol	Description	Pathway	Fold change TP1	Fold change TP5
ATM	Ataxia telangiectasia mutated	DNA damage and repair	−4.0	−6.7
DDB1	Damage-specific DNA binding protein 1, 127 kDa	DNA damage and repair	−2.7	−4.9
ERCC1	Excision repair cross-complementing rodent repair deficiency, compl. group 1	DNA damage and repair	−3.6	−3.5
ERCC3	Excision repair cross-complementing rodent repair deficiency, compl. group 3	DNA damage and repair	−7.2	−3.3
RAD23A	RAD23 homolog A (S. cerevisiae)	DNA damage and repair	−2.3	−2.7
RAD50	RAD50 homolog (S. cerevisiae)	DNA damage and repair	−12.6	−3.9
UNG	Uracil-DNA glycosylase	DNA damage and repair	−2.0	−3.4
XRCC1	X-ray repair complementing defective repair in Chinese hamster cells 1	DNA damage and repair	−2.3	−2.4
XRCC2	X-ray repair complementing defective repair in Chinese hamster cells 2	DNA damage and repair	−3.2	−4.0

explore cellular mechanisms in PDT with the DDPG/DDPC liposomal mTHPC derivative Foslipos, using the prostate carcinoma cell line PC-3 as model.

Our microscopic studies on the cellular uptake showed that Foslipos is quickly accumulating in the cytoplasm of PC-3 cells while always sparing the nucleus. We conclude that liposomal preparations do not affect the intracellular distribution since comparable patterns had been reported for mTHPC in a variety of human cell lines [25—27].

As shown before for PC-3-grafted mice [28], PC-3 cells are highly responsive for mTHPC-mediated PDT. Under our experimental conditions we repetitively observed an over 90% reduced cell count 24 h after PDT with Foslipos compared to untreated controls. However, the kinetics of this reaction were not linear but rather characterized by a two-step process with an initial death of cells, being already significant a few minutes after light application in PDT (i.e. at TP0) and a second — stronger — boost occurring more than 5 h later. Likely, the first ''hit'' is due to direct detrimental actions of short-lived reactive oxygen species (ROS), that are known to be generated in fractions of seconds after PDT and apparently kill a portion of cells immediately. However, the majority of cells seemed to be merely damaged by ROS and eventually undergo a death process that takes several

Table 7 List of genes involved in apoptosis signaling with expression levels altered at least 2-fold in samples subjected to Foslipos-mediated PDT versus untreated controls. TP1: 1 h after illumination, TP5: 5 h after illumination.

Gene symbol	Description	Pathway	Fold change TP1	Fold change TP5
BAX	BCL2-associated X protein	Apoptosis signaling	−2.5	−3.5
BCL2L1	BCL2-like 1	Apoptosis signaling	−4.1	−7.6
CASP8	Caspase 8, apoptosis-related cysteine peptidase	Apoptosis signaling	−2.0	−3.4
CASP10	Caspase 10, apoptosis-related cysteine peptidase	Apoptosis signaling	−2.5	−3.9
FASLG	Fas ligand (TNF superfamily, member 6)	Apoptosis signaling	−3.8	−4.5
TNFRSF1A	Tumor necrosis factor receptor superfamily, member 1A	Apoptosis signaling	−13.4	−6.4
TNFSF10	Tumor necrosis factor (ligand) superfamily, member 10	Apoptosis signaling	−28.0	−4.3

hours. Whether the latter is related to apoptosis was not within the scope of our experiments and will be the focus of further studies.

To investigate the mechanisms leading to the observed photodynamic effects in more detail we performed experiments to characterize damaging effects on nucleic acids. Results for DNA damage, RNA amount and integrity support our above observation of an acute PDT effect that can be documented already shortly after light application.

Since we were unable to localize photosensitizer fluorescence to the cell nucleus, it was surprising that directly after PDT a significant number of DNA strand breaks due to base loss were already detectable. Based on anisotropy imaging studies that showed a localization of mTHPC to the nuclear envelope [29], light activation may have lead to damage of this membrane compartment, allowing for an immediate ROS-related injury of (peripherally residing) DNA. However, results may also be explained by mechanisms similar to those observed in a murine glioma cell line, where mTHPC entered the nucleus during light application [30]. The profound and early DNA damage may account for instant cell destruction but — if not repaired — may also result in, e.g. blocked DNA replication eventually leading to initiation of death cascades. Notably, even within 24 h after PDT no recovery of the number of abasic sites (compared to TP1) was detected, indicating that no DNA repair had been initiated. At the RNA level these results are complemented by the observation that several important genes associated with DNA repair mechanisms had been transcriptionally downregulated or destroyed after PDT with Foslipos. These include the early DNA damage sensor ATM, DDB1, that is a subunit of the damage-specific DNA binding protein complex, the DNA excision repair endonucleases ERCC1 and ERCC3, the postreplication DNA repair genes RAD23A and RAD50, the uracil-DNA glycosylase UNG and the DNA double strand repair proteins XRCC1 and XRCC2. Furthermore, RNA for PCNA, that is involved in base-excision repair pathways, was reduced. However, low DNA repair capacities have dual effects: they confer a cytotoxicity favorable for PDT by triggering cell death but surviving cells are prone to mutations with unpredictable consequences. In worst case this may result in secondary malignancies after PDT. Our data are in accordance with those in murine gliobastoma cells where mTHPC-PDT also resulted in an immediate DNA damage, however, in this study and others activation of repair mechanisms after PDT had been reported [30—33]. Since our data are in contrast to in vitro studies in human myeloid leukaemia and nasopharyngeal carcinoma cells where no DNA damage was found after mTHPC-PDT [34,35], the observed effect may depend on cell line.

The significantly lower readings at TP0 of RNA content per cell after PDT versus all controls indicate that some RNA was initially destroyed, — presumably by an acute and direct effect of ROS on RNA and not by transcriptional regulation. Not unexpected, the major part of specific genes investigated here thus displayed lower transcript numbers after PDT. Since total RNA consists to 90—95% of ribosomal RNA (rRNA), our data may also point towards an impact of PDT on the translational machinery itself. Interestingly, illumination alone (IRR) lead to a significant increase of RNA amounts measured at TP24, so that actually an interaction of effects elicited by light on the one hand and ROS on the other hand may take place after PDT.

Our further RNA expression studies focusing on established genes involved in stress and toxicity indicated a very complex molecular response of PC-3 cells to mTHPC-mediated PDT, including both higher or lower transcript levels of genes with the potential to either support or counter-act PDT actions. While a higher gene expression is due to an upregulation, lower expression scores may be either a sign of PDT-related RNA destruction or of true downregulation. The latter may well be a consequence of the observed oxidative DNA damage after PDT. However, with regard to possible damage of rRNA in PDT it is far from clear whether upregulated transcripts are in fact translated into proteins.

Our study reveals reduced levels of genes involved in cellular defense mechanisms against oxidative and metabolic stress. PDT with other photosensitizers are partly in accordance [36,37] and partly in contrast to our data [38,39]. Because CAT and SOD1 have been shown to protect cells against phototoxic effects of hematophorphyrin derivative or ALA in vitro [40,41] and inhibition of SODs results in increased PDT effects [42], we hypothesize that the reduced ability of the cells to cope with oxidative and metabolic stress may constitute an important mechanism for PDT effects with Foslipos. However, as in other studies [43,44], we found that two antioxidant defense genes (CRYAB and HMOX1) were strongly upregulated. The small heat shock protein CRYAB and the heme oxygenase family member HMOX are known to act as anti-apoptotic molecules that protect cells against oxidative damage [45]. Together with the observation that inhibition of HMOX may increase the efficacy of PDT [44,46], we propose that — if translated — high levels of HMOX or CRYAB may eventually prevent optimal phototoxic effects.

Expression patterns of heat-shock proteins (HSPs) in our study turned out to be very complex. Several previous papers reported the induction of HSP60, HSP70 or HSP90 after PDT with various photosensitizers [47—52]. However, HSPs consist of large protein families and in our study we found that expression of members may be downregulated or upregulated after PDT with Foslipos. Upregulation of the HSP40 member DNAJB4 as well as HSP70 members HSPA1A, HSPA1L and especially HSPA6, that is only induced by severe stress-stimuli, may mirror the extent of damage in our model but also indicate the presence of a (partly) preserved stress-response system. On the other hand it should be noted that RNA levels of several HSP members investigated here are downregulated. Thus protective mechanisms by HSPs may be rather impaired after PDT with Foslipos. Notably, some of the downregulated HSP70 members belong to essential house keeping genes.

PDT with Foslipos may not only have direct destructive effects on cells but may also block proliferation and induce cell cycle arrest in survivors. Since cell damage is obviously so profound that repair mechanisms are not operative, death pathways are eventually activated. As reported in part previously [53—55], transcripts of cyclin family genes CCNC, CCND1 and CCNG1 as well as of PCNA, a protein crucial for DNA replication, were markedly reduced after PDT in our model thereby possibly leading to a diminished

proliferative activity. However, the observed downregulation of cyclin-interacting transcription factor E2F1 may also directly promote cell death, as reported previously for PC-3 cells [56]. The tumor suppressor p53 (TP53) is regarded as a key factor for the regulation of cell growth and death. Interestingly, we and others [57] found that PDT did not change the expression of this gene. However, the expression of one of the main targets of TP53, the cyclin-dependent kinase inhibitor CDKN1A, was reduced after PDT in our study, further supporting an impact of PDT on cell cycle processes. Our data are in contrast to PDT studies that report an increase in CDKN1A [58]. Since MDM2, an important inhibiting factor of p53, was reduced in our study, the ratio of MDM2 to TP53 apparently changed. This may be associated with the potential of increased p53-related pathways and/or reduced p53 degradation followed by cell cycle arrest and apoptosis. Furthermore, we found a strong upregulation of the bZIP transcription factor DDIT3 — notably independent of p53 — after PDT. Since DDIT3 had been implicated in anti-proliferative effects and the induction of apoptosis by certain anti-cancer agents, including in PC-3 cells [59], the observed high levels may have also contributed to growth arrest and apoptotic signaling in our experiment after PDT.

We here report a marked downregulation of IGFBP6 after PDT. Being a relatively specific inhibitor of IGF-II action, high levels of IGFBP-6 had been found to block proliferation and increase apoptosis in vitro, including in PC-3 cells [60,61].

In our study, genes involved in apoptosis signaling all displayed reduced transcript numbers. Most of these genes seem to be damaged early — probably due to direct ROS effects. TNFRSF1A, that binds CASP8, as well as both the apoptosis-inducing ligands TNFSF10 and FASLG are almost completely shut down already at TP1 in our model. The biological consequences of fewer apoptosis-promoting BAX in addition to fewer anti-apoptotic BCL2L1 transcripts in PDT with Foslipos are not clear yet. Of interest is the further reduction of CASP8 and CASP10 RNA over time that is suggestive of a PDT-driven regulatory process. Since many of cell death processes are more adequately investigated at the protein level our data do not generally exclude the activation of apoptotic pathways in Foslipos-mediated PDT. The results may rather be another sign of a breakdown in basic cellular functions.

Taken together, we propose that Foslipos-mediated PDT in PC-3 cells is characterized by a two-stage process. A significant number of cells is disintegrated within minutes, — a process that is likely driven by direct actions of ROS on vital biological components. Even in in vitro systems that ought to contain a homogeneous population of cells and that uniformly accumulate the photosensitizer, the majority of cells survive this attack. Of course we cannot exclude that this is due to our experimental set-up with, e.g. unequal illumination. However, initially surviving cells go into growth arrest and display signs of an oxidative stress response, while many transcripts whose proteins are known to contribute to cellular rescue mechanisms are reduced. Since this is in parallel to severe damages of genomic DNA and the translational system, cells are unable to recover and ultimately die after a delay of several hours.

Acknowledgements

The authors thank Franziska Rossi and Ingrid Briod for their excellent assistance with experiments. The work was supported by the EU FP7 EuroNanoMed ERA-NET grant ''TARGET-PDT''.

References

[1] Allison RR, Bagnato VS, Sibata CH. Future of oncologic photodynamic therapy. Future Oncol 2010;6:929—40.
[2] Brown SB, Brown EA, Walker I. The present and future role of photodynamic therapy in cancer treatment. Lancet Oncol 2004;5:497—508.
[3] Sasnouski S, Pic E, Dumas D, et al. Influence of incubation time and sensitizer localization on meta-tetra(hydroxyphenyl)chlorin (mTHPC)-induced photoinactivation of cells. Radiat Res 2007;168:209—17.
[4] Triesscheijn M, Ruevekamp M, Out R, et al. The pharmacokinetic behavior of the photosensitizer meso-tetrahydroxyphenyl-chlorin in mice and men. Cancer Chemother Pharmacol 2007;60:113—22.
[5] Buchholz J, Kaser-Hotz B, Khan T, et al. Optimizing photodynamic therapy: in vivo pharmacokinetics of liposomal meta-(tetrahydroxyphenyl)chlorin in feline squamous cell carcinoma. Clin Cancer Res 2005;11:7538—44.
[6] Svensson J, Johansson A, Grafe S, et al. Tumor selectivity at short times following systemic administration of a liposomal temoporfin formulation in a murine tumor model. Photochem Photobiol 2007;83:1211—9.
[7] Hansch A, Frey O, Gajda M, et al. Photodynamic treatment as a novel approach in the therapy of arthritic joints. Lasers Surg Med 2008;40:265—72.
[8] Lassalle HP, Dumas D, Grafe S, D'Hallewin MA, Guillemin F, Bezdetnaya L. Correlation between in vivo pharmacokinetics, intratumoral distribution and photodynamic efficiency of liposomal mTHPC. J Control Rel 2009;134:118—24.
[9] Kirveliene V, Sadauskaite A, Kadziauskas J, Sasnauskiene S, Juodka B. Correlation of death modes of photosensitized cells with intracellular ATP concentration. FEBS Lett 2003;553:167—72.
[10] Marchal S, Francois A, Dumas D, Guillemin F, Bezdetnaya L. Relationship between subcellular localisation of Foscan and caspase activation in photosensitised MCF-7 cells. Br J Cancer 2007;96:944—51.
[11] Bressenot A, Marchal S, Bezdetnaya L, Garrier J, Guillemin F, Plenat F. Assessment of apoptosis by immunohistochemistry to active caspase-3, active caspase-7, or cleaved PARP in monolayer cells and spheroid and subcutaneous xenografts of human carcinoma. J Histochem Cytochem 2009;57:289—300.
[12] Yow CM, Mak NK, Leung AW, Huang Z. Induction of early apoptosis in human nasopharyngeal carcinoma cells by mTHPC-mediated photocytotoxicity. Photodiagnosis Photodyn Ther 2009;6:122—7.
[13] Gharehbaghi K, Kubin A, Grusch M, et al. Photodynamic action of meta-tetrahydroxyphenylchlorin (mTHPC) on an ovarian cancer cell line. Anticancer Res 2000;20:2647—52.
[14] Sasnauskiene A, Kadziauskas J, Vezelyte N, Jonusiene V, Kirveliene V. Apoptosis, autophagy and cell cycle arrest following photodamage to mitochondrial interior. Apoptosis 2009;14:276—86.
[15] Merchant S, Sun J, Korbelik M. Dying cells program their expedient disposal: serum amyloid P component upregulation in vivo and in vitro induced by photodynamic therapy of cancer. Photochem Photobiol Sci 2007;6:1284—9.

[16] Mitra S, Goren EM, Frelinger JG, Foster TH. Activation of heat shock protein 70 promoter with meso-tetrahydroxyphenyl chlorin photodynamic therapy reported by green fluorescent protein in vitro and in vivo. Photochem Photobiol 2003;78:615—22.
[17] Schouwink H, Oppelaar H, Ruevekamp M, et al. Oxygen depletion during and after mTHPC-mediated photodynamic therapy in RIF1 and H-MESO1 tumors. Radiat Res 2003;159:190—8.
[18] Sharwani A, Jerjes W, Hopper C, et al. Photodynamic therapy down-regulates the invasion promoting factors in human oral cancer. Arch Oral Biol 2006;51:1104—11.
[19] Yom SS, Busch TM, Friedberg JS, et al. Elevated serum cytokine levels in mesothelioma patients who have undergone pleurectomy or extrapleural pneumonectomy and adjuvant intraoperative photodynamic therapy. Photochem Photobiol 2003;78:75—81.
[20] Muller S, Walt H, Dobler-Girdziunaite D, Fiedler D, Haller U. Enhanced photodynamic effects using fractionated laser light. J Photochem Photobiol B 1998;42:67—70.
[21] Bombelli C, Caracciolo G, Di Profio P, et al. Inclusion of a photosensitizer in liposomes formed by DMPC/gemini surfactant: correlation between physicochemical and biological features of the complexes. J Med Chem 2005;48:4882—91.
[22] Pegaz B, Debefve E, Ballini JP, et al. Photothrombic activity of m-THPC-loaded liposomal formulations: pre-clinical assessment on chick chorioallantoic membrane model. Eur J Pharm Sci 2006;28:134—40.
[23] D'Hallewin MA, Kochetkov D, Viry-Babel Y, et al. Photodynamic therapy with intratumoral administration of lipid-based mTHPC in a model of breast cancer recurrence. Lasers Surg Med 2008;40:543—9.
[24] Dragicevic-Curic N, Scheglmann D, Albrecht V, Fahr A. Temoporfin-loaded invasomes: development, characterization and in vitro skin penetration studies. J Control Rel 2008;127:59—69.
[25] Teiten MH, Bezdetnaya L, Merlin JL, et al. Effect of meta-tetra(hydroxyphenyl)chlorin (mTHPC)-mediated photodynamic therapy on sensitive and multidrug-resistant human breast cancer cells. J Photochem Photobiol B 2001;62:146—52.
[26] Leung WN, Sun X, Mak NK, Yow CM. Photodynamic effects of mTHPC on human colon adenocarcinoma cells: photocytotoxicity, subcellular localization and apoptosis. Photochem Photobiol 2002;75:406—11.
[27] Kiesslich T, Berlanda J, Plaetzer K, Krammer B, Berr F. Comparative characterization of the efficiency and cellular pharmacokinetics of Foscan- and Foslip-based photodynamic treatment in human biliary tract cancer cell lines. Photochem Photobiol Sci 2007;6:619—27.
[28] Sehgal I, Sibrian-Vazquez M, Vicente MG. Photoinduced cytotoxicity and biodistribution of prostate cancer cell-targeted porphyrins. J Med Chem 2008;51:6014—20.
[29] Foster TH, Pearson BD, Mitra S, Bigelow CE. Fluorescence anisotropy imaging reveals localization of meso-tetrahydroxyphenyl chlorin in the nuclear envelope. Photochem Photobiol 2005;81:1544—7.
[30] Rousset N, Keminon E, Eleouet S, et al. Use of alkaline Comet assay to assess DNA repair after m-THPC-PDT. J Photochem Photobiol B 2000;56:118—31.
[31] Ricci F, Pucci S, Sesti F, Missiroli F, Cerulli L, Spagnoli LG. Modulation of Ku70/80, clusterin/ApoJ isoforms and Bax expression in indocyanine-green-mediated photo-oxidative cell damage. Ophthalmic Res 2007;39:164—73.
[32] Yang ZZ, Li MX, Zhang YS, et al. Knock down of the dual functional protein apurinic/apyrimidinic endonuclease 1 enhances the killing effect of hematoporphrphyrin derivative-mediated photodynamic therapy on non-small cell lung cancer cells in vitro and in a xenograft model. Cancer Sci 2009.
[33] Akramiene D, Aleksandraviciene C, Grazeliene G, et al. Potentiating effect of beta-glucans on photodynamic therapy of implanted cancer cells in mice. Tohoku J Exp Med 2010;220:299—306.
[34] McNair FI, Marples B, West CM, Moore JV. A comet assay of DNA damage and repair in K562 cells after photodynamic therapy using haematoporphyrin derivative, methylene blue and meso-tetrahydroxyphenylchlorin. Br J Cancer 1997;75:1721—9.
[35] Yow CM, Chen JY, Mak NK, Cheung NH, Leung AW. Cellular uptake, subcellular localization and photodamaging effect of temoporfin (mTHPC) in nasopharyngeal carcinoma cells: comparison with hematoporphyrin derivative. Cancer Lett 2000;157:123—31.
[36] Du HY, Olivo M, Tan BK, Bay BH. Photoactivation of hypericin down-regulates glutathione S-transferase activity in nasopharyngeal cancer cells. Cancer Lett 2004;207:175—81.
[37] Luo J, Li L, Zhang Y, et al. Inactivation of primary antioxidant enzymes in mouse keratinocytes by photodynamically generated singlet oxygen. Antioxid Redox Signal 2006;8:1307—14.
[38] El-Missiry MA, Abou-Seif M. Photosensitization induced reactive oxygen species and oxidative damage in human erythrocytes. Cancer Lett 2000;158:155—63.
[39] Krusekopf S, Roots I. St. John's wort and its constituent hyperforin concordantly regulate expression of genes encoding enzymes involved in basic cellular pathways. Pharmacogenet Genomics 2005;15:817—29.
[40] Hirakawa K, Mori M, Yoshida M, Oikawa S, Kawanishi S. Photo-irradiated titanium dioxide catalyzes site specific DNA damage via generation of hydrogen peroxide. Free Radic Res 2004;38:439—47.
[41] Chekulayeva LV, Shevchuk IN, Chekulayev VA, Ilmarinen K. Hydrogen peroxide, superoxide, and hydroxyl radicals are involved in the phototoxic action of hematoporphyrin derivative against tumor cells. J Environ Pathol Toxicol Oncol 2006;25:51—77.
[42] Golab J, Nowis D, Skrzycki M, et al. Antitumor effects of photodynamic therapy are potentiated by 2-methoxyestradiol. A superoxide dismutase inhibitor. J Biol Chem 2003;278:407—14.
[43] Nowis D, Legat M, Grzela T, et al. Heme oxygenase-1 protects tumor cells against photodynamic therapy-mediated cytotoxicity. Oncogene 2006;25:3365—74.
[44] Frank J, Lornejad-Schafer MR, Schoffl H, Flaccus A, Lambert C, Biesalski HK. Inhibition of heme oxygenase-1 increases responsiveness of melanoma cells to ALA-based photodynamic therapy. Int J Oncol 2007;31:1539—45.
[45] Parcellier A, Schmitt E, Brunet M, Hammann A, Solary E, Garrido C. Small heat shock proteins HSP27 and alphaB-crystallin: cytoprotective and oncogenic functions. Antioxid Redox Signal 2005;7:404—13.
[46] Kocanova S, Buytaert E, Matroule JY, et al. Induction of heme-oxygenase 1 requires the p38MAPK and PI3K pathways and suppresses apoptotic cell death following hypericin-mediated photodynamic therapy. Apoptosis 2007;12:731—41.
[47] Hanlon JG, Adams K, Rainbow AJ, Gupta RS, Singh G. Induction of Hsp60 by photofrin-mediated photodynamic therapy. J Photochem Photobiol B 2001;64:55—61.
[48] Verwanger T, Sanovic R, Aberger F, Frischauf AM, Krammer B. Gene expression pattern following photodynamic treatment of the carcinoma cell line A-431 analysed by cDNA arrays. Int J Oncol 2002;21:1353—9.
[49] Jalili A, Makowski M, Switaj T, et al. Effective photoimmunotherapy of murine colon carcinoma induced by the combination of photodynamic therapy and dendritic cells. Clin Cancer Res 2004;10:4498—508.
[50] Kuzelova K, Grebenova D, Pluskalova M, Marinov I, Hrkal Z. Early apoptotic features of K562 cell death induced by 5-aminolaevulinic acid-based photodynamic therapy. J Photochem Photobiol B 2004;73:67—78.

[51] Yanase S, Nomura J, Matsumura Y, et al. Enhancement of the effect of 5-aminolevulinic acid-based photodynamic therapy by simultaneous hyperthermia. Int J Oncol 2005;27:193—201.
[52] Prasmickaite L, Cekaite L, Hellum M, Hovig E, Hogset A, Berg K. Transcriptome changes in a colon adenocarcinoma cell line in response to photochemical treatment as used in photochemical internalisation (PCI). FEBS Lett 2006;580:5739—46.
[53] Sugiyama M, Sakahara H, Sato K, et al. Evaluation of 3′-deoxy-3′-18F-fluorothymidine for monitoring tumor response to radiotherapy and photodynamic therapy in mice. J Nucl Med 2004;45:1754—8.
[54] Romanko YS, Tsyb AF, Kaplan MA, Popuchiev VV. Relationship between antitumor efficiency of photodynamic therapy with photoditasine and photoenergy density. Bull Exp Biol Med 2005;139:460—4.
[55] Togashi H, Uehara M, Ikeda H, Inokuchi T. Fractionated photodynamic therapy for a human oral squamous cell carcinoma xenograft. Oral Oncol 2006;42:526—32.
[56] Park C, Lee I, Kang WK. Lovastatin-induced E2F-1 modulation and its effect on prostate cancer cell death. Carcinogenesis 2001;22:1727—31.
[57] Finlan LE, Kernohan NM, Thomson G, Beattie PE, Hupp TR, Ibbotson SH. Differential effects of 5-aminolaevulinic acid photodynamic therapy and psoralen + ultraviolet A therapy on p53 phosphorylation in normal human skin in vivo. Br J Dermatol 2005;153:1001—10.
[58] Crescenzi E, Varriale L, Iovino M, Chiaviello A, Veneziani BM, Palumbo G. Photodynamic therapy with indocyanine green complements and enhances low-dose cisplatin cytotoxicity in MCF-7 breast cancer cells. Mol Cancer Ther 2004;3:537—44.
[59] Lu M, Xia L, Hua H, Jing Y. Acetyl-keto-beta-boswellic acid induces apoptosis through a death receptor 5-mediated pathway in prostate cancer cells. Cancer Res 2008;68:1180—6.
[60] Bach LA. IGFBP-6 five years on; not so 'forgotten'? Growth Horm IGF Res 2005;15:185—92.
[61] Koike H, Ito K, Takezawa Y, Oyama T, Yamanaka H, Suzuki K. Insulin-like growth factor binding protein-6 inhibits prostate cancer cell proliferation: implication for anticancer effect of diethylstilbestrol in hormone refractory prostate cancer. Br J Cancer 2005;92:1538—44.

3

PHOTOSENSITIZER EFFECTS ON HNSCC CELL LINES IN THE DARK

3. Effects of Hypericin and a Chlorin Based Photosensitizer alone or in Combination in Squamous Cell Carcinoma Cells in the Dark

The following manuscript is accepted in *Photodiagnosis and Photodynamic Therapy* Journal.

The contributions of Emina Besic Gyenge to the study: „Dark Activity of Hypericin and a Chlorine Based Photosensitizer alone or in Combination in Squamous Cell Carcinoma Cells" were the following:

1. Cell culturing

2. Proliferation assay experiment in **UMB-SCC 969** cell line **figure 1**

3. Intracellular accumulation of photosensitizers in **UMB-SCC 969** cell line, in particular: **figure 2.1** (confocal imaging of time dependent accumulation of hypericin, Foslipos® and their 1:1 mixture) and **figure 2.2** (fluorescence measurements of time dependent accumulation of hypericin, Foslipos® and their 1:1 mixture)and **figure 3.1** (confocal imaging of time dependent elimination of hypericin, Foslipos® and their 1:1 mixture)and figure 3.2 (fluorescent measurements of time dependent elimination of hypericin, Foslipos® and their 1:1 mixture)

4. Photosensitizer localisation experiments and confocal imaging in **UMB-SCC 969** cell line **figure 4**

5. RNA extraction and RNA integrity number measurements **figure 5** (for both cell lines)

6. DNA damage (comet assays) for UMB-SCC 969 cell line **figure 6**

Photodiagnosis and Photodynamic Therapy (2012) xxx, xxx–xxx

Available online at www.sciencedirect.com

SciVerse ScienceDirect

journal homepage: www.elsevier.com/locate/pdpdt

Effects of hypericin and a chlorin based photosensitizer alone or in combination in squamous cell carcinoma cells in the dark

Emina Besic Gyenge Dr Sc. Nat.[a,*,1], Patrick Forny[a,1], Daniel Lüscher[a], Andrea Laass[a], Heinrich Walt[b], Caroline Maake[a]

[a] Institute of Anatomy, University of Zürich, Winterthurerstr. 190, CH-8057 Zürich, Switzerland
[b] Department of Cranio-Maxillofacial Surgery, University Hospital Zürich, Frauenklinikstr. 24, CH-8091 Zürich, Switzerland

KEYWORDS
Dark toxicity;
Photosensitizer;
Hypericin;
mTHPC;
Head and neck cancer;
Photodynamic therapy

Summary
Introduction: The toxic influence of photosensitizers in the dark is poorly investigated. In our study we used the photosensitizers liposomal meso-tetrahydroxyphenyl chlorin derivative (Foslipos®) and hypericin as well as their 1:1 combination on two different head and neck squamous cell carcinoma (HNSCC) cell lines (UMB-SCC 745 and UMB-SCC 969).
Materials and methods: We examined uptake, efflux and localization of the photosensitizers with confocal microscopy. Fluorescence quantification was measured with a micro-plate spectrometer. Special interest was given to effects on cell proliferation (BrdU proliferation assay), RNA quality (Bioanalyzer measurements) and DNA damage (comet assays) in the dark.
Results: Foslipos® uptake was linear over time and its efflux was not achieved even after 24 h while uptake of hypericin reached a plateau after 5 h and was almost eliminated after 24 h. Localization of Foslipos® was organelle-unspecific. Hypericin was found mainly at membranes and in trans-golgi network. Foslipos® treated cells showed cell toxicity for the highest concentration (10 μg/mL). In contrast, hypericin was toxic for all concentrations (10–0.6 μg/mL). The photosensitizer combination was non-toxic for all concentrations (10–0.6 μg/mL). No changes in RNA quality were monitored. Initial DNA damage was found only in hypericin treated UMB-SCC 745, which recovered after 3 h. No significant DNA damage was found for UMB-SCC 969.
Conclusion: Our data shows that the combinatorial application decrease photosensitizer toxicity, which can be advantageous in PDT treatments.

Introduction

Photodynamic therapy (PDT) has emerged as an alternative treatment modality for patients with head-and-neck squamous cell carcinoma (HNSCC) that may supplement or even replace conventional therapies such as surgery, radio- and/or chemotherapy [1,2]. As with other PDT

* Corresponding author. Fax: +41 446355702.
E-mail address: emina.besicgyenge@uzh.ch (E. Besic Gyenge).
[1] Contributed equally.

1572-1000/$ – see front matter © 2012 Elsevier B.V. All rights reserved.
http://dx.doi.org/10.1016/j.pdpdt.2012.03.006

applications, patients had been reported to benefit from the minimal invasiveness, the biocompatibility with other treatment modalities, the option for repeatability, the absence of serious side effects, the excellent cosmetic or functional outcome and the fast recovery [3,4].

Various first and second generation photosensitizers had been successfully explored for PDT of early primary, secondary and recurrent HNSCC with curative and palliative aims or as an intraoperative adjuvant, including porfimer sodium, haematoporphyrin derivative, talaporfin sodium, 5-aminolevulinic acid-induced protoporphyrin IX, meso-tetrahydroxyphenyl chlorin (mTHPC), chlorin e6 or hypericin [1,2].

In most cases the photosensitizer is administered systemically and shows a preferential accumulation in tumor cells compared to healthy tissue. The reason for the latter is only incompletely understood, but may be related to e.g. an impaired wall integrity of tumor-supplying vessels or changes in the metabolism of cancer cells leading to higher photosensitizer retention. However, the exposition by photosensitizers of somatic cells is considerable in such protocols and may eventually result in an uptake of the photosensitizer into various tissues of the body. Although PDT-mediated cell death only occurs in those photosensitizer-bearing cells that are illuminated with the appropriate wavelength, little is known about cellular and molecular responses that may occur after cellular interaction with photosensitizers in the dark.

Studies from our group indicated that PDT may be improved if a combination of photosensitizers is applied. We reported on a patient who showed unexpected phototoxic effects due to an unintended simultaneous activation of (aminolevulinic acid-induced) protoporphyrin IX and hypericin, that were taken for the diagnosis of breast cancer and as an antidepressant, respectively [5]. Further in vitro studies on keratinocyte and endometrial cancer cell lines confirmed that the combination of these two photosensitizers and white light resulted in a synergistic enhancement of PDT effects [6,7]. In addition, we recently demonstrated that a photosensitizer mixture of mTHPC and hypericin may be advantageous for antimicrobial PDT [8].

Currently, no studies are available that deal with possible beneficial properties of photosensitizer mixtures for PDT of malignant head-and-neck tumors. As a first step towards the evaluation of a combined systemic hypericin/mTHPC-mediated PDT protocol for HNSCC patients, we here investigate possible in vitro dark activities of these photosensitizers alone and in combination.

Materials and methods

Photosensitizers

Foslipos® was kindly donated from Biolitec AG, Jena, Germany and had a concentration of mTHPC in liposomes of 1.5 mg/mL (dissolved in water). Hypericin (1 mg) was purchased from Invitrogen, Basel, Switzerland. It was dissolved in 1 mL of 100% ethanol (EtOH).

Cell culture

The cell lines UMB-SCC 745 and UMB-SCC 969 were derived from oropharynx and tonsil head and neck squamous cell carcinomas, respectively, and were kindly provided by Dr. Robert Mandić, Department of Otolaryngology, Philips University, Marburg, Germany.

The cells were cultured under standard conditions (37 °C, 5% CO_2, 95% air atmosphere) in RPMI growth medium (Invitrogen) supplemented with 10% fetal calf serum (FCS, Sigma–Aldrich, Buchs, Switzerland), 1% 4-(2-hydroxyethyl)-1-piperazineethanesulfonic acid (HEPES, Invitrogen), 1% Minimum Essential Medium Non Essential Amino Acids (MEM NEAA, Invitrogen) and 1% penicillin and streptomycin (Invitrogen).

Every second day the growth medium was replaced. When the cells reached confluence, the cell passaging was done with trypsin (1×, Invitrogen), in general every 2–3 days.

Proliferation assay

The dark cytotoxicity was evaluated using a commercial cell proliferation assay (Cell Proliferation ELISA, BrdU (chemiluminescent), Roche, Basel, Switzerland). The cells were seeded in black 96-well plates (2000 cells/well, Greiner, Solingen, Germany) with 100 μL growth medium and cultured at 37 °C, 5% CO_2 for 24 h. Next, the growth medium was replaced with fresh one containing hypericin or Foslipos® or a combination of both at final concentrations ranging between 10 μg/mL and 0.6 μg/mL. The control samples were treated with the same amount of 100% EtOH as applied in hypericin and phototsensitizer mixture treated cells. After an incubation time of 5 h, the cells were washed with phosphate buffered saline (PBS, Oxoid, Hampshire, United Kingdom) and incubated overnight with fresh growth medium (200 μL/well) containing BrdU-labeling agent. Incorporated BrdU was detected with an ELISA immunoassay according to the manufacturer's protocol. The resulting signal was quantified by measuring the photons using a micro-plate spectrometer with photomultiplier technology (BioTek Instruments, Luzern, Switzerland).

Photosensitizer intracellular accumulation

5000 cells/well were seeded in black 96-well plates (Greiner) and grown overnight at 37 °C. For the accumulation study photosensitizers (hypericin and Foslipos®, 2.5 μg/mL final concentration) and the photosensitizer mixture (1:1 mixture of hypericin and Foslipos®, 1.25 μg/mL each) were incubated for several time points (1 and 30 min, 1 h, 3 h, 5 h, 7 h and 24 h). Sextuplicates were used for each time point and cell line.

Furthermore, cells were incubated with hypericin or Foslipos® and photosensitizer mixture (1:1 mixture of hypericin and Foslipos®), respectively, for 5 h. Subsequently growth medium was replaced with fresh one and left in the incubator during different time points (1 min, 1 h, 3 h, 5 h, 7 h and 24 h).

Please cite this article in press as: Besic Gyenge E, et al. Effects of hypericin and a chlorin based photosensitizer alone or in combination in squamous cell carcinoma cells in the dark. Photodiagnosis and Photodynamic Therapy (2012), http://dx.doi.org/10.1016/j.pdpdt.2012.03.006

For both experiments the cells were washed three times with PBS and fluorescence was subsequently measured quantitatively with a micro-plate spectrometer (Tecan Infinite M1000, Tecan Group Ltd., Männedorf, Switzerland). To exclude cross-talks between photosensitizers each micro-well plate was measured four times with following adjustments: excitation wavelengths 420 nm and 554 nm and emission wavelengths 600 nm and 654 nm.

In addition cells were seeded on poly-L-lysine (PLL, 0.25 mg/mL, Sigma—Aldrich) — coated glass cover slips (50,000 cells, Hecht-Assistant, Sondheim, Germany). The cells were then incubated as reported above. For each condition doublets were made. After treatment cells were washed with PBS, fixed for 15 min with PBS containing 1% paraformaldehyde (PFA, Sigma—Aldrich) and 0.33% saccharose (Sigma—Aldrich), permeabilized with 0.01% Triton X-100 (Roche) for 1.5 min, nuclei stained with 4′-6-diamidino-2-phenylindole (DAPI, 1 μg/mL, Roche) and finally mounted on cover slides with Glycer Gel (Dako, Baar, Switzerland). The monitoring was carried out with a confocal laser scanning microscope (Leica SP2, Heerbrugg, Switzerland). Excitation wavelength for hypericin was 594 nm, for Foslipos® and for the photosensitizer mixture 488 nm. Emission wavelengths were in the range of 640—720 nm for Foslipos®, for hypericin 590—680 nm and for mixture 590—720 nm. Excitation wavelength for the visualisation of DAPI was 350 nm and for detection a wavelength range of 450—500 nm was used.

Photosensitizer localisation (immunocytochemistry): Both cells lines were cultured on PLL coated cover slides and incubated for 5 h with hypericin, Foslipos® and a 1:1 mixture of both at final concentrations of 2.5 μg/mL. After incubation cells were fixed for 15 min with 1% PFA, permeabilized with 0.01% Triton X-100 (Roche) for 1.5 min, then blocked for 30 min at room temperature with 0.1% bovine serum albumin (BSA, Calbiochem, San Diego, USA) and afterwards washed with PBS. For labelling of golgi apparatus and trans golgi network mouse anti-cis golgi matrix protein 130 antibody (GM130, 1:500, stock concentration 0.7 mg/mL, Abcam, Cambridge, United Kingdom) and rabbit anti-trans golgi network protein antibody (TNG46, 1:500, stock concentration 0.5 mg/mL, Abcam), respectively, were used. Visualisation of endoplasmic reticulum was achieved with mouse anti-protein disulfide isomerase antibody (PDI, 1:200, stock concentration 1 mg/mL, Abcam). Mitochondria were stained with Mitotracker Orange (working solution 300 nM, Invitrogen).

The primary antibodies were incubated for 2 h at room temperature or overnight at 4 °C. Subsequently the samples were washed and incubated with FITC-labelled donkey anti-rabbit or anti-mouse antibodies respectively (both 1:500, Sigma—Aldrich) together with DAPI (1 μg/mL) for 1 h at room temperature. After washing samples were mounted and examined with confocal microscopy. Excitation and detection wavelengths for photosensitizers and DAPI were chosen as described above. For FITC detection an excitation wavelength of 488 nm was used and emission was recorded in the range of 490—540 nm.

For all confocal studies control experiments were performed, cells were cultured as described, but photosensitizer-containing medium was replaced with growth medium.

RNA quality

Cells were grown in 6-well plates (500,000 cells/well; doublets for each condition, Greiner) under standard conditions overnight. Next, single photosensitizers (hypericin and Foslipos®) and the photosensitizer mixture (1:1 mixture of hypericin and Foslipos®) were incubated for 5 h at final concentrations of 2.5 μg/mL (1.25 μg/mL each in photosensitizer mixture). Subsequently photosensitizer growth medium was replaced with fresh one without photosensitizers. RNA extraction was made with NucleoSpin RNA II Kit (Macherey-Nagel, Oensingen, Switzerland) according to the provided protocol. The cells were lysed with 350 μL lysis buffer (RA1) containing 3.5 μL β-mercaptoethanol and stored at −20 °C until use. The whole extraction procedure was performed in the dark. The final RNA elution step was done with 40 μL RNase-free-water.

The RNA yield was determined with a Nanodrop-spectrometer (Thermo Fisher Scientific, Essex, United Kingdom) and RNA quality/integrity with a Bioanalyzer Agilent 2100 (Agilent Technologies, Santa Clara, USA). We used either pico-chips for RNA concentrations between 0.2 and 5 ng/μL or nano-chips for concentrations between 50 and 500 ng/μL (both chips from Agilent Technologies). Measurements and corresponding analysis (determination of RNA Integrity Number, RIN) were acquired by the RIN algorithm software of the Bioanalyzer.

DNA damage (comet assays)

500,000 cells/well were seeded in 6 well culture plates (Greiner) and grown overnight. After photosensitizer incubation (hypericin and Foslipos® and 1:1 mixture of both, 2.5 μg/mL total concentration) for 5 h comet assays [9] were performed directly (TP 1 = 0 h) or 3 h (TP 2 = 3 h) after removal of photosensitizer. Briefly, for the first microscopy slide coating 1% normal melting point agarose (Fluka, St. Louis, USA) was used. After the photosensitizer incubation the cells were detached with cell stripper solution (CELLGRO, Manassas, USA) supplemented with 0.05% trypsin (Invitrogen) and subsequently transferred to 1% low melting point agarose (LMPA; Fluka). After placing of 350 μL of LMPA cell solution on microscopy slides the samples were kept at 4 °C for 15 min. The slides were then placed in lysis buffer (2.5 M NaCl, 100 mM EDTA, 10 mM Trizma base, pH 10) for one hour and subsequently electrophoresis (10 M NaOH and 200 mM EDTA, pH > 13) was done for 30 min at 24 V/cm. After neutralisation (0,4 M Tris-buffer, pH 7,5), samples were stained with GelRed Nucleic Acid Staining (Roche Diagnostics), washed and mounted with cover slips. As a positive control staurosporin (1 μg/mL, 3 h) treated cells were used. Examination was performed with wide field microscopy (Leica LX, Heerbrugg, Switzerland). Statistical calculations were made with one way Anova Tukey's Multiple Comparison Test, $p < 0.05$ was considered as significant.

Results

The effects of photosensitizers on cell proliferation in the dark are shown in Fig. 1A and B. Significant reduction of cell viability was found for Foslipos® treated samples at

Please cite this article in press as: Besic Gyenge E, et al. Effects of hypericin and a chlorin based photosensitizer alone or in combination in squamous cell carcinoma cells in the dark. Photodiagnosis and Photodynamic Therapy (2012), http://dx.doi.org/10.1016/j.pdpdt.2012.03.006

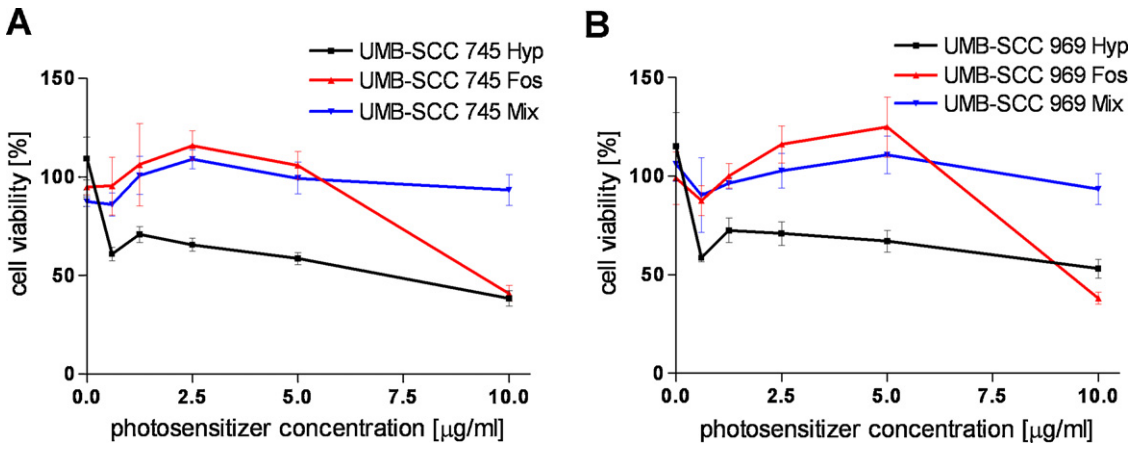

Figure 1 BrdU proliferation assays in UMB-SCC 745 (in A) and UMB-SCC 969 (in B) cells after 5 h incubation of photosensitizers (hypericin in black, Foslipos® in red and mixture of both in blue) at different concentrations ranging from 0 to 10 μg/mL. The concentration of single photosensitizer in the mixture was always half of the overall concentration. (For interpretation of the references to color in this figure legend, the reader is referred to the web version of this article.)

highest (10 μg/mL) photosensitizer concentration (up to 60% of cell viability reduction for both cell lines). Concentrations of 2.5 μg/mL and 5 μg/mL respectively, induced up to 20% cell proliferation increase compared to control samples (not significant) which were set to 100%. The concentrations of 1.25 μg/mL and 0.6 μg/mL did not show significant changes in cell proliferation. The hypericin treated cells (in both cell lines) displayed significant cell viability reduction for all photosensitizer concentrations. The BrdU assay results indicated almost linear cell toxicity distribution for concentrations between 1.25 and 10 μg/mL. The highest cell viability reduction was detected for the hypericin concentration of 10 μg/mL (60% reduction). The concentrations in the range from 5 to 1.25 μg/mL caused a cell reduction between 20 and 36% (Fig. 1A and B). The lowest hypericin concentration (0.6 μg/mL) led to a proliferation reduction of 42% for both cell lines. Despite the same overall photosensitizer concentration in the mixture no significant reduction of cell proliferation was found. This was observed for all applied photosensitizer concentrations from 0.6 μg/mL to 10 μg/mL. Based on these results a photosensitizer concentration of 2.5 μg/mL was used for further studies. For the mixture single photosensitizer concentration was 1.25 μg/mL each.

Subsequently intracellular accumulation of photosensitizers (2.5 μg/mL) over different time periods (0 and 30 min, 1 h, 3 h, 5 h, 7 h and 24 h) was performed. The results of the confocal study for 0 h, 5 h and 24 h for both cell lines and all photosensitizer treatments are depicted in Fig. 2.1 and in addition Fig. 2.2 displays the quantitative fluorescence measurements (time points 0 h, 1 h, 3 h, 5 h, 7 h and 24 h). Fig. 2.1 shows confocal pictures of hypericin uptake which clearly display increase of hypericin aggregates after 5 h in both cell lines. The fluorescence measured for hypericin treated cells followed a Gaussian distribution curve with a maximum of intensity after 5 h of incubation (Fig. 2.2A). The increase of intracellular fluorescence over time for Foslipos® treated cells was continuous. This was visible from confocal pictures and quantitative measurements (Fig. 2.1 and 2.2B). The results for the accumulation of the mixture were consistent with results obtained for single photosensitizers (Fig. 2.1 and 2.2C respectively). The fluorescence intensity was weaker (Fig. 2.2C) compared to single photosensitizer measurements (3.5 times weaker for hypericin and 2.5 times for Foslipos® wavelengths adjustments).

Results of photosensitizer efflux are depicted in Fig. 3.1 and 3.2. Again, the pictures in 3.1 show the cells with corresponding photosensitizer after different time points (0 h, 5 h and 24 h after preceding 5 h of incubation). A reduction of intracellular amounts of hypericin is not visible after 5 h but almost complete cellular clearance occurs within 24 h. Only few hypericin aggregates were detectable after this time. For Foslipos® and mixture, respectively, fluorescence signals were visible even after 24 h. The photosensitizer mixture treated cells displayed higher amount of aggregates as found in hypericin-only treated cells. The quantitative measurements showed that after 24 h the hypericin fluorescence signal is reduced by over 95%, for Foslipos® a reduction of 65% was visible and finally for mixture an over 95% reduction in case of hypericin and reduction up to 65% in case for Foslipos® was detected (Fig. 3.2B). Both cell lines displayed similar behaviour.

Further, we addressed our study to intracellular localisations of photosensitizers after 5 h of incubation. Hypericin was mainly found at cellular membranes (outer cell membranes and nuclear membranes) and the perinuclear region. Well-defined co-localisation was also found with trans golgi network protein (TGN, Fig. 4). Foslipos® did not exhibit any co-localisation with stained cell organelles. The localisation of Foslipos® after 5 h of incubation was limited unspecifically to the cell cytoplasm. These results were found for both cell lines.

The RNA quality measurements after 5 h of photosensitizer incubation (2.5 μg/mL) showed no influence on RNA integrity. The virtual Northern blots are depicted in Fig. 5. The quality of RNA of photosensitizer treated cells was the same as for the control samples, the RNA integrity numbers (RIN) ranged from 10 to 9.8.

Please cite this article in press as: Besic Gyenge E, et al. Effects of hypericin and a chlorin based photosensitizer alone or in combination in squamous cell carcinoma cells in the dark. Photodiagnosis and Photodynamic Therapy (2012), http://dx.doi.org/10.1016/j.pdpdt.2012.03.006

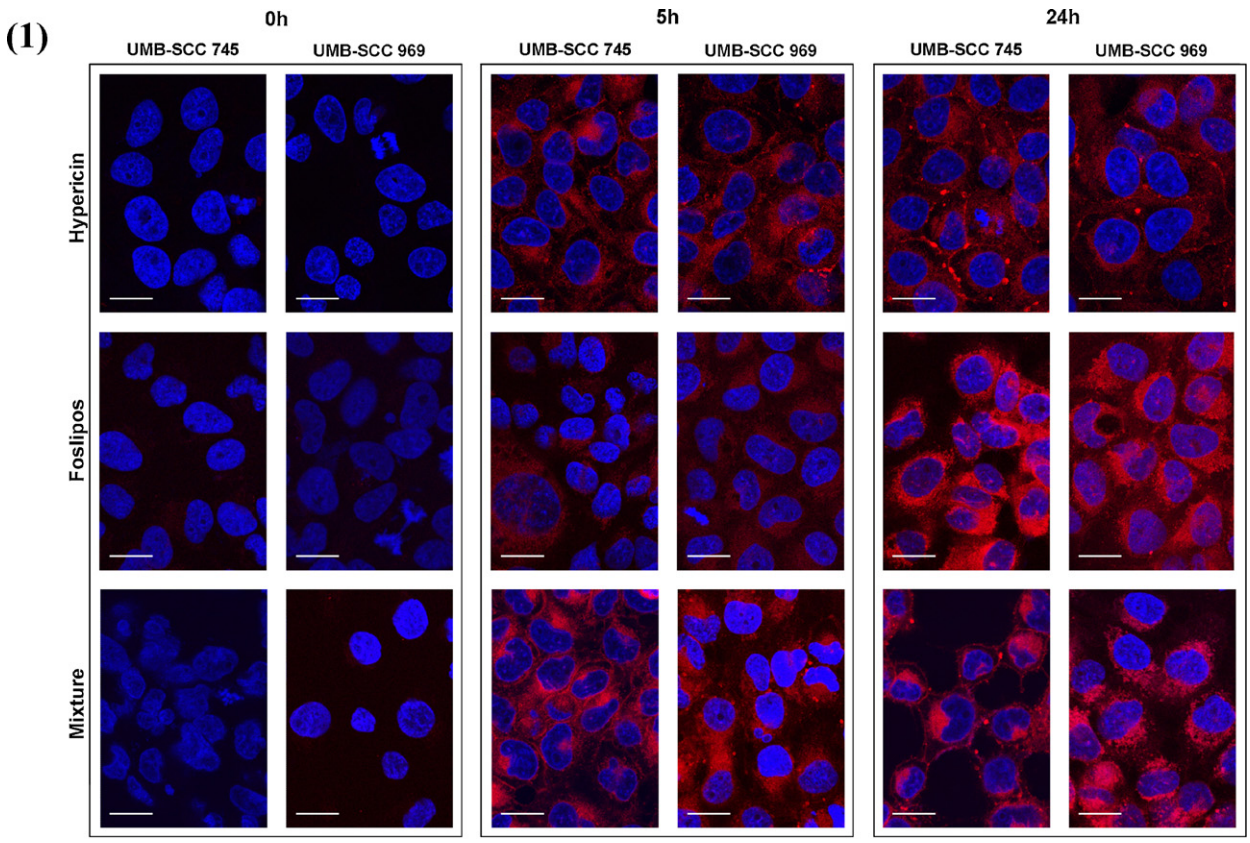

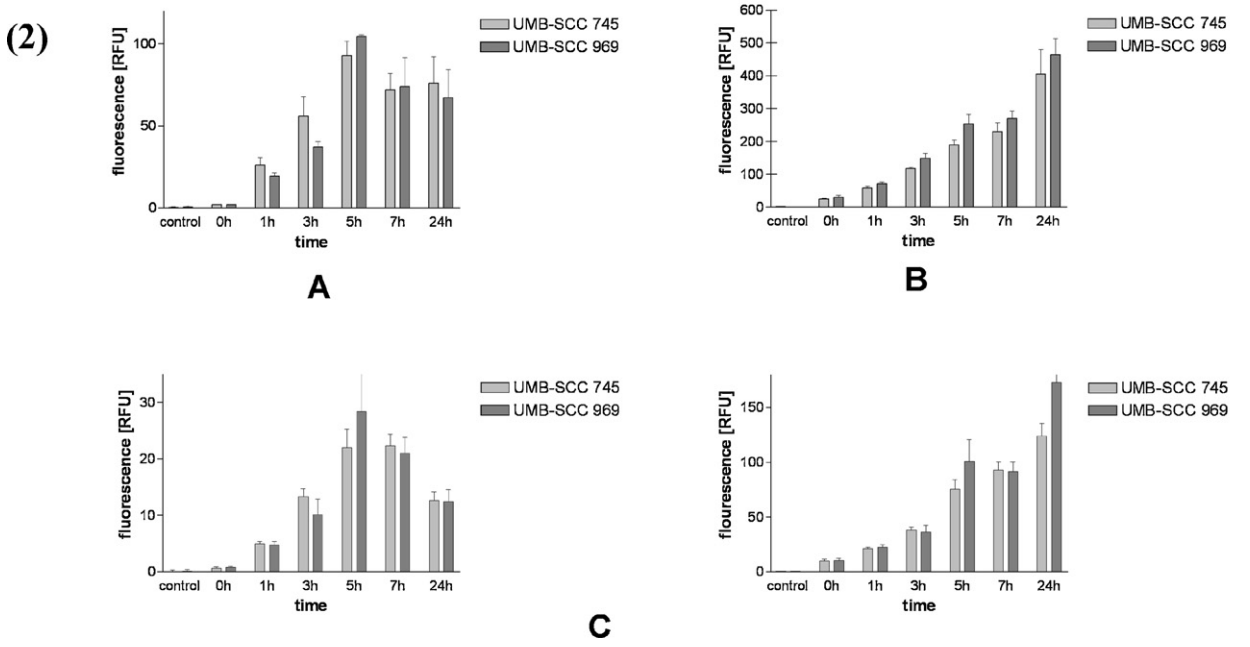

Figure 2 Confocal laser microscopy pictures, shown in 2.1, displaying accumulation of photosensitizer (hypericin, Foslipos® and mixture of both) over different time periods (0 h, 5 h and 24 h) in UMB-SCC 745 and UMB-SCC 969 respectively. Nuclei are shown in blue and photosensitizers in red. Scale bars = 20 μm. The graphs in 2.2 are showing quantitative fluorescence measurements of photosensitizer accumulation (hypericin in A, Foslipos® in B and mixture of both in C) over time (0—24 h) in UMB-SCC 745 and UMB-SCC 969 cells respectively. The fluorescence of photosensitizer mixture was measured once with hypericin adjustments (excitation at 554 nm and detection at 600 nm) shown in 2.2C left and once with Foslipos® adjustments (excitation at 420 nm and detection at 654 nm) shown in 2.2C right. (For interpretation of the references to color in this figure legend, the reader is referred to the web version of this article.)

Please cite this article in press as: Besic Gyenge E, et al. Effects of hypericin and a chlorin based photosensitizer alone or in combination in squamous cell carcinoma cells in the dark. Photodiagnosis and Photodynamic Therapy (2012), http://dx.doi.org/10.1016/j.pdpdt.2012.03.006

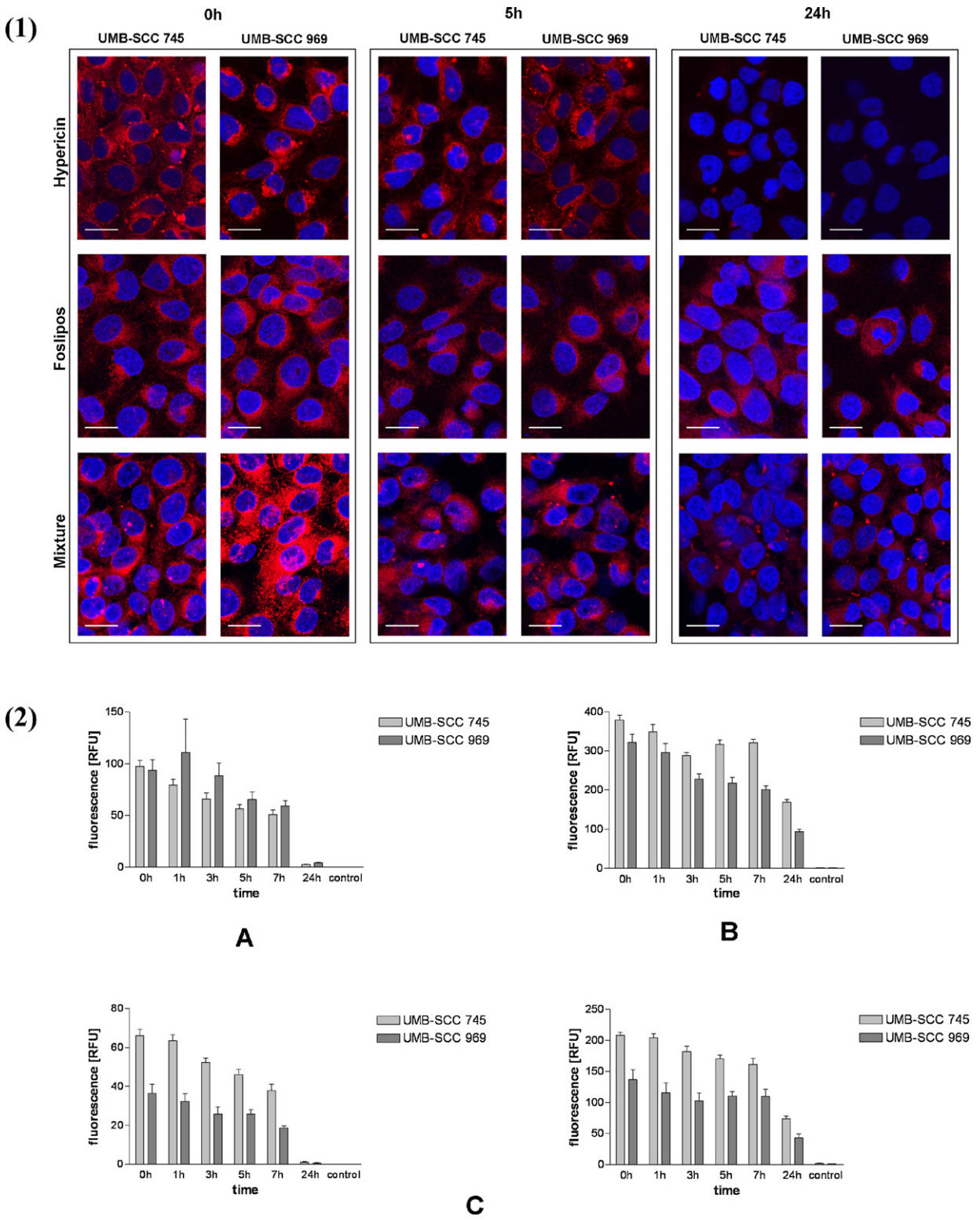

Figure 3 Confocal laser microscopy pictures in 3.1 are displaying elimination of photosensitizers (hypericin, Foslipos® and mixture of both, incubation time 5 h correspond to 0 h in the pictures) over different time periods (0 h, 5 h and 24 h) in UMB-SCC 745 and UMB-SCC 969 respectively. Nuclei are shown in blue and photosensitizers in red. Scale bars = 20 μm. The graphs in 3.2 are showing quantitative fluorescence measurement of photosensitizer elimination (hypericin in A, Foslipos® in B and mixture of both in C, incubation time 5 h) over time (0—24 h) in UMB-SCC 745 and UMB-SCC 969 cells respectively. The fluorescence of photosensitizer mixture was measured once with hypericin adjustments (excitation at 554 nm and detection at 600 nm) shown in 3.2C left and once with Foslipos® adjustments (excitation at 420 nm and detection at 654 nm) shown in 3.2C right. (For interpretation of the references to color in this figure legend, the reader is referred to the web version of this article.)

Please cite this article in press as: Besic Gyenge E, et al. Effects of hypericin and a chlorin based photosensitizer alone or in combination in squamous cell carcinoma cells in the dark. Photodiagnosis and Photodynamic Therapy (2012), http://dx.doi.org/10.1016/j.pdpdt.2012.03.006

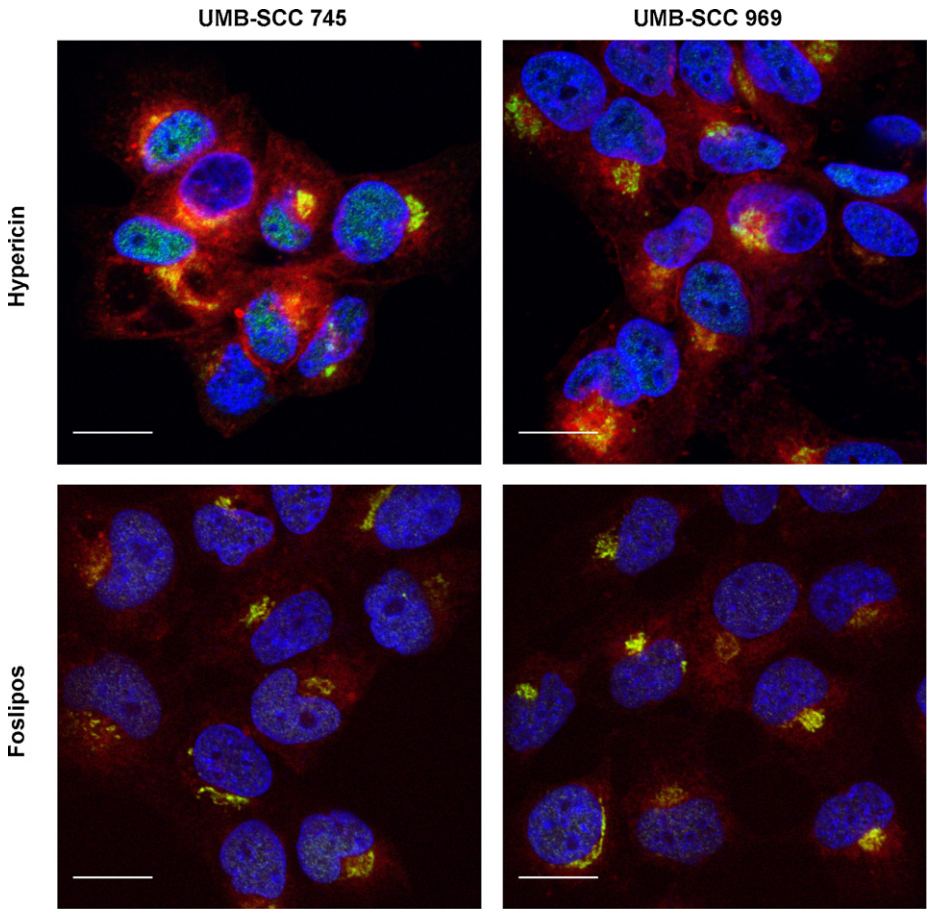

Figure 4 Confocal laser microscopy pictures showing partial (in yellow) co-localization of hypericin (in red) with transgolgi network (TGN, in green) in UMB-SCC 745 and UMB-SCC 969 respectively. Foslipos® did not display any co-localization with TGN. Nuclei are shown in blue and photosensitizers in red. Scale bars = 10 μm. (For interpretation of the references to color in this figure legend, the reader is referred to the web version of this article.)

The DNA damage assay was performed with single cell electrophoresis (comet assay). Fig. 6A shows measurements of comet tail length immediately (TP 1) and 3 h (TP 2) after previous photosensitizer incubation (5 h) compared to untreated cells. The UMB-SCC 969 did not display any significant DNA damage for all applied treatments. In contrast, the UMB-SCC 745 cell line experienced significant DNA damage for hypericin treatment immediately after incubation. The comet tails were 1.4 fold longer then comet tails in untreated cells. After 3 h post incubation of photosensitizer (TP 2), comet tails displayed significant recovery (half as long comet tails as measured immediately after incubation) but the damage was still significant if compared to the untreated cells. In hypericin treated samples we could observe a 2% of cell population (at TP 1) with very long comet tails (high DNA damage). This cell population did not exhibit any recovery even after 3 h (TP 2). Still, the DNA damage (comet tail length) caused with hypericin in comparison to those induced with staurosporin (positive control) was in general negligibly small (Fig. 6B). The UMB-SCC 745 cell line did not exhibit any significant comet tail change for Foslipos® or photosensitizers mixture treatment for both time points. Fig. 6B displays confocal pictures of untreated UMB-SCC 745 cells, hypericin and staurosporin treated cells.

Discussion

PDT is becoming an important alternative treatment modality for head and neck squamous cell carcinoma (HNSCC) [1]. Further, it is reported that every photosensitizer possesses certain benefits for its use in PDT [10,11] and according to our previous studies [7,8] using several photosensitizers simultaneously could improve PDT outcome. It is very important to elaborate and exclude all possible photosensitizer cross effects (chemical and intracellular) in the dark before investigating PDT effects. In our study we applied a liposomal mTHPC derivative (Foslipos®) and one of the most powerful naturally occurring photosensitizers, hypericin, on two different HNSCC cell lines.

Physicochemical photosensitizer properties play a vital role, apart from solubility and biomolecular (proteins and membranes) interaction behaviour, in cellular tolerability. The photosensitizer effects on cell viability in the dark are poorly explored. Hypericin treated cells showed proliferation decrease for all concentrations in both cell lines. This could be due to the light independent inhibition of different enzymes [12] such as protein kinase C, various protein tyrosine kinases or mitochondrial succinoxidase, which play an important role in cell survival, growth, proliferation and

Please cite this article in press as: Besic Gyenge E, et al. Effects of hypericin and a chlorin based photosensitizer alone or in combination in squamous cell carcinoma cells in the dark. Photodiagnosis and Photodynamic Therapy (2012), http://dx.doi.org/10.1016/j.pdpdt.2012.03.006

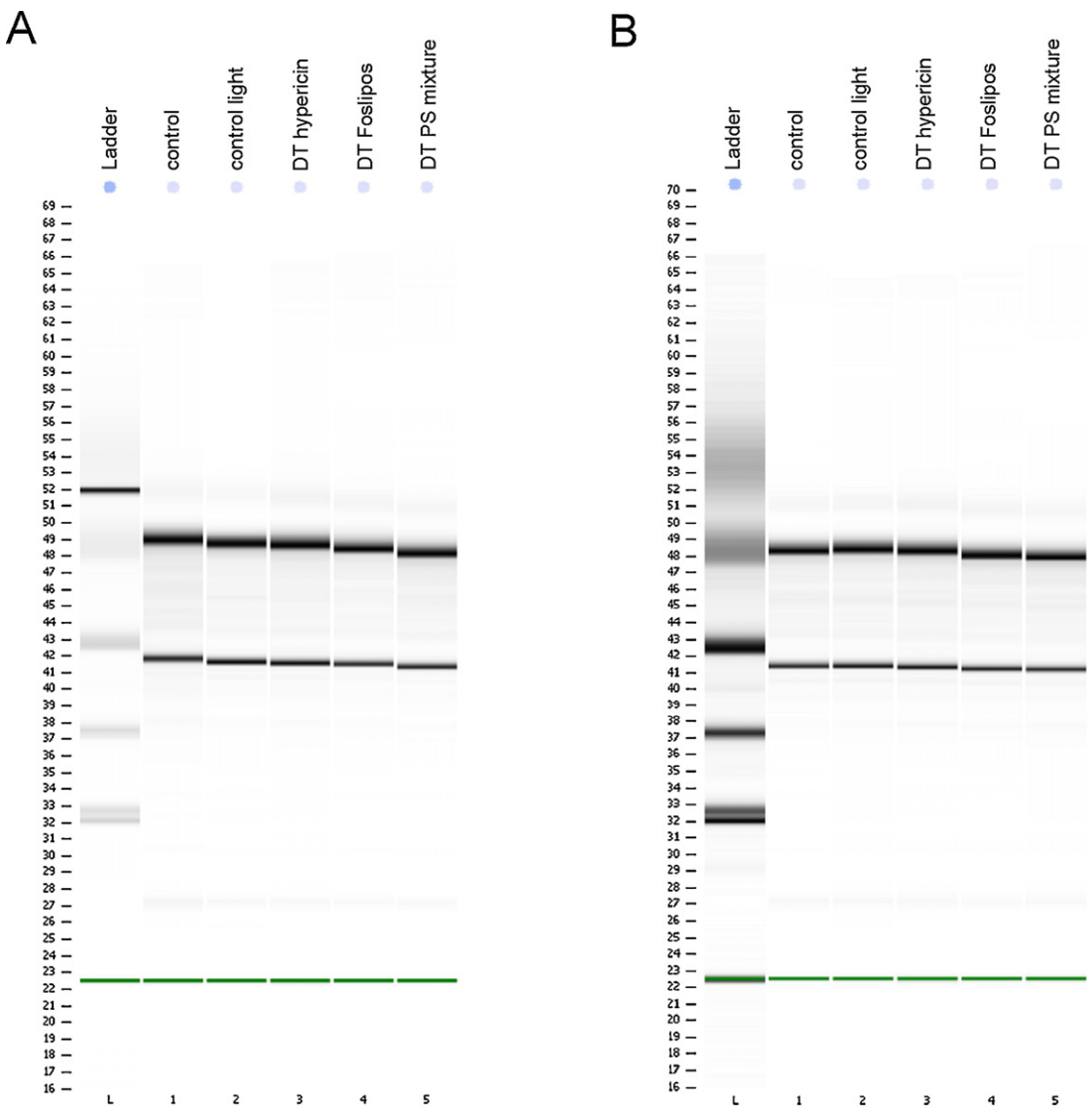

Figure 5 The virtual Northern blots displaying RNA quality after 5 h of incubation. In (A) are displayed results for UMB-SCC 745 cells and in (B) for UMB-SCC 969 cells. The RNA quality measurements were performed with Bioanalyzer Agilent 2100.

death [13,14]. It is reported that in most cases these effects are more prominent under light application and/or if hypericin is slightly chemically modified [15]. In contrast to the above mentioned minor inhibitions, Johnson and Pardini [16] reported that hypericin showed strong light independent inhibitory activity against glutathione reductase (IC_{50} of about 2 nmol/L), which is an important cellular antioxidant. Low intracellular levels of antioxidants can cause oxidative stress and may lead to cell damage. It was also reported that hypericin has a 50% competitive inhibition for several species of cytochrome P450 [17,18], whereupon various metabolic processes could be affected. Additionally, it is known that hypericin can cause reduction in intracellular pH by proton transfer to surrounding molecules leading to pH dependent structural changes in proteins [19]. All these findings could account for affected cell proliferation in our study. Further investigations on this topic were not within the scope of our study but will be the focus of subsequent experiments. Foslipos® treated cells showed only significant changes for highest photosensitizer concentrations (up to 45% viability decrease for 10 μg/mL). The mechanisms which affect cell viability are not yet known. Kiesslich et al. [20] reported that Foslip® (difference to Foslipos® 5% glucose in the solution) has a dark toxic effect in gall bladder cancer (GBC) and bile duct cancer (BDC) cell lines starting from 20 μg/mL (~5% decrease) to 100 μg/mL (~85% decrease) photosensitizer concentration. The additional 5% of glucose in Foslip® can be excluded as a reason for the proliferation decrease in our cell models because both photosensitizer formulations were tested (data not shown). The use of a different cell model is more likely as an explanation. In our study the proliferation assays with photosensitizer mixture application in the dark indicated that even with the highest concentrations (10 μg/mL, hypericin and Foslipos® 5 μg/mL each) cell viability remains the same as for control samples. The decrease in cell proliferation for 5 μg/mL hypericin (showed in a proliferation assay experiment for hypericin alone) was approximately 36%. The mechanisms underlying

Please cite this article in press as: Besic Gyenge E, et al. Effects of hypericin and a chlorin based photosensitizer alone or in combination in squamous cell carcinoma cells in the dark. Photodiagnosis and Photodynamic Therapy (2012), http://dx.doi.org/10.1016/j.pdpdt.2012.03.006

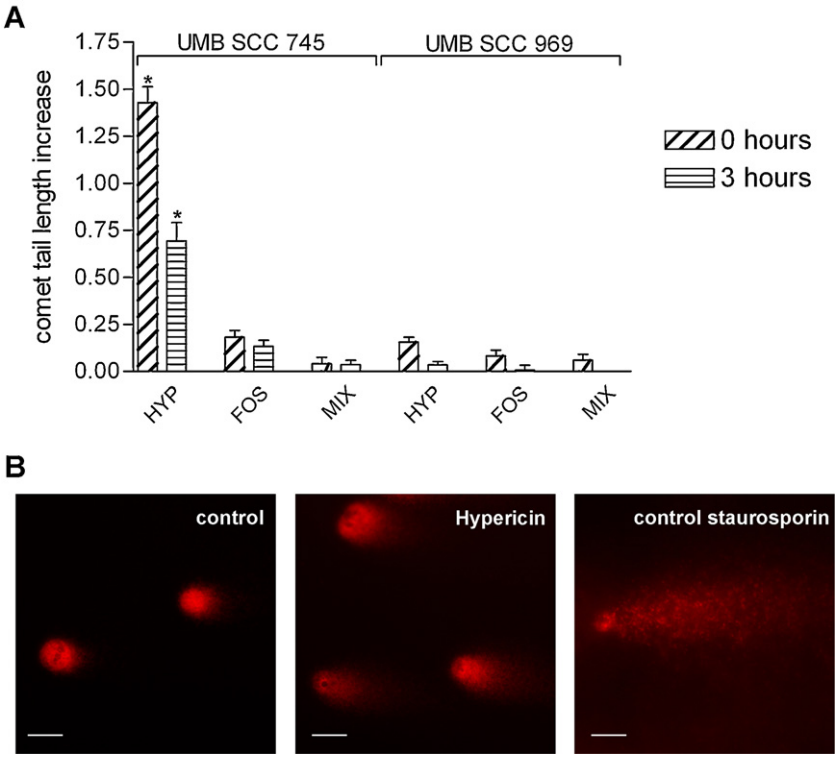

Figure 6 The relative (compared to control samples) fold change of comet tail length of hypericin, Foslipos® and photosensitizer mixture treated cells is shown in (A) after TP 1 = 0 h and TP 2 = 3 h (post previous 5 h of incubation) without illumination in both cell lines (UMB-SCC 745 and UMB-SCC 969). (B) Widefield fluorescent microscopy pictures of comet tails (in red) of untreated, hypericin and staurosporin treated UMB-SCC 745 cells. The scale bars = 10 μm. *$p < 0.001$. (For interpretation of the references to color in this figure legend, the reader is referred to the web version of this article.)

the improved tolerability of the photosensitizer mixture are not clear. However, since hypericin is known to attach to lipoproteins and incorporates into lipid membranes [21], it cannot be excluded that in the mixture hypericin interacts with Foslipos® liposomes, thereby changing its bioactivity.

The cell dependent behaviour of photosensitizer uptake and their efflux were shown in many studies. For example Kiesslich et al. [22] investigated 9 different biliary cancer cell lines on uptake, release and phototoxicity of mTHPC and found great variations in uptake between individual cell lines resulting in even more pronounced differences in phototoxicity. Ritz et al. [23] showed different hypericin uptake in 12 primary human glioma cell cultures. They assumed that the uptake was dependent on an energy dependent uptake process involving LDL receptor-related proteins. Photosensitizer-uptake and -efflux processes in our study were similar for both cell lines. Uptake of hypericin followed a Gaussian curve distribution with a fluorescence maximum after 5 h of incubation. The intracellular aggregation of hypericin was visible in our confocal observations and it was increasing over incubation time. Hypericin aggregates (stacked and planar associations) [24] are well documented and examined. Additionally, it is reported that this leads to fluorescence quenching which we could observe in our quantitative fluorescence measurements. On the one hand aggregate formation prevents the photosensitizer photodegradation [25,26] but on the other hand hypericin diffusion is heavily affected [27] and therewith also its cellular uptake in case the aggregation takes place extracellularly and/or cellular efflux in case it occurs intracellularly. Confocal pictures of hypericin intracellular clearance displayed that hypericin aggregates are present even after 24 h. This can have a negative effect on PDT outcome prolonging photosensitivity if applied in vivo. Foslipos® uptake was continuous over 24 h, corresponding to the results achieved in our study with the prostate carcinoma cell line PC-3 [28] and many other studies [29] including work of Kiesslich et al. [20] who has demonstrated a continuous uptake reaching a plateau of the cellular fluorescence after 36 h. The cellular efflux of Foslipos® in our cell models was slightly different to this study. UMB-SCC 745 displayed 45% and UMB-SCC 969 25% of Foslipos® fluorescence intracellularly after 24 h. The Foslip® retention in GBC and BDC cells was very high even after 48 h (48% for GBC and beyond 70% for BDC cells) post medium exchange, which was high enough even for a suitable PDT effect. The slow release of mTHPC and its derivatives from the cells was reported in several other studies [30,31] and remains unclear. Our slightly different findings in photosensitizer uptake and efflux in HNSCC cell lines could be a result of different cellular and metabolic processes and direct comparison to studies is difficult. Photosensitizer mixture uptake and efflux studies on both UMB-SCC cell lines were comparable to the observations achieved with single photosensitizers. The first observed difference was a higher amount of hypericin aggregates after 24 h in photosensitizer efflux experiment in comparison

Please cite this article in press as: Besic Gyenge E, et al. Effects of hypericin and a chlorin based photosensitizer alone or in combination in squamous cell carcinoma cells in the dark. Photodiagnosis and Photodynamic Therapy (2012), http://dx.doi.org/10.1016/j.pdpdt.2012.03.006

to hypericin alone. Another important observation is that hypericin fluorescence intensity in the uptake study after 5 h (shown in Fig. 2.2) was 3.5 times and after 24 h even 5 times weaker than it theoretically should be. The higher amount of hypericin aggregates and photosensitizers near proximity could eventually cause fluorescence quenching. Taken together these findings indicate slightly different intracellular behaviour of hypericin if combined with Foslipos® and further studies on this topic are needed.

Subcellular localisation of photosensitizers is very important for PDT outcome and it seems to be photosensitizer and cell line dependent. In our study, 5 h post incubation hypericin was mainly found in membranous systems (outer cellular membranes, nuclear membranes, trans golgi network and perinuclearly). In many studies the intracellular localisation of hypericin was investigated. A review of Theodossiou et al. [32] summarised hypericin localisation places in several different cell lines reaching from lipid membranes and nucleus to various cell organelles like mitochondria, ER, Golgi apparatus or lysosomes. The distribution and localisation of hypericin seems to be driven by many factors like photosensitizer concentration, incubation time, cell lines and incubation parameters or presence of serum proteins. A direct data comparison with other studies is therefore rather difficult. Foslipos® did not co-localise with any cell organelle stain and it remained diffuse in cytoplasm of both UMB-SCC cell lines. These findings are similar to those found in our previous study with PC-3 cells [28] or in the study of Kiesslich et al. [22] where Foslipos® accumulation in GBC and BDC cell lines could not be organelle-specifically localized. Also herein the localisation seems to be dependent on the cell models and incubation parameters. In the mixture the localisation of single photosensitizer was due to the overlapping absorption and emission spectral range difficult to separate from each other, therefore well-defined immunocytochemistry in photosensitizer mixture treated cells was not feasible. However, in general the observation of photosensitizer localisation in the mixture was not remarkably different compared to the confocal pictures made for single photosensitizers (Fig. 2.1).

Intracellular accumulation of photosensitizers without illumination did not show any influence on overall RNA quality. These results correspond to our previous study with prostate carcinoma cell line PC-3 [28]. In contrast, transient DNA damage was detected, but only in case of hypericin treated UMB-SCC 745 cells. Since UMB-SCC 745 cells did not show significant differences in photosensitizer uptake, efflux or localisation a plausible explanation for the minor DNA damage could be individual cell line stress management caused by hypericin. The mechanisms of action stay unclear. Nevertheless, compared to staurosporin samples hypericin mediated DNA damage in UMB-SCC 745 was on one side very low and on other the cells recovered after 3 h post photosensitizer removal.

Conclusions

Our study is the first showing that a combination of photosensitizers may reduce dark toxic effects, potentially allowing for the save application of higher photosensitizer doses for PDT of HNSCC. We are aware that our study design relies on cancer cell lines only and that photosensitizer biobehaviour of normal cells or in patients may differ. However, our data will set the stage for further investigations on benefits of photosensitizers in combinations in vitro and in vivo. Possible consequences for PDT of photosensitizer interactions in the mixture are now the focus of ongoing studies.

Acknowledgements

The study was supported by the FP7 ERA-net EuroNanoMed project TARGET-PDT. We are thankful to Urs Ziegler and his team for their help with confocal microscopy. We also thank Biolitec AG for kindly providing Foslipos®.

References

[1] Biel MA. Photodynamic therapy of head and neck cancers. Methods Mol Biol 2010;635:281—93.
[2] Bredell MG, Besic E, Maake C, et al. The application and challenges of clinical PD-PDT in the head and neck region: a short review. J Photochem Photobiol B 2010;101(3):185—90.
[3] O'Connor AE, Gallagher WM, Byrne AT. Porphyrin and nonporphyrin photosensitizers in oncology: preclinical and clinical advances in photodynamic therapy. Photochem Photobiol 2009;85(5):1053—74.
[4] Prasad PS, Schwartz SD, Hubschman JP. Age-related macular degeneration: current and novel therapies. Maturitas 2010;66(1):46—50.
[5] Ladner DP, Steiner RA, Allemann J, et al. Photodynamic diagnosis of breast tumours after oral application of aminolevulinic acid. Br J Cancer 2001;84(1):33—7.
[6] Ladner DP, et al. Synergistic toxicity of delta-aminolaevulinic acid-induced protoporphyrin IX used for photodiagnosis and hypericum extract, a herbal antidepressant. Br J Dermatol 2001;144(4):916—8.
[7] Schneider-Yin X, Kurmanaviciene A, Roth M, et al. Hypericin and 5-aminolevulinic acid-induced protoporphyrin IX induce enhanced phototoxicity in human endometrial cancer cells with non-coherent white light. Photodiagnosis Photodyn Ther 2009;6(1):12—8.
[8] Lüthi M, Gyenge EB, Engström M, et al. Hypericin- and mTHPC-mediated photodynamic therapy for the treatment of cariogenic bacteria. Med Laser Appl 2009;24(4):227—36.
[9] Dhawan A, et al. Protocol for the Single Cell Gel Electrophoresis/Comet Assay for Rapid Genotoxicity Assessment: Marg, India; p. 1—10, http://www.cometassayindia.org/Protocol%20for%20Comet%20Assay.PDF.
[10] Berlanda J, Kiesslich T, Engelhardt V, et al. Comparative in vitro study on the characteristics of different photosensitizers employed in PDT. J Photochem Photobiol B 2010;100(3):173—80.
[11] Allison RR, Downie GH, Cuenca R, Hu X-H, Childs CJH, Sibata CH. Photosensitizers in clinical PDT. Photodiagn Photodyn Ther 2004;1:27—42.
[12] Kubin A, Wierrani F, Burner U, et al. Hypericin — the facts about a controversial agent. Curr Pharm Des 2005;11(2):233—53.
[13] Haimovitz-Friedman A, Balaban N, McLoughlin M, et al. Protein kinase C mediates basic fibroblast growth factor protection of endothelial cells against radiation-induced apoptosis. Cancer Res 1994;54(10):2591—7.
[14] Kim CY, Giaccia AJ, Strulovici B, et al. Differential expression of protein kinase C epsilon protein in lung cancer cell lines by ionising radiation. Br J Cancer 1992;66(5):844—9.
[15] Vandenbogaerde AL, Delaey EM, Vantieghem AM, et al. Cytotoxicity and antiproliferative effect of hypericin and

derivatives after photosensitization. Photochem Photobiol 1998;67(1):119—25.
[16] Johnson SA, Pardini RS. Antioxidant enzyme response to hypericin in EMT6 mouse mammary carcinoma cells. Free Radic Biol Med 1998;24(5):817—26.
[17] Obach RS. Inhibition of human cytochrome P450 enzymes by constituents of St. John's Wort, an herbal preparation used in the treatment of depression. J Pharmacol Exp Ther 2000;294(1):88—95.
[18] Budzinski JW, Foster BC, Vandenhoek S, et al. An in vitro evaluation of human cytochrome P450 3A4 inhibition by selected commercial herbal extracts and tinctures. Phytomedicine 2000;7(4):273—82.
[19] Sureau F, Miskovsky P, Chinsky L, Turpin PY. Hypericin-induced cell photosensitization involves an intracellular pH decrease. J Am Chem Soc 1996;118(40):9484—7.
[20] Kiesslich T, Berlanda J, Plaetzer K, et al. Comparative characterization of the efficiency and cellular pharmacokinetics of Foscan- and Foslip-based photodynamic treatment in human biliary tract cancer cell lines. Photochem Photobiol Sci 2007;6(6):619—27.
[21] Ho YF, Wu MH, Cheng BH, et al. Lipid-mediated preferential localization of hypericin in lipid membranes. Biochim Biophys Acta 2009;1788(6):1287—95.
[22] Kiesslich T, Neureiter D, Alinger B, et al. Uptake and phototoxicity of meso-tetrahydroxyphenyl chlorine are highly variable in human biliary tract cancer cell lines and correlate with markers of differentiation and proliferation. Photochem Photobiol Sci 2009;9(5):734—43.
[23] Ritz R, Muller M, Dietz K, et al. Hypericin uptake: a prognostic marker for survival in high-grade glioma. J Clin Neurosci 2008;15(7):778—83.
[24] Sevenants MR. Pigments of blepharisma undulans compared with hypericin. J Protozool 1965;12(2):240—5.
[25] Martinez RBAG. Photobleaching of sensitisers used in photodynamic therapy. Tetrahedron 2001;57(591):9513—47.
[26] Bonnett R, Martinez G. Photobleaching of compounds of the 5,10,15,20-Tetrakis(m-hydroxyphenyl)porphyrin Series (m-THPP, m-THPC, and m-THPBC). Org Lett 2002;4(12): 2013—6.
[27] Bano G, Stanicova J, Jancura D, et al. On the diffusion of hypericin in dimethylsulfoxide/water mixtures-the effect of aggregation. J Phys Chem B 2011;115(10):2417—23.
[28] Gyenge EB, Hiestand S, Graefe S, et al. Cellular and molecular effects of the liposomal mTHPC derivative Foslipos in prostate carcinoma cells in vitro. Photodiagn Photodyn Ther 2011;8(2):86—96.
[29] Ma L, Moan J, Berg K. Evaluation of a new photosensitizer, meso-tetra-hydroxyphenyl-chlorin, for use in photodynamic therapy: a comparison of its photobiological properties with those of two other photosensitizers. Int J Cancer 1994;57(6):883—8.
[30] Ball DJ, Vernon DI, Brown SB. The high photoactivity of m-THPC in photodynamic therapy. Unusually strong retention of m-THPC by RIF-1 cells in culture. Photochem Photobiol 1999;69(3):360—3.
[31] Mitra S, Foster TH. Photophysical parameters, photosensitizer retention and tissue optical properties completely account for the higher photodynamic efficacy of meso-tetra-hydroxyphenyl-chlorin vs Photofrin. Photochem Photobiol 2005;81(4):849—59.
[32] Theodossiou TA, Hothersall JS, De Witte PA, et al. The multifaceted photocytotoxic profile of hypericin. Mol Pharm 2009;6(6):1775—89.

Please cite this article in press as: Besic Gyenge E, et al. Effects of hypericin and a chlorin based photosensitizer alone or in combination in squamous cell carcinoma cells in the dark. Photodiagnosis and Photodynamic Therapy (2012), http://dx.doi.org/10.1016/j.pdpdt.2012.03.006

4

PDT EFFECTS ON HNSCC CELL LINES

4. Photodynamic Mechanisms induced by Hypericin and a Chlorin Based Photosensitizer in Head and Neck Squamous Cell Carcinoma Cells

The following manuscript is in revision. The journal where the manuscript is submitted is *Photochemistry and Photobiology*.

The contributions of Emina Besic Gyenge to the study: „Optimizing Photodynamic Therapy on Head and Neck Squamous Cell Carcinoma Cells", were the following:

1. Cell culturing

2. Cell viability assay (**figure 5**) for **UMB-SCC 969** cell line

3. Singlet oxygen sensor green assay (**figure 2**)

4. ROS measurements with CM-H_2DCFDA assay including microscopic monitoring in both cell lines (**figure 3**)

5. Live cell imaging after photosensitizer treatment in **UMB-SCC 969** cell line (**figure 6 B**)

6. Death assay with Annexin V experiments including microscopic monitoring for both cell lines (**figures 8 A** and **B**)

7. Cytochrom C release experiments for both cell lines (**figure 9**)

8. RNA extraction and RNA integrity number measurements for both cell lines and rtPCR for **UMB-SCC 969** cell line (**table 1**)

Photochemistry and Photobiology, 20**, **: *–*

Photodynamic Mechanisms induced by a Combination of Hypericin and a Chlorin Based-Photosensitizer in Head and Neck Squamous Cell Carcinoma Cells

Emina Besic Gyenge*,†[1], Daniel Lüscher†[1], Patrick Forny[1], Martina Antoniol[1], Georg Geisberger[2], Heinrich Walt[3], Greta Patzke[2] and Caroline Maake[1]

[1]Institute of Anatomy, University of Zurich, Zurich, Switzerland
[2]Institute of Inorganic Chemistry, University of Zurich, Zurich, Switzerland
[3]Department of Cranio-Maxillofacial Surgery, University Hospital of Zurich, Zurich, Switzerland

Received 15 February 2012, revised 30 July 2012, accepted 2 August 2012, DOI: 10.1111/j.1751-1097.2012.01217.x

ABSTRACT

The aim of this study was to elucidate photodynamic therapy (PDT) effects mediated by hypericin and a liposomal meso-tetrahydroxyphenyl chlorin (mTHPC) derivative, with focus on their 1:1 mixture, on head and neck squamous cell carcinoma cell lines. Absorption, excitation and photobleaching were monitored using fluorescence spectrometry, showing the same spectral patterns for the mixture as measured for single photosensitizers. In the mixture mTHPC showed a prolonged photo-stability. Singlet oxygen yield for light-activated mTHPC was $\Phi_\Delta = 0.66$, for hypericin $\Phi_\Delta = 0.25$ and for the mixture $\Phi_\Delta = \sim 0.4$. A linear increase of singlet oxygen yield for mTHPC and the mixture was found, whereas hypericin achieved saturation after 35 min. Reactive oxygen species fluorescence was only visible after hypericin and mixture-induced PDT. Cell viability was also more affected with these two treatment options under the selected conditions. Examination of death pathways showed that hypericin-mediated cell death was apoptotic, with mTHPC necrotic and the 1:1 mixture showed features of both. Changes in gene expression after PDT indicated strong up-regulation of selected heat-shock proteins. The application of photosensitizer mixtures with the features of reduced dark toxicity and combined apoptotic and necrotic cell death may be beneficial in clinical PDT. This will be the focus of our future investigations.

INTRODUCTION

Photodynamic therapy (PDT) relies on the uptake of a nontoxic photoactivatable drug, the so called "photosensitizer", into cells. Upon local illumination the photosensitizer can be activated to excited triplet state. At this energy level, the photosensitizer is very unstable and may therefore transfer its energy to molecular oxygen or biomolecules in its proximity initiating the generation of singlet oxygen and other reactive oxygen species (ROS; 1), which can cause damage to important cellular compartments such as mitochondria. The initial oxidative cellular damage is occurring at the photosensitizer subcellular localization site due to the short diffusion radius (10–55 nm) of singlet oxygen and other ROS. Depending on the localization of the damage different cellular mechanisms can be activated and can therewith influence the fate of cells, leading to apoptosis or necrosis. For this reason, the localization of the photosensitizer plays a very important role in PDT-induced cellular responses.

So far, PDT has been successfully used for the treatment of different types of pre malignant and malignant lesions, not only including for *e.g.* actinic keratosis or Barrett esophagus but also skin tumors such as squamous cell carcinoma *in situ* (Bowen's disease), bladder transitional cell carcinomas, non small cell lung cancer and head and neck squamous cell carcinoma (HNSCC; 2, 3). In contrast to conventional cancer treatments such as surgery, chemo- or radiotherapy PDT is not or minimally invasive, is repeatable, has low side effects and excellent functional and cosmetic outcome (4). In addition, promising results were reported in treatment of patients with advanced cancer who had failed conventional therapy or were unsuitable for such treatments (5,6).

We recently reported that the combination of two photosensitizers may improve PDT effects. First observations had been reported in a case study where aminolevulinic acid (ALA) was administered as a guide for intraoperative diagnosis and recognition of tumor margins in a breast cancer patient, where hypericin was simultaneously taken as an antidepressant (7). The unintended activation of (ALA-induced) protoporphyrin IX and hypericin showed unexpected high phototoxic effects. Further *in vitro* studies on keratinocyte and endometrial cancer cell lines confirmed that the combination of these two photosensitizers and white light resulted in a synergistic enhancement of PDT effects (7,8). These remarkable results initiated further studies on possible applications of photosensitizer combinations on oral pathogens. We examined PDT effects of hypericin and a liposomal meso-tetrahydroxylphenyl chlorin (mTHPC) derivative (Foslipos®) in a 1:1 mixture on *Streptococcus mutans* and *S. sobrinus* (9). We found that these two oral pathogens could be completely eradicated with the photosensitizer mixture showing high PDT efficacy despite a low dose of single photosensitizers. In addition, our previous study on dark toxicity (Besic Gyenge *et al.* (2012) *Photodiagnosis Photodyn Ther*. (In press, DOI: 10.1016/j.pdpdt.2012.03.006) in HNSCC cell lines showed that application of hypericin and Foslipos® in combination decreases *in vitro*

*Corresponding author email: emina.besicgyenge@uzh.ch (Emina Besic Gyenge)
†Contributed equally.

dark toxicity without influencing photosensitizer physicochemical properties or their intracellular behavior.

These results prompted us to further investigate the potential of photosensitizer mixtures in PDT treatment. In this study, we extensively explored the effects and consequences of PDT with Foslipos® and hypericin in combination, using an *in vitro* HNSCC model.

MATERIALS AND METHODS

Photosensitizers. In our study, we used two different photosensitizers and their 1:1 combinations. Foslipos®, which is a liposomal derivative of mesotetra(hydroxy)phenyl chlorin (mTHPC) was kindly donated from Biolitec AG (Jena, Germany). The stock concentration was 1.5 mg mL^{-1} (2.2 mM). Hypericin, a herbal photosensitizer which is the main photoactive constituent from St. Johns wort was purchased from Invitrogen (Basel, Switzerland). A 1 mg was dissolved in 1 mL 100% ethanol (EtOH; 1.9 mM). For both photosensitizers working solutions (0.3–5 μg mL^{-1}) were prepared in Roswell Park Memorial Institute medium (RPMI) growth medium (Invitrogen) supplemented with 10% fetal calf serum (FCS; Sigma–Aldrich, Buchs, Switzerland), 1% 4-(2-hydroxyethyl)-1-piperazineethanesulfonic acid (HEPES; Invitrogen), 1% MEM non essential amino acids (Invitrogen) and 1% penicillin and streptomycin (Invitrogen).

Cell culture. HNSCC cell lines UMB-SCC 745 and 969 were kindly provided by Dr. Robert Mandić, Department of Otorhinolaryngology, Philips University (Marburg, Germany). The UMB-SCC 745 was derived from the oropharynx tumor of a 48-year-old man and UMB-SCC 969 from the tonsil tumor of a 67-year-old man respectively. The cells were cultured under standard conditions (37°C, 5% CO_2, 95% air atmosphere) in RPMI growth medium. Cells were passaged by trypsination (trypsin 1x; Invitrogen) when reaching confluence, in general every 2–3 days.

Absorption and emission spectra. Absorption and emission spectra of hypericin and Foslipos® were measured using a fluorescence spectrophotometer (Cary Eclipse, Varian, Santa Clara) in 100% EtOH at final concentrations of 1 μg mL^{-1}. In addition, the spectra of the 1:1 combination of hypericin and Foslipos® were recorded. The excitation wavelengths were ranging from 200 to 900 nm (zero order excitation). The absorption and emission spectra were recorded from 300 to 800 nm.

Photobleaching experiments. Freshly prepared solutions of hypericin and Foslipos® were used for photobleaching experiments. Hypericin was dissolved in EtOH and Foslipos® was dissolved in double distilled water to reach final concentrations of 2×10^{-5} M. To investigate the photobleaching of the mixture, both solutions were mixed in a 1:1 ratio. In a 50 mL reaction vessel, which was thermostated at 25°C with a water cooling jacket, the solutions were irradiated under stirring with 10 light bulbs (Osram Dulux®S 865 white, 9 W per 570 lm, spectrum cf. Fig. 4D). The lamps were arranged around the photoreactor vessel in a circular fashion at a distance of 5–6 cm. At given time intervals: 0, 10, 20, 30 and 45 min, 1, 1.5, 2–7 and 21 h 1.5 mL of the solution was collected and analyzed by recording the change of main peaks using a Perkin–Elmer Lambda 650S UV/Vis spectrophotometer.

Cell viability assay. Cell viability after PDT was determined with a colorimetric (3-(4,5-dimethylthiazol-2-yl)-2,5-diphenyltetrazolium bromide (MTT) assay (Invitrogen). Cells were seeded on transparent 96-well plates (5000 cells per well) over night. Photosensitizers and 1:1 combinations of both with final concentrations of 2.5 μg mL^{-1} were incubated for 5 h. Cells were washed and 200 μL per well of growth medium was added. Cells were illuminated with white light (fluorescent tube SYLVANIA standard F15W/154, daylight) for 1 min (6000 Lx; 250 μW; 32 mW cm^{-2}) and then kept in the incubator until the next day. Growth medium was then replaced with growth medium containing 0.5 mg mL^{-1} MTT dye for 3 h. Afterward, growth medium was replaced with 100 μL dimethyl sulfoxide (DMSO; Sigma–Aldrich) and the absorption at 565 nm was measured on a microplate spectrometer (BioTek Instruments, Luzern, Switzerland). For statistical calculations one-way ANOVA Tukey's test and the software GRAPHPAD PRISM were used.

Singlet oxygen yield measurements. Oxygen luminescence: Absorption spectra were recorded on a Perkin–Elmer (Lambda 2, Courtaboeuf, France) UV–visible spectrophotometer. Singlet oxygen spectra were recorded on a SPEX Fluorolog-3 spectrofluorimeter (Jobin Yvon, Longjumeau, France) equipped with a thermostated cell compartment (25°C), using a 450 W Xenon lamp. The detection at 1270 nm was done through a PTI S/N 1565 monochromator, and the emission was monitored using a liquid nitrogen-cooled Ge-detector model (EO-817L; North Coast Scientific Co., Santa Rosa, CA). Two excitation wavelengths were chosen, 415 nm for Foslipos® and 590 nm for hypericin. Rose Bengal has been chosen as a reference solution because of its high $^1O_2$ quantum yield in EtOH (= 0.68, DO = 0.2 at the excitation wavelength).

First experiment: The detection of singlet oxygen was measured at an excitation wavelength of 590 nm. The concentration of hypericin and Foslipos® in the mixture was 1:1. *Second experiment*: The detection of singlet oxygen was measured at an excitation wavelength 415 nm as reported above. The concentration of hypericin and Foslipos® in the mixture was 1:1. Figure in supplementary data (Figure S1).

Singlet oxygen sensor green (SOSG) assay: Stock concentrations of hypericin and Foslipos® were 5 μg mL^{-1} and concentration of the photosensitizer mixture was 2.5 μg mL^{-1} each in TRIS buffer (20 mM). A quantity of 50 μL of photosensitizers (end concentration of single photosensitizers: 2.5 μg mL^{-1}; in the mixture: 1.25 μg mL^{-1}) and 50 μL of SOSG (Molecular Probes, Eugene, OR; 10 μM in 100% methanol [MeOH]) was placed in one well of a black 96-well plate (Cellstar, Frickenhausen, Germany). The measurement was performed for 1 h alternately with an illumination for 30 s with white light (fluorescent tube SYLVANIA standard F15W/154, daylight; 6000 Lx; 250 μW; 32 mW cm^{-2}) and fluorescence measurements every 3 s over 3 min on a microplate spectrometer (BioTek Instruments) at an excitation wavelength of 504 nm and a detection wavelength of 525 nm.

CM-H_2DCFDA ROS measurement. Cells were seeded (50 000 cells per well) on 8-well ibidi slides (μ-slide 8 well, ibiTreat; ibidi GmbH, Munich, Germany). Incubation with photosensitizers and their mixture took place on the next day for 5 h at 37°C in the dark (overall concentration of photosensitizers and their mixture was 2.5 μg mL^{-1}). Ibidi slides were incubated with CM-H_2DCFDA (Invitrogen) for 1 h at a final concentration of 5 μM prior to observation. Growth medium was renewed, cells were illuminated for 1 min (fluorescent tube SYLVANIA standard F15W/154, daylight; 6000 Lx; 250 μW; 32 mW cm^{-2}) and subsequently live cell confocal scanning microscopy (SP5 Leica Microsystems Inc., Bannockburn, IL) was performed. The experiments were repeated three times in doublets.

FLICA™ assay and Hoechst stain. Caspase activity was monitored with fluorescein labelled inhibitors of poly-caspases (FLICA™ Poly Caspases Kit; ImmunoChemistry Technologies, Bloomington, MN). Cells were seeded (50 000 cells per coverslip) on poly-L-lysine (PLL) coated coverslips (Menzel Gläser, Braunschweig, Germany) and grown overnight. The next day, cells were incubated with photosensitizers (2.5 μg mL^{-1}) and their mixture (1.25 μg mL^{-1} each photosensitizer) for 5 h, in the dark at 37°C, growth medium was changed and the cells were illuminated with white light (fluorescent tube SYLVANIA standard F15W/154, daylight; 6000 Lx; 250 μW; 32 mW cm^{-2}) for 1 min. Subsequently, the cells were incubated for 1 h with fresh growth medium supplemented with FLICA™ (30X final concentration) after different time intervals post illumination (0 and 30 min, 1, 1.5, 2, 2.5, 3, 3.5 and 4 h). As controls we created samples illuminated, but without photosensitizers, with photosensitizers, but without illumination and finally neither with photosensitizers nor illumination. One hour after FLICA™ incubation, nuclei were stained with Hoechst 33342 staining medium (1 μg mL^{-1}, provided with FLICA™ Kit) for 5 min. Then, the cells were washed twice with wash buffer (FLICA™ Kit). To fix the cells, fixative (FLICA™ Kit) was added for 15 min. Examination was made using a confocal scanning microscope Leica TCS SP5 (Leica Microsystems Inc.). The fluorescence for FITC was observed using a bandpass filter (excitation 488 nm, emission 490–540 nm) and the fluorescence of the Hoechst 33342 stain with a UV-filter with excitation at 350 nm and emission at 450–500 nm.

Annexin V assay. A quantity of 50 000 cells per well were seeded on 8-well plates (ibidi GmbH). After 24 h, growth medium was removed and replaced by single photosensitizer and 1:1 photosensitizer mixture containing medium (single photosensitizer concentration: 2.5 μg mL^{-1}; photosensitizer mixture: 1.25 μg mL^{-1} for each photosensitizer) and incubated for 5 h. Then, growth medium was renewed and samples were illuminated for 1 min (fluorescent tube SYLVANIA standard F15W/154, daylight; 6000 Lx; 250 μW; 32 mW cm^{-2}). Subsequently, growth medium was replaced with Annexin V-Fluos labelling

reagent (20 μL), propidium iodide (1 μg mL^{-1}) and Hoechst 33342 (1 μg mL^{-1}) in incubation buffer (10 mM HEPES/NaOH, pH 7.4 [Sigma–Aldrich]; 140 mM NaCl [Sigma–Aldrich]; 5 mM $CaCl_2$ [Sigma–Aldrich]) according to the manufacturer's protocol. Cells were observed using a confocal laser scanning microscope Leica TCS SP5 (Leica Microsystems Inc.) after 15 min of incubation and examination was finished 3 h after Annexin V incubation.

Cytochrome C staining. Cells were seeded on round glass cover slides and treated with photosensitizers as reported above in chapter 2.8. After illumination (1 min, fluorescent tube SYLVANIA standard F15W/154, daylight; 6000 Lx; 250 μW; 32 mW cm^{-2}) supernatant was replaced with 1% paraformaldehyde, 0.33% sucrose in PBS for 30 min at different time points after illumination (0, 1 and 3 h). Afterward, cells were washed two times with PBS and permeabilized with 0.01% Triton X-100 (Roche) for 2 min at room temperature. After two washing steps with PBS cells were blocked with 0.1% bovine serum albumine (BSA; Calbiochem, San Diego, CA) for 30 min at room temperature. Cell samples were incubated with sheep anti-cytochrome c (1:1000, stock concentration 1.5 mg mL^{-1}; Sigma–Aldrich) in 0.1% BSA for 1 h at 37°C. Samples were washed and incubated with donkey anti-sheep IgG coupled biotin (1:200; Jackson ImmunoResearch, West Grove, PA) in 0.1% BSA for 1 h at room temperature. Finally, after three washing steps with PBS cells were incubated with Cy5 coupled streptavidin (1:200, Jackson ImmunoResearch) and 4′,6-diamidino-2-phenylindole (DAPI, 1 g mL^{-1}; Roche) in 0.1% BSA for 1 h at room temperature. Subsequently, cells were washed three times in PBS and mounted with GlycerGel mounting medium (Dako, Baar, Switzerland). Samples were monitored using Leica a confocal scanning microscope TCS SP5 (Leica Microsystems Inc.).

Live cell imaging. Cells were seeded (50 000 cells per well) on 8-well plates (ibidi GmbH). After 24 h, growth medium was replaced by medium with single photosensitizers or the 1:1 photosensitizer mixture at concentrations ranging from 0.3 to 10 μg mL^{-1}. Cells were incubated for 5 h. Growth medium was renewed and cells were illuminated for 1 min with white light (fluorescent tube SYLVANIA standard F15W/154, daylight; 6000 Lx; 250 μW; 32 mW cm^{-2}). After illumination ibidi slides were monitored with a live cell imaging wide field microscope Leica LX (Leica Microsystems Inc.). The experiments were performed three times individually each time in doublets. The ibidi slides were screened manually to find appropriate place and differential interference contrast (DIC) images were recorded every 10 min during 18 h.

Quantitative PCR. Cells were grown in 6-well plates (Corning, 500 000 cells per well; doublets for each condition) under standard conditions overnight. Next, single photosensitizer or photosensitizer mixture was incubated for 5 h at final concentrations of 2.5 μg mL^{-1} (1.25 μg mL^{-1} each in the photosensitizer mixture). Subsequently, the photosensitizer growth medium was replaced by fresh one without photosensitizer. Samples were illuminated with white light for 1 min (fluorescent tube SYLVANIA standard F15W/154, daylight; 6000 Lx; 250 μW; 32 mW cm^{-2}). RNA extraction was made using NucleoSpin RNA II Kit (Macherey-Nagel, Oensingen, Switzerland) according to the provided protocol. The cells were lysed with 350 μL lysis buffer (RA1) containing 3.5 μL β-mercaptoethanol at different time points (1, 3 and 5 h) and stored at −20°C until usage. The whole extraction procedure was performed in the dark. The final RNA elution step was done with 40 μL RNase-free-water.

Nanodrop and Bioanalyzer measurements: The RNA yield was determined using a Nanodrop-spectrometer (Thermo Scientific, Wilmington, MA) and RNA quality/integrity with a Bioanalyzer Agilent 2100 (Agilent Technologies, Santa Clara, CA). We used either pico-chips for RNA concentrations between 0.2 and 5 ng μL^{-1} or nano-chips for concentrations between 50 and 500 ng μL^{-1} (both chips from Agilent Technologies).

Reverse transcriptase (RT) reaction: RT reactions were performed for each time point and with both cell lines with 100 ng total RNA and the QuantiTect RT-Kit (Qiagen, Hombrechtikon, Switzerland) according to the manufacturer's instructions. The reactions yielded a final volume of 20 μL. cDNAs were kept at −20°C. Negative controls included omission of RT enzyme.

Quantitative polymerase chain reaction (qPCR): The following combinations were used: for heat-shock 70 kDa protein 6 (HSPA6): sense primer (5′-tcatgaagccgagcagtaca-3′), antisense primer (5′-gtttttggcagccactctgt-3′), probe (5′-gctgagga-3′) and for alpha-crystallin B chain (CRYAB): sense primer (5′-cagctggtttgacactggac-3′) and antisense primer (5′-gcttcacatccaggttgaca-3′), probe (5′-cctggaga-3′). Primer/probes were based on the human Universal ProbeLibrary System (Roche) and primers were synthesized by Microsynth. Protocols for qPCR were performed in triplicates in each 10 μL: 1X Absolute QPCR low ROX mix (ABgene), 0.1 μM FAM-labelled Universal ProbeLibrary probe (Roche), 0.4 μM each sense and antisense primer and 1 μL cDNA. qPCR was run in an Applied Biosystems 7500 Fast Real-time PCR System (Applied Biosystems) under the following conditions: 15 min at 95°C and 40 cycles with 15 s at 95°C and 1 min at 60°C. Statistical analyses were performed using the REST software (http://gene-quantification.com).

RESULTS

Absorption and emission spectra

We determined the absorption and emission spectra of hypericin and Foslipos® and the mixture of both at a range from 300 to 800 nm (Fig. 1). Major absorption bands for hypericin (Fig. 1A) were found in the range of 300–350, 450–500 and 550–600 nm. For Foslipos® absorption maxima (Fig. 1A) were found at 380–450 nm and around 600 nm. For the mixture the absorption bands (Fig. 1A) were the summation of hypericin and Foslipos® bands together. The emission wavelengths for hypericin (Fig. 1B) were detected in the range from 580 to 650 nm. Foslipos® (Fig. 1B) had one emission maximum at 650 nm. Measurements with the photosensitizer mixture (Fig. 1B) displayed the summation of hypericin and Foslipos® emission peaks. Taken together no additional peaks were detected in the mixture; the peak intensity and the peak patterns remained the same if compared to single photosensitizer measurements.

Singlet oxygen luminescence measurements

Singlet oxygen yield measurements for hypericin, Foslipos® and their 1:1 mixture were performed using $^1O_2$ luminescence at 1270 nm. The triplet quantum yield for 100% hypericin in EtOH was $\Phi_\Delta = 0.25$ and for 100% Foslipos® $\Phi_\Delta = 0.66$. The triplet quantum yield for the 1:1 photosensitizer mixture measurements at 590 nm was $\Phi_\Delta = 0.32 \pm 5\%$ and for 415 nm $\Phi_\Delta = 0.45 \pm 5\%$ (data shown in Figure S1).

Singlet oxygen measurement with SOSG reagent

The production of singlet oxygen was additionally observed over 1 h with SOSG reagent, which is highly selective for singlet oxygen. The results are shown in Fig. 2. Singlet oxygen yield produced with hypericin-PDT achieved a plateau approximately after 35 min while the singlet oxygen yield produced with Foslipos®-PDT was increasing linearly over time. The accumulation of singlet oxygen produced with Foslipos® after 1 h was almost five times higher than the values recorded for hypericin. The singlet oxygen yield for the photosensitizer mixture corresponded approximately to the summation of half of the $^1O_2$ yields of single photosensitizers.

ROS measurements with CM-H_2DCFDA reagent

Besides the singlet oxygen yield measurements we observed the intracellular production of other ROS such as hydrogen peroxide H_2O_2, hydroxyl radicals $HO^\bullet$, peroxyl radicals $ROO^\bullet$ and peroxynitrite anions $ONOO^-$. We used the non fluorescent cell-permeable indicator CM-H_2DCFDA for our live cell experiments

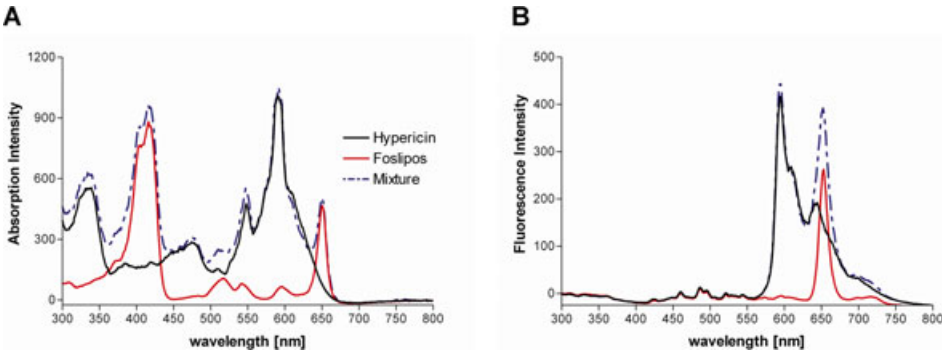

Figure 1. Absorption (A) and emission (B) spectra of photosensitizers used in the study. Shown in black are hypericin spectra, Foslipos® in red and mixture of both in dashed-blue.

(Fig. 3). This substance becomes fluorescent after cellular oxidation and removal of acetate groups by cellular esterases. The pictures showed that both cell lines accumulated high amounts of fluorescent CM-H_2DCFDA directly after hypericin treatment and illumination. The maximum fluorescence intensity in hypericin-treated UMB-SCC 745 cells was found after 2 h. UMB-SCC 969 displayed lower fluorescence intensity but accumulated fluorescent dye was always detectable during examination. In both cell lines membrane blebbing and apoptotic bodies were visible (see Figures S2–S4). After Foslipos® treatment ROS were not detectable in UMB-SCC 745 but CM-H_2DCFDA fluorescence was visible in UMB-SCC 969 immediately after illumination albeit in a weaker manner than observed for hypericin treated UMB-SCC 969 cells. At later time points during the observation Foslipos®-treated cells did not display fluorescent CM-H_2DCFDA. Shrinkage of cells was observed after 2 h. In case of the treatment with both photosensitizers maximum CM-H_2DCFDA fluorescence for UMB-SCC 969 was detectable directly after illumination (0 h) which decreased over time (1 and 2 h). UMB-SCC 745 displayed stronger fluorescence after 1 h if compared to UMB-SCC 969. The maximum fluorescence for UMB-SCC 745 was detected between 1 and 2 h. Membrane blebbing, apoptotic bodies and cell shrinkage was also observable as reported for hypericin-treated cells.

Photosensitizer photobleaching experiments

Singlet oxygen and ROS production is dependent on photosensitizer stability. Photobleaching experiments were performed with two different light sources. The light source which was used for all experiments (6000 Lx; 250 μW; 32 mW cm^{-2}) did not induce photobleaching effects (data not shown). Illumination with 10 light bulbs (9 W per 570 lm, light spectra in Fig. 4D) showed that hypericin was photo-stable even after 23.5 h (Fig. 4A). In contrast, Foslipos® was completely photo-bleached after 6 h (Fig. 4B). In case of the 1:1 mixture of both photosensitizers hypericin did not show any difference in its photo-stability if compared with the single measurement but we could register less intense photobleaching for Foslipos®. After 8 h the Foslipos® peak was still visible. Total photobleaching for the Foslipos® peak in the photosensitizer mixture was achieved after 21 h (Fig. 4C).

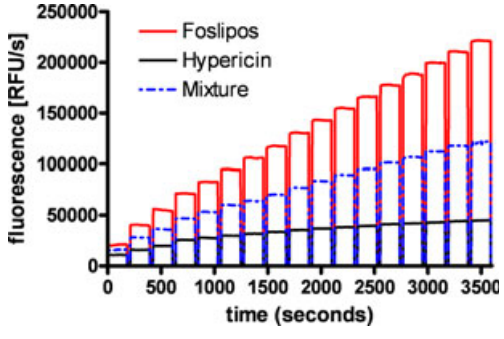

Figure 2. Singlet oxygen measurements performed with Singlet Oxygen Sensor Green (SOSG) assays after PDT with Foslipos® (red), hypericin (black) and the mixture of both photosensitizers (dashed-blue). Photosensitizer concentration was 2.5 μg mL^{-1} for single photosensitizers and in the mixture 1.25 μg mL^{-1} each. Measurements were performed at an excitation wavelength of 504 nm and an emission wavelength at 525 nm.

Cell viability assay

MTT assays were performed 1 day after UMB-SCC 745 and UMB-SCC 969 cells were incubated with hypericin, Foslipos® and their 1:1 mixture for 5 h and illuminated with white light for 1 min (6000 Lx; 250 μW; 32 mW cm^{-2}; Fig. 5). The viability for hypericin-treated cells was reduced by 96% for UMB-SCC 745 and by 90% for UMB-SCC 969. Cell viability for Foslipos®-treated cells was reduced by 83% for both cell lines. Photosensitizer mixture-treated cells displayed a 94% viability reduction for UMB-SCC 745 and a 90% decrease for UMB-SCC 969. Differences for individual photosensitizers between both cell lines were not significant. The statistical evaluation (one-way ANOVA Tukey's test) showed that the PDT effect in Foslipos®-treated UMB-SCC 745 cells differs significantly to hypericin and photosensitizer mixture-treated cells (Tukey's Multiple Comparison Test, $P < 0.05$ was considered statistically significant). Cell viability differences between hypericin and photosensitizer mixture treated UMB-SCC 745 cells were not biologically significant. In case of UMB-SCC 969 cells a significant viability difference was only detectable between hypericin- and Foslipos®-treated cells.

Morphological cell changes after PDT

Morphological cell changes after PDT were monitored with wide field microscopy. In Fig. 6A DIC pictures of UMB-SCC 745 cells and in Fig. 6B DIC pictures of UMB-SCC 969 cells treated with hypericin, Foslipos® and photosensitizer mixture after different time periods (0, 3 and 17 h) are shown (see supporting data). Hypericin-treated cells showed morphological changes immediately after illumination for both cell lines. Directly after illumination individual cells started to shrink, membrane blebbing and membrane vesiculation (microparticle formation)

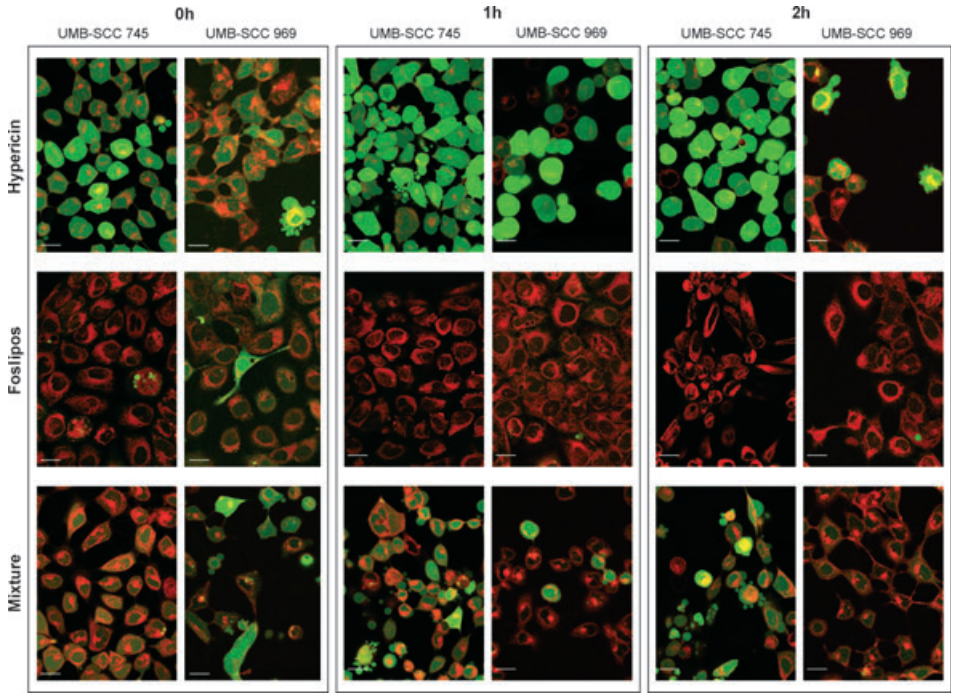

Figure 3. Confocal laser scanning microscopy pictures showing intracellular accumulation of CM-H_2DCFDA (in green) after PDT in both cell lines at different time points (0, 1 and 2 h) and photosensitizer treatments (hypericin, Foslipos® and the mixture of both, red fluorescence). Scale bars = 30 μm.

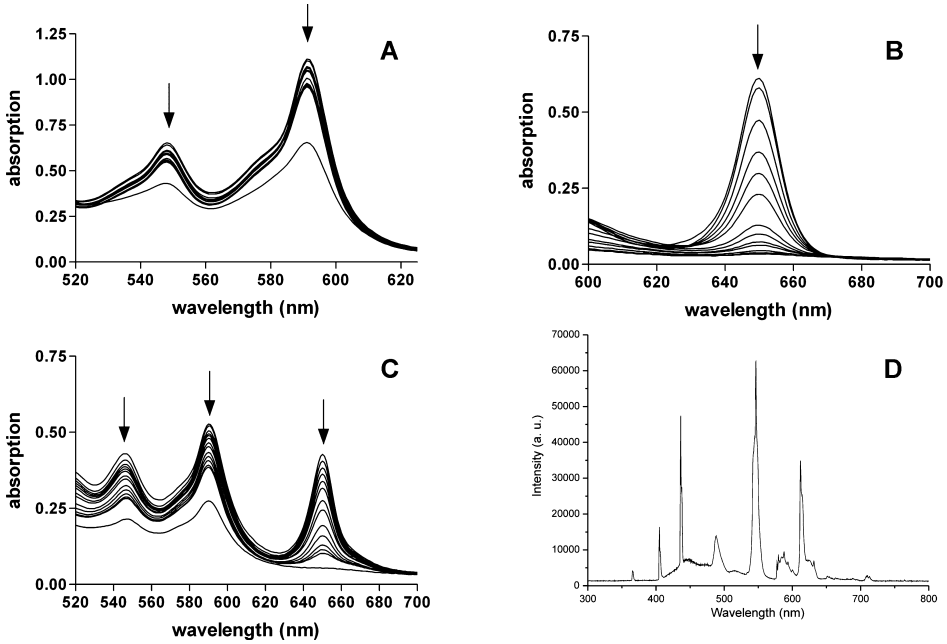

Figure 4. Spectra in (A) are showing photobleaching effect of major hypericin (2×10^{-5} M) emission peaks in ethanol (time: 0, 5, 15, 30 and 45 min, 1, 1.5, 2, 2.5, 3, 3.5, 4, 4.5, 5 and 23.5 h), in (B) photobleaching effects of Foslipos® (2×10^{-5} M) in water (time: 0, 5, 15, 30 and 60 min, 1.5, 2, 2.5, 3, 4, 5 and 6 h) and in (C) the photobleaching effects of the 1:1 mixture of both photosensitizers (time: 0, 10, 20, 30 and 45 min, 1, 1.5, 2, 3, 4, 5, 6, 7 and 21 h). In (D) shown is spectrum of Osram Dulux S 865 white light. The black arrows show decrease of signal intensity.

were visible and finally cell breakage in smaller pieces (apoptotic bodies) was monitored (see supplementary data). After 3 h more than 30% of cells displayed such behavior. The majority of cells died within 12 h. Foslipos® treated cells showed a different behavior post illumination if compared to hypericin-treated ones. Cell contraction, which is an initially visible cell death indicator, was monitored after 4 h for UMB-SCC 745 and 6 h for UMB-SCC 969. Few cells (*ca* 3% of the cell population) showed similar behavior as described for hypericin-treated cells (membrane blebbing and vesiculation, apoptotic bodies), but the majority of cells started to shrink and to detach from the surface. After 12 h cells were found detached in the growth medium in large cell

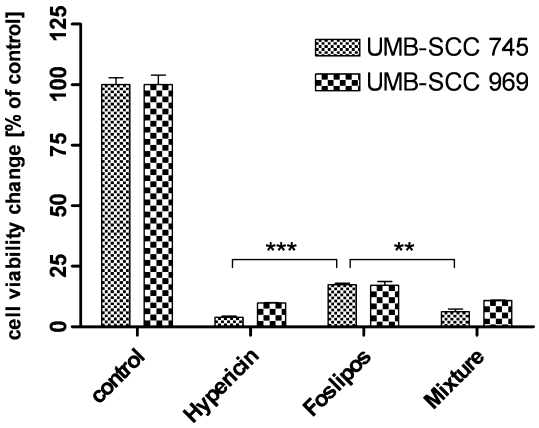

Figure 5. Cell viability change (MTT assays) 24 h after photosensitizer treatment (5 h incubation, 2.5 μg mL^{-1} for single photosensitizer and 1.25 μg mL^{-1} for each photosensitizer in the mixture) and illumination with white light (1 min, 6000 Lx; 250 μW; 32 mW cm^{-2}) on both cell lines. The samples for each condition were in sextuplicates and the experiment was performed independently three times. The software used for statistical analysis (one-way ANOVA Tukey's test) was GRAPHPAD PRISM. The statistical significance was expressed as *P*-values (***$P < 0.001$ and **$P < 0.01$).

aggregates. Morphological changes for photosensitizer mixture-treated cells were visible immediately after illumination. Initially, illuminated cells indicated more resemblance to hypericin-treated cells than to Foslipos®-treated ones. At later time points (5 h post illumination) membrane bulging was observable followed by membrane rupture (data not shown). Cell residues remained immobile and attached on the slide surface. Both cell lines displayed similar behavior.

Cell death pathways

Morphological examinations emphasized that hypericin-treated cells followed rather a programmed (apoptosis) and Foslipos® an un-programmed (necrosis) cell death. The photosensitizer mixture-treated cells displayed characteristics of both apoptosis and necrosis. Active caspases during PDT caused death processes and were detected by covalent binding of FLICA™ agents to active caspases (Fig. 7, additional figures in supplementary data: Figures S2–S4). In UMB-SCC 745 and UMB-SCC 969 cells treated with hypericin caspases were detected 1 h after illumination. Over time, cells were shrinking continuously and at late time points (4 h) cells were round in shape, caspase fluorescence was only visible in a minority of the present cells and Hoechst dye did not stain the nuclei very well. Only few cells could be found on the cover slides. Foslipos®-treated cells first displayed cell shrinkage and detachment from slides. Caspase activity was not observable in UMB-SCC 745 cells. Still, UMB-SCC 969 cells treated with Foslipos® showed low caspase fluorescence in a few cells. Aggregates of dead cells (in both cell lines) were found on slides 4 h post illumination. The nuclei could only partly be stained using Hoechst dye. The photosensitizer mixture-treated cells displayed caspase activity in UMB-SCC 745 after 2 h. UMB-SCC 969 showed caspase activity only in a few cells. Four hours after illumination cells (both cell lines) were shrunken and round, but they did not build cell aggregates as seen in Foslipos®-treated cells. Also, here nuclei staining could not be achieved as in untreated cells.

Annexin V assay results obtained for UMB-SCC 745 cells are shown in Figure 8A (additional figures in supplementary data: Figures S2–S4). Hypericin-treated cells showed first annexin staining of cell membranes between 1 and 2 h. Partial propidium iodide nuclear staining was detectable at later time points (2–3 h). Annexin V maximum fluorescence was detectable between 2 and 3 h. Membrane blebbing and membrane vesiculations were visible. For Foslipos®-treated UMB-SCC 745 cells annexin V as well as nuclear propidium iodide co-staining was detectable between 2 and 3 h. Only a small number of cells (2–3% of the cell population) were not stained with propidium iodide. UMB-SCC 745 cells, which were treated with photosensitizer mixture showed annexin V staining between 2 and 3 h including propidium iodide co-staining. Figure 8B shows the annexin V assay results achieved for the UMB-SCC 969 cell line. Annexin V staining for hypericin-treated cells after 1 h was not pronounced as in UMB-SCC 745, but after 2 h the staining effect was equally prominent. Partial propidium iodide nuclear staining was detectable at later time points (2–3 h). Foslipos®-treated UMB-SCC 969 cells displayed comparable results achieved for the UMB-SCC 745 cell line. Photosensitizer mixture treated UMB-SCC 969 cells at later time points (2–3 h) displayed more annexin V and propidium iodide co-staining if compared to UMB-SCC 745 cells.

Cytochrome C after PDT was monitored after three different time periods (0, 1 and 3 h). Figure 9 (additional figures in supplementary data: Figures S2–S4) displays cytochrome C staining for all three photosensitizer treatments over 1 and 3 h. The UMB-SCC 745 cells displayed well-defined mitochondria staining for all photosensitizers after 1 h. No cytochrome C release was observed. After 3 h a partly cytochrome C-release was observable. Hypericin-treated UMB-SCC 969 cells displayed already after 1 h cytochrome C-staining in the cytoplasm and after 3 h cytoplasmic staining was even more prominent. Foslipos®-treated UMB-SCC 969 cells displayed well-defined mitochondria staining for all time points. Photosensitizer-mixture treated UMB-SCC 969 cells displayed similar results as reported for hypericin treatment in this cell line. Staining in the cytoplasm was less pronounced, but cytochrome C-release was detectable.

Relative quantification of gene expression

Analyses of qPCR data revealed that in controls HSPA6 mRNA was expressed whereas CRYAB transcripts were barely detectable. However, after PDT with Foslipos®, hypericin or the mixture, both genes were highly up-regulated over time in UMB-SCC 745 and UMB-SCC 969 compared to untreated controls. The detailed results of qPCR data are presented in Table 1.

DISCUSSION

The use of PDT in cancer treatment gained on importance during the last decade, however, the urge in improving the efficiency of this treatment modality is still high. For this purpose PDT had been combined with *e.g.* hyperthermia (10,11), radiation (12–14) and chemotherapy (15–17), showing in most cases synergistic or additive effects. In contrast, little is known about possible advantages of combining different types of photosensitizers for PDT (7, 8). In our previous study (Besic Gyenge *et al.* (2012) *Photodiagnosis Photodyn. Ther*. (In press, DOI: 10.1016/j.pdpdt.2012.03.006) we thus examined possible effects of the combination of hypericin and Foslipos® on two HNSCC cell lines in the dark. We showed that

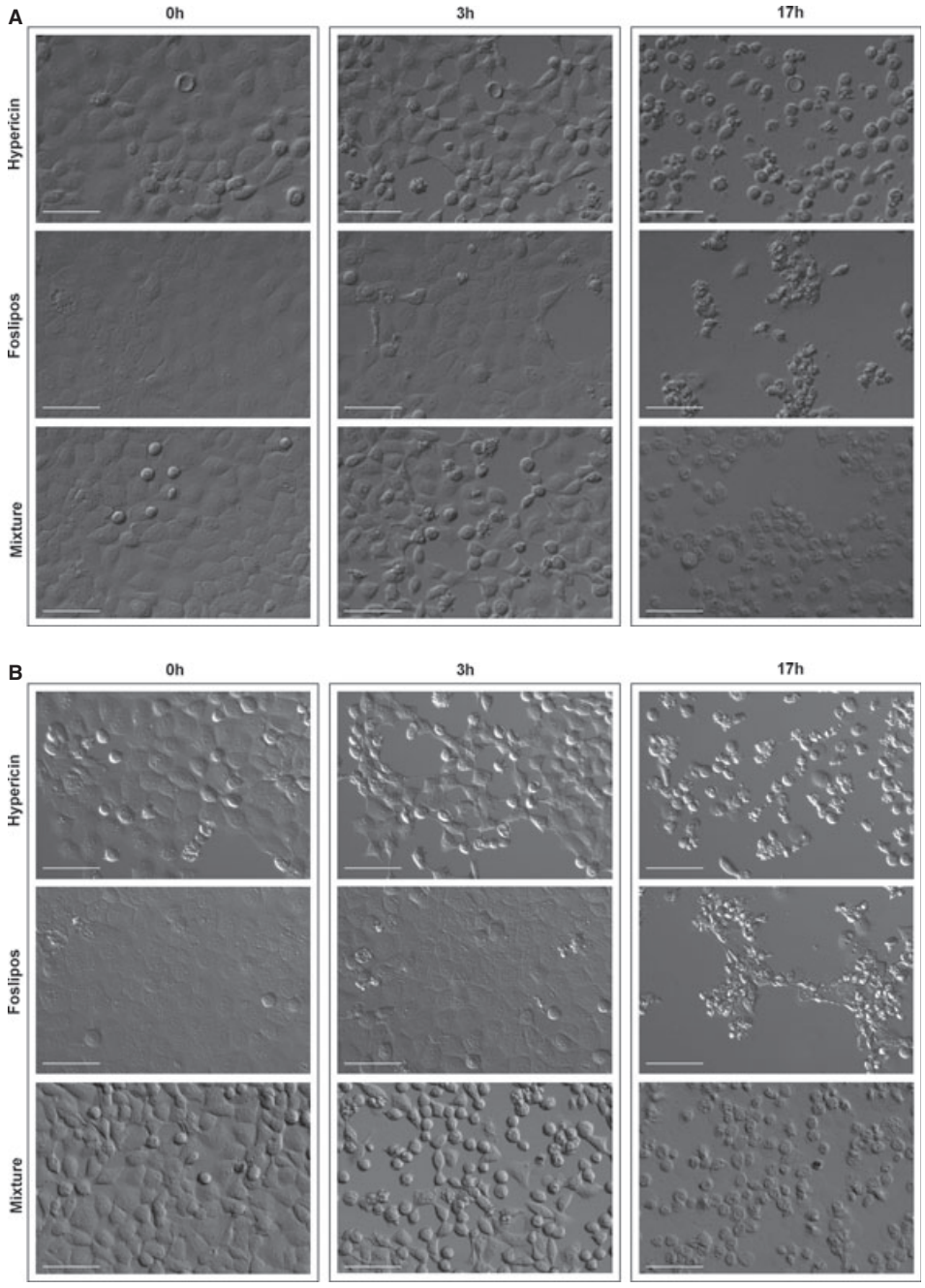

Figure 6. Live cell wide field microscopy pictures after PDT in (A) UMB-SCC 745 and (B) UMB-SCC 969. Incubation time of photosensitizers was 5 h (concentration of single photosensitizer was 2.5 μg mL^{-1} and in the mixture 1.25 μg mL^{-1} for each photosensitizer), illumination 1 min with white light (6000 Lx; 250 μW; 32 mW cm^{-2}). Scale bars = 100 μm.

applying these photosensitizers in combination is decreasing *in vitro* dark toxicity without influencing their physicochemical properties or behavior. These promising results prompted us to now explore possible advantages of a combination of hypericin and Foslipos® for PDT, using the same HNSCC cell models.

We found that the absorption and emission spectra of the photosensitizer combination did not show any mutual quenching and fluorescence interactions, *i.e.* peak pattern remained unchanged if compared to single photosensitizer measurements. It is thus possible to apply illumination conditions established for single photosensitizers. Since the absorption bands in the photosensitizer mixture were the combination of the bands of single photosensitizers one should keep in mind for later applications that the light source has to cover the whole range of absorption spectra for both photosensitizers. For this purpose, the application of white light or a combination of light-emitting diodes (18,19) could be very effective and at low costs compared to lasers.

Because PDT effects are highly dependent on the photosensitizer's singlet oxygen and ROS production efficacy, three different assays were performed to elaborate yields in the photosensitizer mixture compared to single photosensitizers and to explore possible quenching effects in the mixture. The oxygen triplet quantum yield measurement for Foslipos® (in EtOH) yielded in 0.66 which is higher than reported before for mTHPC

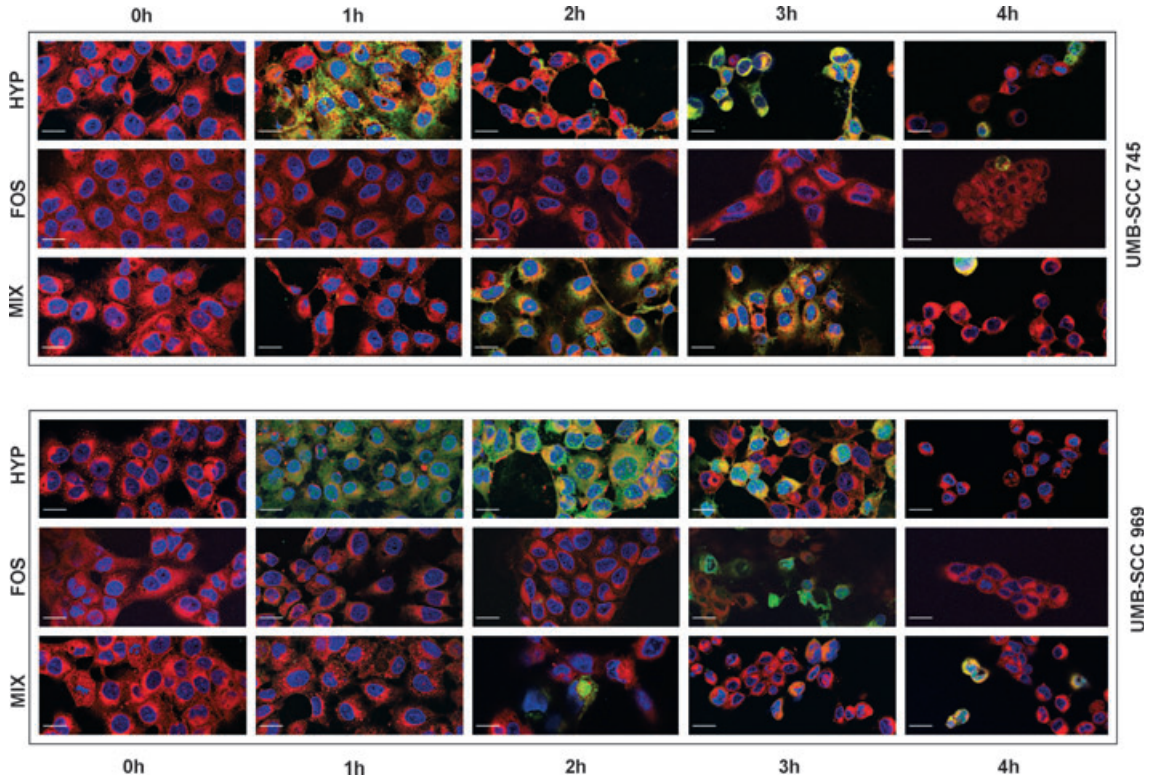

Figure 7. Confocal laser scanning microscopy pictures of caspase activity on both cell lines after PDT and illumination (1 min, 6000 Lx; 250 μW; 32 mW cm^{-2}). The concentration of single photosensitizer was 2.5 μg mL^{-1} and in the mixture concentration was 1.25 μg mL^{-1} for each photosensitizer. Shown in blue are nuclei, in red photosensitizers and in green caspases. Scale bars = 30 μm.

(Φ_Δ = 0.3) (20), but correlates with measurements of mTHPC loaded into human serum albumin (HSA) nanoparticles in D_2O (Φ_Δ = 0.65; 21). Hypericin triplet quantum yield in methanol was found before to be 0.39 (22), in our study we measured it in EtOH and obtained 0.25. The inconsistencies could be explained by differences in measurement conditions and purity of the hypericin extraction. It is known that hypericin triplet state is susceptible to quenching not only by oxygen but also by its tautomeric form and/or other energy acceptors and donors present in the solution (23). In addition, formation of hypericin aggregates may lead to a decreased singlet oxygen production (24). When applying photosensitizers in the mixture it should be considered that photons are divided between photosensitizers and the production of singlet oxygen or ROS is highly dependent on both photosensitizers and their direct biological environment. Singlet oxygen yield measurements (at 417 and 590 nm) for the photosensitizer mixture did not display any synergistic effects. It was higher if compared to the singlet oxygen yield generated by hypericin, but lower if compared to Foslipos® treatment alone.

Another approach for singlet oxygen measurement included a highly $^1O_2$ selective SOSG assay. We found that after 35 min hypericin-mediated accumulation of singlet oxygen achieved a plateau whereas in case of Foslipos® a continuous increase was detected. Achieving a plateau in case of hypericin-mediated $^1O_2$ generation cannot be explained by photobleaching effects because we could not observe photodegradation with our illumination conditions (6000 Lx; 250 μW; 32 mW cm^{-2}). However, impurities in the hypericin extract, possible chemical reactions between hypericin and SOSG agent and/or formation of hypericin aggregates may have been causative. Because mTHPC is embedded in liposomes, photosensitizer aggregation or chemical reactions with SOSG agent are less possible as reported for mTHPC in solution (25). Singlet oxygen generation and therewith related Foslipos® fast relaxation to the ground state coupled with photosensitizer photo-stability may have allowed the continuous SOSG fluorescence increase. Data for the photosensitizer 1:1 mixture were in line with the theoretically expected values, but, in summary, were better than hypericin alone and worse than Foslipos® alone.

Microscopic evaluations of CM-H_2DCFDA showed that PDT with hypericin resulted in a generation of ROS whereas for Foslipos®-treated cells no ROS accumulation could be detected. However, the latter does not generally exclude ROS production by Foslipos®-mediated PDT in our models, because the known fast kinetics of this process (26) may have led to an early disruption of the plasma membrane and an associated release of detectable ROS. Notably, after the treatment with the photosensitizer mixture ROS fluorescence was less compared to treatment with hypericin alone, possibly reflecting the fact that in the mixture only half of hypericin molecules are present.

It is reported that the excited state for mTHPC in solution has an apparent triplet state life time of *ca* 250 ns in air (27). The triplet state life time for hypericin was found to be 370 ns (23). These findings indicated that as long as the photosensitizer molecule is not degraded/photobleached it can return to the ground state and under repeated illumination and available molecular oxygen singlet oxygen and ROS production can be

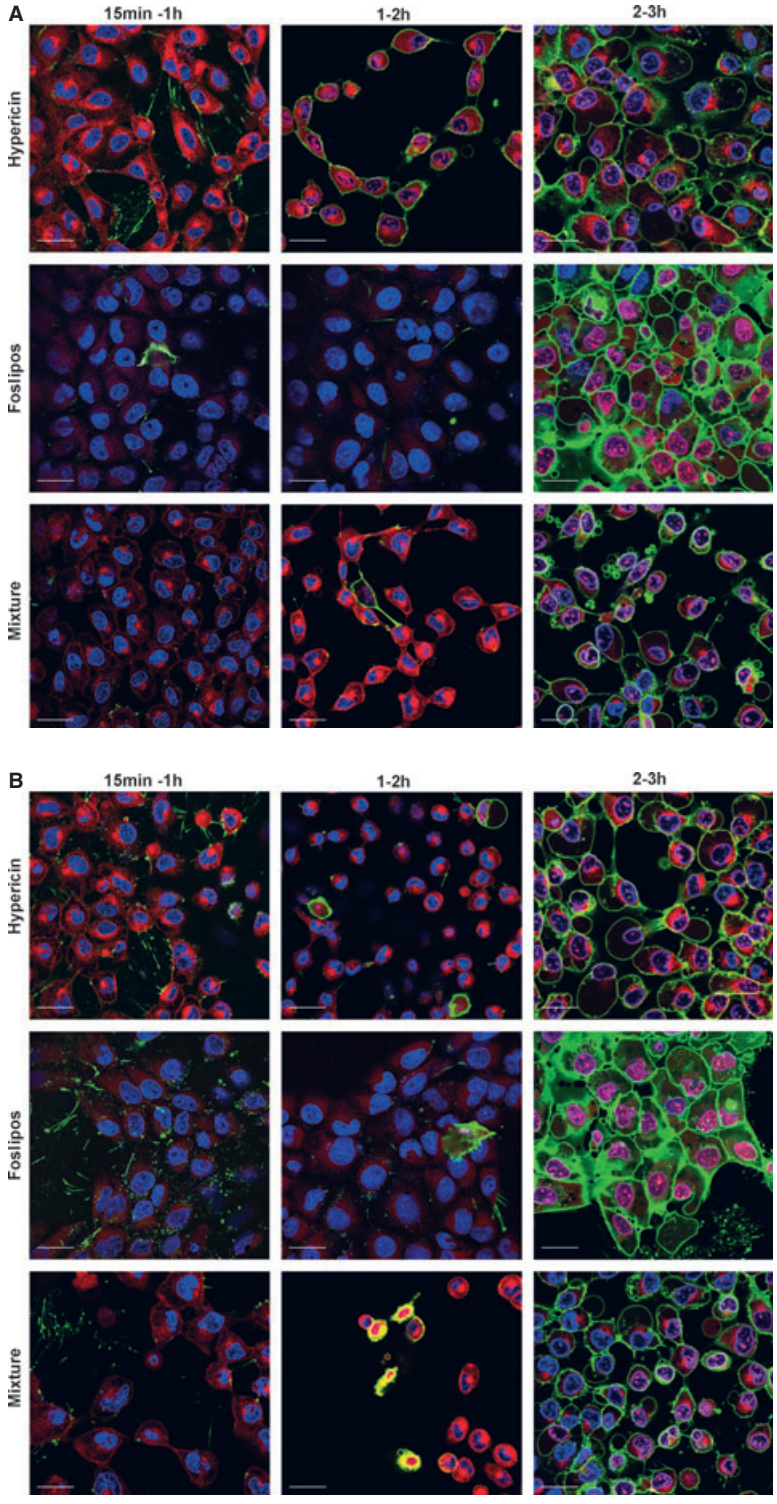

Figure 8. Live cell confocal laser scanning microscopy pictures of annexin V and PI? exposure after PDT on (A) UMB-SCC 745 and (B) UMB-SCC 969 cells at different time points. Incubation time of photosensitizers was 5 h and concentrations were 2.5 μg mL^{-1} for single photosensitizer and 1.25 μg mL^{-1} in the mixture for each photosensitizer. Illumination time was 1 min with 6000 Lx; 250 μW; 32 mW cm^{-2}. In green is shown annexin V, in blue nuclei, in red photosensitizers and in magenta propidium iodide. Scale bars = 30 μm.

expected. Stability of photosensitizers is thus on the one hand very important for effective PDT, but on the other hand major drawbacks may occur if applied *in vivo* (long persistence of skin photosensitivity) (28).

With our illumination conditions (6000 Lx; 250 μW; 32 mW cm^{-2}), no photobleaching of the photosensitizers could be observed (neither alone nor in the mixture) within a time frame of 3 h. Many studies showed that light doses and available

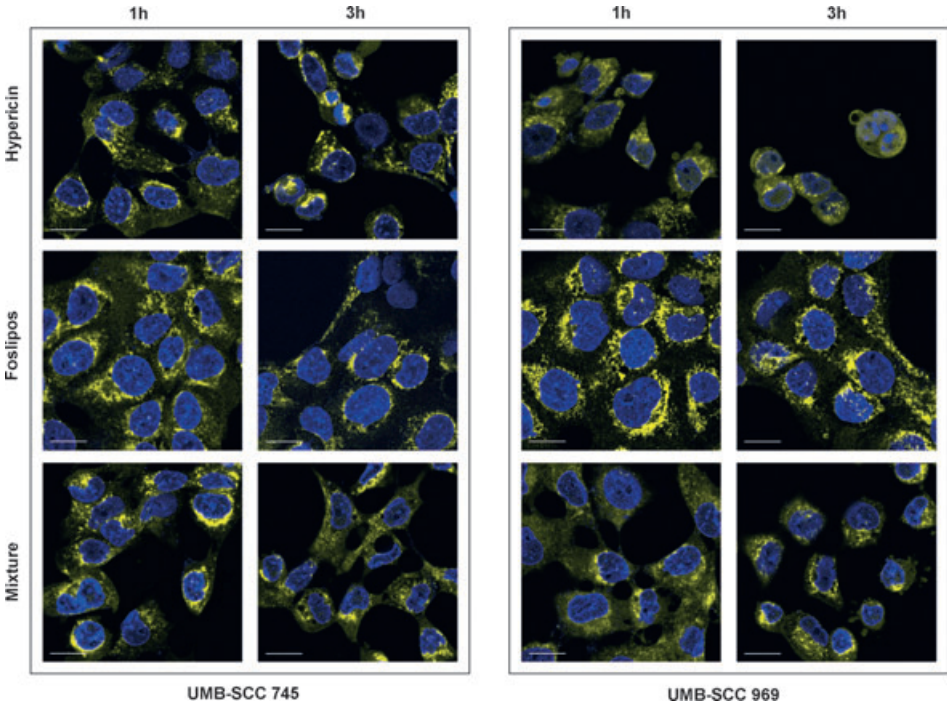

Figure 9. Cytochrome C staining in both cell lines over 1 and 3 h. Incubation time of photosensitizers was 5 h and concentrations were 2.5 μg mL^{-1} for single photosensitizer and 1.25 μg mL^{-1} of each photosensitizer in the mixture. Illumination time was 1 min with 6000 Lx; 250 μW; 32 mW cm^{-2}. Shown in yellow is cytochrome C staining and in blue cell nuclei staining (DAPI). Scale bars = 25 μm.

Table 1. Quantitative analysis of real-time polymerase chain reaction 1, 3 and 5 h after PDT with Foslipos® (FOS), hypericin (HYP) and the 1:1 mixture of both photosensitizers (MIX) in UMB-SCC 745 (745) and UMB-SCC 969 (969) cell lines. Relative expression ratios of heat shock 70 kDa protein 6 (HSPA6) and alpha-crystallin B chain (CRYAB), expressed as fold changes compared to untreated controls (all samples normalized to glyceraldehyde-3-phosphate dehydrogenase).

		1 h			3 h			5 h		
Gene	Cell line	FOS	HYP	MIX	FOS	HYP	MIX	FOS	HYP	MIX
HSPA6	745	+1526.3	+779.3	+1585.0	+9311.3	+20790.4	+15678.5	+24849.0	+38007.6	+102273.1
	969	+1792.0	+834.8	+777.9	+7305.0	+21081.2	+7847.9	+13252.7	+63861.8	+16459.5
CRYAB	745	+3.2	+1.9	+2.4	+22.6	+36.0	+59.8	+137.4	+74.9	+173.6
	969	+6.4	+2.1	+4.5	+29.6	+14.0	+33.4	+72.8	+171.6	+168.6

molecular oxygen play a crucial role in photosensitizer photobleaching (29). Although higher illumination rates can induce high photosensitizer photobleaching and hypoxia, it had been reported that lower fluence-rates give favorable PDT treatment responses (30). Stability of the photosensitizer may be important for effective PDT, since undegraded/non bleached photosensitizers can return to the ground state and may be repetitively activated.

However, to investigate whether or not in the mixture, photosensitizers are subjected to changed bleaching kinetics we used higher light doses. Compared to photobleaching of single photosensitizers, the mixture displayed a strongly delayed bleaching of Foslipos®, indicating that in the mixture this photosensitizer may have a prolonged activity. With lower mTHPC doses in combination with a greater dose of light strong tumor necrosis during PDT treatment and only a minor damage to normal tissue was observed (31). Photobleaching is closely related to singlet oxygen production. The observed lower singlet oxygen yield in the mixture (compared to Foslipos® alone) may therefore be the explanation for prolonged photobleaching kinetics. Photosensitizer aggregations or influence on their photo-physics due to their near proximity could also have an impact on Foslipos® photobleaching behavior.

Under our experimental conditions, number of viable cells were comparable after PDT with hypericin and the photosensitizer mixture, whereas cell survival was slightly higher after Foslipos®-induced PDT. A cell viability difference was also detectable between the two cell lines. The high efficiency of PDT with hypericin (32, 33) and mTHPC formulations (32) had been previously shown. However, direct comparisons between our studies and other studies are generally difficult due to the use of different light sources, cell lines and incubation conditions.

Investigated morphologically and with different assays we found that PDT with our photosensitizers resulted in different modes of cell death: hypericin-treated cells showed features of apoptotic cell death, Foslipos®-treated cells displayed characteristics of necrotic cell death and photosensitizer mixture-treated cells showed a combination of initially apoptotic and later necrotic cell death features. However, it had been shown in many studies that

the cell death mechanisms in PDT depend on many parameters, including *e.g.* photosensitizer concentrations, light doses, cellular redox systems or cell line (34). The different modes of cell death in our study may be related to the observed differences in intracellular localization of the two photosensitizers (diffuse distribution of Foslipos® and membrane-associated localization of hypericin, Besic Gyenge *et al.* (2012) *Photodiagnosis Photodyn. Ther.* (In press, DOI: 10.1016/j.pdpdt.2012.03.006). Destruction of organelles may induce release of pro- and anti-apoptotic proteins and in combination with cell specific redox systems different death pathway are possible. Interestingly, we could show that apoptotic death pathways were triggered by different mechanisms dependent on used cell line. In contrast to UMB-SCC 969 cells, hypericin-mediated apoptotic pathways for UMB-SCC 745 were not initiated by cytochrome C release (Figure 9 and supplementary Figure S2). Provoking certain types of cell death pathways is important in the clinical context, especially in inducing immune responses (35; antitumor activity of inflammatory cells and tumor-sensitized immune reactions) and further *in vivo* studies on trigger mechanisms in PDT would be an important contribution to the understanding and application of PDT.

Analyses of our qPCR data revealed that all PDT regimes induced a pronounced expression of HSP70 and HSP20 family members HSPA6 and CRYAB respectively. Both were among the most prominently up-regulated genes in our previous study on Foslipos®-mediated PDT effects in PC-3 cells (36). We found that HSPA6 mRNA increased from low (UMB-SCC 745) or undetectable (UMB-SCC 969) levels in controls to a several 1000-fold up-regulation at 5 h post illumination. HSP70 is known to be induced by oxidative stress of PDT, as previously reported for mTHPC, hypericin, Photofrin or ALA-induced protoporphyrin IX in different models (36–42). However, while in our study the singlet oxygen quantum yield considerably varied with the photosensitizer, fold changes of HSPA6 mRNA did not significantly differ between hypericin, Foslipos® or the mixture of both. The functional consequences of high HSPA6 levels in HNSCC cell lines used are not clear yet. Although we have not investigated the respective protein in our study, likely, translation to HSP70B' (the protein derived from HSPA6) is initiated after PDT,—especially because (ribosomal) RNA quality does not seem to be compromised. In the light of our data on PDT-related highly effective cell killing, we propose that HSP70B' may rather play a role in promoting cell death mechanisms than to prevent them (43). Our results are in contrast to other PDT studies that reported on cytoprotective effects of HSP70 (42, 44, 45). However, it should be noted that the data from our group are the first to focus on HSPA6 expression in PDT and that it had been shown that different HSP70 members have opposing functions (46). A possible role of up-regulated HSPA6 with regard to anticancer immune activation (39) in our cell lines is investigated in ongoing studies.

After PDT with hypericin, Foslipos® and the mixture, we also observed a strong induction of CRYAB expression that compared to HSPA6, was slightly retarded and failed to reach such extremely high levels over time. However, CRYAB acts as a chaperone and its up-regulation may thus be interpreted as an—eventually unsuccessful—cellular rescue response aiming at capturing oxidative stress-damaged proteins and preventing cell death (47). On the other hand, it should be kept in mind that alpha-crystallin has the ability to complex with hypericin in its monomeric form, thereby extending the lifetime of its triplet excited state (48).

In our previous study, we have shown that the mixture of Foslipos® and hypericin features a reduced dark toxicity *in vitro*, potentially allowing for increased photosensitizer doses *in vivo* (Gyenge *et al.* (2012) *Photodiagnosis Photodyn. Ther.* (In press, DOI: 10.1016/j.pdpdt.2012.03.006). We have herein shown that especially with regard to direct killing effects of tumor cells in PDT the application of the mixture does not show an apparent advantage over the use of single photosensitizers. However, the observed occurrence of a combined apoptotic and necrotic cell death in PDT with the photosensitizer mixture may be clinically beneficial in terms of PDT-related activation of the immune system. This hypothesis is currently under investigation in our laboratories.

Acknowledgements—The study was supported by the FP7 ERA-net EuroNanoMed project TARGET-PDT. We are thankful to Urs Ziegler and his team for their help with confocal microscopy. We also thank Céline Frochot and her team for performing luminescence singlet oxygen measurements. Thanks to Biolitec AG for kindly providing Foslipos®P and to Heidi Roschitzki-Voser and Anina Schneider for their technical assistance.

SUPPORTING INFORMATION

Additional Supporting Information may be found in the online version of this article:

Figure S1. Singlet oxygen quantum yields of hypericin (in red) and Foslipos® (in blue) at excitation wavelengths of 415 nm for Foslipos® (with increasing hypericin concentration) and 590 nm for hypericin (with increasing Foslipos® concentration). Rose Bengal was used as a reference solution.

Figure S2. The figure is exemplarily illustrating different cell stainings and morphological changes post PDT mediated by hypericin treatment in head and neck squamous cell carcinoma cells. (A) DIC and confocal pictures (CM-H_2DCFDA staining) of UMB-SCC 969 cell line indicating different stages of cell death (A1: control cells, A2: cells 2 h after illumination and A3: cells 3 h after illumination). (B) confocal scanning pictures illustrating (on top) the cells stained with FLICA™ caspases assay (DAPI in blue, hypericin in red and caspase stain in green) immediately after illumination and 2 h later (UMB-SCC 969), (in the middle) annexin V death assay (DAPI in blue, hypericin in red and annexin V stain in green) after 1 and 3 h post illumination (UMB-SCC 745) and (on the bottom) cytochrome C staining (DAPI in blue and cytochrome C in yellow) directly after illumination and 3 h later (UMB-SCC 969). Scale bars = 30 μm.

Figure S3. The figure is exemplarily illustrating different cell stainings and morphological changes post PDT mediated by Foslipos® treatment in head and neck squamous cell carcinoma cells. (A) DIC and confocal pictures (CM-H_2DCFDA staining) of UMB-SCC 969 cell line indicating different stages of cell death (A1: control cells, A2: cells 2 h after illumination and A3: cells 4 h after illumination). (B) confocal scanning pictures illustrating (on top) the cells stained with FLICA™ caspases assay (DAPI in blue, hypericin in red and caspase stain in green) immediately after illumination and 3 h later (UMB-SCC 969), (in the middle) annexin V death assay (DAPI in blue, hypericin in red and annexin V stain in green) after 1 and 3 h post illumination (UMB-SCC 745)and (on the bottom) cytochrome C staining (DAPI in blue and cytochrome C in yellow) directly after illumination and 3 h later (UMB-SCC 969). Scale bars = 30 μm.

Figure S4. The figure is exemplarily illustrating different cell stainings and morphological changes post PDT mediated by mixture of hypericin and Foslipos® treatment. (A) DIC and confocal pictures (CM-H_2DCFDA staining) of UMB-SCC 969 cell line indicating different stages of cell death (A1: control cells, A2: cells 2 h after illumination and A3: cells 3 h after illumination). (B) confocal scanning pictures illustrating (on top) the cells stained with FLICA™ caspases assay (DAPI in blue, hypericin in red and caspase stain in green) immediately after illumination and 3 h later (UMB-SCC 745), (in the middle) annexin V death assay (DAPI in blue, hypericin in red and annexin V stain in green) after 1 and 3 h post illumination (UMB-SCC 745) and (on the bottom) cytochrome C staining (DAPI in blue and cytochrome C in yellow) directly after illumination and 3 h later (UMB-SCC 969). Scale bars = 30 μm.

Movie S1. The live cell monitoring after the hypericin treatment (2.5 μg mL^{-1}, 5 h of incubation, 1 min illumination with 6000 Lx; 250 μW; 32 mW cm^{-2}). Pictures were made with wide field microscope Leica LX every 10 min during 18 h.

Movie S2. The live cell monitoring after the Foslipos treatment (2.5 μg mL^{-1}, 5 h of incubation, 1 min illumination with 6000 Lx; 250 μW; 32 mW cm^{-2}). Pictures were made with wide field microscope Leica LX every 10 min during 18 h.

Movie S3. The live cell monitoring after the photosensitizer mixture treatment (1.25 μg mL^{-1} each photosensitizer, 5 h of incubation, 1 min illumination with 6000 Lx; 250 μW; 32 mW cm^{-2}). Pictures were made with wide field microscope Leica LX every 10 min during 18 h.

Please note: Wiley-Blackwell are not responsible for the content or functionality of any supporting materials supplied by the authors. Any queries (other than missing material) should be directed to the corresponding author for the article.

REFERENCES

1. De Saint-Hubert, M., K. Prinsen, L. Mortelmans, A. Verbruggen and F. M. Mottaghy (2009) Molecular imaging of cell death. *Methods* **48** (2), 178–187.
2. Agostinis, P., K. Berg, K. A. Cengel, T. H. Foster, A. W. Girotti, S. O. Gollnick, S. M. Hahn, M. R. Hamblin, A. Juzeniene, D. Kessel, M. Korbelik, J. Moan, P. Mroz, D. Nowis, J. Piette, B. C. Wilson and J. Golab (2011) Photodynamic therapy of cancer: An update. *CA Cancer J. Clin.* **61**(4), 250–281.
3. Dougherty, T. J., C. J. Gomer, B. W. Henderson, G. Jori, D. Kessel, M. Korbelik, J. Moan and Q. Peng (1998) Photodynamic therapy. *J. Natl. Cancer Inst.* **90**(12), 889–905.
4. Brown, S. B., E. A. Brown and I. Walker (2004) The present and future role of photodynamic therapy in cancer treatment. *Lancet Oncol.* **5**(8), 497–508.
5. Biel, M. A. (2010) Photodynamic therapy of head and neck cancers. *Methods Mol. Biol.* **635**, 281–293.
6. Jerjes, W., T. Upile, H. Radhi and C. Hopper (2011) Photodynamic therapy and end-stage tongue base cancer: Short communication. *Head Neck Oncol.* **3**, 49.
7. Ladner, D. P., S. D. Klein, R. A. Steiner and H. Walt (2001) Synergistic toxicity of delta-aminolaevulinic acid-induced protoporphyrin IX used for photodiagnosis and hypericum extract, a herbal antidepressant. *Br. J. Dermatol.* **144**(4), 916–918.
8. Schneider-Yin, X., A. Kurmanaviciene, M. Roth, M. Roos, A. Fedier, E. I. Minder and H. Walt (2009) Hypericin and 5-aminolevulinic acid-induced protoporphyrin IX induce enhanced phototoxicity in human endometrial cancer cells with non-coherent white light. *Photodiagnosis Photodyn. Ther.* **6**(1), 12–18.
9. Lüthi, M., G. E. B, M. Engström, M. Bredell, K. Grätz, H. Walt, R. Gmür and C. Maake (2009) Hypericin- and mTHPC-mediated photodynamic therapy for the treatment of cariogenic bacteria. *Med. Laser Appl.* **24**(4), 227–236.
10. Yanase, S., J. Nomura, Y. Matsumura, Y. Watanabe and T. Tagawa (2009) Synergistic increase in osteosarcoma cell sensitivity to photodynamic therapy with aminolevulinic acid hexyl ester in the presence of hyperthermia. *Photomed. Laser Surg.* **27**(5), 791–797.
11. Yanase, S., J. Nomura, Y. Matsumura, T. Nagata, T. Fujii and T. Tagawa (2006) Synergistic interaction of 5-aminolevulinic acid-based photodynamic therapy with simultaneous hyperthermia in an osteosarcoma tumor model. *Int. J. Oncol.* **29**(2), 365–373.
12. Luksiene, Z., P. Juzenas and J. Moan (2006) Radiosensitization of tumours by porphyrins. *Cancer Lett.* **235**(1), 40–47.
13. Pogue, B. W., J. A. O'Hara, E. Demidenko, C. M. Wilmot, I. A. Goodwin, B. Chen, H. M. Swartz and T. Hasan (2003) Photodynamic therapy with verteporfin in the radiation-induced fibrosarcoma-1 tumor causes enhanced radiation sensitivity. *Cancer Res.* **63**(5), 1025–1033.
14. Allman, R., P. Cowburn and M. Mason (2000) Effect of photodynamic therapy in combination with ionizing radiation on human squamous cell carcinoma cell lines of the head and neck. *Br. J. Cancer* **83**(5), 655–661.
15. Zuluaga, M. F. and N. Lange (2008) Combination of photodynamic therapy with anti-cancer agents. *Curr. Med. Chem.* **15**(17), 1655–1673.
16. Creekmore, S. P. and D. S. Zaharko (1983) Modification of chemotherapeutic effects on L1210 cells using hematoporphyrin and light. *Cancer Res.* **43**(11), 5252–5257.
17. DeWys, W. D. (1975) Current concepts of chemotherapy combined with other modalities for head and neck cancer. *Can. J. Otolaryngol.* **4**(2), 195–204.
18. Neupane, J., S. Ghimire, S. Shakya, L. Chaudhary and V. P. Shrivastava (2010) Effect of light emitting diodes in the photodynamic therapy of rheumatoid arthritis. *Photodiagnosis Photodyn. Ther.* **7**(1), 44–49.
19. Mordon, S. and V. Maunoury (2006) Using white light during photodynamic therapy: Visualization only or treatment? *Eur. J. Gastroenterol. Hepatol.* **18**(7), 765–771.
20. Hadjur, C., L. Norbert, J. Rebstein, P. Monnier, H. van den Bergh and G. Wagnières (1998) Spectroscopic studies of photobleaching and photoproduct formation of meta(tetrahydroxyphenyl)chlorin (m-THPC) used in photodynamic therapy The production of singlet oxygen by m-THPC. *J. Photochem. Photobiol. B, Biol.* **45**(2–3), 170–178.
21. Wacker, M., K. Chen, A. Preuss, K. Possemeyer, B. Roeder and K. Langer (2010) Photosensitizer loaded HSA nanoparticles. I: Preparation and photophysical properties.. *Int. J. Pharm.*, **393**, (1–2), 253–262.
22. Roslaniec, M., H. Weitman, D. Freeman, Y. Mazur and B. Ehrenberg (2000) Liposome binding constants and singlet oxygen quantum yields of hypericin, tetrahydroxy helianthrone and their derivatives: Studies in organic solutions and in liposomes. *J. Photochem. Photobiol. B, Biol.*, **57**, (2–3), 149–158.
23. Darmanyan, A. P. and J. W.S. (1999) Quenching of excited triplet state hyericin with energy acceptors and donors and acceptors of electrons. *J. Phys. Chem. B.* **103**, 3323–3331.
24. Van De Putte, M., T. Roskams, G. Bormans, A. Verbruggen and P. A. De Witte (2006) The impact of aggregation on the biodistribution of hypericin. *Int. J. Oncol.* **28**(3), 655–660.
25. Belitchenko, I., V. Melnikova, L. Bezdetnaya, H. Rezzoug, J. L. Merlin, A. Potapenko and F. Guillemin (1998) Characterization of photodegradation of meta-tetra(hydroxyphenyl)chlorin (mTHPC) in solution: Biological consequences in human tumor cells. *Photochem. Photobiol.* **67**(5), 584–590.
26. Kalyanasundaram, K. and M. Grätzel (1993) Photosensitization and photocatalysis using inorganic and organometallic compounds. In *Catalysis by Metal Complexes* (Edited by K. A. P. Group), pp. 113–155. Kluwer Academic Publishers, Dordrecht.
27. Howe, L., A. Sucheta, O. Einarsdottir and J. Z. Zhang (1999) Time-resolved studies of the excited-state dynamics of meso-tetra(hydroxylphenyl)chlorin in solution. *Photochem. Photobiol.* **69**(6), 617–623.
28. Dougherty, T. J., M. T. Cooper and T. S. Mang (1990) Cutaneous phototoxic occurrences in patients receiving Photofrin. *Lasers Surg. Med.* **10**(5), 485–488.
29. Bonnett, R. and G. Martinez (2001) Photobleaching of sensitisers used in photodynamic therapy. *Tetrahedron* **57**, 9513–9547.
30. Ericson, M. B., C. Sandberg, B. Stenquist, F. Gudmundson, M. Karlsson, A. M. Ros, A. Rosen, O. Larko, A. M. Wennberg and I. Rosdahl (2004) Photodynamic therapy of actinic keratosis at varying

fluence rates: Assessment of photobleaching, pain and primary clinical outcome. *Br. J. Dermatol.* **151**(6), 1204–1212.
31. Ris, H. B., H. J. Altermatt, C. M. Stewart, T. Schaffner, Q. Wang, C. K. Lim, R. Bonnett and U. Althaus (1993) Photodynamic therapy with m-tetrahydroxyphenylchlorin *in vivo*: Optimization of the therapeutic index. *Int. J. Cancer* **55**(2), 245–249.
32. Berlanda, J., T. Kiesslich, V. Engelhardt, B. Krammer and K. Plaetzer (2010) Comparative *in vitro* study on the characteristics of different photosensitizers employed in PDT. *J. Photochem. Photobiol. B, Biol.* **100**(3), 173–180.
33. Wang, X., Y. Guo, S. Yang, C. Wang, X. Fu, J. Wang, Y. Mao, J. Zhang and Y. Li (2010) Cellular and molecular mechanisms of photodynamic hypericin therapy for nasopharyngeal carcinoma cells. *J. Pharmacol. Exp. Ther.* **334**(3), 847–853.
34. Karioti, A. and A. R. Bilia (2010) Hypericins as potential leads for new therapeutics. *Int. J. Mol. Sci.* **11**(2), 562–594.
35. Castano, A. P., P. Mroz and M. R. Hamblin (2006) Photodynamic therapy and anti-tumour immunity. *Nat. Rev. Cancer* **6**(7), 535–545.
36. Gyenge, E. B., S. Hiestand, S. Graefe, H. Walt and C. Maake (2011) Cellular and molecular effects of the liposomal mTHPC derivative Foslipos in prostate carcinoma cells *in vitro*. *Photodiagnosis Photodyn. Ther.* **8**(2), 86–96.
37. Paba, V., M. Quarto, L. Varriale, E. Crescenzi and G. Palumbo (2001) Photo-activation of hypericin with low doses of light promotes apparent photo-resistance in human histiocytic lymphoma U937 cells. *J. Photochem. Photobiol., B*, **60** (2–3), 7–96.
38. Sanovic, R., B. Krammer, S. Grumboeck and T. Verwanger (2009) Time-resolved gene expression profiling of human squamous cell carcinoma cells during the apoptosis process induced by photodynamic treatment with hypericin. *Int. J. Oncol.* **35**(4), 921–939.
39. Korbelik, M., J. Sun and I. Cecic (2005) Photodynamic therapy-induced cell surface expression and release of heat shock proteins: Relevance for tumor response. *Cancer Res.* **65**(3), 1018–1026.
40. Merchant, S. and M. Korbelik (2010) Heat shock protein 70 is acute phase reactant: Response elicited by tumor treatment with photodynamic therapy. *Cell Stress Chaperones* **16**(2), 153–162.
41. Etminan, N., C. Peters, D. Lakbir, E. Bunemann, V. Borger, M. C. Sabel, D. Hanggi, H. J. Steiger, W. Stummer and R. V. Sorg (2011) Heat-shock protein 70-dependent dendritic cell activation by 5-aminolevulinic acid-mediated photodynamic treatment of human glioblastoma spheroids *in vitro*. *Br. J. Cancer* **105**(7), 961–969.
42. Mitra, S., B. R. Giesselman, F. J. De Jesus-Andino and T. H. Foster (2011) Tumor response to mTHPC-mediated photodynamic therapy exhibits strong correlation with extracellular release of HSP70. *Lasers Surg. Med.* **43**(7), 632–643.
43. Arya, R., M. Mallik and S. C. Lakhotia (2007) Heat shock genes—integrating cell survival and death. *J. Biosci.* **32**(3), 595–610.
44. Nonaka, M., H. Ikeda and T. Inokuchi (2004) Inhibitory effect of heat shock protein 70 on apoptosis induced by photodynamic therapy *in vitro*. *Photochem. Photobiol.* **79**(1), 94–98.
45. Gomer, C. J., S. W. Ryter, A. Ferrario, N. Rucker, S. Wong and A. M. Fisher (1996) Photodynamic therapy-mediated oxidative stress can induce expression of heat shock proteins. *Cancer Res.* **56**(10), 2355–2360.
46. Hageman, J., M. A. van Waarde, A. Zylicz, D. Walerych and H. H. Kampinga (2011) The diverse members of the mammalian HSP70 machine show distinct chaperone-like activities. *Biochem. J.* **435**(1), 127–142.
47. Ganea, E. (2001) Chaperone-like activity of alpha-crystallin and other small heat shock proteins. *Curr. Protein Pept. Sci.* **2**(3), 205–225.
48. Sgarbossa, A., N. Angelini, D. Gioffre, T. Youssef, F. Lenci and J. E. Roberts (2000) The uptake, location and fluorescence of hypericin in bovine intact lens. *Curr. Eye Res.* **21**(2), 597–601.

5

GENERAL DISCUSSION

5. General Discussion

Photodynamic therapy (PDT) is an emerging treatment modality with a constantly growing area of application. The long-term treatment experiences, especially from the dermatology field, have shown that there are some advantages in using PDT as opposed to conventional therapy. PDT treatment has resulted in excellent functional as well as aesthetic outcomes. Furthermore, this therapy may be repeated as often as needed with minimal damage to normal tissue structures. PDT also shows promising results in the treatment of patients with unsalvageable tumours where other treatments have failed. These treatments are in the developmental phase and need further improvement [1].

The PDT mode of action is known to involve three key factors: a photosensitizer, light and molecular oxygen. The development of novel photosensitizers and light delivery systems is an ongoing process. In general, the terms of improvement are photosensitizer systemic tolerance, good solubility under physiological conditions, high yield of singlet oxygen and ROS, low photobleaching and light absorbance preferably in deep red region. Some of the established photosensitizers exhibit excellent singlet oxygen and ROS yield and have low photobleaching but they may still suffer from systemic intolerance or poor solubility. Therefore, in the last few years encapsulation in virus-like nanocarriers, liposome, albumine nanoparticles or polymeric micelles has aroused scientific interest [2]. It has been shown that different formulation/ encapsulations of existing drugs exhibit not only potent anti-tumour activity, but they also display highly reduced side effects. In our work on silica-based nanoparticles with $[Ru(byp)_3]Cl_2$ core as a fluorescent dye [3] nanoparticle bio-behaviour in HNSCC cell lines with the aim of developing novel therapeutic strategies was investigated. In this study the interactions of core-shell silica nanoparticles interactions with HNSCC cells and their complex internalisation was elucidated. Gaining this information is essential before active pharmaceutical agents are encapsulated.

In our work we explored *in vitro* possibilities for improving the efficiency of PDT. Furthermore, we have contributed to the understanding of PDT mechanisms of the two most powerful photosensitizers nowadays: a liposomal mTHPC derivative (Foslipos®, a second-generation photosensitizer) and hypericin, the strongest natural occurring photosensitizer. In addition, this is the first study that examined the effects of photosensitizer mixtures in treatments of cancer cells and microorganisms *in vitro*. In the following pages, the most

important results gained from the extensive studies conducted, which are described in detail in enclosed publications and submitted manuscripts (chapters 2-4 and 7) are discussed.

Physico-chemical properties of photosensitizers

In a first step, the physico-chemical properties of applied photosensitizers were examined with a main focus on their mixture. The absorption and emission spectra of the photosensitizer combination did not show any cross effects. Peak pattern and intensity remained unchanged when compared to single photosensitizer measurements. Three different measurement approaches were performed (singlet oxygen luminescence, singlet oxygen sensor green and ROS selective CM-H_2DCFDA reagents) to elaborate singlet oxygen yields and ROS production efficacy and to explore possible quenching effects in the photosensitizer mixture.

The oxygen triplet quantum yield measurements are, in general, dependent on the parameters used, such as chosen measurement solution. Results from our study with Foslipos® correlated with measurements of Wacker et al. [4] where mTHPC was loaded in HSA nanoparticles, but it was higher than reported in the literature where mTHPC [5] was measured alone. Hypericin triplet quantum yield was found to be slightly lower than previously reported [6]. This difference could be explained by individually measurement conditions, hypericin purity and/ or time-dependent formation of hypericin aggregates, which has an high impact on its bio-distribution and singlet oxygen production as reported in the literature [7]. Singlet oxygen yield measurement at 415 nm and 590 nm did not display any cross effects for the photosensitizer mixture.

Additionally, singlet oxygen measurement was conducted with a highly $^1O_2$ selective SOSG reagent. In this measurement hypericin-mediated accumulation of singlet oxygen achieved a plateau after 35 minutes. When Foslipos® was applied, a continuous increase of fluorescence was detected. Collected data for SOSG assay measurements for the photosensitizer mixture were in line with the theoretical values expected. It was assumed that in the case of hypericin mediated $^1O_2$ generation achieving the plateau was connected to the photosensitizer photobleaching effect. Yet in the measurements obtained in our study, photodegradation was not detected when illuminated with used white light. Most likely, remains from plant extraction and/ or hypericin aggregation play a crucial role on this effect. Furthermore, possible chemical reactions between hypericin and SOSG agent and the formation of hypericin aggregates tend to be a more feasible explanation for this observation.

It can be assumed that the results of Foslipos® mediated fluorescence generation and accumulation may be understood to support results obtained. mTHPC, which is embedded in liposomes, most likely prevents the photosensitizer aggregation, and chemical reactions with SOSG agent are less possible for mTHPC in solution [8].

Detection of ROS with CM-H_2DCFDA was performed on HNSCC cell lines and it showed an accumulation of fluorescent dye in hypericin and the photosensitizer mixture treated cells while for Foslipos® treated cells no accumulation was detected. The explanation for the lack of accumulation of the fluorescent CM-H_2DCFDA form for Foslipos® treated cells was found in the deficient cell membrane integrity, which was seen in live cell imaging and/ or confocal pictures.

The experiments on photosensitizer photobleaching with lower light doses indicated that no significant photobleaching could be detected. Therefore, higher light doses were applied in order to examine the possible cross effects in the photosensitizer mixture. Surprisingly, the time for complete Foslipos® bleaching in the mixture was approximately two hours longer then for the single photosensitizer. Since in the mixture both photosensitizers equally absorbed photons and singlet oxygen production was generated by both photosensitizers photobleaching had to be related to these events. Additionally, the photosensitizer aggregations or the influence on their photo-physics due to their near proximity could also have an impact on their photobleaching behaviour.

Photosensitizer uptake, distribution and localisation studies

After the examination of the chemical properties of the photosensitizer, including the generation of singlet oxygen and ROS, photo-stability in solution and possible interactions in the mixture, the uptake kinetics on cancer cells and microorganisms were examined microscopically and spectroscopically. The performed microscopic uptake studies showed quick photosensitizer accumulation in the cells (PC-3 and HNSCC cells) and an even faster accumulation in microorganisms (*Streptococcus sobrinus, Streptococcus mutans, Candida albicans, Aggregibacter aphrophilus, Capnocytophaga ochracea* and *Fusobacterium nucleatum* (data not shown)).

The photosensitizer-uptake and -efflux processes in these studies were similar between cell lines. Uptake of Foslipos® in the initial studies for PC-3, and in subsequent studies for HNSCC, was continuous over 24 hours, while hypericin treated HNSCC cells followed a Gaussian curve distribution with a fluorescence maximum after five hours of incubation.

Other studies [9, 10] found great variations in uptake between individual cell lines resulting in even more pronounced differences in phototoxicity. Additionally, in accordance with many studies, which were done on a variety of human cell lines [11-13], the liposomal preparation of mTHPC did not affect the intracellular distribution when compared with mTHPC alone. Intracellular clearance results, which were made for HNSCC cells displayed that major amount of hypericin was cleared within 24 h with some hypericin aggregates remaining, while Foslipos® clearance was much slower. The slow release of mTHPC and its derivatives from the cells has been reported in several other studies [14, 15] and the reasons remain unclear. The photosensitizer mixture uptake and efflux studies on both UMB-SCC cell lines were comparable to the observations achieved with the single photosensitizers. The two differences were a higher amount of hypericin aggregates after 24 h in the photosensitizer efflux experiment when compared to hypericin alone and lower fluorescence intensity in the uptake study after five hours. The higher amount of hypericin aggregates and the photosensitizers near proximity could eventually cause fluorescence quenching resulting in lower fluorescence intensity. Taken together, these findings indicate slightly different intracellular behaviour of hypericin when combined with Foslipos®.
Interestingly, the uptake studies for microorganisms indicated much faster uptake kinetics. An incubation time of 15 minutes was sufficient to achieve total PDT mediated eradication of examined pathogens, while the intracellular amount of photosensitizers during this incubation time did not affect cells. The short incubation protocols in pathogen treatment are definitely safer and more tolerable for surrounding tissue. They may provide a novel therapy modality on local infections in oral regions.

The PDT effects are highly dependent on intracellular localization places. Thus extensive localization studies were performed in the HNSCC cell- and microorganisms model system. The photosensitizer subcellular localization studies in HNSCC cells indicated that hypericin was mainly found in membranous systems (outer cellular membranes, nuclear membranes, in trans golgi network and perinuclearly), while Foslipos® did not co-localise with any cell organelle stain and it remained diffuse in cytoplasm of both UMB-SCC cell lines and PC-3 cells. In many studies, such as those of Theodossiou et al. [16] or Kiesslich et al. [9] intracellular localisation of photosensitizers was investigated and the results correspond partially with the findings in our studies. Microscopic analyses in examined microorganisms showed similar distribution picture in gram-positive and gram-negative species. *S. sobrinus* and *S. mutans* as well as *C. albicans*, *A. aphrophilus*, *C. ochracea* and *F. nucleatum* (data not

shown) accumulated all used photosensitizers intracellularly. The intracellular photosensitizer localization seems to be driven by many factors such as photosensitizer concentration, incubation time, cell model systems, incubation parameters and/ or environment of the photosensitizer (such as presence of serum proteins or other substances). This was clearly evident from the study performed on microorganisms where photosensitizers were applied in combination with chitosan-thioglycolic acid (TGA), which acted as an enhancer for antimicrobial PDT effects. Here, uptake of Foslipos® was prevented through chitosan-TGA incubation for some microorganisms, resulting in a shift from intracellular to extracellular Foslipos® localization in gram-negative bacteria. In comparision, *C. albicans* and *S. sobrinus* did not display this behaviour. The underlying mechanisms are not clear yet but they may be related to the known lipid-binding capabilities of chitosan [17] and more probable species-specific factors such as cell wall structure.

Cell viability studies without illumination

The photosensitizer mechanisms on cell viability in the dark have, up to date, received very little scientific investigation, most likely due to their complexity. Our study partially examined the said mechanisms. The results demonstrated that Foslipos® treated cells (PC-3 and HNSCC) displayed a significant proliferation decrease only for highest concentration used (10 µg/ mL), while hypericin treatment affected cell viability for all applied concentrations. Many studies have reported dark toxicity of Foslipos® [13], but the mechanisms which affect cell viability were not further investigated. The cell toxic concentrations differ from study to study which might be explained by use of different cell models. Hypericin effects in the dark could be a result of the light independent inhibition of various enzymes [18] such as protein kinase C, protein tyrosine kinases or mitochondrial succinoxidase, all of which play important roles in cell growth, proliferation, survival and death [19, 20]. In addition, hypericin showed a strong light independent inhibitory activity against glutathione reductase and against several species of cytochrome P450 [21, 22], by which various metabolic processes could be affected. Hypericin may also reduce intracellular pH by proton transfer to surrounding molecules leading to pH dependent structural changes in proteins [23]. Any of those findings could account for affected cell proliferation in our study. Surprisingly, the proliferation assays with photosensitizer mixture application in the dark indicated that even with the highest concentrations cell viability remained as in the control samples. The mechanisms underlying the improved tolerability of the photosensitizer mixture

are not clear. However, since hypericin is known to attach to lipoproteins, and is preferably incorporated into lipid membranes [24], it cannot be excluded that in the mixture hypericin interacts with Foslipos® liposomes, thereby changing its bioactivity.
Furthermore, the examinations of RNA quality in HNSCC cell lines and in PC-3 cell line indicated that the overall RNA quality was not influenced by the intracellular accumulation of photosensitizers without illumination. There was not observable difference between the two HNSCC cell lines. Contrasting these results, in the case of hypericin treated UMB-SCC 745 and Foslipos® treated PC-3 cells DNA damage was detected. Since UMB-SCC 745 cells did not show significant differences in photosensitizer uptake, efflux or localisation when compared to UMB-SCC 969 a plausible explanation for the minor DNA damage could be found in the fact that different cell lines were used.

In the study focusing on oral pathogens [25], viability of *S. sobrinus* in the dark was not found to be affected by the photosensitizers used (hypericin, Foslipos® and 1:1 mixture), while *S. mutans* showed high toxic effects when incubated with Foslipos® or the photosensitizer mixture. Furthermore, ineffectiveness of hypericin-mediated PDT in *S. mutans* was observed. These results were unexpected since both microorganisms are traditionally grouped in a common taxonomic cluster. The highly differing sensitivities of the two *Streptococcus* species may be explained by the differences found in the molecular phylogenetic analyses of glucan-producing enzymes and superoxide dismutases, indicating that the two bacteria strains are in fact genetically separate [26-28]. The mechanisms of these effects are unknown and further investigations of the molecular and cellular properties are needed.

In summary, the results from other studies and our own results on cancer cells (PC-3 and HNSCC) and oral pathogens indicate how little we actually understand about the factors that govern photosensitizer generated cellular and bacterial toxicity in the dark. The complex molecular mechanisms behind the photosensitizer dark toxicity remain unclear but further investigations will be in the focus of our future studies.

Cell viability studies after illumination

The cell viability results after illumination on all three cell lines and applied photosensitizers were decreased significantly when compared to control samples. The initial study on PC-3 cells for mTHPC- mediated PDT indicated that kinetics of the reaction were characterised by a two-step process with an initial cell death few minutes after light

application and a second – a stronger one - five hours later. The first PDT effect is likely due to direct reactive oxygen species (ROS) damage. Generation of ROS occurs in fractions of a second after PDT and may kill a population of cells immediately. However, damage caused by ROS seems to merely affect the majority of the cells which rather undergo death processes that takes several hours. Excellent PDT results were achieved also on HNSCC cell lines. Noteworthy are effects with low light and low photosensitizer doses in the mixture conditions especially when compared with Foslipos® treatment alone. The cell viability difference was also detectable between the two cell lines. According to many other studies similar results for Foslipos® and hypericin induced PDT were found [29, 30]. Unfortunately the PDT effects of the photosensitizer combination were not examined in other studies.

The PDT treatments of gram-positive and gram-negative bacteria when combined with TGA-chitosan are very attractive. Our results showed that this treatment modality, with appropriate protocols, may result in 100% bacterial death. The advantages of PDT in comparison to conventional treatments are its proven efficacy on antibiotic-resistant strains, low potential for mutagenicity and photoresistance as well as its broad target spectrum [31]. Interestingly, despite the large spectrum of photoactive agents available only a limited number have been investigated with regards to their antimicrobial applicability. However, it should be emphasised that the application of a mixture of photosensitizer has great potential to target complex microbial populations, as such found in most infections.

Cell death and morphological changes after illumination

The monitoring of morphological cellular changes and the examination of cell death pathways after light application was extensively examined on HNSCC cell lines. Hypericin treated HNSCC cells showed features of apoptotic cell death (cell shrinkage, membrane blebbing and vesiculation, formation of apoptotic bodies), while for Foslipos® treated cells more necrotic cell death outcome (shrinkage of the cells and detaching from the surface) was detected. The photosensitizer mixture treated cells showed initial apoptotic death features and at later points in time necrotic cell death features. The cellular death pathways were verified with caspases activity assay, annexin V death assay and staining of cytochrome C. Foslipos® mediated cell death in both HNSCC cell lines were necrotic by nature. Interestingly, the experiments conducted demonstrated that apoptotic death pathways in hypericin-induced PDT were triggered by different mechanisms depending on the cell line used. The apoptotic pathway for the UMB-SCC 745 cell line was not initiated by cytochrome C release in contrast

to UMB-SCC 969 cells. Programmed cell death seems to be complicated but obviously there are many alternative possibilities to avoid potential intracellular problems resulting in apoptosis. The study by Panzarini et al. showed such a cellular death flexibility [32] by demonstrating that rose bengal acetate could trigger apoptosis by at least four different pathways during the observed time (0 - 12 h) in HeLa cells. The initial apoptosis pathway was the intrinsic pathway, followed by the activation of the extrinisic, caspase-12-dependent and caspases-independent pathways. Finally, apoptosis was rapidly followed by autophagy. Quality-control mechanism of autophagy served as a necrosis protection and Panzarini et al. could predominantly registered apoptosis in HeLa. Necrosis was always negligible in their study. In addition to the cell model used, the intracellular photosensitizer localization places, photosensitizer concentration and applied light doses contribute significantly to the cell death pathways, as reported in many other studies [16, 18, 29, 30, 33-37]. The PDT- mediated cell death pathways are complicated and it seems that apoptosis and necrosis co-exist and interrelate in different proportions. Cellular death trigger mechanisms in PDT are still under investigation. These are very important studies in the clinical context and they will make significant contribution to the understanding and application of PDT *in vivo*.

Molecular mechanisms after illumination

The investigation of affected molecular mechanisms was performed by characterizing the damaging effects on nucleic acids which was supported by RNA- integrity and quality experiments. Surprisingly, directly after illumination a significant number of DNA strand breaks were detected in Foslipos®- treated PC-3 and in hypericin-, Foslipos®- and photosensitizer mixture- treated HNSCC cells (data not shown). Anisotropy imaging studies of mTHPC [38] showed its localization to the nuclear envelope. In addition, our own observations of hypericin's preferably perinuclearly localization might be the reason for the damage of membrane compartments, allowing an immediate ROS-related injury of (peripherally residing) DNA. Rousset et al. [39] reported possible nuclear mTHPC entering during light application in the murine glioma cell line. This could also be an explanation for the DNA damage in our study. The profound and early DNA damage may account for instant cell destruction or initiation of death cascades but also to cell mutation – if DNA repair capacities are too low – and in surviving cells which may result in secondary malignancies after PDT. In our study on PC-3 cells a recovery of a-basic sites (no DNA repair initiation)

could not be detected even within 24h after PDT, nor could a recovery of comet tails in the single cell electrophoresis study on HNSCC cell lines (data not shown, paper in preparation).
RNA-integrity and quality experiments show a clear degradation pattern in Foslipos®- treated PC-3 cells. The RNA degradation in photosensitizer treated HNSCC cell lines was similar between applied photosensitizer conditions (hypericin, Foslipos® and 1:1 mixture) but was lower if compared to PC-3 cells (data not shown).
These results were complemented at the RNA level by the observation of several important genes associated with DNA repair mechanisms. The gene expression analyses for PC-3 cells were performed with an array system of 84 genes involved in stress-response pathways. The gene expression in HNSCC cell lines were observed for 16 specific selected genes (paper in preparation). The early DNA damage sensors ATM, DDB1, the excision repair endonucleases ERCC1 and 3, the post-replication DNA repair genes RAD23A and 50, the uracil-DNA glycosylase UNG and the DNA double strand repair proteins XRCC1 and 2 were transcriptionally down-regulated or destroyed after PDT with Foslipos® in PC-3 treated cells. Our data are comparable with those in murine glioblastoma cells where mTHPC mediated PDT also resulted in an immediate DNA damage. However, in this and other studies, activation of repair mechanisms had been reported [39-41]. Since our data are contradictory to studies in human myeloid leukaemia and nasopharyngeal carcinoma cells where no DNA damage was found after mTHPC-PDT [42, 43], it can be assumed that the observed effects might be dependent on cell line used. Molecular response of PC-3 cells to mTHPC- induced PDT seems to be very complex. Further RNA expression studies on genes involved in cellular stress and defence mechanisms response showed that two antioxidant defence genes (CRYAB and HMOX1) were strongly upregulated. The small heat shock protein CRYAB, which was between 6 and 7-fold up-regulated also for all the photosensitizer treatments in HNSCC cells and the heme oxygenase family member HMOX1 is known to act as a molecular chaperon preventing the aggregation of denaturated proteins. Furthermore they interact with cytoskeletal components such as microtubules, intermediate filaments and microfilaments in response to different stress situations [44] protecting cells from oxidative damage [45]. Together with the observation that inhibition of HMOX1 may increase the efficacy of PDT [46, 47], it can be suggested that high levels of HMOX1 or CRYAB may eventually prevent optimal phototoxic effects.
Expression of heat shock proteins (HSPs) such as HSP60, HSP70 or HSP90 after PDT with various photosensitizers was reported to be up-regulated [48-51]. In our study we found that expression of HSPs members may be down- or up-regulated after PDT with Foslipos® in PC-

3 cells. Up-regulation of the HSP40 member DNAJB4 as well as HSP70 members HSPA1, HSPA1L and especially HSPA6 that is only induced by severe stress-stimuli may mirror the extent of damage in our model but also may indicate the presence of a (partly) preserved stress-response system.

The heat shock protein gene HSPA6 was as well highly up-regulated after all PDT treatments in both HNSCC cell lines. This correlates with different studies on PDT-induced heat shock protein expressions [1, 52]. The 70kDa heat shock proteins (molecular chaperons) generally have cell protective functions in stressful conditions and additionally they serve as markers for elimination by immune system [53]. An increase of intracellular concentration of HSP70 proteins may enhance the ability of a cell to deal with resulting accumulation of abnormally folded proteins after PDT treatment. Interestingly, our results show that not only apoptotic (hypericin treated cells) but also necrotic cells (Foslipos® treated cells) and cells displaying features of both death pathways (1:1 mixture treated cells) have an up-regulated HSPA6 expression. The HSPA6 up-regulation in the UMB-SCC 745 and in the UMB-SCC 969 cell line was immensely high that the interpretation of the data and drawing conclusions concerning possible differences between these two cell lines and different treatments was not possible.

The cell damage after PDT in the PC-3 cell model was obviously so profound that repair mechanisms were not functional. Therefore, the possible activation of death pathways was examined. It was reported that cyclin family genes which are crucial for DNA replication, were markedly reduced after PDT [54, 55]. Findings in our model correspond to these studies. The down-regulation of cyclin-interacting transcription factors may lead to a diminished proliferative activity or it may directly promote cell death. Interestingly, the expression of the tumor suppressor p53 (TP53), a key factor for the regulation of cell growth and death, was not affected. This has been reported previously [56]. However, the cyclin-dependent kinase inhibitor CDK1A, one of the main targets of TP53, was in contrast to other studies [57] reduced after PDT in our study. This result supports the assumption of an impact of PDT on cell cycle processes. Additionally, MDM2, an important inhibiting factor of p53, was also reduced. This may be associated with the potential of increased p53-related pathway and/ or reduced p53 degradation followed by cell cycle arrest and apoptosis. Furthermore, a strong up-regulation of bZIP transcription factor DDIT3 was found. DDIT3 had been implicated in anti-proliferative effects and the induction of apoptosis by certain anti-cancer agents, including PC-3 cells [58]. The high levels may have also contributed to growth arrest and apoptotic signalling in the experiments performed.

The genes involved in apoptosis signalling in our study either displayed reduced transcript numbers, or were almost completely shut down. Most of these genes seemed to be damaged early – probably due to direct ROS damage. The biological consequences are not clear yet. In general, the observation of various cell death processes seems to be more adequately investigated at the protein level. The monitoring of apoptotic pathways in Foslipos®-mediated PDT in PC-3 cells was not the scope of our study but the data did not exclude their activation as observed in caspases activity assay (FLICA) in HNSCC cell lines. Rather, the obtained results in PC-3 cells might be another sign of a breakdown in basic cellular functions.

Summary

In summary, our study focusing on PC-3 cells with Foslipos®-mediated PDT is characterized by a two-stage process, a combination of acute and delayed lethal effects. The first step is most likely driven by the direct actions of ROS on vital biological components allowing the temporary cell survival, initiating growth arrest, oxidative stress and rescue responses. The second step, a few hours later, was characterized by severe damage of the genomic DNA and the translational system which prevented recovery of the cells and lead to unavoidable cell death.

The studies on the HNSCC cell lines demonstrated different death pathways (necrosis and apoptosis) which seem to be dependent mainly on the photosensitizer. Further, evidence was provided that hypericin could induce two different apoptosis pathways (mitochondrial dependent and independent death pathways) relying upon the cell line used. Finally, these studies showed that the application of a photosensitizer mixture with lower single photosensitizer concentrations had an excellent PDT effect in our cell models.

Based on these results, the application of photosensitizer mixture could be beneficial not only in cancer treatment, but it also could help in the fight against microorganisms. This simple but innovative approach could open new treatment possibilities in PDT.

Outlook

In the near future we plan to examine the effects and the mechanisms of photosensitizers and their mixture without illumination. Also PDT effects with established conditions in HNSCC multicellular spheroids will be examined. The comparison of the data

obtained in monolayer could give more detailed insight to PDT understanding, which is essential before PDT application *in vivo*. Additionally, we intend to further investigate on antimicrobial PDT and we are planning to combine cancer PDT with hyperthermia, where we can enhance PDT effects through additional cellular stress. The initial study is ongoing and results are very promising.

5.1 References

1. Dougherty, T.J., et al., *Photodynamic therapy.* J Natl Cancer Inst, 1998. **90**(12): p. 889-905.
2. Konan, Y.N., R. Gurny, and E. Allemann, *State of the art in the delivery of photosensitizers for photodynamic therapy.* J Photochem Photobiol B, 2002. **66**(2): p. 89-106.
3. Besic Gyenge, E., et al., *Uptake and fate of surface modified silica nanoparticles in head and neck squamous cell carcinoma.* J Nanobiotechnology, 2011. **9**: p. 32.
4. Wacker, M., et al., *Photosensitizer loaded HSA nanoparticles. I: Preparation and photophysical properties.* Int J Pharm, 2010. **393**(1-2): p. 253-62.
5. Hadjur, C., et al., *Spectroscopic studies of photobleaching and photoproduct formation of meta(tetrahydroxyphenyl)chlorin (m-THPC) used in photodynamic therapy. The production of singlet oxygen by m-THPC.* Journal of Photochemistry and Photobiology B: Biology, 1998. **45**(2-3): p. 170-178.
6. Roslaniec, M., et al., *Liposome binding constants and singlet oxygen quantum yields of hypericin, tetrahydroxy helianthrone and their derivatives: studies in organic solutions and in liposomes.* J Photochem Photobiol B, 2000. **57**(2-3): p. 149-58.
7. Van de Putte, M., et al., *Elucidation of the tumoritropic principle of hypericin.* Br J Cancer, 2005. **92**(8): p. 1406-13.
8. Belitchenko, I., et al., *Characterization of photodegradation of meta-tetra(hydroxyphenyl)chlorin (mTHPC) in solution: biological consequences in human tumor cells.* Photochem Photobiol, 1998. **67**(5): p. 584-90.
9. Kiesslich, T., et al., *Uptake and phototoxicity of meso-tetrahydroxyphenyl chlorine are highly variable in human biliary tract cancer cell lines and correlate with markers of differentiation and proliferation.* Photochem Photobiol Sci, 2009. **9**(5): p. 734-43.
10. Ritz, R., et al., *Hypericin uptake: a prognostic marker for survival in high-grade glioma.* J Clin Neurosci, 2008. **15**(7): p. 778-83.
11. Teiten, M.H., et al., *Effect of meta-tetra(hydroxyphenyl)chlorin (mTHPC)-mediated photodynamic therapy on sensitive and multidrug-resistant human breast cancer cells.* J Photochem Photobiol B, 2001. **62**(3): p. 146-52.
12. Leung, W.N., et al., *Photodynamic effects of mTHPC on human colon adenocarcinoma cells: photocytotoxicity, subcellular localization and apoptosis.* Photochem Photobiol, 2002. **75**(4): p. 406-11.
13. Kiesslich, T., et al., *Comparative characterization of the efficiency and cellular pharmacokinetics of Foscan- and Foslip-based photodynamic treatment in human biliary tract cancer cell lines.* Photochem Photobiol Sci, 2007. **6**(6): p. 619-27.
14. Ball, D.J., D.I. Vernon, and S.B. Brown, *The high photoactivity of m-THPC in photodynamic therapy. Unusually strong retention of m-THPC by RIF-1 cells in culture.* Photochem Photobiol, 1999. **69**(3): p. 360-3.
15. Mitra, S. and T.H. Foster, *Photophysical parameters, photosensitizer retention and tissue optical properties completely account for the higher photodynamic efficacy of meso-tetra-hydroxyphenyl-chlorin vs Photofrin.* Photochem Photobiol, 2005. **81**(4): p. 849-59.
16. Theodossiou, T.A., et al., *The multifaceted photocytotoxic profile of hypericin.* Mol Pharm, 2009. **6**(6): p. 1775-89.
17. Rodriguez, M.S. and L.E. Albertengo, *Interaction between chitosan and oil under stomach and duodenal digestive chemical conditions.* Biosci Biotechnol Biochem, 2005. **69**(11): p. 2057-62.

18. Kubin, A., et al., *Hypericin--the facts about a controversial agent.* Curr Pharm Des, 2005. **11**(2): p. 233-53.
19. Haimovitz-Friedman, A., et al., *Protein kinase C mediates basic fibroblast growth factor protection of endothelial cells against radiation-induced apoptosis.* Cancer Res, 1994. **54**(10): p. 2591-7.
20. Kim, C.Y., et al., *Differential expression of protein kinase C epsilon protein in lung cancer cell lines by ionising radiation.* Br J Cancer, 1992. **66**(5): p. 844-9.
21. Obach, R.S., *Inhibition of human cytochrome P450 enzymes by constituents of St. John's Wort, an herbal preparation used in the treatment of depression.* J Pharmacol Exp Ther, 2000. **294**(1): p. 88-95.
22. Budzinski, J.W., et al., *An in vitro evaluation of human cytochrome P450 3A4 inhibition by selected commercial herbal extracts and tinctures.* Phytomedicine, 2000. **7**(4): p. 273-82.
23. Sureau, F., Miskovsky, P. , Chinsky, L., Turpin,P. Y., *Hypericin-Induced Cell Photosensitization Involves an Intracellular pH Decrease.* J. Am. Chem. Soc., 1996. **118** (40): p. 9484-9487.
24. Ho, Y.F., et al., *Lipid-mediated preferential localization of hypericin in lipid membranes.* Biochim Biophys Acta, 2009. **1788**(6): p. 1287-95.
25. Lüthi, M., et al., *Hypericin- and mTHPC-mediated photodynamic therapy for the treatment of cariogenic bacteria.* Med. Laser App., 2009. **24**(4): p. 227-236.
26. Shiroza, T., S. Ueda, and H.K. Kuramitsu, *Sequence analysis of the gtfB gene from Streptococcus mutans.* J Bacteriol, 1987. **169**(9): p. 4263-70.
27. Abo, H., et al., *Peptide sequences for sucrose splitting and glucan binding within Streptococcus sobrinus glucosyltransferase (water-insoluble glucan synthetase).* J Bacteriol, 1991. **173**(3): p. 989-96.
28. Poyart, C., et al., *Identification of streptococci to species level by sequencing the gene encoding the manganese-dependent superoxide dismutase.* J Clin Microbiol, 1998. **36**(1): p. 41-7.
29. Berlanda, J., et al., *Comparative in vitro study on the characteristics of different photosensitizers employed in PDT.* J Photochem Photobiol B, 2010. **100**(3): p. 173-80.
30. Wang, X., et al., *Cellular and molecular mechanisms of photodynamic hypericin therapy for nasopharyngeal carcinoma cells.* J Pharmacol Exp Ther, 2010. **334**(3): p. 847-53.
31. Jori, G., et al., *Photodynamic therapy in the treatment of microbial infections: basic principles and perspective applications.* Lasers Surg Med, 2006. **38**(5): p. 468-81.
32. Panzarini, E., V. Inguscio, and L. Dini, *Timing the multiple cell death pathways initiated by Rose Bengal acetate photodynamic therapy.* Cell Death Dis, 2011. **2**: p. e169.
33. Piette, J., et al., *Cell death and growth arrest in response to photodynamic therapy with membrane-bound photosensitizers.* Biochem Pharmacol, 2003. **66**(8): p. 1651-9.
34. Davids, L.M., et al., *Hypericin phototoxicity induces different modes of cell death in melanoma and human skin cells.* J Photochem Photobiol B, 2008. **91**(2-3): p. 67-76.
35. Dubessy, C., et al., *Spheroids in radiobiology and photodynamic therapy.* Crit Rev Oncol Hematol, 2000. **36**(2-3): p. 179-92.
36. Gyenge, E.B., et al., *Cellular and molecular effects of the liposomal mTHPC derivative Foslipos in prostate carcinoma cells in vitro.* Photodiagnosis Photodyn Ther, 2011. **8**(2): p. 86-96.
37. Agostinis, P., et al., *Regulatory pathways in photodynamic therapy induced apoptosis.* Photochem Photobiol Sci, 2004. **3**(8): p. 721-9.

38. Foster, T.H., et al., *Fluorescence anisotropy imaging reveals localization of meso-tetrahydroxyphenyl chlorin in the nuclear envelope.* Photochem Photobiol, 2005. **81**(6): p. 1544-7.
39. Rousset, N., et al., *Use of alkaline Comet assay to assess DNA repair after m-THPC-PDT.* J Photochem Photobiol B, 2000. **56**(2-3): p. 118-31.
40. Ricci, F., et al., *Modulation of Ku70/80, clusterin/ApoJ isoforms and Bax expression in indocyanine-green-mediated photo-oxidative cell damage.* Ophthalmic Res, 2007. **39**(3): p. 164-73.
41. Yang, Z.Z., et al., *Knock down of the dual functional protein apurinic /apyrimidinic endonuclease 1 enhances the killing effect of hematoporphrphyrin derivative-mediated photodynamic therapy on non-small cell lung cancer cells in vitro and in a xenograft model.* Cancer Sci, 2009. **101**(1): p. 180-7.
42. McNair, F.I., et al., *A comet assay of DNA damage and repair in K562 cells after photodynamic therapy using haematoporphyrin derivative, methylene blue and meso-tetrahydroxyphenylchlorin.* Br J Cancer, 1997. **75**(12): p. 1721-9.
43. Yow, C.M., et al., *Cellular uptake, subcellular localization and photodamaging effect of temoporfin (mTHPC) in nasopharyngeal carcinoma cells: comparison with hematoporphyrin derivative.* Cancer Lett, 2000. **157**(2): p. 123-31.
44. Launay, N., et al., *Cell signaling pathways to alphaB-crystallin following stresses of the cytoskeleton.* Exp Cell Res, 2006. **312**(18): p. 3570-84.
45. Parcellier, A., et al., *Small heat shock proteins HSP27 and alphaB-crystallin: cytoprotective and oncogenic functions.* Antioxid Redox Signal, 2005. **7**(3-4): p. 404-13.
46. Frank, J., et al., *Inhibition of heme oxygenase-1 increases responsiveness of melanoma cells to ALA-based photodynamic therapy.* Int J Oncol, 2007. **31**(6): p. 1539-45.
47. Kocanova, S., et al., *Induction of heme-oxygenase 1 requires the p38MAPK and PI3K pathways and suppresses apoptotic cell death following hypericin-mediated photodynamic therapy.* Apoptosis, 2007. **12**(4): p. 731-41.
48. Hanlon, J.G., et al., *Induction of Hsp60 by Photofrin-mediated photodynamic therapy.* J Photochem Photobiol B, 2001. **64**(1): p. 55-61.
49. Verwanger, T., et al., *Gene expression pattern following photodynamic treatment of the carcinoma cell line A-431 analysed by cDNA arrays.* Int J Oncol, 2002. **21**(6): p. 1353-9.
50. Kuzelova, K., et al., *Early apoptotic features of K562 cell death induced by 5-aminolaevulinic acid-based photodynamic therapy.* J Photochem Photobiol B, 2004. **73**(1-2): p. 67-78.
51. Prasmickaite, L., et al., *Transcriptome changes in a colon adenocarcinoma cell line in response to photochemical treatment as used in photochemical internalisation (PCI).* FEBS Lett, 2006. **580**(24): p. 5739-46.
52. Mitra, S., et al., *Activation of heat shock protein 70 promoter with meso-tetrahydroxyphenyl chlorin photodynamic therapy reported by green fluorescent protein in vitro and in vivo.* Photochem Photobiol, 2003. **78**(6): p. 615-22.
53. Multhoff, G. and L.E. Hightower, *Cell surface expression of heat shock proteins and the immune response.* Cell Stress Chaperones, 1996. **1**(3): p. 167-76.
54. Romanko, Y.S., et al., *Relationship between antitumor efficiency of photodynamic therapy with photoditasine and photoenergy density.* Bull Exp Biol Med, 2005. **139**(4): p. 460-4.
55. Togashi, H., et al., *Fractionated photodynamic therapy for a human oral squamous cell carcinoma xenograft.* Oral Oncol, 2006. **42**(5): p. 526-32.

56. Finlan, L.E., et al., *Differential effects of 5-aminolaevulinic acid photodynamic therapy and psoralen + ultraviolet A therapy on p53 phosphorylation in normal human skin in vivo.* Br J Dermatol, 2005. **153**(5): p. 1001-10.
57. Crescenzi, E., et al., *Photodynamic therapy with indocyanine green complements and enhances low-dose cisplatin cytotoxicity in MCF-7 breast cancer cells.* Mol Cancer Ther, 2004. **3**(5): p. 537-44.
58. Lu, M., et al., *Acetyl-keto-beta-boswellic acid induces apoptosis through a death*

6

UNPUBLISHED DATA

6. Establishment of Three Dimensional Head and Neck Squamous Cell Carcinoma (HNSCC) Cell Culture (Multicellular Spheroids)

6.1 Introduction

Nowadays cell culture models are a very important and indispensable instrument in cancer, pharmacological and other experimental biology research. Monolayer or suspension cell cultures are known for 70 years and revolutionised the way of molecular research. Cell monolayers offer the possibility to simplify complex living systems enormously and therewith give insight in basic biological functions such as cellular interactions with drugs or various cellular pathways important for cell survival or death. The simplicity of this system is at the same time its major disadvantage. Drawing conclusions from work with cell cultures and extrapolating them to complex living systems is very challenging and it can lead to inaccurate context. Beside that, cell cultures are far away to represent complex and well organised appearance of tissue or tumours. In 1970 three dimensional cell cultures, so called multicellular spheroids, were introduced by experimental radiotherapists [1]. Since then tumour multicellular cultures were used in many different research areas such as photodynamic therapy, pharmacological research, hyperthermia and antibody-based immunotherapy as well as chemotherapy. This cellular model system made immense contribution to our knowledge about cellular responses to many therapeutic approaches [2]. Compared to monolayer cultures, 3D cell cultures offer similar conditions and microenvironments as found in tumours *in vivo*. They represent avascular tumour nodules or regions of solid tumour more accurately [3]. This cell model is gaining increasing value in cancer research as an essential tool for pharmacodynamic and pharmacokinetic predictions such as drug transportation, cellular resistance, tumour cell-matrix interactions, differentiation and invasion processes.

Part of our study was to establish HNSCC multicellular spheroids protocol for the application of photodynamic therapy *in vitro*. It is known that photodynamic therapy is dependent on the concentration of photosensitizer, molecular oxygen present and light penetration [4], therefore multicellular spheroids with their complex morphology appear to be suitable for examination of PDT-based mechanisms of action.

6.2 Materials and Methods

6.2.1 Cell lines

Monolayer: UMB-SCC 745 and UMB-SCC 969 were kindly provided by Dr. Robert Mandić, Department of Otolaryngology, Philipps University, Marburg, Germany. The cells were cultured under standard conditions (37°C, 5% CO_2, 95% air atmosphere) in RPMI growth medium (Invitrogen) supplemented with 10% fetal calf serum (FCS, Sigma-Aldrich, Buchs, Switzerland), 1% (4-(2-hydroxyethyl)-1-piperazineethanesulfonic acid (HEPES, Invitrogen), 1% Minimum Essential Medium Non Essential Amino Acids (MEM NEAA, Invitrogen) and 1% penicillin and streptomycin (Invitrogen). Every second day the growth medium was replaced. When the cells reached confluence, the cell passaging was done with 1x trypsin (Invitrogen), in general every 2-3 days.

***Multicellular spheroids (3D cell culture)*:** For generation of multicellular spheroids we applied a modified and for our cells optimised hanging drop method [5]. The following parameters were modified:

i) volume of agar in 96-well plate
ii) volume of growth medium per well
iii) volume of cell suspension drops on the lid
iv) cell concentration per drop
v) hanging time
vi) time dependent development of spheroids in wells

The detailed work is described in Marco Etter's medical doctoral thesis manuscript.

Briefly, the optimized version: 96-well plates were coated with 60 µl of 1.5% agarose (Sigma-Aldrich) per well, in RPMI medium without FCS. Then 20 µl drops of UMB-SCC cell solution (5000 cells/ 20 µl for UMB-SCC 745 and 10'000 cells/ 20 µl for UMB-SCC 969) were placed onto the plate lid, the lid was positioned back to the plate and then kept in the incubator (37°C, 5% CO_2) overnight. The following day, 80 µl growth medium were added to each well; the plates were centrifuged shortly and returned to the incubator. In order to avoid vibration, which would have had an influence on the formation of spheroids, the incubator

was not opened for the first 48 hours. After this initial time spheroids were stable in their form and reached the desired diameter of 150 μm two days later.

6.2.2 Microscopy

Microscopes: The development of multicellular spheroids was monitored with different microscopic techniques. Leica LX wide field microscope (Leica Microsystems, Wetzlar, Germany) was used for time dependent live cell observation of morphological development of spheroids. Transmission electron microscopy (TEM) with Philips CM 100 (Royal Philips Electronics, Amsterdam, Netherlands) was used to examine the cell differentiations and connections inside of spheroids. Scanning electron microscopy (SEM) with Gemini Zeiss SUPRA 50VP (Leica Microsystems) was used for examination of surface area of spheroids.

Preparation Protocols: Two different time-dependent live cell imaging experiments were performed. Firstly, development of spheroid over time was monitored. Eight spheroids were removed from 96-well plates, washed 2 times with PBS and subsequently placed on 18-well ibidi slides (Vitaris, Baar, Switzerland) in PBS and monitored for 20 minutes. Used spheroids were discarded after observation and for the subsequent experiment next eight spheroids from 96-well plates were used. The observation was made every second day until day eleven. Secondly, we observed behaviour of multiple spheroids in the same well over 5 h.

Samples for TEM were high pressure frozen and freeze-substituted (at -90°C, -60°C, -30°C) in water-free acetone and 2% osmium tetroxide (OsO_4). The samples were embedded first into 33% Epon (Sigma-Aldrich) followed by 66% for 1,5 hours and finally into 100% Epon. The polymerisation was in a 60°C heated oven over night. The 60 nm thick sample sections were placed onto 200 mesh grids and contrasted with 2% uranyl acetate (Sigma-Aldrich) and Reynold's lead citrate (Sigma-Aldrich).

SEM samples were performed according to the standard protocol. Briefly, samples were fixed for 30 minutes with 2.5% glutaraldehyde and 2% OsO_4, PBS and washed with distilled water. Subsequently samples were dehydrated in ascending EtOH series (60 %, 70%, 80%, 90 % and 100 %), critical point dried (CPD O30, Leica) and mounted on 12 mm aluminium stubs. Sputter coat for 80 seconds with platinum followed subsequently. Additionally, behaviour of spheroids was also monitored with SEM. Several spheroids were left on poly-L-lysine (PLL) coated slides for 20 minutes. The fixation protocol was as described above.

6.3 Results

Live cell imaging: Time dependent development of spheroids in the well was observed over 11 days. One day after cell suspension drops centrifugation spheroids were perfectly round in shape with a diameter between 75 µm and 150 µm. Until the sixth day spheroids did not show changes in their shape but only in their dimensions. Grown spheroids displayed a diameter from approximately 250 µm - 300 µm. From eighth day detaching of the cells on the surface was visible which was on eleventh day very pronounced. Both cell lines displayed similar behaviour. In figure 1 time dependent spheroid development of UMB-SCC 745 cell line is shown as an example.

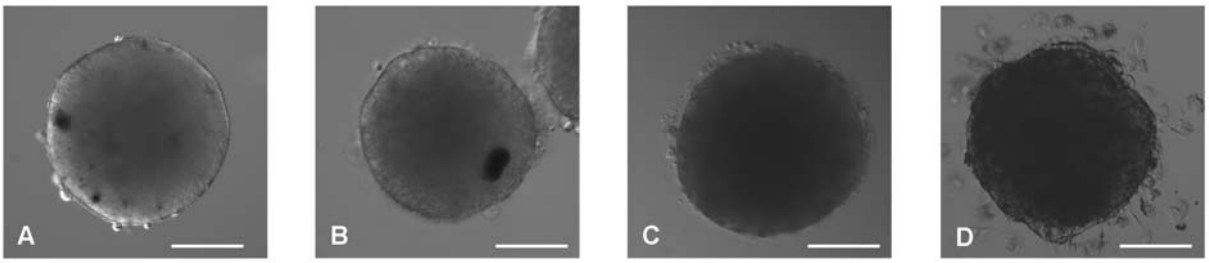

Figure 1: Live cell imaging pictures of UMB-SCC 745 spheroids after different time periods: in A after two days, in B after six days, in C after eight days and in D after eleven days. The differential interference contrast (DIC) pictures were made by wide-field Leica LX microscope. Scale bars in A = 50 µm and in B-D = 100 µm.

During live cell imaging we observed very interesting spheroids behaviour. If spheroids are in very near proximity to each other they tended to dock to each other and fuse (fig. 2). The fusing time was within five hours. Due to the semi-transparency of spheroids dynamic movements of the cells inside spheroid were observable. The black spots (probably necrotic areas) in spheroids were shifted through whole spheroid over time.

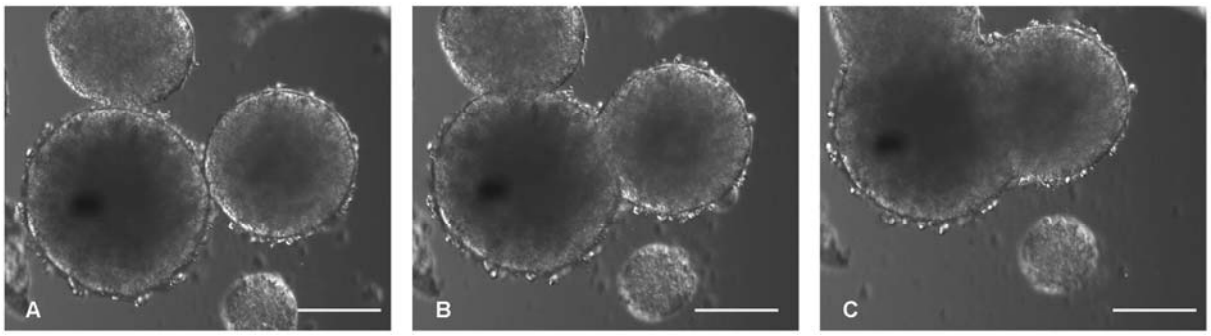

Figure 2: Live cell imaging pictures of UMB-SCC 745 spheroids. In picture A DIC picture of zero time point (spheroids docking) is shown, in B fusing after 2,5 hours and in C totally fusion after 5 hours. The DIC pictures were made by wide-field Leica LX microscope every 10 minutes. Scale bars = 100 µm.

SEM imaging: Surface and form of spheroids were examined with SEM. In figure 3 A UMB-SCC 745 spheroids after 4 days of growth are shown. The spheroids are perfectly round in shape and had an even and smooth surface. Figure 3 B is an enlarged section of spheroid surface. In this picture tight packed cells with strong pronounced cell-cell contacts are visible. The cells on the surface of spheroid build a unifying and tightly connected cell layer.

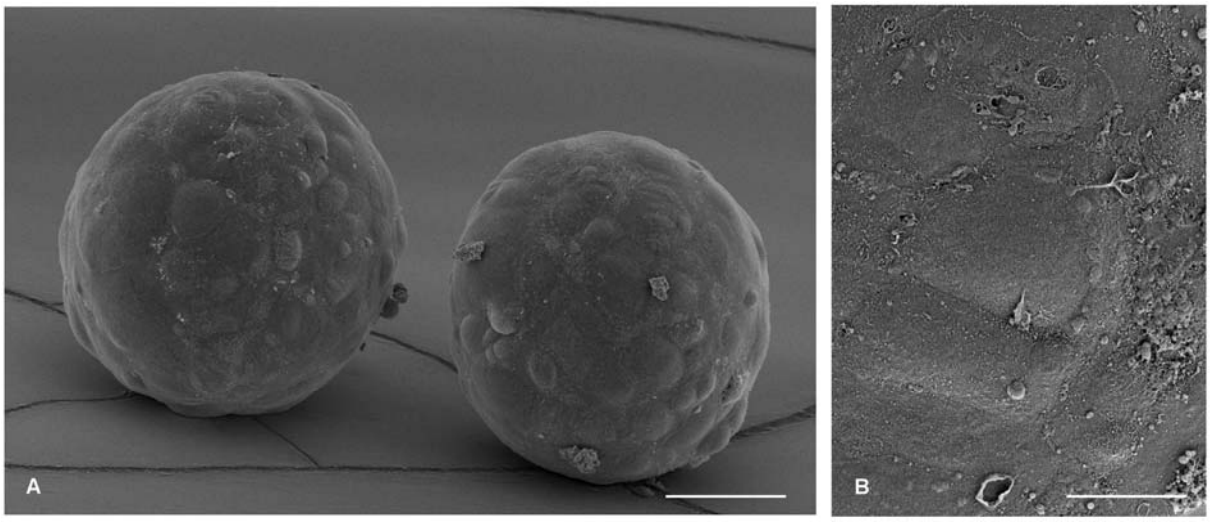

Figure 3: SEM pictures of UMB-SCC 745 spheroids. In picture A are shown two spheroids after 4 days. In picture B is shown the surface of spheroids. Nicely visible are single cells and cell-cell contacts. Scale bar in A = 50 µm in B =10 µm.

As already described spheroids demonstrate highly dynamic behaviour. Living spheroids were left on PLL coated cover slides for 20 minutes and then fixed for SEM as reported. In figure 4 A a spheroid with round shape and smooth surface at the time point zero is shown. Picture 4 B shows spheroids after 20 minutes on PLL coated cover slides. The first remarkable observation was rapid spheroid form change. Within 20 minutes spheroid were flattened and cells started to develop filopodia extensions on the cover slide surface, which is displayed in figure 4 C.

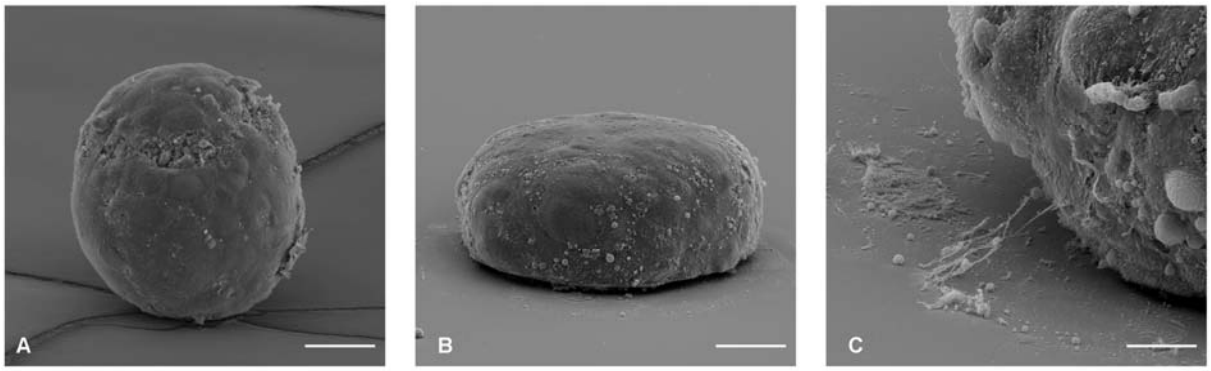

Figure 4: SEM pictures of UMB-SCC 745 spheroids on PLL coated cover slides over 20 minutes. In picture A spheroid at time point zero is shown, in B after 20 minutes. In C enlarged picture of cell filopodia after 20 minutes is shown. Scale bars in A and B = 50 µm and in C = 10 µm.

TEM imaging: High pressure frozen spheroid ultra-thin sample sections were used to examine structures and cellular organisation inside the spheroids. In figure 5 an overview picture of a UMB-SCC 745 spheroid with four pictures of detailed structures (A-D) are shown. In the overview picture is visible that the cell density is decreasing towards the spheroid centre. The cells display necrotic and autophagic features such as large vacuoles, degradation of intracellular content, multilamellar bodies (figure 6) and loss of cell-cell contacts. The cells which are near to spheroid surface (fig. 5 B and C) are tightly packed and have an extremely pronounced filopodia maze which serves as mechanical cellular anchors ensuring cohesion of the cells.

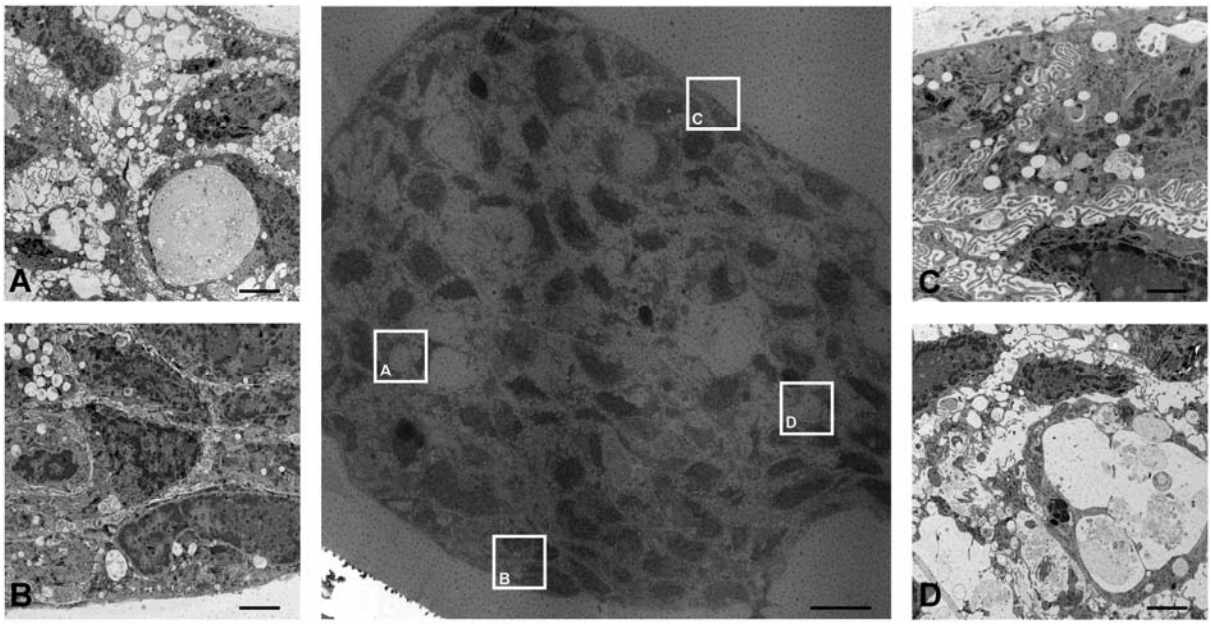

Figure 5: TEM pictures of high pressure frozen UMB-SCC 745 spheroid. In the middle an overview picture of a spheroid is shown. In A and D cells which display predominantly autophagic features (many vacuoles, degradation of cell organelles, multilamellar bodies and loss of cell-cell contacts) are shown. In B and C healthy

cells with pronounced filopodia-cell-cell contacts, smooth spheroid surface and healthy cell organelles and nuclei are shown. Scale bars for A - D = 5 µm and for overall spheroid picture = 20 µm.

Figure 6 A is a detailed picture of autophagy compartments inside the spheroid and in 6 B close-up picture of multilamellar bodies. The self-digestion of cells in nutrient-poor spheroid compartments is often found.

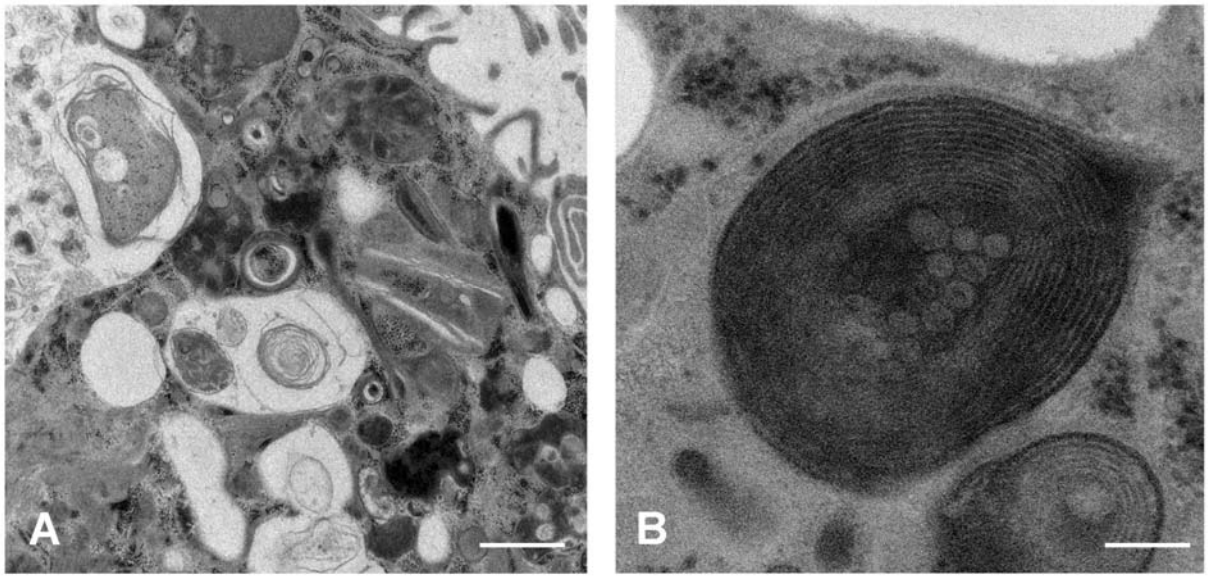

Figure 6: TEM pictures of multilamellar bodies inside high pressure frozen UMB-SCC 745 spheroid. In A an overview picture with several vacuoles with multilamellar bodies and other digested cell compartments is shown. In B a detailed picture with multilamellar bodies and glycogen storages is shown. Scale bars in A = 500 nm and in B = 100 nm.

In summary, the examination of UMB-SCC 745 multicellular spheroids revealed a complex morphological architecture with heterogeneous pathophysiological characteristics similar to those found in solid tumours such as three dimensional cell-cell interactions, necrotic and autophagic compartments and presence of nutrient gradient.

6.4 Discussion and Conclusion

The multicellular spheroids represent an accurate and powerful *in vitro* model for various biological research areas. Until now many different protocols for generation of 3D cell cultures were described. Still, there are not many research groups using multicellular spheroids for their research. This could be due to the complex multicellular spheroid culture technique and multiple possibilities to analyse the treated spheroids. The conventional generation of multicellular spheroids is based on cell-cell coupling by resisting cell-surface interactions [2]. This is used in variety of methods such as agitation of the cell suspension [3], cellular aggregation by sedimentation at concaves, usage of microcapsules with Ca-alginate- [6] or alginate-chitosan [7] gel membranes, cell adhesion resistant surfaces such as agarose [8] or poly-hydroxyethyl methacrylate [9] or a droplet's air-liquid interface [5, 10, 11]. The major working challenge with multicellular spheroids is lack of fully developed high-throughput manipulation and analysis methods as available for 2D monolayer cell cultures. The monitoring of spheroids with different microscopy methods (widefield microscopy, multiphoton confocal microsocopy, SEM and TEM,) are well established and widely used. It is possible to monitor viable and intact spheroids as well as high pressure frozen, chemically fixed or paraffin-embedded multicellular spheroid cultures. Further more, it is possible to perform a broad range of immunocytochemical stainings on ultra-thin cross-sections. Performance of assays in intact and viable spheroids in contrast is often limited due to the complex spheroid morphology which makes penetration of substances difficult. Nowadays cell survival in spheroids is monitored with different approaches such as observation of respiratory-, lactate dehydrogenase- or acid phosphatase activity [12-14]. Molecular methods such as examination of gene expression response may also be applied to multicellular spheroids. However, the requirement of large amount of spheroids for the experimental set-ups should be taken in account. Nevertheless, it was shown that gene expression patterns are much closer related to the *in vivo* situation than results achieved with 2D monolayer cultures [15-17].

Two dimensional monolayer cultures are widely used in PDT research but this approach is inadequate since oxygen gradient as well as heterogeneous population of cells (proliferating, quiescent and hypoxic cells) is lacking. Important parameters for good PDT efficacy are photosensitizer intracellular concentration (penetration and accumulation), light dose and amount of molecular oxygen present. A three dimensional cell model system with radially decreasing oxygen gradient [19] offers an excellent insight in processes induced by

oxygen dependent therapies such as PDT. Photosensitizer fluorescence features enable an easy monitoring and tracking of photosensitizer distribution and for light dosimetry - which is very important for accurate *in vivo* PDT - a number of different strategies is proposed [18]. In our study we established and elaborated an easy and low cost protocol for generation of HNSCC spheroids which can be applied to any cell type. Results of our previous studies on 2D monolayer HNSCC cell cultures will serve as a basis for further research in HNSCC multicellular spheroids.

In summary, multicellular spheroids represent an *in vitro* system between 2D monolayers and tumours in situ. This model closely mimics the situation of micro-environment in solid tumours and is characterised by complex structural features as well as by oxygen, nutrient, pH gradients. Therefore application of different treatments (e.g. drug screenings, experimental radiotherapy, antibody-based immunotherapy or photodynamic therapy) in 3D cell culture is gaining outstanding importance.

6.5 References

1. Sutherland, R.M., et al., *A multi-component radiation survival curve using an in vitro tumour model.* Int J Radiat Biol Relat Stud Phys Chem Med, 1970. **18**(5): p. 491-5.
2. Hirschhaeuser, F., et al., *Multicellular tumor spheroids: an underestimated tool is catching up again.* J Biotechnol, 2010. **148**(1): p. 3-15.
3. Friedrich, J., R. Ebner, and L.A. Kunz-Schughart, *Experimental anti-tumor therapy in 3-D: spheroids--old hat or new challenge?* Int J Radiat Biol, 2007. **83**(11-12): p. 849-71.
4. Dubessy, C., et al., *Spheroids in radiobiology and photodynamic therapy.* Crit Rev Oncol Hematol, 2000. **36**(2-3): p. 179-92.
5. Kelm, J.M. and M. Fussenegger, *Microscale tissue engineering using gravity-enforced cell assembly.* Trends Biotechnol, 2004. **22**(4): p. 195-202.
6. Sakai, S., et al., *Multicellular tumor spheroid formation in duplex microcapsules for analysis of chemosensitivity.* Cancer Sci, 2011.
7. Tsoi, A.M., et al., *[Microencapsulated multicellular tumor spheroids: preparation and use as a novel in vitro model for drug screening].* Biomed Khim, 2010. **56**(6): p. 674-85.
8. Friedrich, J., et al., *Spheroid-based drug screen: considerations and practical approach.* Nat Protoc, 2009. **4**(3): p. 309-24.
9. Ivascu, A. and M. Kubbies, *Rapid generation of single-tumor spheroids for high-throughput cell function and toxicity analysis.* J Biomol Screen, 2006. **11**(8): p. 922-32.
10. Foty, R., *A simple hanging drop cell culture protocol for generation of 3D spheroids.* J Vis Exp, 2011(51).
11. Timmins, N.E. and L.K. Nielsen, *Generation of multicellular tumor spheroids by the hanging-drop method.* Methods Mol Med, 2007. **140**: p. 141-51.
12. Torisawa, Y.S., et al., *A multicellular spheroid-based drug sensitivity test by scanning electrochemical microscopy.* Oncol Rep, 2005. **13**(6): p. 1107-12.
13. De Witt Hamer, P.C., et al., *Quantification of viability in organotypic multicellular spheroids of human malignant glioma using lactate dehydrogenase activity: a rapid and reliable automated assay.* J Histochem Cytochem, 2005. **53**(1): p. 23-34.
14. Friedrich, J., et al., *A reliable tool to determine cell viability in complex 3-d culture: the acid phosphatase assay.* J Biomol Screen, 2007. **12**(7): p. 925-37.
15. Cichon, M.A., et al., *Growth of lung cancer cells in three-dimensional microenvironments reveals key features of tumor malignancy.* Integr Biol (Camb), 2011.
16. Cody, N.A., et al., *Influence of monolayer, spheroid, and tumor growth conditions on chromosome 3 gene expression in tumorigenic epithelial ovarian cancer cell lines.* BMC Med Genomics, 2008. **1**: p. 34.
17. Chang, T.T. and M. Hughes-Fulford, *Monolayer and spheroid culture of human liver hepatocellular carcinoma cell line cells demonstrate distinct global gene expression patterns and functional phenotypes.* Tissue Eng Part A, 2009. **15**(3): p. 559-67.
18. Madsen, S.J., et al., *Multicell tumor spheroids in photodynamic therapy.* Lasers Surg Med, 2006. **38**(5): p. 555-64.
19. Gorlach, A. and H. Acker, *pO2- and pH-gradients in multicellular spheroids and their relationship to cellular metabolism and radiation sensitivity of malignant human tumor cells.* Biochim Biophys Acta, 1994. **1227**(3): p. 105-12.

7

APPENDIX

7.1 Uptake and fate of surface modified silica nanoparticles in head and neck squamous cell carcinoma

The contributions of Emina Besic Gyenge to the study: „Uptake and fate of surface modified silica nanoparticles in head and neck squamous cell carcinoma" were the following:

1. Spheroid cell culturing

2. Elaboration of experiment designs

3. Nanoparticle uptake experiments (in both cell lines) and microscopic monitoring, in particular: **figure 2** (nanoparticle internalisation mode), **figure 3** (time dependent uptake of Ru@SiO_2-OH nanoparticles), f**igure 4** (time dependent uptake of Ru@SiO_2-NH_2 nanoparticles), **figure 6** (time dependent uptake of Ru@SiO_2-PEG nanoparticles), **figure 7** (time dependent uptake of Ru@SiO_2-NH_2 nanoparticles in spheroids).

4. Nanoparticle intracellular localisation and distribution (in both cell lines) and microscopic monitoring, in particular **figure 5** (intracellular localisation of Ru@SiO_2-OH and Ru@SiO_2-NH_2 nanoparticles), **figure 8** (intracellular co-localisation of Ru@SiO_2-OH and Ru@SiO_2-NH_2 nanoparticles) and **figure 10** (Ru@SiO_2-NH_2 nanoparticles distribution during cell division)

JOURNAL OF NANOBIOTECHNOLOGY

RESEARCH Open Access

Uptake and fate of surface modified silica nanoparticles in head and neck squamous cell carcinoma

Emina Besic Gyenge[1*†], Xenia Darphin[1†], Amina Wirth[2], Uwe Pieles[2], Heinrich Walt[3], Marius Bredell[3] and Caroline Maake[1]

Abstract

Background: Head and neck squamous cell carcinoma (HNSCC) is currently the eighth leading cause of cancer death worldwide. The often severe side effects, functional impairments and unfavorable cosmetic outcome of conventional therapies for HNSCC have prompted the quest for novel treatment strategies, including the evaluation of nanotechnology to improve e.g. drug delivery and cancer imaging. Although silica nanoparticles hold great promise for biomedical applications, they have not yet been investigated in the context of HNSCC. In the present in-vitro study we thus analyzed the cytotoxicity, uptake and intracellular fate of 200-300 nm core-shell silica nanoparticles encapsulating fluorescent dye tris(bipyridine)ruthenium(II) dichloride with hydroxyl-, aminopropyl- or PEGylated surface modifications ($Ru@SiO_2$-OH, $Ru@SiO_2$-NH_2, $Ru@SiO_2$-PEG) in the human HNSCC cell line UMB-SCC 745.

Results: We found that at concentrations of 0.125 mg/ml, none of the nanoparticles used had a statistically significant effect on proliferation rates of UMB-SCC 745. Confocal and transmission electron microscopy showed an intracellular appearance of $Ru@SiO_2$-OH and $Ru@SiO_2$-NH_2 within 30 min. They were internalized both as single nanoparticles (presumably via clathrin-coated pits) or in clusters and always localized to cytoplasmic membrane-bounded vesicles. Immunocytochemical co-localization studies indicated that only a fraction of these nanoparticles were transferred to early endosomes, while the majority accumulated in large organelles. $Ru@SiO_2$-OH and $Ru@SiO_2$-NH_2 nanoparticles had never been observed to traffic to the lysosomal compartment and were rather propagated at cell division. Intracellular persistence of $Ru@SiO_2$-OH and $Ru@SiO_2$-NH_2 was thus traceable over 5 cell passages, but did not result in apparent changes in cell morphology and vitality. In contrast to $Ru@SiO_2$-OH and $Ru@SiO_2$-NH_2 uptake of $Ru@SiO_2$-PEG was minimal even after 24 h.

Conclusions: Our study is the first to provide evidence that silica-based nanoparticles may serve as useful tools for the development of novel treatment options in HNSCC. Their long intracellular persistence could be of advantage for e.g. chronic therapeutic modalities. However, their complex endocytotic pathways require further investigations.

Keywords: nanoparticles, silica dioxide, surface properties, tumor cell line, uptake, endocytosis, cellular fate

1. Introduction

Head and neck squamous cell carcinoma (HNSCC) comprise a group of epithelial cancers that arise from e. g. the lips, the oral or nasal cavity, salivary glands, paranasal sinuses, pharynx or larynx [1]. With a worldwide incidence of more than 600'000 new cases per year, HNSCC accounts for about 6% of all malignant diseases diagnosed (http://globocan.iarc.fr). If detected early, patients have cure rates of about 90%. However, 60% of patients present with advanced disease or loco-regional lymph node metastasis at the time of diagnosis and have a poor prognosis [2,3].

Currently, treatment options for HNSCC patients include surgery, radiotherapy, chemotherapy or a combination of them [4,5]. Due to the distinct localization of these tumors in regions with anatomic structures

* Correspondence: emina.besicgyenge@uzh.ch
† Contributed equally
[1]Institute of Anatomy, University of Zürich, Winterthurerstr. 190, 8057 Zürich, Switzerland
Full list of author information is available at the end of the article

important to e.g. breathing, mastication, swallowing or phonation, invasive treatment regimes frequently leading to severe functional impairments - often accompanied by unfavorable cosmetic outcomes. This is true despite significant advancements made in the reconstructive abilities over past two decades. Moreover, radiation may have long-term effects on surrounding healthy structures such as parts of the brain, the spinal cord or salivary glands. However, while surgery or radiation therapy is local, chemotherapy is applied systemically and may thus result in severe adverse effects e.g. on blood cell production (anaemia, neutropenia, thrombopenia), the mucosa (mucositis), the auditory and vestibular system (ototoxicity) or the kidneys (nephrotoxicity). Despite this aggressive therapeutic regime, to date many patients with advanced disease cannot be cured and more then half of them die within five years [6-8]. HNSCC is thus currently the eighth leading cause of cancer death worldwide.

To overcome at least some of the challenges in the therapy of patients with advanced HNSCC, the application of nanoparticles has been evaluated with regard to their advantages for chemotherapeutic/medicinal, radiation and imaging strategies. Previous data indicates that cytotoxic drugs such as mitoxantron, cisplatin or paclitaxel as well as the photosensitizer 5,10,15,20-tetrakis (meso-hydroxyphenyl)porphyrin (mTHPP) encapsulated in superparamagnetic, liposome, albumin or methoxy poly(ethylene glycol)-poly(lactide-co-glycolide) (MPEG-PLGA) nanoparticles or polymeric micelles not only exhibit potent antitumor activity, but also displayed reduced side effects [9-13]. Furthermore, it has been reported that beta-emitting radionuclides attached to liposomes showed promising results when applied intratumorally and gold nanoparticles or nanoparticles with antisense oligonucleotides against the gene ataxia-telangiectasia-mutated (ATM) improved radiosensitivity in rodent head and neck cancer models [14-16]. In addition, superior imaging in head and neck cancers resulted from the use of superparamagnetic iron oxide nanoparticles, gold nanoparticles or gadolinium-labelled phosphorescent polymeric nanomicelles [17-22].

In the past years, silica-based nanoparticles have gained increasing interest for medical applications because of their biocompatibility, versatility and stability. Numerous in-vitro and in-vivo studies pointed towards their great potential for improving the efficacy of therapeutic agents in tumor cells by e.g. circumventing solubility and stability problems of certain drugs or enabling targeted delivery and controlled release strategies [23-25]. Moreover, silica nanomaterials have been proposed as promising medical tools for biosensing [26,27] and imaging purposes [28].

However, to our knowledge, silica nanoparticles have not yet been investigated in the context of head and neck cancers. In this work, we assess the biological in-vitro behaviour of core-shell silica based nanoparticles on the HNSCC cell line UMB-SCC-745 with regard to their cytotoxicity, uptake, localization and intracellular fate.

2. Materials and methods

2.1. Synthesis of nanoparticles

Spherical core-shell silica nanoparticles encapsulating tris(bipyridine)ruthenium(II) dichloride $[Ru(bpy)_3]Cl_2$ as fluorescent dye were produced as described before [29]. The method is based on an oil-in-water microemulsion of n-hexanol-TritonX100-cyclohexane, $[Ru(bpy)_3]Cl_2$, tetraethyl-orthosilicate (TEOS) and ammonia. The surface chemistry of mono-shell silica nanoparticles was modified by the addition of a mixture of TEOS and other organosilanes, such as 3-aminopropyltriethoxysilane (APTES) to generate aminopropyl and hydroxyl functionalities ($Ru@SiO_2$-NH_2 and $Ru@SiO_2$-OH) at the nanoparticle surface. Similarly, PEGylated $[Ru(bpy)_3]Cl_2$-labeled dual-shell nanoparticles ($Ru@SiO_2$-PEG) have been synthesized as previously described, using a mixture of TEOS and bis(silylated)polyethylene glycol (SPEGS) for growth of a PEGylated second shell [30]. All the three types of nanoparticles have been fully characterized, as precedently described and have an average size ranging between 200 and 300 nm [30]. The surface charge and the hydrophilic character of nanoparticles have been explored based on their electrophoretic mobility in nanopure water at neutral pH (Zetasizer Nano ZS, Malvern Instruments Ltd., UK).

2.2. Cell Culture

The head and neck squamous carcinoma cell line UMB-SCC-745 was kindly provided by Dr. Robert Mandić, Department of Otolaryngology, Philips University, Marburg, Germany. The UMB-SCC-745 was derived from the tonsil tumor of a 48-year-old man and has a distinct p53 single point mutation and loss of heterozygosity [31].

Monolayer

UMB-SCC-745 cells were cultured under standard conditions (37°C, 5% CO_2, 95% air atmosphere) in growth medium, i.e. RPMI Medium (Invitrogen, Basel, Switzerland) supplemented with 10% fetal calf serum (FCS, Sigma-Aldrich, Buchs, Switzerland), 1% HEPES (Invitrogen), 1% MEM non essential amino acids (Invitrogen) and 1% penicillin and streptomycin (Invitrogen). The growth medium was changed every second day. The passage of the cells was performed by trypsination (trypsin 1×, Invitrogen) when reaching confluence, in general every 2-3 days.

Multicellular spheroids (3D cell culture)

For generation of multicellular spheroids, we applied a modified hanging drop method [32]. Briefly, 96-well plates were coated with 60 μl of 1.5% agarose (Sigma-Aldrich) per well, in RPMI medium without FCS. Then 20 μl drops of UMB-SCC 745 cell solution (5000 cells/20 μl) were placed on the plate lid, the lid was positioned back to the plate and then kept overnight in the incubator (37°C, 5% CO_2). The following day, 80 μl growth medium was added to the wells, the plates were shortly centrifuged and returned to the incubator. In order to avoid vibration, which has an influence on the formation of spheroids, the incubator should not be opened for the first 48 hours. After this initial time spheroids were stable in their form and reached the desired diameter of 150 μm two days later.

2.3. Proliferation assay

The cytotoxicity of nanoparticles was evaluated using a commercial cell proliferation assay (Cell Proliferation ELISA, BrdU, chemiluminescent, Roche, Basel, Switzerland). For this experiment the cells were cultured in black Greiner-96-well plates (2000 cells/well, Cellstar, Frickenhausen, Germany) with 100 μl growth medium at 37°C, 5% CO_2 for 24 h. Subsequently the growth medium was replaced with fresh one containing Ru@SiO_2-OH, Ru@SiO_2-NH_2 or Ru@SiO_2-PEG nanoparticles at final concentrations ranging between 0.03 mg/ml - 0.5 mg/ml. Nanoparticles were ultrasonicated for 2 h before incubation to ensure their homogeneity. After nanoparticle incubation for 5 h, the cells were washed with phosphate buffered saline (PBS, Oxoid, Hampshire, United Kingdom) and incubated overnight with fresh growth medium containing BrdU-labeling agent. BrdU, which is incorporated only in viable cells during DNA synthesis, was detected with an ELISA immunoassay according to the recommendation of the manufacturer. The resulting signal was quantified by measuring the photons using a micro-plate luminometer with photomultiplier technology (BioTek, Luzern, Switzerland). The relative light units/second (rlu/s) directly correlates to the amount of DNA synthesis and hereby to the number of proliferating cells in the respective microcultures.

2.4. Exposure protocols of nanoparticles

For all experiments, nanoparticles were ultrasonicated for 2 h directly prior to use in cell culture.

For the uptake study the cells were seeded either on six-well plates (1'000'000 cells/well) for transmission electron microscopy (TEM) or on poly-L-lysine (PLL, 0.25 mg/ml, Sigma-Aldrich) -coated glass cover slips (50'000 cells, Hecht-Assistant, Sondheim, Germany) for confocal laser scanning microscopy (CLSM). The cells were then incubated with either Ru@SiO_2-OH, Ru@SiO_2-NH_2 or Ru@SiO_2-PEG nanoparticles (final concentrations 0.125 mg/ml) for different time periods (30 min, 1 h, 2 h, 5 h, 7 h, 12 h and 24 h) under cell culture conditions. After each time point cell aliquots were used for microscopic monitoring by CLSM and TEM.

Alternatively, multicellular spheroids were grown for 4 days in 96-well plates and also exposed to Ru@SiO_2-OH and Ru@SiO_2-NH_2 nanoparticles for 5 h and 24 h, respectively, at final concentrations of 0.125 mg/ml under cell culture conditions. The nanoparticle distribution in spheroids was monitored only by CLSM.

For long-time experiments, cells were grown in six-well culture plates and incubated under cell culture conditions with Ru@SiO_2-OH and Ru@SiO_2-NH_2 nanoparticles for 5 h (final concentrations 0.125 mg/ml). Following an extensive washing step with PBS, cells were directly passaged, re-seeded (500'000 cells/well) in cell culture plates and kept in culture until confluence (three days). The growth medium was exchanged every day. Passaging of the cells was continued until fifth passage. After each passage aliquots of the cells were used for evaluation by both CLSM and TEM.

For control experiments, cells or spheroids were cultured as above, but nanoparticle-containing medium was replaced by growth medium.

Protocols for CLSM (TCS-SP2 and TCS-SP5, Leica, Heerbrugg, Switzerland)**:** After exposure to nanoparticles and washing steps, cells on cover slips were fixed for 15 min with PBS containing 1% paraformaldehyde (PFA, Sigma-Aldrich) and 0.33% saccharose (Sigma-Aldrich). Visualisation of nuclei were performed by incubation with 4'-6-diamidion-2-phenylindole (DAPI, 1 μg/ml, Roche) and mounted with GlycerGel mounting medium (Dako, Baar, Switzerland).

In experiments concerning multicellular spheroids, nuclei were stained with Hoechst staining dye (1 μg/ml, Sigma-Aldrich), which was added for the last hour of incubation. After incubation, the spheroids were collected, washed with PBS, fixed with PBS containing 1% PFA for 30 minutes, washed again with PBS and then monitored by confocal microscopy.

$[Ru(byp)_3]^{2+}$ complexes were excited with a 458 nm laser and detected in the range of 570 - 650 nm. Visualisation of nuclei (DAPI and Hoechst staining) was achieved with an excitation wavelength of 350 nm and a detection wavelength range of 450 - 500 nm.

Protocols for TEM (CM100, TEM, Philips, Guildford, UK)**:** After nanoparticle incubation and washing steps cells were fixed with 2.5% glutaraldehyde (GA, Electron Microscopy Sciences, Hatfield, USA) and 0.8% PFA in 0.05 M dimethylarsenic acid sodium salt trihydrate (Na-Caco, Merck, Darmstadt, Germany) buffer at 1:9 ratio

for 30 minutes. The samples were washed once with 0.05 M Na-Caco buffer and then fixed for 1 h with 2% osmium-tetra-oxide and 3% potassium hexacyano-ferrate (II) trihydrate (Sigma-Aldrich) at 1:1 ratio. After washing and centrifugation, cell pellets were transferred to 2.5% bacto agar (Agar Scinetific, Wetzlar, Germany), dehydrated in 70-100% ethanol and embedded in embedding medium (Glycidether 100 (Promega); dodecenylsuccinic-anhydride (Sigma-Aldrich); nadic methyl anhydride (Sigma-Aldrich) and N, N-dimethylbenzylamin purum (Sigma-Aldrich) as activator) for 24 h at 80° C. Sections (70 nm) were contrasted with uranyl acetate dihydrate (Sigma-Aldrich) and lead (II) citrate (Sigma-Aldrich) for 20 minutes each.

2.5. Immunocytochemistry

UMB-SCC-745 cells cultured on PLL coated cover slides were incubated for 5 hours with Ru@SiO_2-PEG, Ru@SiO_2-OH and Ru@SiO_2-NH_2 nanoparticles at final concentrations of 0.125 mg/ml. After incubation cells were fixed for 15 min with 1% PFA in PBS, permeabilized with 0.01% Triton-X 100 (Roche) for 1.5 min, blocked for 30 min at room temperature with 0.1% bovine serum albumine (BSA, Calbiochem, San Diego, USA) and washed with PBS. For labelling of early endosomes, rabbit anti-EEA1 antibody (1:300, stock concentration 1.3 mg/ml, Sigma-Aldrich) was used. Rabbit anti-Rab7 antibody (1:300, stock concentration 1.2 mg/ml, Sigma-Aldrich) was used to visualize late endosomes and for labelling of Golgi apparatus mouse anti-GM130 antibody (1:500, stock concentration 0.7 mg/ml, Abcam, Cambridge, UK) was used. Cells were incubated with primary antibodies for 2 h at room temperature or overnight at 4°C, washed and incubated with FITC-labelled donkey anti-rabbit or anti-mouse antibodies, respectively (both 1:500, Sigma-Aldrich), together with DAPI (1 μg/ml) for 1 h at room temperature. Lysosomes and mitochondria were visualized with Lysotracker Red and Mitotracker Orange respectively (working concentration for both 300 nM, Invitrogen). For examination by CLSM (Leica), $[Ru(byp)_3]^{2+}$ complexes and nuclei have been detected as described above, while for FITC excitation and detection wavelengths of 488 nm and 490-540 nm, respectively, have been used.

3. Results

Electrophoretic mobility of Ru@SiO_2-OH particles revealed a ζ-potential of -40 mV, which is in good agree, ζ-potentials of +11.3 mV and +4.29 mV have been obtained, respectively. As a prerequisite for our studies we first determined optimal concentrations of the different surface-modified nanoparticles in our in-vitro model (Figure 1). BrdU proliferation assays indicated for all types of nanoparticles that concentrations ranging between 0.03 - 0.125 mg/ml had no statistic-ment with the values measured for bare (non doped) SiO_2 nanoparticles, whereas in the case of amino- and PEG-modified particlesally significant effect on cell proliferation compared to untreated controls. Ru@SiO_2-PEG had no impact on cell growth even at higher concentrations (0.25 - 0.5 mg/ml). However, 0.25 and 0.5 mg/ml of Ru@SiO_2-NH_2 nanoparticles negatively affected proliferation rates, leading to an average of 21% and 31% reduced incorporation of BrdU, respectively. Ru@SiO_2-OH nanoparticles diminished cell proliferation up to 41% at highest nanoparticle concentrations (0.5 mg/ml), while a reduction below 10% was observed at 0.25 mg/ml. Based on these results we decided to use concentrations of 0.125 mg/ml for all three Ru@SiO_2 nanoparticles for further experiments.

To obtain information about the cellular uptake of Ru@SiO_2-PEG, Ru@SiO_2-OH and Ru@SiO2-NH_2 we conducted electron microscopic studies in UMB-SCC 745 cells. Generally, nanoparticle incubation did not result in an obvious ultrastructural damage compared to untreated controls. Both Ru@SiO_2-OH and Ru@SiO_2-NH_2 were detected intracellularly already 30 min after nanoparticle incubation. In case of single nanoparticles, internalization involved invaginations of the plasma membrane that are lined by electron dense material at the cytoplasmic side. Furthermore, clusters of nanoparticles were internalized by membrane ruffling (Figure 2). In all cases, nanoparticles were found in membrane-bounded vesicles within the cytoplasm. Intracellular amounts of Ru@SiO_2-OH and Ru@SiO_2-NH_2 nanoparticles steadily increased between 30 min and 5 h post incubation (Figure 3 and 4). However after 24 h, large vesicles with many nanoparticles were found in favour of vesicles with single nanoparticles (Figure 5). Despite multiple washing steps during sample preparation for TEM, considerable amounts of nanoparticles were attached to the cell surface at all time points investigated.

In contrast to the other studied nanoparticles, the uptake of Ru@SiO_2-PEG into UMB-SCC 745 cells was minimal (Figure 6). Very few Ru@SiO_2-PEG nanoparticles were observed after 5 h of incubation and then only in a minority of cells. Neither an increase in uptake over time nor an affinity to the outer cell membrane as with the other nanoparticles could be observed. These data lead us to exclude Ru@SiO_2-PEG from further experiments.

The uptake of Ru@SiO_2-OH and Ru@SiO_2-NH_2 nanoparticles had been additionally investigated in a 3D cell culture system (Figure 7). Confocal microscopy revealed that an intense $[Ru(bpy)_3]Cl_2$ fluorescence was visible after 5 h in the cytoplasm of cells constituting

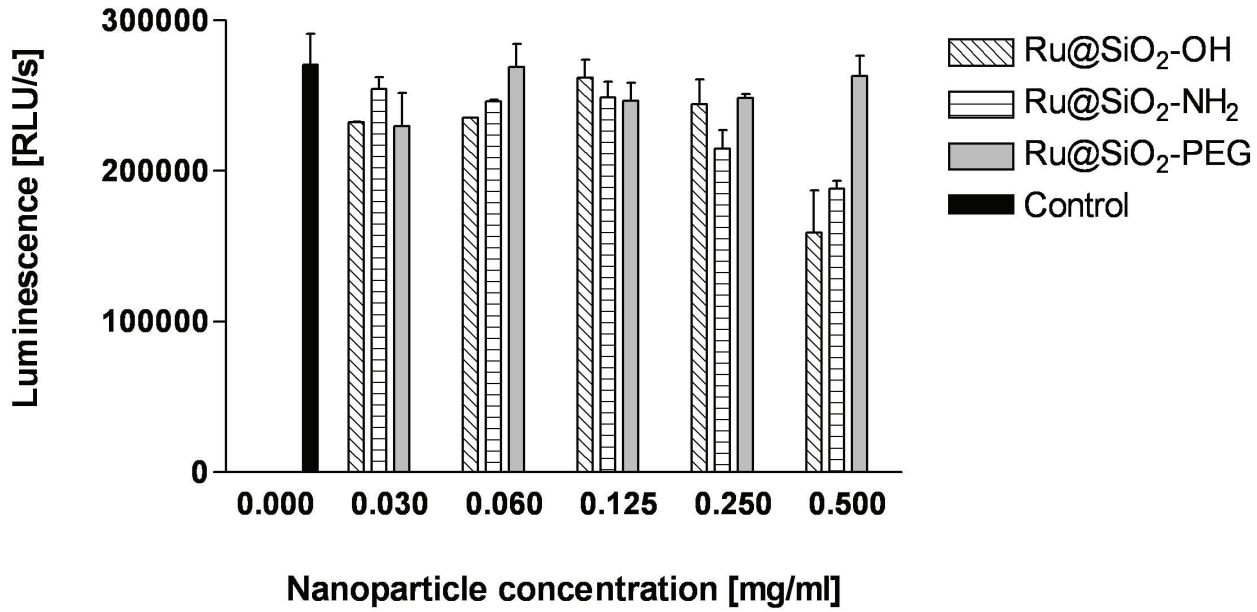

Figure 1 Proliferation effects of different surface modified nanoparticles on UMB-SCC 745. BrdU proliferation assays in UMB-SCC 745 cells after incubation (5 h) of nanoparticles with different surface modifications (Ru@SiO_2-OH, Ru@SiO_2-NH_2 and Ru@SiO_2-PEG) at concentration ranges of 0-0.5 mg/ml.

the outer layer of spheroids while inner cells were devoid of such signals.

With the aim to better characterize the intracellular fate of nanoparticles, immunohistochemical studies with antibodies against markers of endocytotic pathways were performed. CLSM analyses showed that at all time points investigated immunoreactions for Rab7, GP 120, Mitotracker and Lysotracker were present, but never co-localized with Ru@SiO_2-OH or Ru@SiO_2-NH_2 nanoparticles. In contrast, a subfraction of EEA1 immunosignals coexisted with Ru@SiO_2-OH and Ru@SiO_2-NH_2 fluorescence after 2 h of incubation, reaching a maximum at 5 h (Figure 8). This observation was slightly more pronounced in Ru@SiO_2-OH. However, the majority of [Ru$(bpy)_3$]Cl_2 fluorescent nanoparticles was not located together with EEA1 immunoreactivity. Co-localization with EEA1 after 24 h of incubation was negligibly low for both nanoparticle types, even if it was slightly higher for Ru@SiO_2-OH.

In addition, we investigated the presence of Ru@SiO_2-OH or Ru@SiO_2-NH_2 nanoparticles over a time span of 15 days (i.e. over five cell passages) in UMB-SCC 745 cells (Figure 9). During the whole experiment no signs of degradation of Ru@SiO_2 nanoparticles could be observed. During the first two days after Ru@SiO_2-OH or Ru@SiO_2-NH_2 incubation all cells contained large numbers of nanoparticles. However, at day four, Ru@SiO_2-OH nanoparticles were detected only in about 50% of cells, while Ru@SiO_2-NH_2 nanoparticles were still present in more than 70% of the cell population. Nine days after incubation, Ru@SiO_2-OH and Ru@SiO_2-NH_2 nanoparticles were visible in less then 30% and about 50% of all cells, respectively. Generally, we found that during mitosis nanoparticles were either only propagated to one daughter cell or distributed between both daughter cells (Figure 10). At day 12 all cells exhibited a cytoplasm free of Ru@SiO_2-OH. In contrast, Ru@SiO_2-NH_2 nanoparticles were found up to day 15, however, the detectable amounts were low.

4. Discussion

The large data corpus of recent years provides evidence that silica nanomaterials may have the potential to strongly improve cancer treatment and diagnosis. Silica nanomaterials feature the versatility necessary for tumor-specific modifications, stability in the often harsh environments of the body, ease of production and - more importantly - they are generally regarded as biocompatible. However, the latter clearly depends on many parameters such as particle size, surface modification, dose, exposure time or cell type used as model [33]. With the aim to explore the suitability of silica nanoparticles for new concepts in the treatment of head and neck cancers we investigated as a first step the biological in-vitro behaviour of non-targeted 200-300 nm core-shell silica nanoparticles with three different surface modifications.

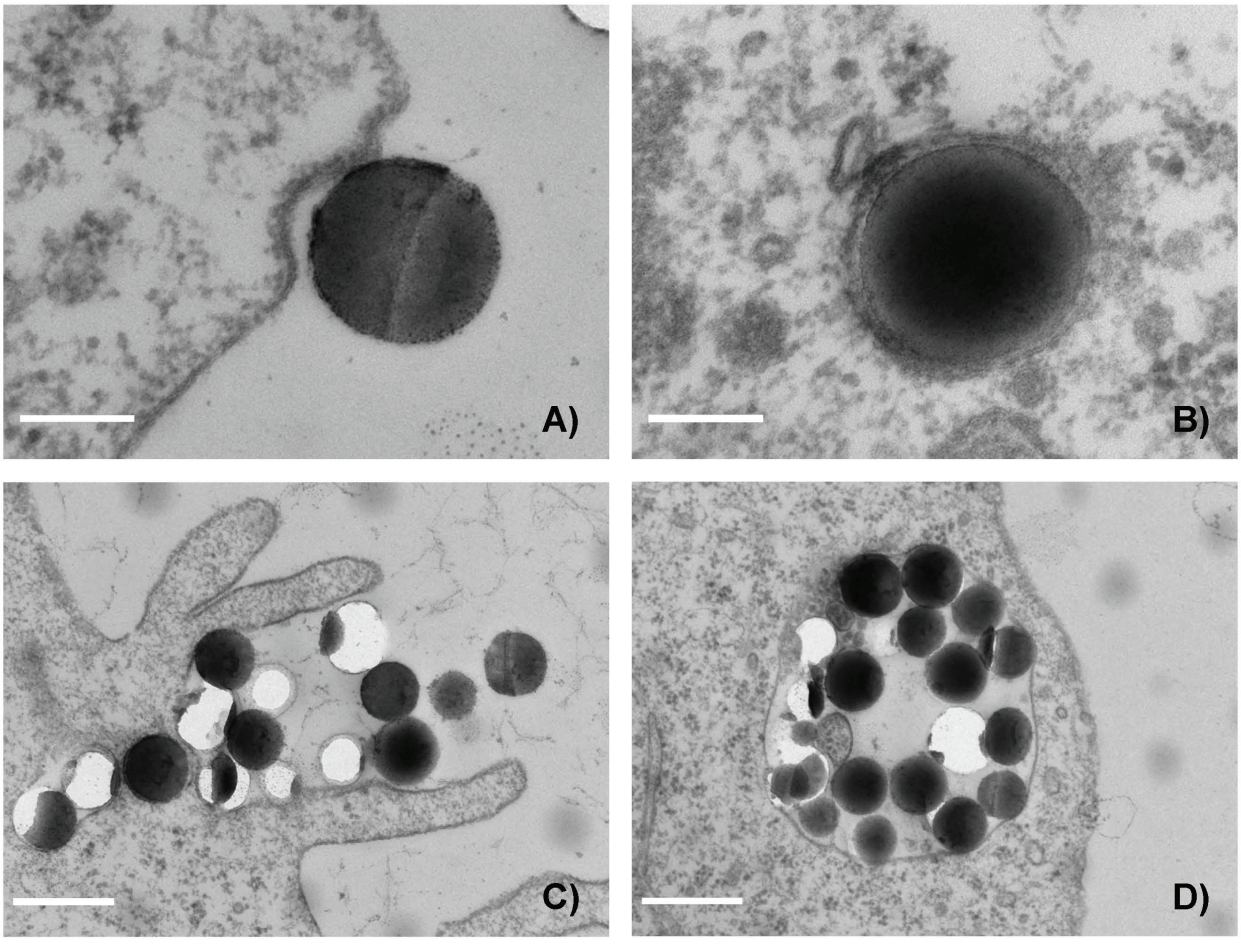

Figure 2 Nanoparticle internalisation. Transmission electron microscopy pictures of nanoparticle internalisation in UMB-SCC 745 exemplarily shown for Ru@SiO_2-NH_2. Uptake occurred either as single nanoparticle (A, B, scale bars = 100 nm), or nanoparticle clusters (C, D, scale bars = 500 nm).

While both Ru@SiO_2-OH and Ru@SiO_2-NH_2 nanoparticles displayed high uptake rates in our model, internalization of PEGylated silica nanoparticles was almost completely lacking under the same experimental conditions. Although we observed this effect in the related HNSCC line UMB-SCC 969 and in the human prostate carcinoma cell line PC-3 as well (unpublished data), other studies showed, in contrast to our results, that PEGylated silica nanoshells are at least able to attach to the outside of MCF-7 cells [34]. However, PEG is known for its cell-repelling properties [35-37], but uptake efficiency may be increased by the addition of targeting ligands [38]. Since grafting of nanoparticles with PEG has been reported to be advantageous for in-vivo applications - basically due to its increased half-live in circulation - and helpful for targeting, the generation of optimized Ru@SiO_2-PEG may be worthwhile (work in preparation).

Although the plasma membrane is negatively charged, the different surface charges of (negatively charged) Ru@SiO_2-OH and (positively charged) Ru@SiO_2-NH_2 nanoparticles had no considerable influence on cellular uptake kinetics in our model. This is in contrast to reports indicating that negatively charged nanomaterials are less effectively internalized [39]. However, a large number of studies show that both cationic and anionic nanoparticles are capable of effectively passing the cell membrane [39].

Our data indicates that at nanoparticle concentrations of 0.125 mg/ml and below, no perturbances in cell cycle progression have been detected under our experimental conditions. An increase of cancer cell proliferation could be dangerous and hold dire consequences in clinical settings. This phenomenon has been reported in-vitro for melanoma cells and mesoporous silica nanoparticles [40], but has never been observed in our experiments.

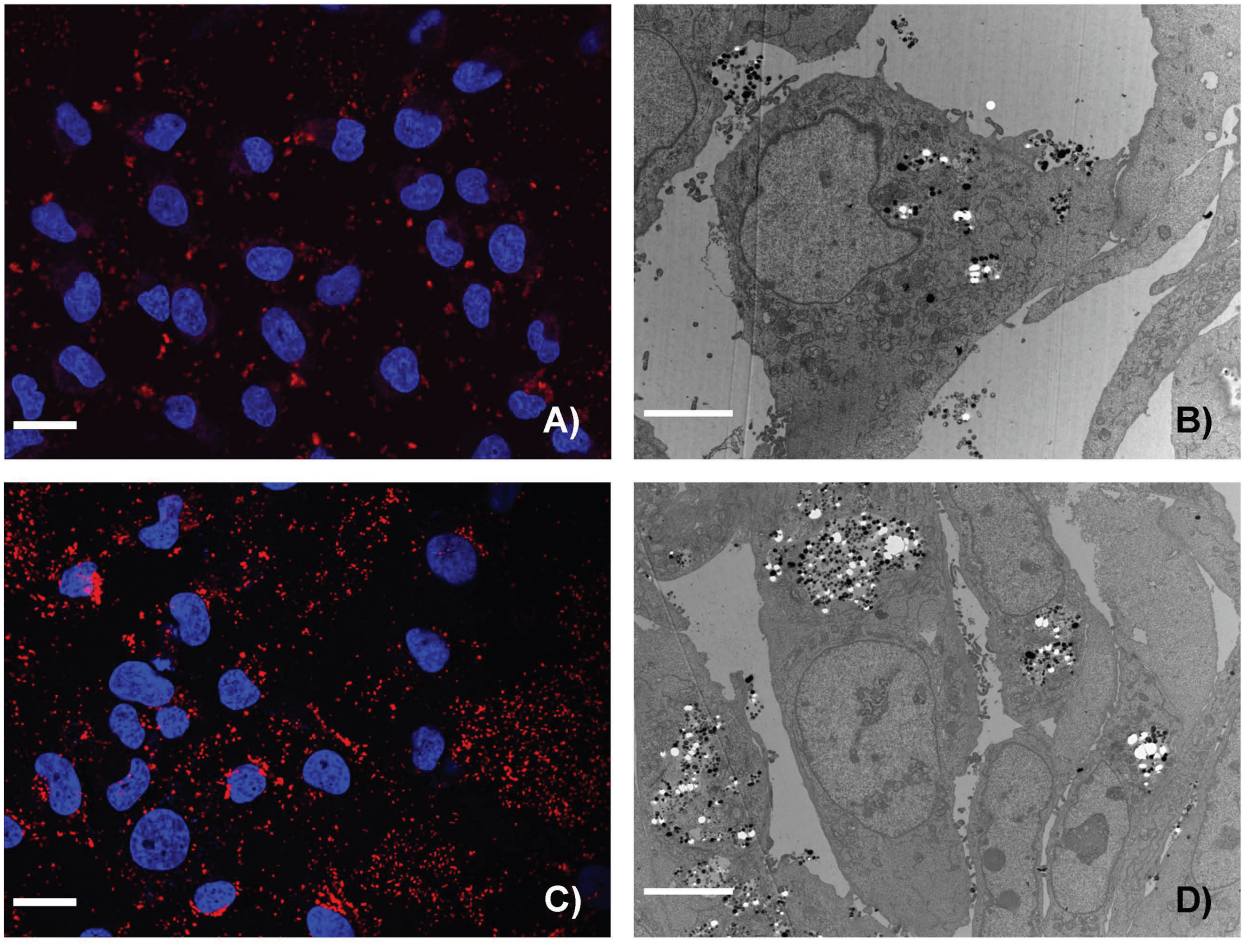

Figure 3 Time dependent uptake of Ru@SiO_2-OH nanoparticles. Ru@SiO_2-OH nanoparticle uptake over 2 h (A and B) and 24 h (C and D) in UMB- SCC 745. A, C: confocal laser scanning microscopy, showing nuclei in blue and Ru@SiO_2-OH nanoparticles in red, scale bars = 20 μm. B, D: transmission electron microscopy, scale bars = 10 μm.

However, higher concentrations of Ru@SiO_2-OH and Ru@SiO_2-NH_2 lead to reduced proliferation rates. While a slowdown in growth of tumor cells may be generally regarded as a positive effect in cancer treatment it should be emphasized that the underlying pathomechanisms in HNSCC are not clear yet. Previous in-vitro studies in other cancer cell lines have shown that cytotoxicity of silica nanoparticles, in relation to size and incubation time, may be due to oxidative stress with lipid peroxidation and membrane damage and/or an inflammatory response [41,42]. A detailed analysis of the complex molecular pathways involved is therefore needed in order to estimate possible (wanted or unwanted) consequences for future therapeutic strategies. Because of the different experimental design (e.g. longer incubation times, different particle sizes, other cell lines) it is impossible to directly compare our cytotoxicity data with previous studies. However, head and neck cancer cells seem to display cell toxic effects at concentrations comparable to other cancer cells, e.g. cervical adenocarcinoma cells [43], osteosarcoma cells [42], lung adenocarcinoma cells [37,41], and gastric and colon cancer cells [44]. Despite this, nanoparticle concentrations have to be carefully adjusted: using the same nanoparticles and experimental conditions as here, PC-3 human prostate cancer cells displayed a proliferation stagnation of about 15 days after nanoparticle incubation, although metabolic rates have been found to be higher (Besic Gyenge et al., unpublished).

With regard to internalization processes of nanoparticles into cells, phagocytosis, pinocytosis and caveolin- or clathrin-driven endocytosis have all been proposed and seem to strongly depend on particle form, size and cell type used. With our experimental set-up, apparently two different routes of nanoparticle uptake occur in parallel: on the one hand, single particles enter HNSCC cells via

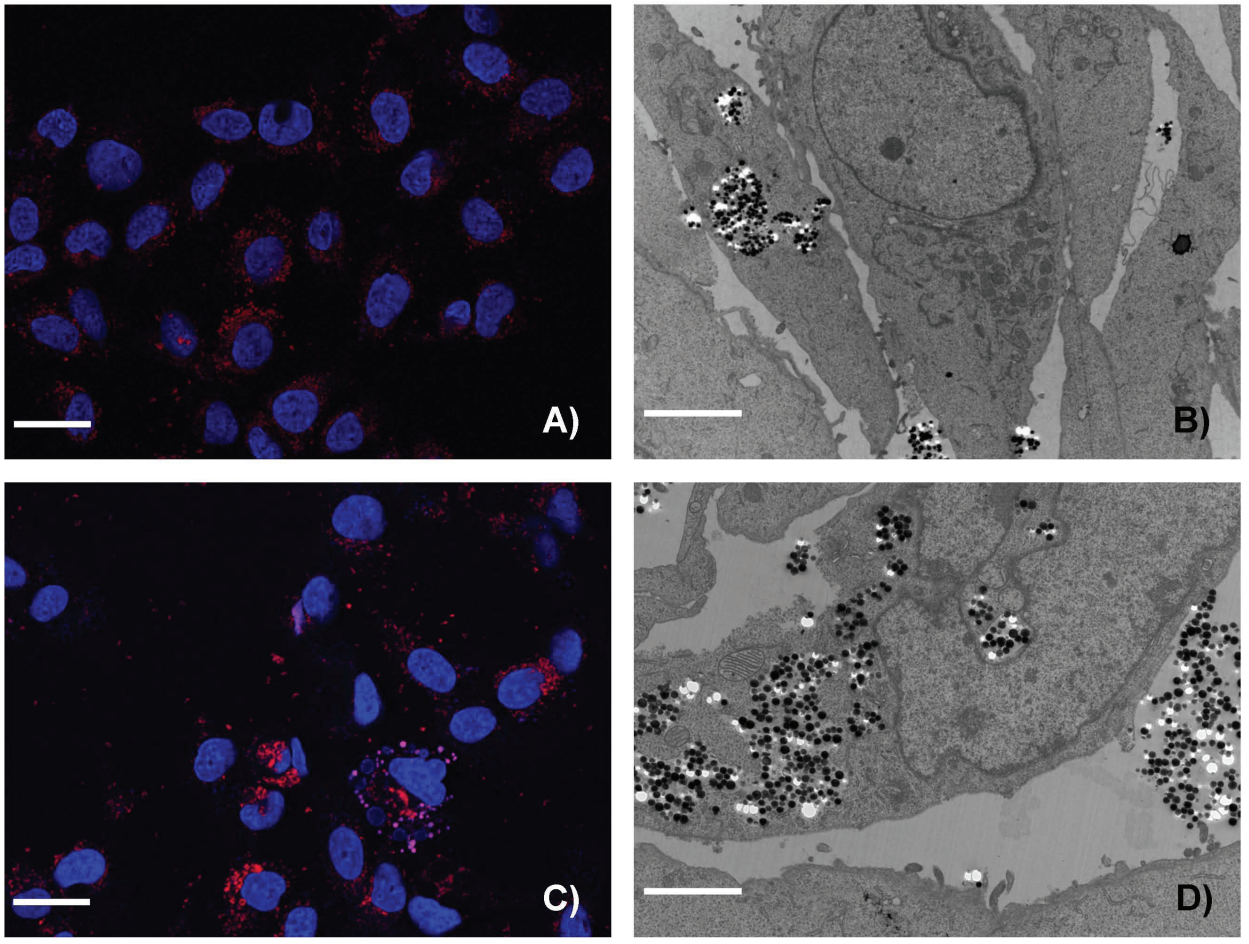

Figure 4 Time dependent uptake of $Ru@SiO_2$-NH_2 nanoparticles. $Ru@SiO_2$-NH_2 nanoparticles uptake over 2 h (A and B) and 24 h (C and D) in UMB-SCC 745. A, C: confocal laser scanning microscopy, showing nuclei in blue and $Ru@SiO_2$-NH_2 nanoparticles in red, scale bars = 20 μm. B, D: transmission electron microscopy, scale bars = 10 μm.

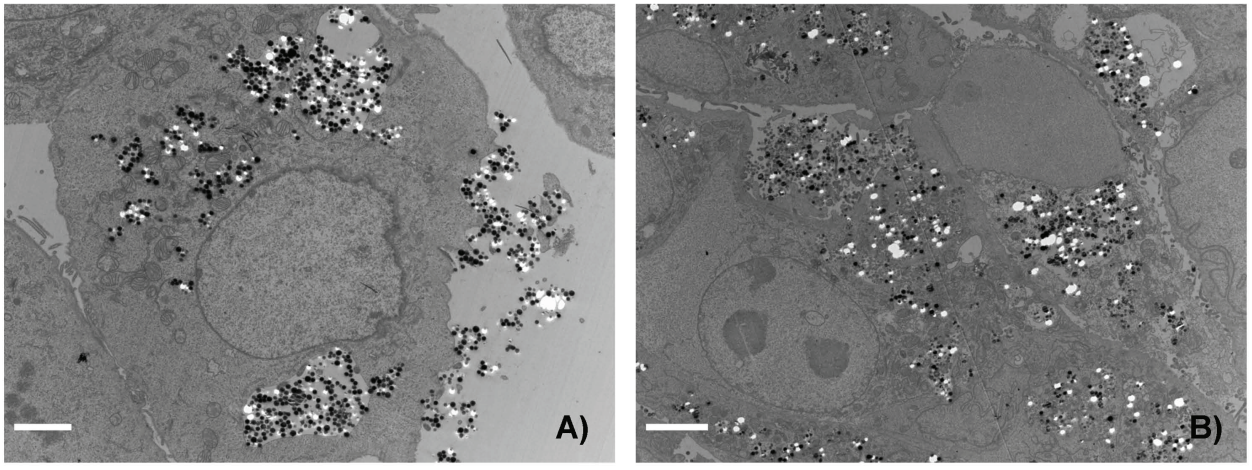

Figure 5 Intracellular localisation of $Ru@SiO_2$-OH and $Ru@SiO_2$-NH_2 nanoparticles after 24 h. Transmission electron microscopy showing intracellular localisation of nanoparticles in UMB-SCC 745 after 24 h of incubation. A) $Ru@SiO_2$-NH_2 nanoparticles and B) $Ru@SiO_2$-OH nanoparticles. Scale bars = 5 μm.

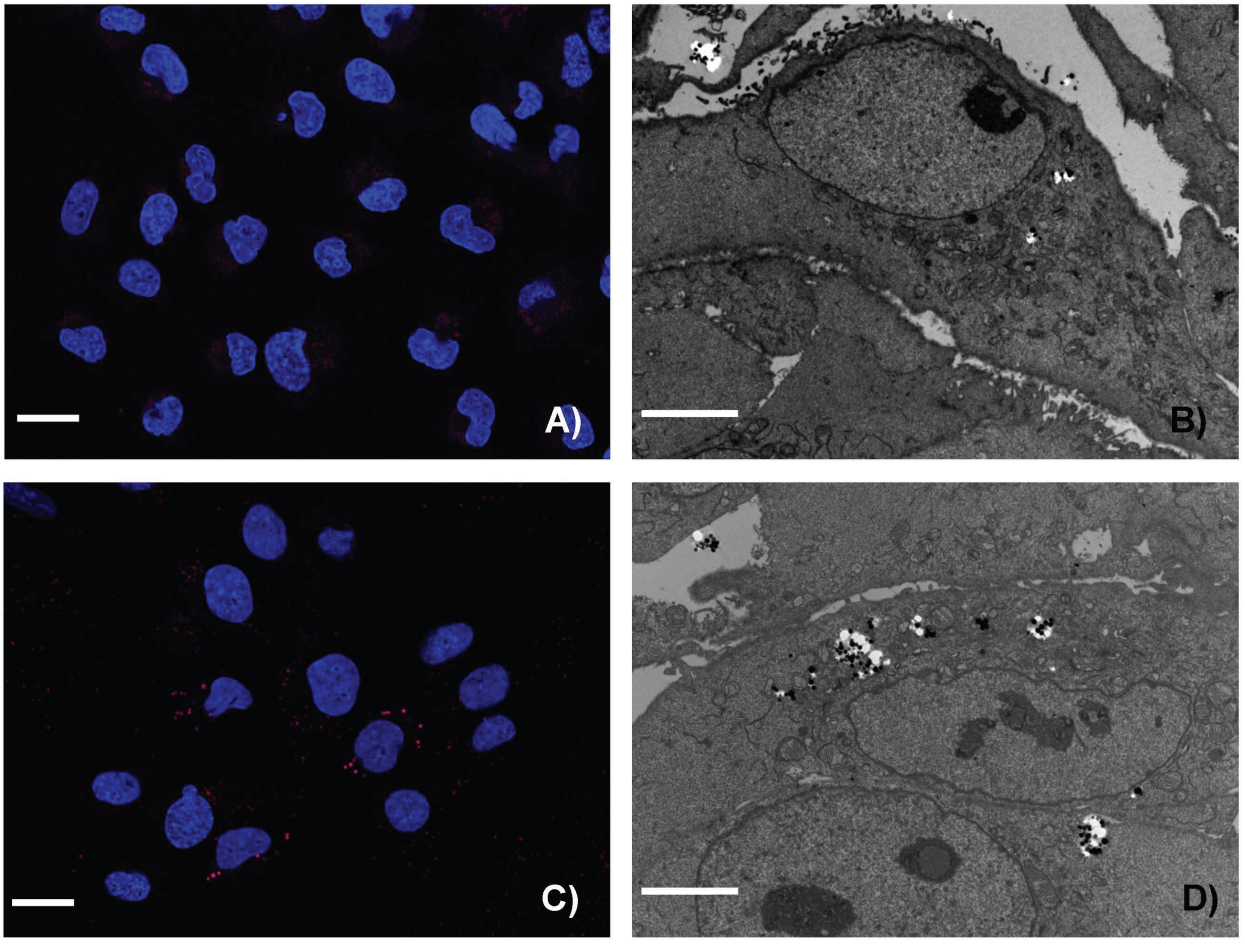

Figure 6 Time dependent uptake of Ru@SiO_2-PEG nanoparticles. Ru@SiO_2-PEG nanoparticle uptake after 2 h (A and B) and 24 h (C and D) in UMB-SCC 745. A, C: confocal laser scanning microscopy, showing nuclei in blue and Ru@SiO_2-PEG nanoparticles in red, scale bars = 20 μm. B, D: transmission electron microscopy, scale bars = 10 μm.

membrane invaginations that ultrastructurally resemble clathrin-coated pits. The involvement of clathrin-coated pits in internalization mechanisms of silica nanoparticles had also been proposed in several previous in-vitro studies using specific inhibitors or confocal methods [45-48]. On the other hand, the observed bulk internalization of nanoparticles is likely related to non-clathrin mediated endocytosis. The latter process rather displays features of macropinocytosis, such as membrane ruffling. Notably, the different surface charges of our nanoparticles did not play an apparent role with regard to the observed uptake mechanisms. Detailed studies are now needed to further characterize the events taking place at the plasma membrane upon contact with our silica nanoparticles. However, the incidence of such different simultaneous endocytosis modes of silica nanoparticles is in accordance with a recent paper, where also discrete entry pathways have been observed for single and agglomerated amorphous silica nanoparticles [48]. Furthermore, in mouse melanoma cells, internalization of latex particles of 200 nm (that corresponds approx. to the size of our particles) involved clathrin-coated pits, while latex particles of 500 nm (that corresponds approx. to our nanoparticle clusters) preferentially entered the cells via a clathrin-independent caveolin-associated pathway [49].

To characterize the intracellular fate of our silica nanoparticles within HNSCC, we next investigated their possible delivery into early and late endosomes and lysosomes. The localization of Ru@SiO_2-OH and Ru@SiO_2-NH_2 in early endosomes indicates their processing to endocytotic pathways, however, a considerable number of particles obviously used a different route of trafficking, that did not involve EEA1-positive organelles. As long as these organelles have not been characterized, a possible role of nanoparticle's surface charge for

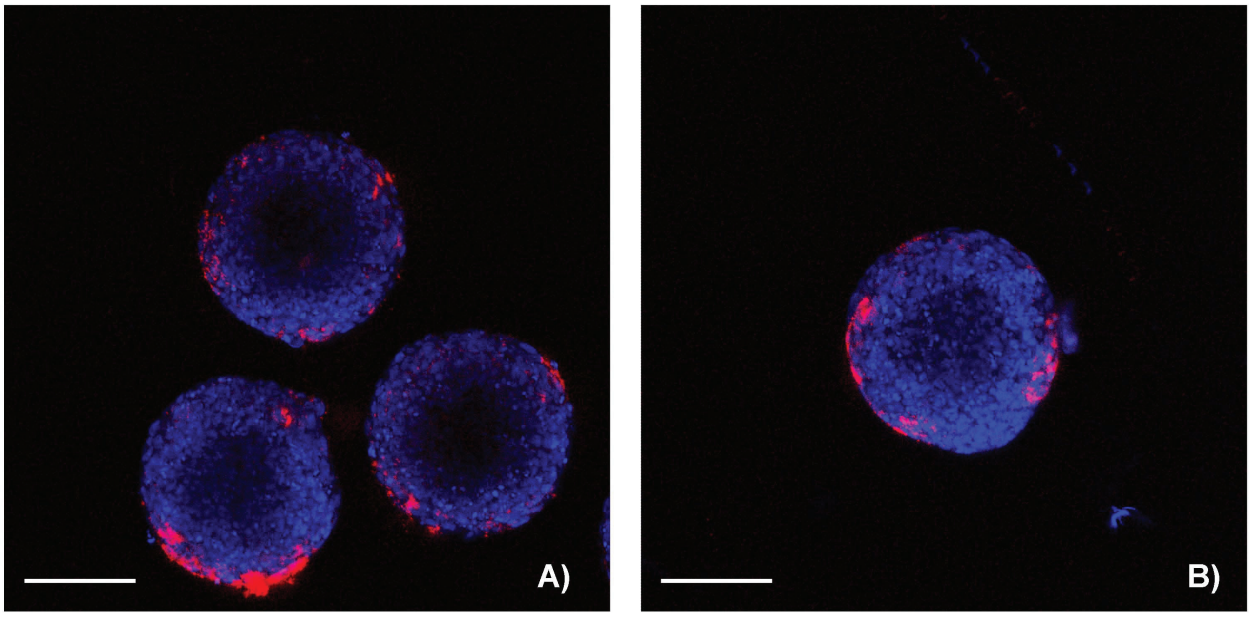

Figure 7 Ru@SiO_2-OH and Ru@SiO_2-NH_2 nanoparticle uptake in multicellular spheroids. Uptake of nanoparticles in UMB-SCC 745 multicellular spheroids after 5 hours. Confocal laser scanning microscopy pictures, showing Ru@SiO_2-OH (A) and Ru@SiO_2-NH_2 (B) in red and cell nuclei in blue. Scale bars = 100 μm.

endocytic processes cannot be defined. However, the acidic pH of early endosomes may explain the slightly higher frequency of (negatively charged) Ru@SiO_2-OH in EEA1-containing vesicles.

While we cannot exclude that some Ru@SiO_2-OH and Ru@SiO_2-NH_2 may have been shuttled back to the plasma membrane for segregation, the majority of nanoparticles remained intracellularly and accumulated in rather large vesicles 24 h after incubation. We propose that the latter is related to homotypic vesicle fusion. No transfer to Golgi apparatus-related pathways has been detected. More importantly, we found that nanoparticle-bearing vesicles did neither mature from early endosomes into (Rab7-positive) late endosomes nor locate to lysosomes. While both the known stability of silica-shell nanoparticles and possible cancer-related changes in

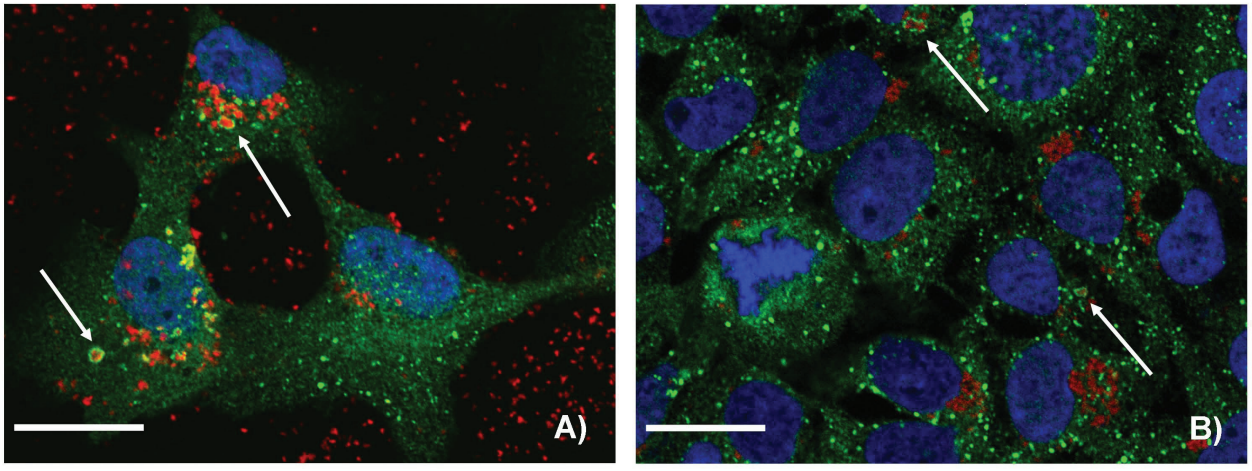

Figure 8 Co-localisation of Ru@SiO_2-OH and Ru@SiO_2-NH_2 nanoparticles with early endosomes. Confocal laser scanning microscopy pictures showing a partial co-localisation after 2 h of incubation of Ru@SiO_2-OH (A, in red) or Ru@SiO_2-NH_2 (B, in red) fluorescence with immunosignals for early endosomes protein 1 (A, B, in green). Cell nuclei are stained in blue. Arrows denote large early endosomes, which contain high amounts of nanoparticles. Scale bars = 30 μm.

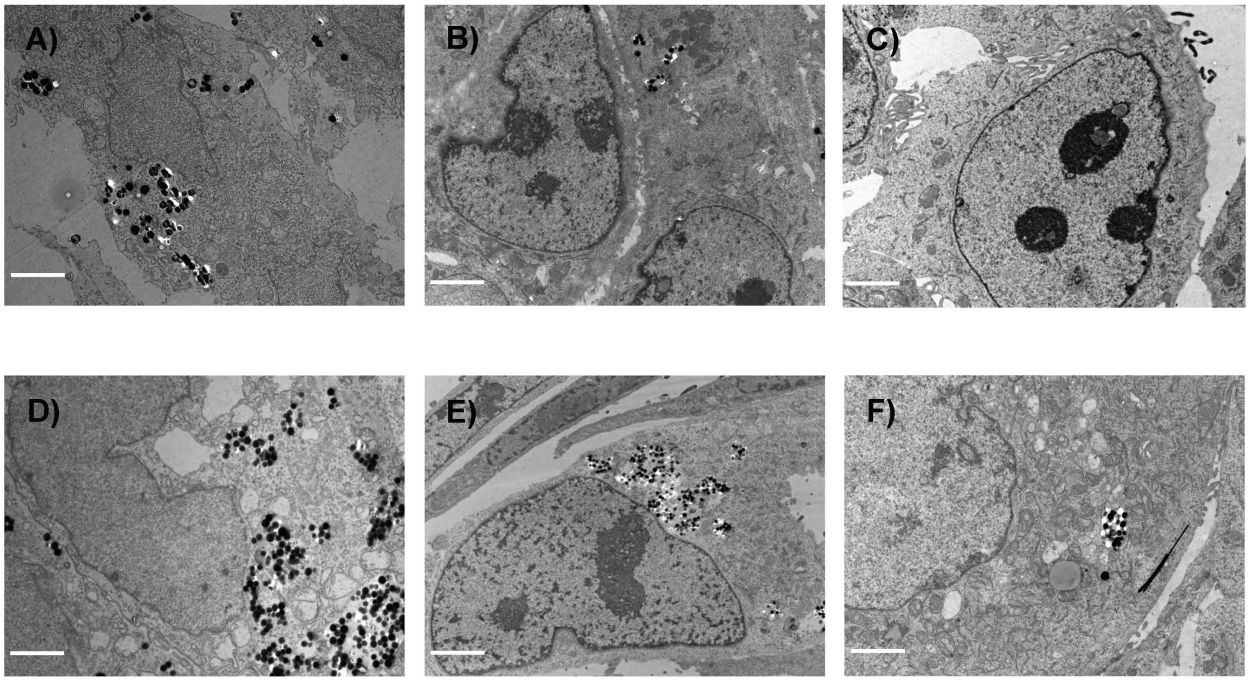

Figure 9 Intracellular long time retention of nanoparticles. Transmission electron microscopy pictures of UMB-SCC 745 after nanoparticle incubation over a time period of 15 days. A-C) 2, 9 and 12 days after incubation of Ru@SiO_2-OH nanoparticles. D-F) 2, 9 and 12 days after incubation of Ru@SiO_2-NH_2 nanoparticles. Scale bars for A-E) = 5 μm and for F) = 0.5 μm.

endosomal sorting mechanisms may have prevented their targeting to degradation pathways, our data is in contrast to other studies showing that silica nanoparticles are in fact transferred to lysosomes [46,47,50]. Our results also differ from those of Rejman et al. [49] where a size-dependency of endocytotic pathways had been proposed. In this study, at least smaller latex particles (200 nm) passaged to late endosomes/lysosomes while only large particles (500 nm) did not [49]. We therefore conclude that intracellular fate of nanoparticles not only depends on their size (or agglomeration status) but presumably also on cell line.

Although the exact nature of different endocytotic organelles in our model has to await further

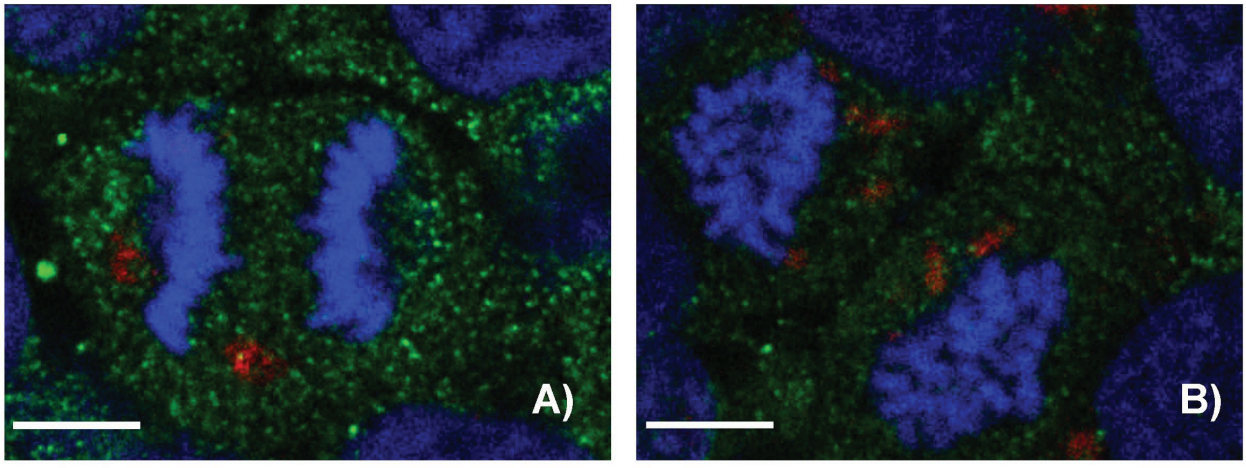

Figure 10 Nanoparticle distribution during cell division. Confocal laser scanning microscopy showing distribution of RuSiO_2-NH_2 nanoparticles during cell division (third passage) of UMB-SCC 745. A) metaphase and B) telophase, nucleus in blue and nanoparticles in red. Scale bars = 10 μm.

characterization, the strictly vesicle-associated occurrence of Ru@SiO_2-OH and Ru@SiO_2-NH_2 in HNSCC may have contributed to their biocompatibility. In human melanoma cells it had been reported that an escape of silica nanoparticles to the cytoplasm resulted in changes of the cytoskeleton as well as of adhesion and migration properties [51]. Whether the vesicular enclosure of our nanoparticles is a useful feature in the case of intracellular drug delivery strategies in HNSCC remains to be proven.

In addition to their relatively large diameter [52,53], the absence of free Ru@SiO_2-OH and Ru@SiO_2-NH_2 within the cytoplasm of HNSCC may have been the reason that nanoparticles never passed the nuclear membrane. Even though localizations of silica nanoparticles within the nucleus had been observed before [54], our data is in accordance with results from previous studies [53,55,56]. Recently, it had been shown that labeling with fluorophores may affect uptake kinetics and intracellular pathways of certain probes [57]. However, due to encapsulation of the dye in our study, it is unlikely that $[Ru(bpy)_3]Cl_2$ may have influenced routes of nanoparticles within cells. Until now, very little is known about the intracellular long-term fate of silica nanoparticles and possible consequences of their persistence in biological systems. In human lung epithelial cells, Stayton et. al. observed a slow but active transfer of silica nanoparticles from the cytoplasm to the exterior environment [58]. They showed that during the first 24 h almost 50% of nanoparticles exited the cells. In contrast, our data implicates that both internalized Ru@SiO_2-OH and Ru@SiO_2-NH_2 remain within the cell and are apparently distributed between daughter cells at cell division. During the course of several passages, initially high nanoparticle amounts in individual cells become "diluted", but ultrastructurally are still found in vesicles. The reason for the observed differences in long-time persistence of Ru@SiO_2-OH and Ru@SiO_2-NH_2 are not clear yet, but may also be related to as yet uncharacterised charge-dependent effects of nanoparticles on endolysosomal pathways. However, in addition of not featuring acute cell toxic effects, the presence of our silica nanoparticles over 15 days caused no visible changes in viability, proliferation or morphology in HNSCC. Of note, over the time course studied, ultrastructure of nanoparticles appears to remain unchanged. However, it cannot be excluded that discrete processes of nanoparticle degradation occurred. Recently, it had been reported that, depending on functionalization, integrity of silica nanoparticles may be impaired step-wise over time in simulated body fluid with regard to e.g. surface area, pore width or pore volume [59,60].

Although the high uptake efficiency of Ru@SiO_2-OH and Ru@SiO_2-NH_2 in our in-vitro mono-layer model was promising, optimized conditions are needed in case of solid HNSCC tumors where conditions of poorer vascularisation may exist. Our results in HNSCC spheroids, an established minitumor model, show that penetration depth of Ru@SiO_2-OH and Ru@SiO_2-NH_2 does not reach beyond the first (outer) cell layer - independent of nanoparticle surface charge. This observation provides further evidence that our nanoparticles are not actively exocytosed. Stayton et. al. showed in-vitro that nanoparticles which were exocytosed in growth medium were taken up by other cells if not removed from growth medium [58]. Given that nanoparticles are not transported transcellularly and apparently are incapable of passing the intercellular junction complexes, new delivery strategies have to be developed for multicellular poorly vascularized cancers.

5. Conclusion

In summary, our study is the first to provide evidence that core-shell silica nanoparticles may be useful tools for the development of novel therapeutic strategies with cancers of the head and neck region. However, before an encapsulation of pharmaceutical compounds or a functionalization with targeting and imaging moieties may be considered, a better understanding of how these nanoparticles interact with HNSCC cells on contact and after internalization is needed. Starting from our first steps towards clarification of endocytic pathways, further microscopic, immunocytochemical and molecular biological studies will elucidate nanoparticle sorting as well as their further intracellular fate, including possible degradation processes, or nanoparticle-mediated molecular cell responses.

Acknowledgements

We are thankful to Urs Ziegler and his team, especially Therese Bruggmann and Gery Barmettler for their help with confocal and transmission electron microscopy. We are also thankful to Tu-My Diep and Martin Steuble for their help in immunocytochemistry and fruitful scientific discussions.

Author details

[1]Institute of Anatomy, University of Zürich, Winterthurerstr. 190, 8057 Zürich, Switzerland. [2]University of Applied Sciences Northwestern Switzerland, School of Life Sciences, Institute of Chemistry and Bioanalytics, CH-4132 Muttenz, Switzerland. [3]Clinic for Cranio-Maxillofacial Surgery, University Hospital of Zürich, Frauenklinikstr. 24, 8091 Zürich, Switzerland.

Authors' contributions

CM and EBG designed all of the experiments and wrote the manuscript. EBG and XD performed all the experiments together. HW and MB contributed clinical expertise. AWH and UP synthesized and characterized the nanoparticles. All authors read and approved the final manuscript.

Competing interests

The authors declare that they have no competing interests.

Received: 8 February 2011 Accepted: 11 August 2011
Published: 11 August 2011

References

1. Tobias JS: **Cancer of the head and neck.** *Bmj* 1994, **308**:961-966.
2. Amir Z, Kwan SY, Landes D, Feber T, Williams SA: **Diagnostic delays in head and neck cancers.** *Eur J Cancer Care (Engl)* 1999, **8**:198-203.
3. Hunter KD, Parkinson EK, Harrison PR: **Profiling early head and neck cancer.** *Nat Rev Cancer* 2005, **5**:127-135.
4. Marur S, Forastiere AA: **Head and neck cancer: changing epidemiology, diagnosis, and treatment.** *Mayo Clin Proc* 2008, **83**:489-501.
5. Vermorken JB, Specenier P: **Optimal treatment for recurrent/metastatic head and neck cancer.** *Ann Oncol* **21(Suppl 7)**:vii252-vii261.
6. Berrino F, Gatta G: **Variation in survival of patients with head and neck cancer in Europe by the site of origin of the tumours.** *Eur J Cancer* 1998, **34**:2154-2161.
7. Conway DI, McKinney PA, McMahon AD, Ahrens W, Schmeisser N, Benhamou S, Bouchardy C, Macfarlane GJ, Macfarlane TV, Lagiou P, *et al*: **Socioeconomic factors associated with risk of upper aerodigestive tract cancer in Europe.** *Eur J Cancer* 2009, **46**:588-598.
8. Conway DI, McMahon AD, Smith K, Black R, Robertson G, Devine J, McKinney PA: **Components of socioeconomic risk associated with head and neck cancer: a population-based case-control study in Scotland.** *Br J Oral Maxillofac Surg* **48**:11-17.
9. Alexiou C, Jurgons R, Schmid RJ, Bergemann C, Henke J, Erhardt W, Huenges E, Parak F: **Magnetic drug targeting–biodistribution of the magnetic carrier and the chemotherapeutic agent mitoxantrone after locoregional cancer treatment.** *J Drug Target* 2003, **11**:139-149.
10. Damascelli B, Patelli G, Ticha V, Di Tolla G, Frigerio LF, Garbagnati F, Lanocita R, Marchiano A, Spreafico C, Mattavelli F, *et al*: **Feasibility and efficacy of percutaneous transcatheter intraarterial chemotherapy with paclitaxel in albumin nanoparticles for advanced squamous-cell carcinoma of the oral cavity, oropharynx, and hypopharynx.** *J Vasc Interv Radiol* 2007, **18**:1395-1403.
11. Boulikas T: **Clinical overview on Lipoplatin: a successful liposomal formulation of cisplatin.** *Expert Opin Investig Drugs* 2009, **18**:1197-1218.
12. Gao C, Pan J, Lu W, Zhang M, Zhou L, Tian J: **In-vitro evaluation of paclitaxel-loaded MPEG-PLGA nanoparticles on laryngeal cancer cells.** *Anticancer Drugs* 2009, **20**:807-814.
13. Cohen EM, Ding H, Kessinger CW, Khemtong C, Gao J, Sumer BD: **Polymeric micelle nanoparticles for photodynamic treatment of head and neck cancer cells.** *Otolaryngol Head Neck Surg* **143**:109-115.
14. Zou J, Qiao X, Ye H, Zhang Y, Xian J, Zhao H, Liu S: **Inhibition of ataxia-telangiectasia mutated by antisense oligonucleotide nanoparticles induces radiosensitization of head and neck squamous-cell carcinoma in mice.** *Cancer Biother Radiopharm* 2009, **24**:339-346.
15. French JT, Goins B, Saenz M, Li S, Garcia-Rojas X, Phillips WT, Otto RA, Bao A: **Interventional therapy of head and neck cancer with lipid nanoparticle-carried rhenium 186 radionuclide.** *J Vasc Interv Radiol* **21**:1271-1279.
16. Hainfeld JF, Dilmanian FA, Zhong Z, Slatkin DN, Kalef-Ezra JA, Smilowitz HM: **Gold nanoparticles enhance the radiation therapy of a murine squamous cell carcinoma.** *Phys Med Biol* **55**:3045-3059.
17. Curvo-Semedo L, Diniz M, Migueis J, Juliao MJ, Martins P, Pinto A, Caseiro-Alves F: **USPIO-enhanced magnetic resonance imaging for nodal staging in patients with head and neck cancer.** *J Magn Reson Imaging* 2006, **24**:123-131.
18. El-Sayed I, Huang X, Macheret F, Humstoe JO, Kramer R, El-Sayed M: **Effect of plasmonic gold nanoparticles on benign and malignant cellular autofluorescence: a novel probe for fluorescence based detection of cancer.** *Technol Cancer Res Treat* 2007, **6**:403-412.
19. Mack MG, Rieger J, Baghi M, Bisdas S, Vogl TJ: **Cervical lymph nodes.** *Eur J Radiol* 2008, **66**:493-500.
20. Popovtzer R, Agrawal A, Kotov NA, Popovtzer A, Balter J, Carey TE, Kopelman R: **Targeted gold nanoparticles enable molecular CT imaging of cancer.** *Nano Lett* 2008, **8**:4593-4596.
21. Kumar R, Ohulchanskyy T, Turowski S, Thompson ME, Seshadri M, Prasad PN: **Combined magnetic resonance and optical imaging of head and neck tumor xenografts using Gadolinium-labelled phosphorescent polymeric nanomicelles.** *Head Neck Oncol* 2010, **2**:35.
22. Xie H, Wang ZJ, Bao A, Goins B, Phillips WT: **In vivo PET imaging and biodistribution of radiolabeled gold nanoshells in rats with tumor xenografts.** *Int J Pharm* 2010, **395**:324-330.
23. Slowing II, Vivero-Escoto JL, Wu CW, Lin VS: **Mesoporous silica nanoparticles as controlled release drug delivery and gene transfection carriers.** *Adv Drug Deliv Rev* 2008, **60**:1278-1288.
24. Manzano M, Colilla M, Vallet-Regi M: **Drug delivery from ordered mesoporous matrices.** *Expert Opin Drug Deliv* 2009, **6**:1383-1400.
25. Vivero-Escoto JL, Slowing II, Trewyn BG, Lin VS: **Mesoporous silica nanoparticles for intracellular controlled drug delivery.** *Small* 2010, **6**:1952-1967.
26. Wang H, Yang R, Yang L, Tan W: **Nucleic acid conjugated nanomaterials for enhanced molecular recognition.** *ACS Nano* 2009, **3**:2451-2460.
27. Zhong W: **Nanomaterials in fluorescence-based biosensing.** *Anal Bioanal Chem* 2009, **394**:47-59.
28. Lucignani G: **Nanoparticles for concurrent multimodality imaging and therapy: the dawn of new theragnostic synergies.** *Eur J Nucl Med Mol Imaging* 2009, **36**:869-874.
29. Legrand S: **Controlling silica nanoparticles properties for biomedical applications through surface modification.** 2008.
30. Fent K, Weisbrod CJ, Wirth-Heller A, Pieles U: **Assessment of uptake and toxicity of fluorescent silica nanoparticles in zebrafish (Danio rerio) early life stages.** *Aquat Toxicol* **100**:218-228.
31. Mandic R, Rodgarkia-Dara CJ, Zhu L, Folz BJ, Bette M, Weihe E, Neubauer A, Werner JA: **Treatment of HNSCC cell lines with the EGFR-specific inhibitor cetuximab (Erbitux) results in paradox phosphorylation of tyrosine 1173 in the receptor.** *FEBS Lett* 2006, **580**:4793-4800.
32. Kelm JM, Timmins NE, Brown CJ, Fussenegger M, Nielsen LK: **Method for generation of homogeneous multicellular tumor spheroids applicable to a wide variety of cell types.** *Biotechnol Bioeng* 2003, **83**:173-180.
33. Napierska D, Thomassen LC, Lison D, Martens JA, Hoet PH: **The nanosilica hazard: another variable entity.** *Part Fibre Toxicol* 2010, **7**:39.
34. Huang Y, Swarup VP, Bishnoi SW: **Rapid Raman imaging of stable, functionalized nanoshells in mammalian cell cultures.** *Nano Lett* 2009, **9**:2914-2920.
35. Tziampazis E, Kohn J, Moghe PV: **PEG-variant biomaterials as selectively adhesive protein templates: model surfaces for controlled cell adhesion and migration.** *Biomaterials* 2000, **21**:511-520.
36. Blummel J, Perschmann N, Aydin D, Drinjakovic J, Surrey T, Lopez-Garcia M, Kessler H, Spatz JP: **Protein repellent properties of covalently attached PEG coatings on nanostructured SiO(2)-based interfaces.** *Biomaterials* 2007, **28**:4739-4747.
37. Akhtar MJ, Ahamed M, Kumar S, Siddiqui H, Patil G, Ashquin M, Ahmad I: **Nanotoxicity of pure silica mediated through oxidant generation rather than glutathione depletion in human lung epithelial cells.** *Toxicology* 2010, **276**:95-102.
38. Bartlett DW, Davis ME: **Physicochemical and biological characterization of targeted, nucleic acid-containing nanoparticles.** *Bioconjug Chem* 2007, **18**:456-468.
39. Verma A, Stellacci F: **Effect of surface properties on nanoparticle-cell interactions.** *Small* **6**:12-21.
40. Huang X, Zhuang J, Teng X, Li L, Chen D, Yan X, Tang F: **The promotion of human malignant melanoma growth by mesoporous silica nanoparticles through decreased reactive oxygen species.** *Biomaterials* 2010, **31**:6142-6153.
41. Lin W, Huang YW, Zhou XD, Ma Y: **In vitro toxicity of silica nanoparticles in human lung cancer cells.** *Toxicol Appl Pharmacol* 2006, **217**:252-259.
42. Choi SJ, Oh JM, Choy JH: **Toxicological effects of inorganic nanoparticles on human lung cancer A549 cells.** *J Inorg Biochem* 2009, **103**:463-471.
43. Slowing I, Trewyn BG, Lin VS: **Effect of surface functionalization of MCM-41-type mesoporous silica nanoparticles on the endocytosis by human cancer cells.** *J Am Chem Soc* 2006, **128**:14792-14793.
44. Chang JS, Chang KL, Hwang DF, Kong ZL: **In vitro cytotoxicitiy of silica nanoparticles at high concentrations strongly depends on the metabolic activity type of the cell line.** *Environ Sci Technol* 2007, **41**:2064-2068.
45. Chung TH, Wu SH, Yao M, Lu CW, Lin YS, Hung Y, Mou CY, Chen YC, Huang DM: **The effect of surface charge on the uptake and biological function of mesoporous silica nanoparticles in 3T3-L1 cells and human mesenchymal stem cells.** *Biomaterials* 2007, **28**:2959-2966.

46. Lu CW, Hung Y, Hsiao JK, Yao M, Chung TH, Lin YS, Wu SH, Hsu SC, Liu HM, Mou CY, *et al*: **Bifunctional magnetic silica nanoparticles for highly efficient human stem cell labeling.** *Nano Lett* 2007, **7**:149-154.
47. Hsiao JK, Tsai CP, Chung TH, Hung Y, Yao M, Liu HM, Mou CY, Yang CS, Chen YC, Huang DM: **Mesoporous silica nanoparticles as a delivery system of gadolinium for effective human stem cell tracking.** *Small* 2008, **4**:1445-1452.
48. Orr GA, Chrisler WB, Cassens KJ, Tan R, Tarasevich BJ, Markillie LM, Zangar RC, Thrall BD: **Cellular recognition and trafficking of amorphous silica nanoparticles by macrophage scavenger receptor A.** *Nanotoxicology* .
49. Rejman J, Oberle V, Zuhorn IS, Hoekstra D: **Size-dependent internalization of particles via the pathways of clathrin- and caveolae-mediated endocytosis.** *Biochem J* 2004, **377**:159-169.
50. Hocine O, Gary-Bobo M, Brevet D, Maynadier M, Fontanel S, Raehm L, Richeter S, Loock B, Couleaud P, Frochot C, *et al*: **Silicalites and Mesoporous Silica Nanoparticles for photodynamic therapy.** *Int J Pharm* **402**:221-230.
51. Huang X, Teng X, Chen D, Tang F, He J: **The effect of the shape of mesoporous silica nanoparticles on cellular uptake and cell function.** *Biomaterials* 2009, **31**:438-448.
52. Chen M, von Mikecz A: **Formation of nucleoplasmic protein aggregates impairs nuclear function in response to SiO2 nanoparticles.** *Exp Cell Res* 2005, **305**:51-62.
53. Nabeshi H, Yoshikawa T, Matsuyama K, Nakazato Y, Arimori A, Isobe M, Tochigi S, Kondoh S, Hirai T, Akase T, *et al*: **Size-dependent cytotoxic effects of amorphous silica nanoparticles on Langerhans cells.** *Pharmazie* **65**:199-201.
54. Tao Z, Toms BB, Goodisman J, Asefa T: **Mesoporosity and functional group dependent endocytosis and cytotoxicity of silica nanomaterials.** *Chem Res Toxicol* 2009, **22**:1869-1880.
55. Yu-Shen Lin, C-P T, Hsing-Yi Huang, Chieh-Ti Kuo, Yann Hung, Dong-Ming Huang, Yao-Chang Chen, Chung-Yuan Mou: **Well-Ordered Mesoporous Silica Nanoparticles as Cell Markers.** *Chem Mater* 2005, **17(18)**:4570-4573.
56. Yu K, Grabinski C, Schrand A, Murdock R, Wang W, Gu B, Schlager J, Hussain S: **Toxicity of amorphous silica nanoparticles in mouse keratinocytes.** *Journal of Nanoparticle Research* 2009, **11**:15-24.
57. Puckett CA, Barton JK: **Fluorescein redirects a ruthenium-octaarginine conjugate to the nucleus.** *J Am Chem Soc* 2009, **131**:8738-8739.
58. Stayton I, Winiarz J, Shannon K, Ma Y: **Study of uptake and loss of silica nanoparticles in living human lung epithelial cells at single cell level.** *Anal Bioanal Chem* 2009, **394**:1595-1608.
59. Cauda V: **ASaTB: Bio-degradationnext term study of colloidal mesoporous previous termsilica nanoparticles:next term Effect of surface functionalization with organo-silanes and poly(ethylene glycol).** *Microporous and Mesoporous Materials* 2010, **132**:60-71.
60. He QJS, Min Zhua, Yu Chen, Feng Chen: **The three-stage in vitro degradation behavior of mesoporous silica in simulated body fluidnext term.** *Microporous and Mesoporous Materials* 2010, **131**:314-320.

doi:10.1186/1477-3155-9-32
Cite this article as: Besic Gyenge *et al.*: Uptake and fate of surface modified silica nanoparticles in head and neck squamous cell carcinoma. *Journal of Nanobiotechnology* 2011 **9**:32.

7.2 Hypericin- and mTHPC-mediated Photodynamic Therapy for the Treatment of Cariogenic Bacteria

The contributions of Emina Besic Gyenge to the study: „Hypericin- and mTHPC-mediated photodynamic therapy for the treatment of cariogenic bacteria" were the following:

1. Supervising of medical student

2. Contribution to elaboration of experiment designs

3. Partially collection of data, in particular: **figure 2** (Foslipos® and hypericin mediated photodynamic effects in *Streptococcus sobrinus*) and **figure 3** (Mixture (1:1 Foslipos® and hypericin) mediated photodynamic effects in *Streptococcus sobrinus)*

4. Collection of microscopic imaging, in particular: **figure 1** (time dependent accumulation of Foslipos® and hypericin in the dark in *Streptococcus sobrinus*) and **figure 4** (time dependent accumulation of Foslipos® and hypericin in the dark in *Streptococcus mutans*

5. Cover picture of the "Medical Laser Application" Journal, Volume 24, 2009

Available online at www.sciencedirect.com
ScienceDirect
Medical Laser Application 24 (2009) 227–236
Medical Laser Application
www.elsevier.de/mla

Hypericin- and mTHPC-mediated photodynamic therapy for the treatment of cariogenic bacteria

Martin Lüthi [a], Emina Besic Gyenge [b], Mathias Engström [a], Marius Bredell [b], Klaus Grätz [b], Heinrich Walt [b], Rudolf Gmür [c], Caroline Maake [a,*]

[a] *Institute of Anatomy, University of Zurich, Winterthurerstrasse 190, 8057 Zurich, Switzerland*
[b] *Clinic for Cranio-Maxillofacial Surgery, University Hospital of Zurich, Frauenklinikstrasse 24, 8091 Zurich, Switzerland*
[c] *Institute of Oral Biology, University Hospital of Zurich, Plattenstrasse 11, 8032 Zurich, Switzerland*

Received 21 July 2009; accepted 30 July 2009

Abstract

Objective: Dental caries is one of the most common diseases in Western countries. Its pathoetiology is multifactorial, however, bacteria including *Streptococcus mutans* and the closely related *Streptococcus sobrinus* are regarded as key factors involved in this process. The fact that therapeutic approaches to eradicate these microorganisms are still limited prompted us to investigate the treatment potential of photodynamic therapy with the photoactive compounds hypericin (HYP) and meso-tetra(hydroxyphenyl)chlorin (mTHPC) *in vitro*.

Material and methods: *S. mutans* and *S. sobrinus* were cultivated under standard conditions and incubated with HYP (Invitrogen, Basel, Switzerland), the liposomal mTHPC derivative Foslipos (FOS, Biolitec, Jena, Germany), or a mixture of both at concentrations ranging between 0.625 and 10 μg/ml for various time points. Following a thorough washing step, bacteria were irradiated with a dental polymerization instrument (400–505 nm). All samples were subjected to serial dilutions and spiral plating on blood agar plates. Viable colony counts were determined after 48 h in culture. Photosensitizer fluorescence of bacteria was visualized by confocal microscopic techniques.

Results: One hundred percent of *S. sobrinus* could be killed by a 15 min incubation with as little as 2.5 μg/ml HYP, 5 μg/ml FOS or a mixture of 1.25 μg/ml of each photosensitizer followed by light activation of 120 s. In contrast to *S. sobrinus*, *S. mutans* displayed a significant dark toxicity for FOS (10–1.25 μg/ml) and no relevant PDT effects using HYP (10–0.625 μg/ml) under these conditions. HYP-mediated PDT effects (10 μg/ml) could be enhanced to more than 99.9% by prolonging photosensitizer incubation to 30 min and fractional illumination (2 × 120 s). Complete eradication of *S. mutans* was achieved by incubation for 15 min with a mixture of 0.625 μg/ml each of FOS and HYP and illumination for 120 s.

Conclusion: For both *S. mutans* and *S. sobrinus*, short PDT protocols with FOS and/or HYP could be established that completely eradicated these cariogenic bacteria in suspension. Our study, however, indicated that careful optimization of PDT conditions may be necessary for successful treatment of even closely related bacterial species. In multispecies microbial populations, the application of photosensitizer combinations for PDT may be useful.

Keywords: Photodynamic therapy; Bacteria; mTHPC; Hypericin; Gram-positive

*Corresponding author. Tel.: +41 44 6355338; fax: +41 44 6355702.
E-mail address: cmaake@anatom.uzh.ch (C. Maake).

1615-1615/$ - see front matter © 2009 Elsevier GmbH. All rights reserved.
doi:10.1016/j.mla.2009.07.004

Introduction

The oral cavity harbors a plenitude of microorganisms that together constitute the normal flora. However, under pathologic conditions this complex system may be disturbed, eventually contributing to the etiology of various inflammatory diseases that may even spread outside the *cavitas oralis* [1].

The most prevalent of microorganism-related oral diseases is caries. Among the different pathogens involved, the contribution of the Gram-positive facultative anaerobic bacteria *Streptococcus mutans* and the related *Streptococcus sobrinus* are thought to play key roles for the progression of this condition [2].

It is well-known that appropriate oral hygiene strongly reduces the risk for caries; however, the current number of affected patients is considerable, creating substantial health care costs [3]. In most cases, caries treatment consists of debridement of the oral plaque (i.e. the biofilm where the cariogenic species reside within an extracellular polymer matrix) or excavation, disinfection and sealing of the infected dentin. The limitations of these non-specific and invasive treatment options recently rekindled interest in a method whose basic effects on microorganisms have been known for 100 years i.e. photodynamic therapy (PDT) [4]. Briefly, PDT is a non- or minimally invasive treatment method relying on the ability of a photoactive non-toxic drug (the so-called photosensitizer) which upon activation with light rapidly generates free radicals or singlet oxygen that can oxidize cellular constituents and eventually lead to cell death [5].

In the past decades, numerous studies have underlined the potential of PDT to destroy bacteria, protozoa, fungi and viruses [6]. Although published data on PDT for oral pathogens are relatively limited and most of the studies had been performed *in vitro*, was proposed that PDT either alone or in combination with other strategies may be a useful option to treat pathogens involved in periodontitis [7], peri-implantitis [8], endodontitis [9] and caries [10].

Of the broad spectrum of photosensitizers available today, several had been successfully applied for PDT on the cariogenic bacteria *S. mutans* and *S. sobrinus*. These included tricyclic dyes [11–20] or tetrapyrroles belonging to the classes of porphyrines [16,20], chlorins [21] and phthalocyanines [22,23]. However, to the best of our knowledge, neither meso-tetra(hydroxyphenyl)chlorin (mTHPC) nor hypericin (HYP) have been tested for treatment of *S. mutans* or *S. sobrinus* by PDT.

mTHPC is currently regarded as one of the most potent second-generation photosensitizers. While the vast majority of reports concern its high efficiency to destroy cancer cells [24], effects on bacteria are anecdotal and only include successful treatment of methicillin-resistant *Staphylococcus aureus* with a liposomal mTHPC formulation [25].

Hypericin is a phenanthroperylene quinine pigment naturally occurring in plants such as St. John's Wort (Hypericum species). It is currently among the most popular drugs against mild depression in complementary medicine. In addition to its potent photo-damaging effects on cancer cells [26], several studies have indicated that HYP is active against various Gram-positive bacteria [27–29].

In order to gain further insight into the effects and potential of new photosensitizers for clinical application the first study was used to investigate the antimicrobial effects on the cariogenic Gram-positive bacteria, *S. mutans* and *S. sobrinus*, of mTHPC and HYP alone and in combined, in PDT.

Materials and methods

Bacterial culture

S. mutans (OMZ 918) and *S. sobrinus* (OMZ 176) were obtained from the culture collection of the Institute of Oral Biology, University of Zurich, Switzerland and routinely grown aerobically over night at 37 °C in fluid universal medium (FUM) as described by Gmür and Guggenheim [30] until the late log phase.

Photosensitizers

Foslipos (FOS), a novel liposomal uncharged mTHPC compound was kindly donated by Biolitec, Jena, Germany. A stock solution (1.5 mg/ml) of FOS was prepared in water. HYP was purchased from Invitrogen, Basel, Switzerland and dissolved as a stock at 1 mg/ml in ethanol. All photosensitizer stock solutions were kept at 4 °C in the dark and further diluted in FUM.

Confocal microscopy

After incubation of bacteria in the dark with FOS or HYP (5 μg/ml) for 5, 15 or 30 min, respectively all samples were fixed by drying on microscopic slides and mounted in Glycergel® (Dako, Glostrup, Denmark). Analyses were performed with a confocal laser scanning microscope (TCS SP2 and SP5, Leica, Wetzlar, Germany).

PDT protocols

Planktonic bacteria were centrifuged and FUM was replaced by FOS (0.625–10 μg/ml), HYP (0.625–10 μg/ml) or a 1:1 mixture (MIX) of both (0.625–10 μg/ml each).

Bacteria were incubated for 1–30 min at 37 °C in the dark, followed by two thorough washing steps in physiological NaCl solution. Thereafter samples were exposed at a 3-cm distance to the culture surface to visible light from a halogen polymerization device (Optilux500, KerrHawe, Bioggio, Switzerland) for 120 s. According to the specifications of the manufacturer, this lamp has a wavelength range of 400–505 nm and an intensity of 1070 mW/cm^2. The light source had an illuminance of 40,000 lx at the surface and of 21,400 lx at the bottom of the incubation tube. Additional experiments were performed as a sequential light application for two times 120 s, with a 30 min vortex step in between.

Numbers of viable colony forming units (CFU) were obtained after 48 h from serial dilutions of all samples in FUM and spiral plating on Columbia Blood Agar Base (Becton, Dickinson and Co., Le Pont de Claix, France) supplemented with 5% hemolyzed human blood. Controls included the following: bacteria received (1) no treatment (neither light nor photosensitizer), (2) only photosensitizers, but no light ("dark toxicity") and (3) no photosensitizer, but light.

Data analyses and statistics

All experiments were at least performed in triplicate. Data are presented as means with standard deviations of the mean. Data were normalized against untreated controls (set to 100%) and expressed as a percentage of surviving or killed bacteria of these untreated controls. The *t*-tests were regarded as significant with *p*-values ≤ 0.05.

Results

Streptococcus sobrinus

Microscopic analyses showed that incubations with FOS and HYP lead to a pronounced fluorescent signal at *S. sobrinus* already after 5 min. The fluorescence intensity was further increased after 15 min but did not appear to be considerably stronger after 30 min incubation (Fig. 1).

Controls indicated that growth of untreated *S. sobrinus* was not impaired by irradiation with the dental polymerization tool. Furthermore, when compared with untreated controls, no significant dark toxic effects were detected after incubations with FOS or HYP (0.625–10 μg/ml) without light activation. In untreated controls, an average of 2.16E + 8 CFU/ml was obtained.

When irradiated after incubation with photosensitizers, a strong PDT effect was elicited, resulting in 100% bacterial death at concentrations between 10 and 2.5 μg/ml HYP or 10 and 5 μg/ml FOS, when incubated for 15 min and light activated for 120 s. A reduced bacterial count of $\leq$E + 05 was still observed down to 1.25 μg/ml FOS or HYP, respectively (Fig. 2). Generally, PDT with FOS resulted in higher counts of the CFU (in the order of 10-fold) compared with PDT with HYP. This observation was most apparent at low photosensitizer concentrations and is illustrated in Fig. 2.

Application of MIX for 15 min and illumination for 120 s revealed that *S. sobrinus* could be 100% eradicated using concentrations between 5 and 1.25 μg/ml of each of the photosensitizers, while the lower concentrated mixture (each photosensitizer 0.625 μg/ml) led only to a 1.53E + 02-fold reduction of CFU counts (Fig. 3). In comparative analyses of treatment effects with single photosensitizers, we found that the bactericidal activity of the MIX with 1.25 μg/ml of each FOS and HYP was the same as with 2.5 μg/ml HYP alone (Fig. 2). Neither PDT with FOS nor HYP at 1.25 μg/ml led to a complete destruction of *S. sobrinus* (99.988% and 99.998%, respectively).

Streptococcus mutans

In *S. mutans*, we observed a fluorescence pattern in confocal microscopy that was comparable to that in *S. sobrinus* with a maximum signal being reached after 15 min incubation with either photosensitizer (Fig. 4). Controls consisting of illumination only indicated no light sensitivity of *S. mutans*. In this bacterial strain, untreated controls reached a mean of 4.16E + 07 CFU/ml.

Studies dealing with possible dark toxic effects revealed that treatment with FOS between 0.625 and 10 μg/ml was already effective in killing 97.500–99.999% of bacteria without light activation (Fig. 5). Additional treatment with light further improved destruction of bacteria at all FOS concentrations investigated, ranging from 100% at concentrations between 10 and 1.25 μg/ml to 99.997% at the lowest concentration tested (0.625 μg/ml) (Fig. 5).

In contrast to FOS, not even the highest concentrations of HYP displayed toxicity in the dark (mean bacterial survival rate of 88.923% at 10 μg/ml HYP compared with controls). However, when bacteria were irradiated (120 s) after incubations with HYP bacterial survival rates were still high. Even PDT with 10 μg/ml HYP only resulted in an E + 02 reduction in *S. mutans*, while with low concentrations (1.25 or 0.625 μg/ml) 65.965% or 90.894%, respectively, of bacteria survived (Fig. 6). Using the highest concentration of HYP (10 μg/ml) in combination with a prolongation of photosensitizer incubation time to 30 min and sequential light application of 2×120 s, a 99.988% destruction of bacteria could be achieved (Fig. 6).

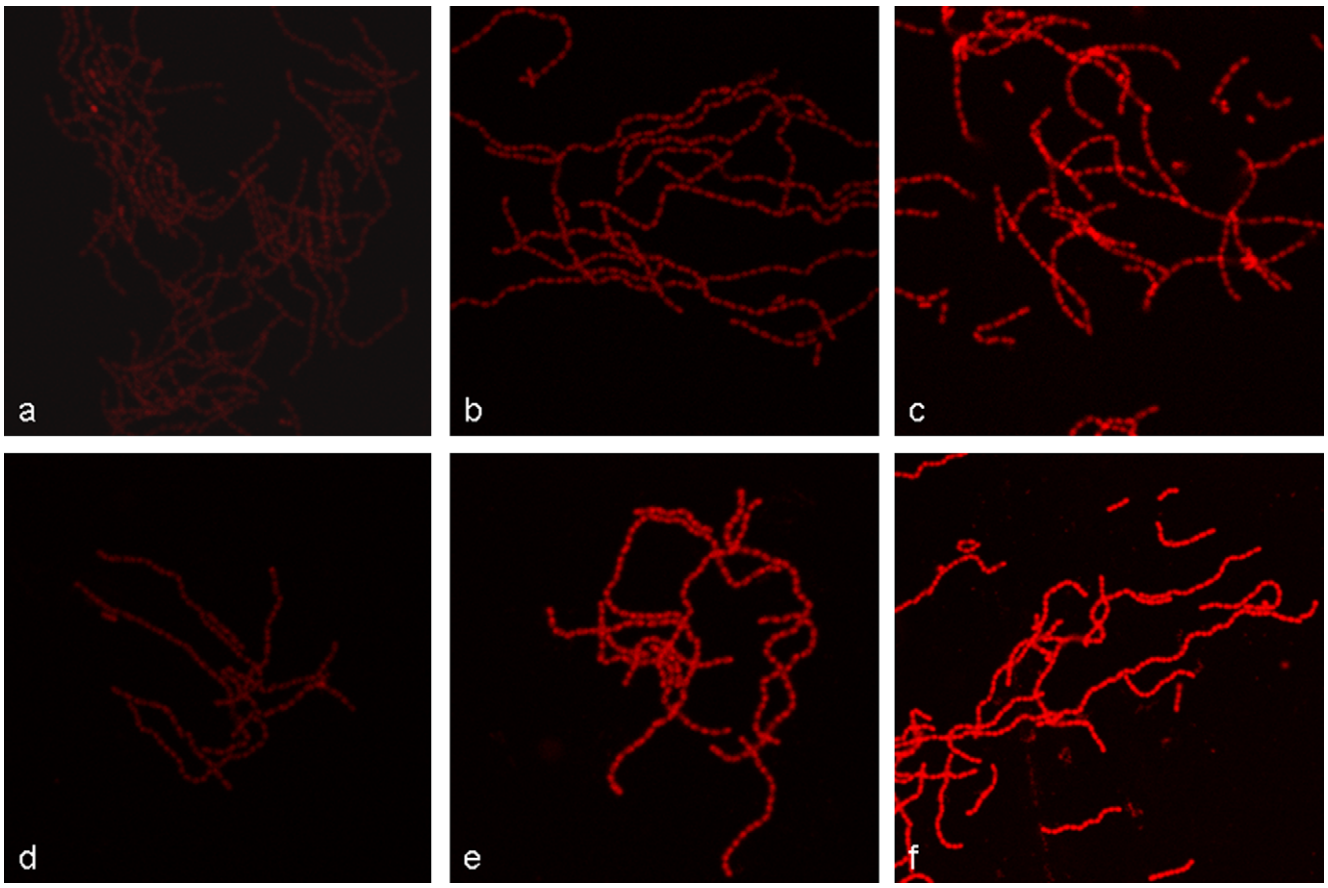

Fig. 1. *Streptococcus sobrinus* after incubation with Foslipos (a–c) and hypericin (d–f) in the dark. Confocal microscopy was performed after incubation times of 5 min (a,d), 15 min (b,e) and 30 min (c,f). Images were acquired with a 63 × 1.4 numerical aperture (NA) oil immersion objective lens providing an optical section thickness of 200 nm.

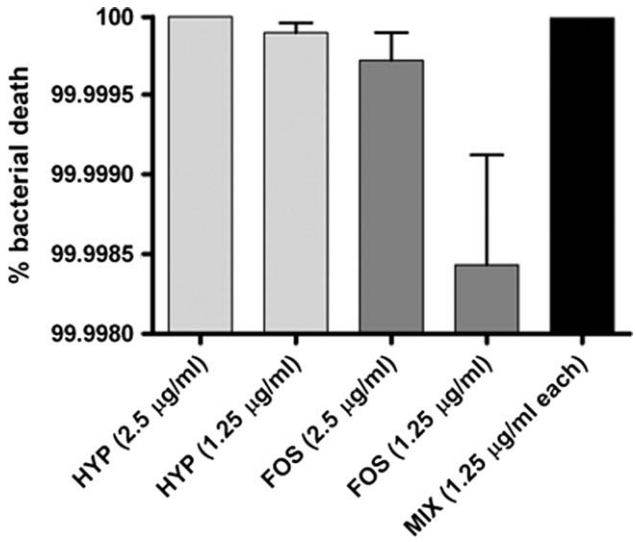

Fig. 2. Photodynamic effects in *Streptococcus sobrinus*. Photosensitizers (Foslipos and/or hypericin) at the concentrations indicated had been incubated for 15 min and light (400–505 nm) was applied for 120 s.

Generally, the 1:1 MIX of photosensitizers displayed the same dark toxicity as the respective concentrations of FOS alone. To obtain information about PDT using the MIX, we focused only on 0.625 µg/ml of each photosensitizer, since this concentration showed a significant PDT effect for FOS when compared with its dark toxicity ($p = 0.0063$). While we found that under the above conditions PDT with the MIX completely (100%) eradicated *S. mutans*, PDT with neither FOS nor HYP alone at concentrations of 0.625 µg/ml was able to do so (survival rate: 0.002% and 90.89%, respectively; Fig. 7). The same 100% effect could be obtained by PDT with 1.25 µg/ml FOS (Fig. 7).

Discussion

PDT is characterized by features that make this treatment modality especially attractive to combat microbial pathogens. These include its efficacy on antibiotic-resistant strains, its broad target spectrum as

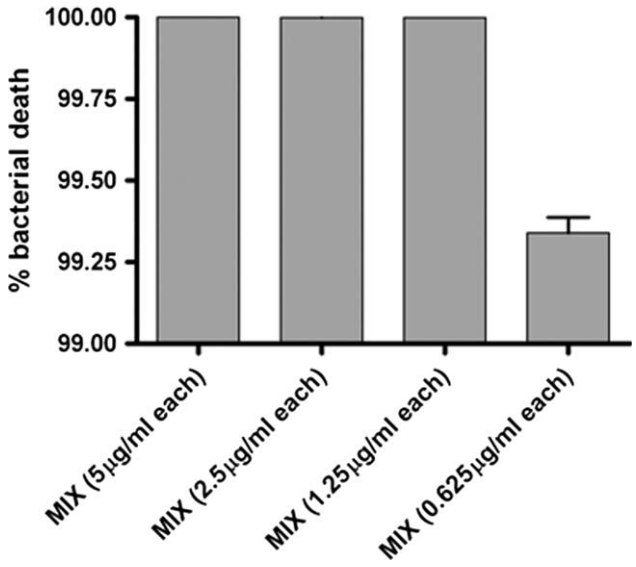

Fig. 3. Photodynamic effects in *Streptococcus sobrinus* after 15 min incubation with varying concentrations of a 1:1 mixture of the photosensitizers Foslipos and hypericin and illumination (400–505 nm) for 120 s.

well as its very low potential for mutagenicity and photoresistance [6]. However, of the large spectrum of photoactive agents available to date, only a limited number have so far been investigated with regard to their antimicrobial applicability.

To the best of our knowledge, our study is the first to investigate bactericidal PDT effects of mTHPC (FOS) or HYP on *S. sobrinus* and *S. mutans*. However, PDT data from previous studies in *mutans streptococci* are available for a few other photosensitizers, including toluidine blue O [11,12,14,17,18,20], methylene blue [16,19], erythrosine [15,16], hematoporphyrin derivative [16,20], native and lysine-conjugated chlorin e6 [21], aluminium disulphonated or cationic Zn(II) phthalocyanine [22,23], and Rose Bengal [13]. Our results as well as the vast majority of the above published data underlined the usefulness of PDT to destroy *mutans streptococci*, supporting the general observation that Gram-positive bacteria are susceptible to inactivation by photodynamic procedures [31]. Since many experimental parameters such as cell culture conditions, photosensitizer concentrations and their incubation times,

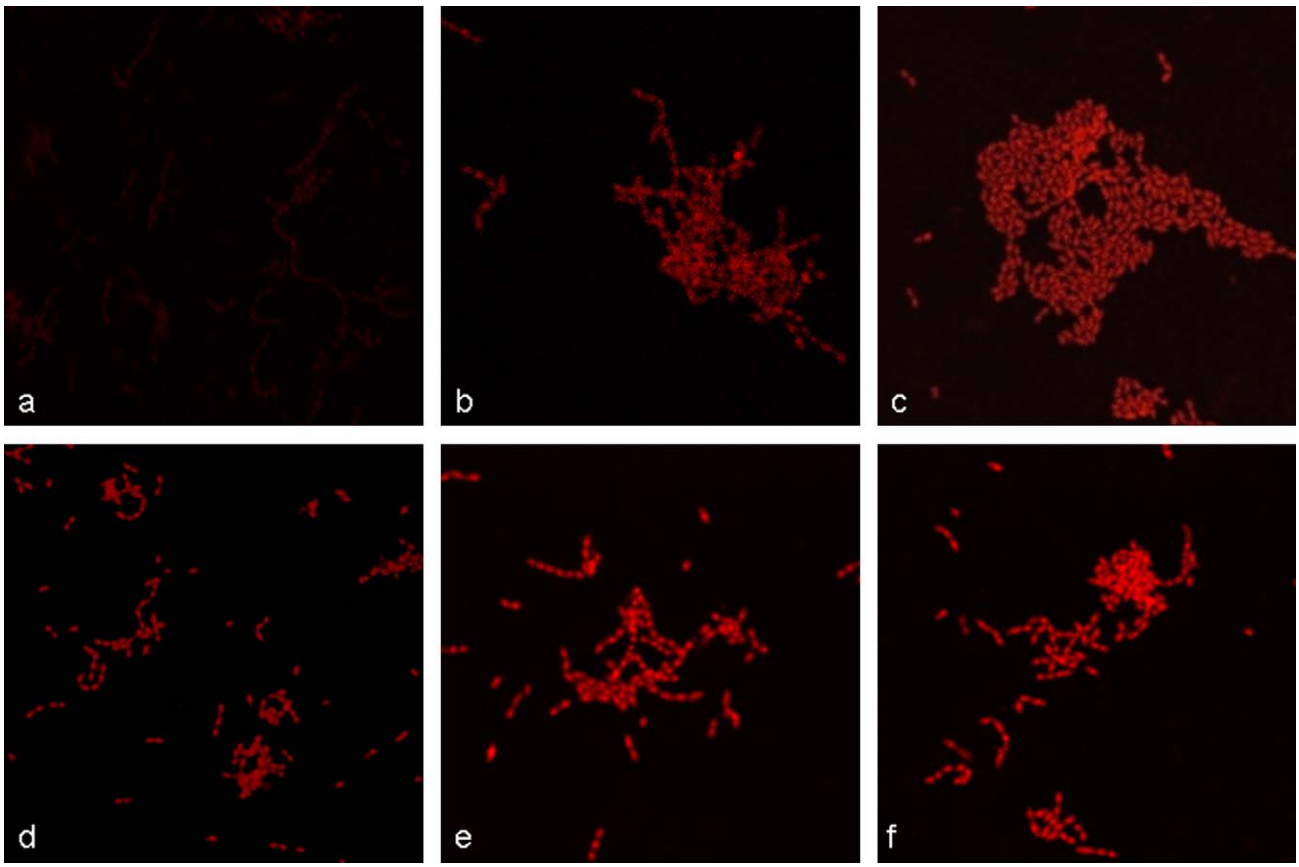

Fig. 4. *Streptococcus mutans* after incubation with Foslipos (a–c) and hypericin (d–f) in the dark. Confocal microscopy was performed after incubation times of 5 min (a,d), 15 min (b,e) and 30 min (c,f). Images were acquired with a 63×1.4 NA oil immersion objective lens providing an optical section thickness of 200 nm.

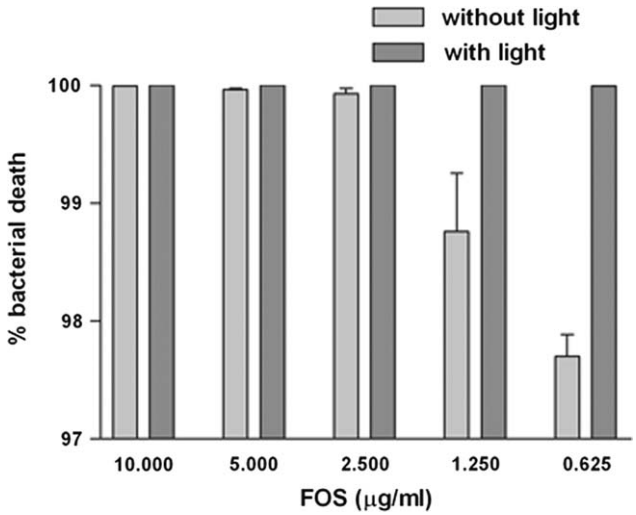

Fig. 5. Incubation of *Streptococcus mutans* with varying concentrations of Foslipos for 15 min with consecutive light activation (120 s) or without light activation.

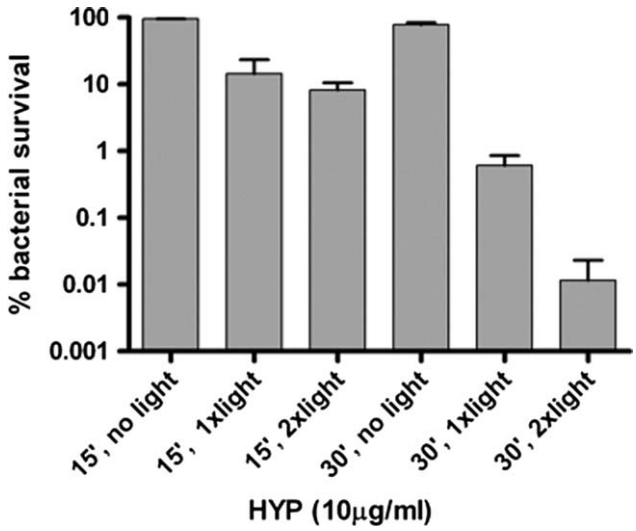

Fig. 6. Effects of hypericin incubated for either 15 or 30 min in *Streptococcus mutans*. Bacterial cultures had been either kept in the dark (no light), or illuminated for 15 min (1 × light) and two times 15 min with an intermittant vortex step of 30 s (2 × light).

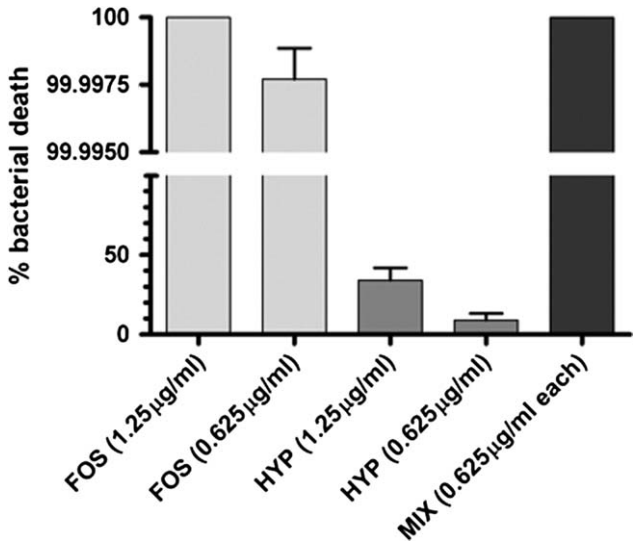

Fig. 7. Photodynamic effects in *Streptococcus mutans*. Photosensitizers (Foslipos and/or hypericin) at the concentrations indicated had been incubated for 15 min and light (400–505 nm) was applied for 120 s.

light sources, illumination intensities and times, differ considerable both between studies and our set-up, a comparison of experiments is only of limited value.

However, when analyzing data or establishing protocols, it should be kept in mind that with respect to the extremely fast growth of *mutans streptococci*, PDT killing rates of bacteria may be statistically significant but clinically insufficient. Our study shows that short PDT protocols with FOS and HYP can be established that have the capacity to completely kill these bacteria in suspension. Among all previously published studies, only two also used planktonic cultures (*S. mutans*) as models, showing that PDT protocols with either 0.5 μg/ml Rose Bengal or 100 μg/ml toluidine blue O resulted in a complete bacterial eradication [13,18]. All PDT reports dealing with single- or multispecies oral biofilms (with *mutans streptococci*) were only able to reduce viable bacterial counts [14–17,19,20,23]. It is well-known that pathogens organized in biofilms are more resistant towards antimicrobial modalities compared to planktonic cultures. This may also hold true for our PDT protocols, since preliminary studies with *mutans streptococci* grown in sucrose-supplemented media also displayed a reduced bactericidal efficiency.

For the light source in our study we used a halogen hand-held unit routinely applied for polymerization of light-cured dental materials. Successful elimination of bacteria in our setting indicated that it may be an interesting alternative to the commonly used lasers; especially since the polymerization tool is safer, cheaper and readily available in most dentists' offices. While for cancer PDT light sources with longer wavelengths are preferred because of deeper penetration needs, the superficial sites of cariogenic bacteria are easily accessible with our device. Its wavelength range (400–505 nm) is perfectly suitable for activation of FOS, since the Soret band of this photosensitizer is at 420 nm [32]. The spectrum of HYP contains a very broad absorption band near 460 nm but, notably, main peaks are outside the wavelength range of our lamp [33]. Our study is not the first using non-laser light for PDT [34] and previously, another brand of hand-held photopolymerizer was successfully applied for activation of Rose Bengal in *S. mutans* [13].

Both *S. mutans* and *S. sobrinus* are traditionally grouped in a common taxonomic cluster – the mutans group – based on shared phenotypic reactions. The strongly different experimental sensitivity of the two *Streptococcus* species observed in our study was therefore rather unexpected and question the close relationship. Our data support earlier molecular phylogenetic analyses of glucan-producing enzymes and superoxide dismutases indicating that the two bacteria are in fact genetically separate [35–37]. From *in-vitro* cancer studies – including our own (unpublished data) – the different behavior of photosensitizers in related types of tumor cells is actually well-known, underlining the complexity of biomechanisms initiated by PDT.

Basically, the observed differences in sensitivity concerned two parameters: (1) high levels of dark toxicity of FOS in *S. mutans* vs. *S. sobrinus* and (2) ineffectiveness of HYP-mediated PDT in *S. mutans* – at least under the conditions effective in *S. sobrinus*.

Currently, no comparable data of our mTHPC formulation are available for other microorganisms. In ongoing studies we are thus investigating whether *S. mutans* has an extremely high tolerance or *S. sobrinus* is extraordinarily sensitive towards this compound. However, we propose that the observed dark toxic effects of FOS should not impose any clinical treatment consequences. In contrast, inefficiency of HYP-mediated PDT in *S. mutans* under the same experimental conditions as in *S. sobrinus* would necessitate the development of protocol modifications. Since our microscopic analyses indicated that the fluorescence signal of HYP was no different morphologically from that of *S. sobrinus* we conclude that lack of adherence and/or uptake was not the underlying problem. Details of these processes, however, have not been investigated here. Notably, the light source used in our setting had a sub-optimal wavelength range for activation of HYP. The improvement of PDT effects by a fractionated illumination may indicate that the failure with our standard protocols is – at least in part – related to this factor. Our data are in line with earlier studies showing that HYP-mediated PDT effects can be enhanced by sequential light application [38]. Another critical factor may be the known complexity of HYP biological effects [39]. These appear to involve an array of light-dependent and -independent mechanisms whose roles may vary under different circumstances. It had been reported, for example, that HYP activity may be strongly and specifically protein-dependent, resulting in either promotion or inhibition of PDT effects in the presence of certain highly related isoforms of glutathione *S*-transferases [40]. The HYP used in our study was a plant extract of 99% purity (according to the manufacturer's specification) and the remaining 1% unspecified herbal components may have further contributed to the observed differences of bioeffects. In none of our experiments, however, did we observe increased growth rates after treatment with HYP as reported for *S. aureus* [41].

In our study, we also investigated the consequences of a combined application of FOS and HYP for PDT. While this is the first report on *mutans streptococci*, combined photosensitizer approaches have been investigated before in a limited number of studies. In *S. aureus*, the combination of HYP and mTHPC was reported to be counterproductive since bacterial growth was stimulated and PDT effects inhibited [41], while in contrast the combination of mTHPC and a hematoporphyrin derivative resulted in a superior (additive) PDT effect in this species [42]. In human endometrial cancer cells, in a breast cancer patient as well in a mouse mammary cancer model photosensitizer combinations (5-aminolevulinic) acid/HYP and Photofrin II/meso-tetra-(4-sulfonatophenyl)-porphine, respectively) led to an enhanced phototoxicity [43,44]. To explore possible advantages of an FOS/HYP combination in our model system, we focused on concentrations for photosensitizers that – when given alone – were unable to completely kill *S. mutans* or *S. sobrinus*. With both bacteria investigated here, PDT after a short incubation with the MIX completely sterilized planktonic cultures, indicating the high efficiency of this treatment procedure. It is of note that PDT with 1.25 μg/ml FOS in *S. mutans* or with 2.5 μg/ml HYP in *S. sobrinus* had the same 100% killing effect as the respective optimal MIX. Therefore, the effects of low-dose single photosensitizers were enhanced in the MIX, but no clear advantage towards the application of the total dose by a single photoactive compound was evident in our set-up. However, in many clinical settings, multispecies microbial communities have to be treated. Given a non-uniform response of these pathogens towards certain photosensitizing agents (as in our models of cariogenic bacteria), the application of mixtures may have distinct advantages by targeting a whole array of microorganisms in one treatment session.

Conclusions

Our study gives further support to the fact that PDT with second-generation photosensitizers may be an effective treatment modality to eradicate cariogenic pathogens. Short protocols within less than 20 min treatment time may be feasible. However, the differential results on closely related bacterial species indicate how little we actually understand about the factors that govern PDT-generated cell death in bacteria. For the achievement of clinically relevant effects, great care must be taken to adjust PDT parameters depending on specific microorganisms to be targeted. Future investigations of molecular and cellular events elicited by photosensitizer incubation and PDT may reveal whether

reduced doses of photosensitizers applied in a combinated treatment will result in favorable clinical effects, e.g. with regards to immune responses *in vivo*. However, the strength of mixtures of photosensitizers for antimicrobial PDT may be in their potential to target complex microbial populations such as in supragingival plaque.

Acknowledgement

Martin Lüthi and Emina Besic Gyenge contributed equally to this study. The authors thank Martin Gander as well as Urs Ziegler (Center of Microscopy and Image Analysis, University of Zurich) for their for excellent technical support. The study was supported by the Swiss Dental Association.

Zusammenfassung

Hypericin- und mTHPC-vermittelte photodynamische Therapie zur Behandlung kariogener Bakterien

Zielsetzung: Karies gehört zu den häufigsten Erkrankungen in den westlichen Ländern. Wenngleich vermutlich multiple Faktoren eine ursächliche Rolle spielen, so wird doch den verwandten Bakterien *Streptococcus mutans* und *Streptococcus sobrinus* eine Schlüsselrolle für die Pathoätiologie von Karies zugesprochen. Da geeignete antibakterielle Behandlungsmöglichkeiten zur Zeit fehlen, haben wir in der vorliegenden Arbeit das Potential einer photodynamischen Therapie (PDT) mit den photoaktiven Substanzen Hypericin (HYP) und meso-Tetra(hydroxyphenyl)chlorin (mTHPC) *in vitro* untersucht.
Material und Methoden: *S. mutans* und *S. sobrinus* wurden routinemässig kultiviert und mit HYP (Invitrogen, Basel, Schweiz), dem liposomalen mTHPC-Derivativ Foslipos (FOS, Biolitec, Jena, Deutschland) oder einer Mischung aus beiden mit Konzentrationen von 0.625–10 μg/ml unterschiedlich lang inkubiert. Nach sorgfältigen Wasch-Schritten wurden die Bakterien mit einer zahnärztlichen Polymerisationslampe bei 400–505 nm bestrahlt. Die Proben wurden dann seriell verdünnt und auf Blut-Agar-Platten ausspiralisiert. Überlebende Kolonien wurden nach 48 h ausgezählt. Ausserdem wurde die Fluoreszenz der Photosensibilisatoren an den Bakterien mit einem Konfokalmikroskop untersucht.
Ergebnisse: *S. sobrinus* konnte zu 100% abgetötet werden durch eine 15-minütige Inkubation mit 2,5 μg/ml HYP, 5 μg/ml FOS oder einer Mischung von 1.25 μg/ml beider Photosensibilisatoren und anschließender Lichtaktivierung für 120 s. Im Gegensatz zu *S. sobrinus* zeigte *S. mutans* unter diesen Bedingungen eine signifikante Dunkeltoxizität für FOS (10–1.25 μg/ml) und keine relevanten PDT-Effekte für HYP (10–0.625 μg/ml). HYP-bedingte PDT-Effekte (10 μg/ml) konnten aber durch Verlängerung der Inkubationszeit auf 30 min und eine fraktionierte Bestrahlung (2 × 120 s) auf mehr als 99.9% erhöht werden. Eine vollständige Eliminierung von *S. mutans* konnte durch eine 15-minütige Behandlung mit einer Mischung von je 0.625 μg/ml FOS und HYP und einer Belichtung von 120 s erzielt werden.
Schlussfolgerungen: Sowohl für *S. mutans* wie auch für *S. sobrinus* konnten kurze PDT-Protokolle mit FOS und/oder HYP entwickelt werden, welche zur vollständigen Abtötung dieser beiden kariogenen Keime in Suspension führten. Unsere Studie zeigte aber auch, dass die Behandlung verwandter Keime eine sorgfältige Optimierung der PDT-Bedingungen notwendig machen kann. Die Verwendung von Photosensibilisator-Kombinationen könnte für die Therapie von mikrobiellen Multispezies-Populationen hilfreich sein.

Schlüsselwörter: Photodynamische Therapie; Bakterien; mTHPC; Hypericin; Gram-positiv

References

[1] Parahitiyawa NB, Jin LJ, Leung WK, Yam WC, Samaranayake LP. Microbiology of odontogenic bacteremia: beyond endocarditis. Clin Microbiol Rev 2009;22(1):46–64.
[2] Takahashi N, Nyvad B. Caries ecology revisited: microbial dynamics and the caries process. Caries Res 2008;42(6):409–18.
[3] Bagramian RA, Garcia-Godoy F, Volpe AR. The global increase in dental caries. A pending public health crisis. Am J Dent 2009;22(1):3–8.
[4] Ackroyd R, Kelty C, Brown N, Reed M. The history of photodetection and photodynamic therapy. Photochem Photobiol 2001;74(5):656–69.
[5] Plaetzer K, Krammer B, Berlanda J, Berr F, Kiesslich T. Photophysics and photochemistry of photodynamic therapy: fundamental aspects. Lasers Med Sci 2009;24(2):259–68.
[6] Jori G, Fabris C, Soncin M, Ferro S, Coppellotti O, Dei D, et al. Photodynamic therapy in the treatment of microbial infections: basic principles and perspective applications. Lasers Surg Med 2006;38(5):468–81.
[7] Meisel P, Kocher T. Photodynamic therapy for periodontal diseases: state of the art. J Photochem Photobiol B 2005;79(2):159–70.
[8] Hayek RR, Araújo NS, Gioso MA, Ferreira J, Baptista-Sobrinho CA, Yamada AM, et al. Comparative study between the effects of photodynamic therapy and conventional therapy on microbial reduction in ligature-induced peri-implantitis in dogs. J Periodontol 2005;76(8):1275–81.
[9] Garcez AS, Nuñez SC, Hamblin MR, Ribeiro MS. Antimicrobial effects of photodynamic therapy on

patients with necrotic pulps and periapical lesion. J Endodont 2008;34(2):138–42.
[10] Walsh LJ. The current status of laser applications in dentistry. Aust Dent J 2003;48(3):146–55.
[11] Burns T, Wilson M, Pearson GJ. Sensitisation of cariogenic bacteria to killing by light from a helium–neon laser. J Med Microbiol 1993;38(6):401–5.
[12] Williams JA, Pearson GJ, Colles MJ, Wilson M. The photo-activated antibacterial action of toluidine blue O in a collagen matrix and in carious dentine. Caries Res 2004;38(6):530–6.
[13] Paulino TP, Ribeiro KF, Thedei Jr G, Tedesco AC, Ciancaglini P. Use of hand held photopolymerizer to photoinactivate *Streptococcus mutans*. Arch Oral Biol 2005;50(3):353–9.
[14] Zanin IC, Gonçalves RB, Junior AB, Hope CK, Pratten J. Susceptibility of *Streptococcus mutans* biofilms to photodynamic therapy: an in vitro study. J Antimicrob Chemother 2005;56(2):324–30.
[15] Metcalf D, Robinson C, Devine D, Wood S. Enhancement of erythrosine-mediated photodynamic therapy of *Streptococcus mutans* biofilms by light fractionation. J Antimicrob Chemother 2006;58(1):190–2.
[16] Wood S, Metcalf D, Devine D, Robinson C. Erythrosine is a potential photosensitizer for the photodynamic therapy of oral plaque biofilms. J Antimicrob Chemother 2006;57(4):680–4.
[17] Zanin IC, Lobo MM, Rodrigues LK, Pimenta LA, Höfling JF, Gonçalves RB. Photosensitization of in vitro biofilms by toluidine blue O combined with a light-emitting diode. Eur J Oral Sci 2006;114(1):64–9.
[18] Bevilacqua IM, Nicolau RA, Khouri S, Brugnera Jr A, Teodoro GR, Zângaro RA, et al. The impact of photodynamic therapy on the viability of *Streptococcus mutans* in a planktonic culture. Photomed Laser Surg 2007;25(6):513–18.
[19] Müller P, Guggenheim B, Schmidlin PR. Efficacy of gasiform ozone and photodynamic therapy on a multispecies oral biofilm in vitro. Eur J Oral Sci 2007;115(1):77–80.
[20] Giusti JS, Santos-Pinto L, Pizzolito AC, Helmerson K, Carvalho-Filho E, Kurachi C, et al. Antimicrobial photodynamic action on dentin using a light-emitting diode light source. Photomed Laser Surg 2008;26(4):281–7.
[21] Rovaldi CR, Pievsky A, Sole NA, Friden PM, Rothstein DM, Spacciapoli P. Photoactive porphyrin derivative with broad-spectrum activity against oral pathogens in vitro. Antimicrob Agents Chemother 2000;44(12): 3364–3367.
[22] Burns T, Wilson M, Pearson GJ. Killing of cariogenic bacteria by light from a gallium aluminium arsenide diode laser. J Dent 1994;22(5):273–8.
[23] Wood S, Nattress B, Kirkham J, Shore R, Brookes S, Griffiths J, et al. An in vitro study of the use of photodynamic therapy for the treatment of natural oral plaque biofilms formed in vivo. J Photochem Photobiol B 1999;50(1):1–7.
[24] Kvaal SI, Warloe T. Photodynamic treatment of oral lesions. J Environ Pathol Toxicol Oncol 2007;26(2):127–33.
[25] Bombelli C, Bordi F, Ferro S, Giansanti L, Jori G, Mancini G, et al. New cationic liposomes as vehicles of *m*-tetrahydroxyphenylchlorin in photodynamic therapy of infectious diseases. Mol Pharmacol 2008;5(4):672–9.
[26] Agostinis P, Vantieghem A, Merlevede W, de Witte PA. Hypericin in cancer treatment: more light on the way. Int J Biochem Cell Biol 2002;34(3):221–41.
[27] Avato P, Raffo F, Guglielmi G, Vitali C, Rosato A. Extracts from St. John's Wort and their antimicrobial activity. Phytother Res 2004;18(3):230–2.
[28] Conforti F, Statti GA, Tundis R, Bianchi A, Agrimonti C, Sacchetti G, et al. Comparative chemical composition and variability of biological activity of methanolic extracts from *Hypericum perforatum* L. Nat Prod Res 2005;19(3):295–303.
[29] Cecchini C, Cresci A, Coman MM, Ricciutelli M, Sagratini G, Vittori S, et al. Antimicrobial activity of seven hypericum entities from central Italy. Planta Med 2007;73(6):564–6.
[30] Gmür R, Guggenheim B. Antigenic heterogeneity of *Bacteroides intermedius* as recognized by monoclonal antibodies. Infect Immun 1983;42(2):459–70.
[31] Musk Jr DJ, Hergenrother PJ. Chemical countermeasures for the control of bacterial biofilms: effective compounds and promising targets. Curr Med Chem 2006;13(18):2163–77.
[32] Kachatkou D, Sasnouski S, Zorin V, Zorina T, D'Hallewin MA, Guillemin F, et al. Unusual photoinduced response of mTHPC liposomal formulation (Foslip). Photochem Photobiol 2009;85(3):719–24.
[33] Weitman H, Roslaniec M, Frimer AA, Afri M, Freeman D, Mazur Y, et al. Solvatochromic effects in the electronic absorption and nuclear magnetic resonance spectra of hypericin in organic solvents and in lipid bilayers. Photochem Photobiol 2001;73(2):110–18.
[34] Brancaleon L, Moseley H. Laser and non-laser light sources for photodynamic therapy. Lasers Med Sci 2002;17(3):173–86.
[35] Shiroza T, Ueda S, Kuramitsu HK. Sequence analysis of the gtfB gene from *Streptococcus mutans*. J Bacteriol 1987;169(9):4263–70.
[36] Abo H, Matsumura T, Kodama T, Ohta H, Fukui K, Kato K, et al. Peptide sequences for sucrose splitting and glucan binding within *Streptococcus sobrinus* glucosyltransferase (water-insoluble glucan synthetase). J Bacteriol 1991;173(3):989–96.
[37] Poyart C, Quesne G, Coulon S, Berche P, Trieu-Cuot P. Identification of streptococci to species level by sequencing the gene encoding the manganese-dependent superoxide dismutase. J Clin Microbiol 1998;36(1):41–7.
[38] Saw CL, Heng PW, Olivo M. Potentiation of the photodynamic action of hypericin. J Environ Pathol Toxicol Oncol 2008;27(1):23–33.
[39] Kober M, Pohl K, Efferth T. Molecular mechanisms underlying St. John's wort drug interactions. Curr Drug Metab 2008;9(10):1027–37.
[40] Lu WD, Atkins WM. A novel antioxidant role for ligandin behavior of glutathione *S*-transferases: attenuation of the photodynamic effects of hypericin. Biochemistry 2004;43(40):12761–9.
[41] Kubin A, Wierrani F, Jindra RH, Loew HG, Grünberger W, Ebermann R, et al. Antagonistic effects of combination

photosensitization by hypericin, meso-tetra-hydroxyphenyl-chlorin (mTHPC) and photofrin II on *Staphylococcus aureus*. Drugs Exp Clin Res 1999;25(1):13–21.

[42] Wierrani F. Experimental investigations and clinical use of photodynamic therapy (PDT) in the Rudolf Foundation Hospital. Gynakol Geburtshilfliche Rundsch 1999; 39(4):217–25.

[43] Nelson JS, Liaw LH, Lahlum RA, Cooper PL, Berns MW. Use of multiple photosensitizers and wavelengths during photodynamic therapy: a new approach to enhance tumor eradication. J Natl Cancer Inst 1990;82(10):868–73.

[44] Schneider-Yin X, Kurmanaviciene A, Roth M, Roos M, Fedier A, Minder EI, et al. Hypericin and 5-aminolevulinic acid-induced protoporphyrin IX induce enhanced phototoxicity in human endometrial cancer cells with non-coherent white light. Photodiagnosis Photodyn Ther 2009;6(1):12–18.

7.3 Combining Chitosan and Photodynamic Effects for the Treatment of Oral Microorganisms

The following manuscript is submitted in January 2012 in *Journal of Translational Medicine*.

The contributions of Emina Besic Gyenge to the study: „Combining Chitosan and Photodynamic Effects for the Treatment of Oral Microorganisms" were the following:

1. Student supervision and introduction into the filed of research

2. Collection of microscopic imaging data, in particular: **figure 3** (Accumulation of hypericin and chitosan-TGA in *Candida albicans*), **figure 5** (Accumulation of hypericin and chitosan-TGA in *Aggregibacter aphrophilus*), **figure 6** (Accumulation of Foslipos® and chitosan-TGA in *Aggregibacter aphrophilus*), **figure 8** (Accumulation of hypericin and chitosan-TGA in *Capnocytophaga ochracea*), **figure 9** (Accumulation of Foslipos® and chitosan-TGA in *Capnocytophaga ochracea*), **figure 11** (Accumulation of hypericin and chitosan-TGA in *Streptococcus sobrinus*) and **figure 12** (Accumulation of Foslipos® and chitosan-TGA in *Streptococcus sobrinus*)

Combining Chitosan and Photodynamic Effects for the Treatment of Oral Microorganisms

Doris Hinger[1+], Georg Geisberger[2+], Emina Besic Gyenge[1], Tobias Gilomen[1], Rudolf Gmür[3], Klaus Grätz[4], Heinrich Walt[4], Greta R. Patzke[2], Caroline Maake[1]*

[+]contributed equally

[1] Institute of Anatomy, University of Zurich, Zurich, Switzerland

[2] Institute of Inorganic Chemistry, University of Zurich, Zurich, Switzerland

[3]Institute of Oral Biology, University of Zurich, Zurich, Switzerland

[4]Clinic of Cranio-Maxillofacial Surgery, University Hospital of Zurich, Zurich, Switzerland

*Corresponding author email: cmaake@anatom.uzh.ch (C. Maake)

Abstract

Photodynamic therapy (PDT) had been proposed as a promising treatment option for oral biofilm-mediated diseases. However, susceptibility of oral microorganisms towards PDT varies among and within species and depends on the photosensitizer used. We thus investigated whether PDT (using the meso-tetrahydroxyphenyl-chlorine, mTHPC, derivative Foslipos [FOS] or hypericin [HYP]) in combination with chitosan-thioglycolic acid (chitosan-TGA) can improve antimicrobial effects on *Candida albicans*, *Aggregatibacter aphrophilus*, *Capnocytophaga ochracea* and *Streptococcus sobrinus*. Using confocal microscopy, chitosan-TGA was found to aggregate bacteria and adhere extracellularly, while both photosensitizers accumulated within cells. The combination of HYP with chitosan-TGA did not change these cellular localization patterns. In contrast, FOS distribution was affected upon addition of chitosan-TGA in bacteria, resulting in a colocalization with chitosan-TGA. Colony forming assays revealed that chitosan-TGA improved FOS-mediated photodynamic effects in all species. Chitosan-TGA enhanced photodynamic effects of HYP only in *C. albicans* and *A. aphrophilus*, while in *S. sobrinus* and *C. ochracea* this combination impaired the outcome to varying degrees compared to HYP-PDT alone. Our results indicate that the addition of chitosan-TGA to PDT protocols may be beneficial for the treatment of multispecies odontogenic infections, but some photosensitizers (such as mTHPC) may be better suitable for such an approach.

Introduction

The oral cavity harbors a large population of different microorganisms that form a complex community under healthy conditions (1). Most of these microorganisms are resident bacteria, that within multispecies biofilms, colonize the oral surfaces (2, 3). In addition, fungi, protozoa and viruses have all been isolated (4).

If intact, this endogenous flora constitutes an important part of human health since it helps to maintain local and systemic immunity, contributes to digestion and prevents growth of harmful exogenous pathogens. However, the normal microbial environment in the mouth is fragile and its specific balance may be affected by e.g. poor oral hygiene, diseases or drugs. With these predisposing conditions, certain oral microorganisms may become pathogenic and/or growth of some species may be promoted, thereby changing the number and proportion of members of the healthy flora. Oral and dental infections arising from the endogenous flora of the oral cavity therefore play an important role in daily clinical practice and the most prevalent odontogenic diseases, i.e. dental caries and periodontal diseases, are thought to originate from opportunistic bacteria of dental or oral soft tissue biofilms.

Current treatment of periodontal diseases mostly include one or more of the following: mechanical debridement of the microbiota with or without surgical intervention, disinfection and/or antibiotics in certain cases (1). Notably, insufficient treatment of oral infections may not only lead to persistent local problems, but also bears the risk of systemic spread of bacteria or their products. Although the causative relations have not been fully understood, it had been proposed that oral infections may contribute to e.g. endocarditis, diabetes mellitus, stroke, preterm delivery and respiratory disease (5, 6). However, treatment of odontogenic infections is still challenging due to the sheer number of the opportunistic pathogens, their high multiplication rates, the complex topography of the oral cavity, the protective character of biofilms against drugs and the rising bacterial resistance to antibiotics (1). The search for new treatment modalities is therefore ongoing.

Numerous studies indicate that photodynamic therapy (PDT) may have significant clinical potential for local treatment of oral infections. As with other PDT applications, antimicrobial PDT relies on the activation with light of a photosensitizer and the generation of singlet oxygen and other reactive oxygen species (ROS) that attack vital components of microorganisms (7). It had been shown in-vitro and in-vivo that PDT is successful in killing bacteria as well as fungi involved in periodontitis, endodontitis, periimplantitis, caries and oral mucosal infections (8). The effectiveness of photodynamic interventions on antibiotic-resistant strains had also been demonstrated for oral species (9) and beneficial immunomodulatory effects in the context of oral antimicrobial PDT had been reported (10, 11).

Despite these promising results, it had been observed that certain oral microorganisms - even in planktonic culture - are insufficiently sensitive or refractory to photodynamic killing. This especially applies to various gram-negative species and strains or yeasts, that are equipped with cell wall structures that prevent the binding and/or uptake of some photosensitizers (7, 12).

Among the substances that have recently been proposed to improve the antimicrobial effects of PDT is chitosan, a natural hydrophilic polysaccharide, produced by partial deacetylation of chitin (13). An important feature of chitosan and its chemical derivatives is its broad-spectrum antimicrobial activity. In the context of oral infections, chitosans have been reported to effectively inhibit growth, viability and/or adhesion of gram-positive, gram-negative bacteria and of fungi (14-24).

With the aim to further improve the efficacy of PDT against oral microorganisms we here explore for the first time the combination of meso-tetrahydroxyphenyl-chlorine (mTHPC) - or hypericin-mediated PDT with chitosan-thioglycolic acid (chitosan-TGA), a chitosan conjugate with strong bioadhesive and permeation-enhancing properties (25).

Materials and Methods

Microbial cultures

All microorganisms were obtained from the cell culture collection of the Institute of Oral Biology, University of Zurich, Switzerland. *Streptococcus sobrinus* (OMZ 176) and *Candida albicans* (OMZ 110) were cultured in fluid universal medium (FUM, (26)) in 10% CO_2 at 37°C. *Capnocytophaga ochracea* (OMZ 362) and *Aggregatibacter aphrophilus* (OMZ 359) were cultured anaerobically at 37°C in FUM or in FUM supplemented with 5% horse serum in case of the *Capnocytophaga* strain. All microorganisms were grown until late log phase of growth.

Preparation of chitosan-TGA

Chitosan (low molecular weight, LMW, 50-190 kDa, >85% deacetylated), thioglycolic acid (TGA, 99+ %) and 1-ethyl-3-(3-dimethylaminopropyl)carbodiimide hydrochloride (98+ %) were obtained from Sigma-Aldrich, Buchs, Switzerland and used as received.

Chitosan-TGA was prepared as described previously (27). In short, chitosan (500 mg) was dissolved in diluted HCl (0.09 M, 50 ml) to obtain a 1 % solution of chitosan hydrochloride. 1-ethyl-3-(3-dimethylaminopropyl)carbodiimide hydrochloride (1.20 g, 6.26 mmol) was dissolved in this solution under stirring and subsequently thioglycolic acid (0.38 ml, 5.43 mmol) was added. The pH was adjusted to 5 by addition of NaOH (0.5 M) and the reaction mixture was stirred at room temperature for 3 h followed by dialysis in cellulose membrane tubings with a molecular cut-off of 12 kDa (5 days, 8 °C). The dialysis media were the following; day 1: HCl (5 mM), day 2 and 3: HCl (5 mmol) containing 1 % NaCl, day 4 and 5: HCl (1 mM). The medium was exchanged twice a day. Afterwards, the product was lyophilized and stored at 4 °C in the dark. For microbiological experiments, chitosan-TGA was dissolved in 0.9% NaCl solution and further diluted with FUM.

The zeta potential of chitosan-TGA (0.5 mg/ml) was measured with a Zetasizer Nano ZS90 (Malvern Instruments, Herrenberg, Germany) in folded capillary cells containing the solution under investigation.

Preparation of FITC-chitosan-TGA

Chitosan-TGA (30 mg) was dissolved in 3 ml distilled H_2O. To this solution a solution of fluorescein isothiocyanate (FITC, 3 mg, Sigma) in dry MeOH (4.5 ml) was added yielding a fluorescent orange mixture, which was stirred for 4 h in the dark at room temperature. Afterwards, the solvent was reduced to 1 ml under vacuum and an orange solid precipitated upon addition of ethanol. The solid was washed thoroughly with ethanol until the washing solution showed no fluorescence. The product was dried under high vacuum and stored in the dark at 4 °C. For microscopy studies, FITC-chitosan-TGA was dissolved in 0.9 % NaCl solution and further diluted with FUM.

Photosensitizers

The photosensitizer Foslipos (FOS; Biolitec AG, Jena, Germany) consists of meso-tetrahydroxyphenyl-chlorine (mTHPC) encapsulated into dipalmitoylphosphatidylcholine/dipalmitoylphosphatidylglycerol (DPPC/DPPG) liposomes. Concentration of mTHPC in liposomes was 1.5 mg/ml. A stock solution of FOS (1.5 mg/ml) was prepared in water. Hypericin (HYP; Invitrogen, Basel, Switzerland) was prepared as a 1.0 mg/ml stock solution in ethanol. All stock solutions were further diluted in FUM and stored at 4 °C in the dark.

UV spectra

Absorption spectra of FOS (3.5 μg/ml), HYP (3.4 μg/ml) and a mixture of chitosan-TGA (0.75 μg/ml) with either FOS or HYP (3.5 μg/ml and 3.4 μg/ml final concentration) were measured with a fluorescence spectrophotometer (Lambda 650 S, Perkin Elmer, Waltham, USA) in water.

Confocal microscopy

Microorganisms were incubated with either 4 mg/ml FITC-chitosan-TGA, 10 μg/ml FOS or 10 μg/ml HYP for 30 min in the dark at 37 °C. Alternatively, microorganisms were incubated with a combination of 4 mg/ml FITC-chitosan-TGA and either 10 μg/ml FOS or 10 μg/ml HYP for 30 min in

the dark at 37 °C (all final concentrations). Thereafter, samples were washed twice with 0.9% NaCl solution, dried, fire-fixed and mounted in Glycergel (Dako, Glostrup, Denmark). Imaging was performed with a confocal laser scanning microscope (TCS SP2 and SP5; Leica, Wetzlar, Germany).

PDT protocols

Density of planktonically cultured microorganisms was determined spectrophotometrically at 550 nm and adjusted to OD 1.0. Afterwards they were incubated with (1) either chitosan-TGA (4 mg/ml for *C. albicans, A. aphrophilus* and *C. ochracea* and 1 mg/ml for *S. sobrinus*), HYP (10 µg/ml for *C. albicans* and *C. ochracea*; 2.5 µg/ml for *A. aphrophilus*; 1.25 µg/ml for *S. sobrinus*) or FOS (10 µg/ml for C. albicans and C. ochracea; 2.5 µg/ml for A. aphrophilus; 1.25 µg/ml for S. sobrinus) or (2) chitosan-TGA (at final concentrations indicated above) together with a photosensitizer (at finals concentrations indicated above) for 30 min in the dark at 37° C. The microorganisms were washed twice with 0.9 % NaCl and samples containing photosensitizers were irradiated with a halogen polymerization device (Optilux 500, KerrHawe, Bioggio, Switzerland) for 120 s from a distance of 3 cm. The device has a wavelength range between 400 and 505 nm with an irradiation intensity of 1070 mW/cm^2. Serial dilutions of all samples in 0.9 % NaCl were spiral plated on Columbia Blood Agar Base plates supplemented with 5 % human blood. The plates were cultured as indicated above for 1-2 days and colony forming units (CFU) were counted.

Data analyses and statistics

Experiments were performed in triplicate and repeated at least twice. Data are given in means of three to six values with standard deviations of the mean. Values are normalized against the controls (which was set to 100%) and presented as percentage of surviving microorganisms or microbial death with respect to untreated controls.

Results

General

Zeta potential measurements of chitosan-TGA revealed a value of 6.8 ± 3.3 mV for a concentration of 0.5 mg/ml chitosan-TGA at pH 7.5 (fig. 1). Lowering the pH lead to increased zeta potentials (pH 4: 63.2 mV and pH 7: 13.9 mV) while a higher pH reduced zeta potentials (pH 8: 1.8 mV and pH 8.75: -3.4 mV).

Measurement of UV spectra showed that the addition of chitosan-TGA to photosensitizers did not change the pattern of absorption peaks (fig. 2). At wavelengths of up to 400 nm absorbance was slightly higher in HYP/chitosan-TGA and FOS/chitosan-TGA mixtures compared to photosensitizers alone. Peaks of HYP at 547 nm and 594 nm were red-shifted each by 6 nm in the mixture. UV spectra of FOS/chitosan-TGA and FOS alone were matching. Importantly, all spectra were identical within the wavelength range of our PDT light source (400-500 nm).

We observed that the combination of chitosan-TGA with FOS initiated the formation of small aggregates. This was not the case with HYP.

Candida albicans

Analyses by confocal microscopy showed that HYP is taken up by all *C. albicans* cells. It was visible as a strong fluorescent signal throughout the cytoplasm in a granular manner. FOS-related fluorescence was also detected in all cells, but the signal was very weak. In contrast, signals for chitosan-TGA were confined to the cell envelope and not found intracellularly. The combination of the photosensitizers with chitosan-TGA showed the same distributions and intensities as with the substances alone (fig. 3 for HYP and chitosan-TGA).

Results of colony counts are shown in fig. 4. Incubation with chitosan-TGA leads to a 99.977 % reduced number *of C. albicans* colonies, compared to controls. Treatment with HYP-PDT resulted in 32.483 % whereas the same treatment with FOS resulted in 95.596 % reduced colony numbers, respectively. With the combination of chitosan-TGA and HYP-PDT, death of 99.975 % of *C. albicans*

colonies was observed, in comparison with controls. Combination of chitosan-TGA with FOS-PDT could diminish number of colonies by 99.984 %.

Aggregatibacter aphrophilus

Microscopic images are depicted in figg. 5 and 6. Fluorescence images showed that HYP was accumulated in all *A. aphrophilus* cells under our conditions. The same was true for FOS, but its intracellular fluorescence signal was much stronger than with HYP. Incubation with chitosan-TGA was followed by a loose aggregation of the majority of *A. aphrophilus* cells in solution. Chitosan-TGA was visible only at these bacterial aggregates but not at single bacteria. The cytoplasm of cells appears to be free of chitosan-TGA signals. Incubation of HYP and chitosan-TGA in combination leads to similar results as documented for HYP or chitosan-TGA alone: HYP was accumulated in all cells whereas chitosan-TGA was adhering only to aggregates, omitting single bacteria. In contrast, cells incubated with FOS and chitosan-TGA in combination displayed a relocation of FOS, so that FOS colocalized to 100 % extracellularly with chitosan-TGA. As a consequence, FOS when combined with chitosan-TGA was not accumulated within cells as reported for single FOS incubation.

Data of CFU counts are shown in fig. 7. *A. aphrophilus* treatment with chitosan-TGA alone caused bacterial death of 99.001%, compared to controls. With regard to photodynamic effects, we found that HYP and FOS resulted in 44.831% and 43.321% reduced numbers of colonies, respectively. The combination of chitosan-TGA with HYP-PDT as well as the combination of chitosan-TGA with FOS-PDT eradicated the bacteria completely.

Capnocytophaga ochracea

Microscopic analysis (figg. 8 and 9) showed that HYP fluorescence was detected within all *C. ochracea* cells. The fluorescence signal of FOS treated cells was also found intracellularly in all bacteria, but was weaker compared to HYP. As with *A. aphrophilus*, the incubation of chitosan-TGA caused bacterial aggregation. FITC-chitosan-TGA was observed at bacterial aggregates only, but not

at single bacteria. When incubated with HYP and chitosan-TGA together, cells displayed a fluorescence distribution comparable with the pattern of the substances alone. In contrast, when bacteria were incubated with FOS and chitosan-TGA simultaneously, FOS fluorescence was found extracellularly and colocalized at aggregates with chitosan-TGA.

Effects of treatments on CFU counts are illustrated in fig. 10. In *C. ochracea* chitosan-TGA treatment killed 80.579 % of cells, compared to controls. Photodynamic treatment with HYP and FOS induced 99.997 % and 73.736 % lower colony numbers, respectively. The combination of HYP-PDT with chitosan-TGA impaired the effect of HYP-mediated PDT, leading to 95.751 % fewer colonies in comparison to controls. After treatment with FOS-PDT plus chitosan-TGA 98.582 % less colonies were observed compared to controls.

Treatment with HYP-PDT in *C. ochracea* also affected bacterial growth patterns: bacteria were growing much slower and forming smaller colonies which were very difficult to spot. Only 64 h after HYP-PDT the bacteria had recovered from treatment and colonies could be reliably identified as viable.

Streptococcus sobrinus

Microscopic pictures (figg. 11 and 12) presented fluorescence for both HYP and FOS within the cytoplasm in a granular manner, but with a stronger signal for HYP compared to FOS. Chitosan-TGA was found in association with the surface of bacteria and bacterial aggregates. Incubation with chitosan-TGA plus HYP resulted in the same fluorescence patterns as with single compounds, while the combination of chitosan-TGA plus FOS indicated that FOS was not only present in cells, but also colocalized with chitosan-TGA extracellularly.

Fig. 13 shows treatment effects in *S. sobrinus*. Chitosan-TGA alone caused a 99.548 % bacteriostatic effect, while HYP and FOS-mediated PDT reduced CFU counts by 99.983 % and 94.594 %, respectively. When HYP-PDT was combined with chitosan-TGA, colony numbers were reduced by

99.850 %. Furthermore, FOS-PDT combined with chitosan-TGA lead to a CFU reduction of 99.871 % in comparison to controls.

Discussion

PDT has emerged as a promising antimicrobial treatment option, with enormous clinical potential particularly for the therapy of difficult or (multiply) antibiotic-resistant strains. However, numerous studies provided evidence that not all microorganisms are equally susceptible to PDT. While gram-positive bacteria have been reported to interact with many different photosensitizers, treatment of gram-negative bacteria is strongly improved by (or even require) the use of cationic photosensitizers (12). As described in detail elsewhere, this phenomenon may be linked to the presence of anionic cell wall components in gram-negative bacteria and fungi (12).

Due to their charge characteristics, some of the photosensitizers with highest singlet oxygen quantum yields therefore do not qualify for broad-band antimicrobial PDT. Among others this may apply to neutral mTHPC and anionic hypericin, that we found to both effectively kill gram-positive *mutans* and *sobrinus streptococci* (28), but may be less suitable for gram-negative strains (Besic Gyenge *et al.,* unpublished).

To overcome these limitations we attempted to combine for the first time mTHPC- or hypericin-mediated PDT with the chitosan derivative, chitosan-TGA, using oral microorganisms as models. Chitosan, a polycationic biopolymer, is generally known for its strong antimicrobial properties towards gram-negative strains and fungi (29) and may thus complement the effects of our photosensitizers in PDT. As a first step we here present our data on CFU counts after treatment, but at this stage no conclusions with regard to the fundamental biological processes (cell death and/or growth reduction) can be drawn.

In our study we report for the first time that a short 30 min treatment with chitosan-TGA had a strong broad-band antimicrobial effect on yeast, as well as on selected oral gram-positive and gram-negative bacteria. With our data we therefore contribute to the growing list of antimicrobially active

chitosans (30, 31). At 4 mg/ml (i.e. the highest possible concentration due to solubility limits), the effectiveness of chitosan-TGA was *S. sobrinus* > *C. albicans* > *A. aphrophilus* >> *C. ochracea*. It should be noted, that only in *S. sobrinus* 4 mg/ml chitosan-TGA lead to a complete eradication. Lower chitosan-TGA concentrations (1 mg/ml) were thus used to better explore in *S. sobrinus* the combined effects of chitosan-TGA and PDT.

Previous studies provided evidence that the mechanisms of chitosan action relate to the adherence of the positively charged free amino groups of chitosans with anionic microbial cell wall components followed by a fatal disturbance of barrier integrity (29, 32-35). Zeta potential measurements confirmed the positive charge at physiological pH of our chitosan-TGA preparation, which was slightly higher than described in the literature (4.3 ± 0.74 mV (36)).

In our study we found that chitosan-TGA induced aggregation of bacteria, especially of the two gram-negative species. Such a behaviour had been described before for various chitosan derivatives (15, 37-39) and seems to be associated with detrimental effects on the cell wall (37). Since it is known for a long time that the formation of biofilms is prevented by bacterial aggregation (40) we suggest that this effect of chitosan-TGA may be a beneficial feature for therapy of patients.

Presumably due to the cationic nature of chitosan-TGA, our confocal microscopy studies always revealed a close physical proximity of chitosan-TGA to microbial cells, even after extensive washing steps. However, while chitosan-TGA clearly attached to the cell envelope of *C. albicans*, we found that the majority of *A. aphrophilus* and *C. ochracea* and all *S. sobrinus* appeared to be embedded in more compact masses of chitosan-TGA. Notably, these differences had no impact on antimicrobial effects of chitosan-TGA. Taking into account the solely extracellular localization of chitosan-TGA, its primary targets will be microbial cell wall and/or cytoplasmic membrane components rather than microbial DNA and transcription factors (29, 35).

Since the microscopic picture of chitosan-TGA fluorescence in *C. ocheacea* was very similar to the one in *A. aphrophilus*, the comparably low efficacy of chitosan-TGA on *C. ochracea* was unexpected. We assume that differences may be related to specific characteristics of *C. ochracea* cell envelope,

like e.g. those that allow for gliding motility on smooth surfaces (the other microorganisms investigated here are non-motile). Furthermore, we cannot exclude that the addition of horse serum to the culture of *C. ochracea* may have interfered with chitosan-TGA activity. Previous studies have provided evidence that chitosan may bind to serum proteins with resulting altered transfection efficacy (41).

Our study confirmed our previous data on bactericidal PDT effects on *S. sobrinus* with the mTHPC derivative FOS and HYP (28). Aditionally, we here provide new PDT informations with these photosensitzers against selected gram-negative bacteria and yeast. In our present study, photosensitizer concentrations had been choosen that that did not result in complete killing of microorganisms after light activation. Generally and in contrast to chitosan-TGA, both photosensitizers penetrated cell walls of all species investigated within 30 min of incubation.

Our study supplied the first data on PDT for *A. aphrophilus* und *C. ochracea*. Although gram-negative bacteria are generally regarded as less sensitive to non-positively charged photosensitizers (12), we found that both HYP- and FOS-mediated PDT is capable of strongly reducing CFU counts in both species. As especially evident with *C. ochracea*, the intensity of confocal fluorescence signals of photosensitizers correlated with efficiency of PDT (i.e. stronger fluorescence was associated with lower CFU counts after treatment).

Several papers have underlined the general usefulness of PDT for the treatment of *Candida* (9, 42). However, little or no results with regard to HYP (43) or FOS, respectively, are available. In our study we found that PDT with HYP had only very limited antifungal effect on *C. albicans*, although this photosensitizer accumulated at high rates in all cells. In contrast, FOS, that showed a decidedly weaker intracellular fluorescence than HYP in *C. albicans*, killed over 95% of cultures. These results highlight the complexity of PDT processes and indicate that the efficiency of a given photosensitizer does not necessarily (like in gram-negative bacteria) depend on the cellular fluorescence of photosensitizers within cells. Since nothing is known about the subcellular localization or molecular responses within *C. albicans*, we cannot exclude that the observed differences in PDT effects are

related to differences in intracellular targets, trafficking pathways or activation of certain signaling cascades (44). Furthermore, we cannot exclude a self-quenching effect of FOS fluorescence signals, that have been reported when concentrations of liposomal mTHPC are high (45, 46).

Initial tests confirmed that the combination of FOS or HYP with chitosan-TGA does not change the spectroscopic properties of photosensitizers at the wavelength range of our light source. Notably, the Q-band of FOS at 652 nm was also not affected by co-incubation with chitosan-TGA. However, HYP is often activated at 593 nm and for this peak a red-shift of 6 nm was observed. This data is in line with a previous study, where interactions of Photogem with chitosan resulted in a red-shift of the Q-band of Photogem (47).

Our results revealed that the effects of a combined treatment with chitosan-TGA plus PDT may be photosensitizer and/or species-dependent.

Under our experimental conditions, the admixture of chitosan-TGA to FOS always improved its photodynamic outcome (as judged from CFU counts and compared to FOS-PDT alone). Furthermore, this combination was also slightly better than chitosan-TGA alone. The underlying mechanisms are, however, not clear yet. The agglomeration occurring when chitosan-TGA is mixed with (liposomal) FOS in solution may be related to the known lipid-binding capabilities of chitosan (48). However, the observation that FOS uptake was prevented upon chitosan-TGA incubation (resulting in a shift from intracellular to extracellular FOS localization) in gram-negative bacteria while in *C. albicans* and *S. sobrinus* this was not the case, may indicate that direct interactions between chitosan-TGA and FOS are not the general driving force of this improvement. Rather, species-specific factors at e.g. the cell wall may have an impact, but this hypothesis requires further investigations.

The combined protocol of HYP-PDT and chitosan-TGA yielded an incongruent picture. In line with our above data, the combination of chitosan-TGA and HYP-mediated PDT was also slightly superior to chitosan-TGA alone. In *C. albicans* and *A. aphrophilus* this combination was better, but in *C. ochracea* and *S. sobrinus* worse than PDT with HYP alone. The reason for this difference is currently not

known, especially since the uptake and intracellular localization of HYP did not appear to be impaired with chitosan-TGA.

In a recent paper it had been shown that unmodified chitosan (LMW, 75-85% deacetylation) improved PDT with hematophorphyrin or toluidine blue for treatment of gram-positive *Staphylococcus aureus, Staphylococcus epidermidis, Streptococcus pyogenes* and gram-negative *Pseudomonas aeruginosa* and *Acinetobacter baumannii*, respectively (13). Since in this study, chitosan itself had no antibacterial effect, the underlying mechanisms are likely to be different to the ones operative in our setup. Another study found that chitosan particles doped with the photosensitizer Photogem displayed reduced activity against the gram-positive Staphylococcus aureus compared to Photogem in solution (47). However, these results were obtained without light irradiation and had been explained by an interaction of negatively charged groups of Photogem with positive moieties of chitosan (47).

Taken together our study provided first evidence that the combination of chitosan-TGA with PDT (especially using mTHPC) may be suitable for antimicrobial therapy. With such combined protocols lower doses of photosensitizers may be applicable, thereby reducing both side effects and costs. Typically, odontogenic infections are polymicrobial, and their treatment may thus benefit from modalities as proposed here, that affect gram-positive and gram-negative bacteria as well as fungi. Compared to unmodified chitosans, thiolated chitosans (including chitosan-TGA) feature improved mucoadhesion as well as better solubility and diffusive permeability (25, 49) and therefore may offer new options for local PDT treatment of infections within the oral cavity.

Acknowledgements

We acknowledge Martin Gander and Helga Lüthi-Schaller, Institute for Oral Biology, University Hospital Zurich for excellent technical support and the Center for Microscopy and Image Analysis, University of Zurich, for assistance with microscopy. We furthermore wish to thank Biolitec AG for

their generous gift of Foslipos. The study was supported by a grant from the Swiss Dental Association.

References

1. S. S. Socransky and A. D. Haffajee (2002) Dental biofilms: difficult therapeutic targets. *Periodontol 2000*, **28**, 12-55.
2. J. A. Aas, B. J. Paster, L. N. Stokes, I. Olsen and F. E. Dewhirst (2005) Defining the normal bacterial flora of the oral cavity. *J Clin Microbiol*, **43**, 5721-5732.
3. N. Suzuki, A. Yoshida and Y. Nakano (2005) Quantitative analysis of multi-species oral biofilms by TaqMan Real-Time PCR. *Clin Med Res*, **3**, 176-185.
4. J. M. Hardie and G. H. Bowden (1974) The normal microbial flora of the mouth. *Soc Appl Bacteriol Symp Ser*, **3**, 47-83.
5. G. J. Seymour, P. J. Ford, M. P. Cullinan, S. Leishman and K. Yamazaki (2007) Relationship between periodontal infections and systemic disease. *Clin Microbiol Infect*, **13 Suppl 4**, 3-10.
6. C. Hayashi, C. V. Gudino, F. C. Gibson, 3rd and C. A. Genco (2010) Review: Pathogen-induced inflammation at sites distant from oral infection: bacterial persistence and induction of cell-specific innate immune inflammatory pathways. *Mol Oral Microbiol*, **25**, 305-316.
7. N. S. Soukos and J. M. Goodson (2010) Photodynamic therapy in the control of oral biofilms. *Periodontol 2000*, **55**, 143-166.
8. N. S. Soukos, P. S. Chen, J. T. Morris, K. Ruggiero, A. D. Abernethy, S. Som, F. Foschi, S. Doucette, L. L. Bammann, C. R. Fontana, A. G. Doukas and P. P. Stashenko (2006) Photodynamic therapy for endodontic disinfection. *J Endod*, **32**, 979-984.
9. M. A. Biel (2010) Photodynamic therapy of bacterial and fungal biofilm infections. *Methods Mol Biol*, **635**, 175-194.
10. P. Braham, C. Herron, C. Street and R. Darveau (2009) Antimicrobial photodynamic therapy may promote periodontal healing through multiple mechanisms. *J Periodontol*, **80**, 1790-1798.

11. A. S. Carvalho, M. H. Napimoga, J. Coelho-Campos, V. J. Silva-Filho and G. Thedei (2011) Photodynamic Therapy Reduces Bone Resorption and Decreases Inflammatory Response in an Experimental Rat Periodontal Disease Model. *Photomed Laser Surg*.

12. G. Jori, C. Fabris, M. Soncin, S. Ferro, O. Coppellotti, D. Dei, L. Fantetti, G. Chiti and G. Roncucci (2006) Photodynamic therapy in the treatment of microbial infections: basic principles and perspective applications. *Lasers Surg Med*, **38**, 468-481.

13. T. Tsai, H. F. Chien, T. H. Wang, C. T. Huang, Y. B. Ker and C. T. Chen (2011) Chitosan augments photodynamic inactivation of gram-positive and gram-negative bacteria. *Antimicrob Agents Chemother*, **55**, 1883-1890.

14. B. K. Choi, K. Y. Kim, Y. J. Yoo, S. J. Oh, J. H. Choi and C. Y. Kim (2001) In vitro antimicrobial activity of a chitooligosaccharide mixture against Actinobacillus actinomycetemcomitans and Streptococcus mutans. *Int J Antimicrob Agents*, **18**, 553-557.

15. H. Sano, K. Shibasaki, T. Matsukubo and Y. Takaesu (2001) Comparison of the activity of four chitosan derivatives in reducing initial adherence of oral bacteria onto tooth surfaces. *Bull Tokyo Dent Coll*, **42**, 243-249.

16. C. Virga, D. Beltramo, C. Landa, N. Passalacqua and S. Dorronsoro (2002) A comparative study in vivo of the therapeutic effect of triclosan, hexetidine and chitosan. *Acta Odontol Latinoam*, **15**, 3-9.

17. K. Bae, E. J. Jun, S. M. Lee, D. I. Paik and J. B. Kim (2006) Effect of water-soluble reduced chitosan on Streptococcus mutans, plaque regrowth and biofilm vitality. *Clin Oral Investig*, **10**, 102-107.

18. Y. Hayashi, N. Ohara, T. Ganno, K. Yamaguchi, T. Ishizaki, T. Nakamura and M. Sato (2007) Chewing chitosan-containing gum effectively inhibits the growth of cariogenic bacteria. *Arch Oral Biol*, **52**, 290-294.

19. H. J. Busscher, E. Engels, R. J. Dijkstra and H. C. van der Mei (2008) Influence of a chitosan on oral bacterial adhesion and growth in vitro. *Eur J Oral Sci*, **116**, 493-495.

20. A. R. Sarasam, P. Brown, S. S. Khajotia, J. J. Dmytryk and S. V. Madihally (2008) Antibacterial activity of chitosan-based matrices on oral pathogens. *J Mater Sci Mater Med*, **19**, 1083-1090.

21. Q. X. Ji, Y. Zhong de, R. Lu, W. Q. Zhang, J. Deng and X. G. Chen (2009) In vitro evaluation of the biomedical properties of chitosan and quaternized chitosan for dental applications. *Carbohydr Res*, **344**, 1297-1302.

22. P. A. Norowski, Jr. and J. D. Bumgardner (2009) Biomaterial and antibiotic strategies for peri-implantitis: a review. *J Biomed Mater Res B Appl Biomater*, **88**, 530-543.

23. N. C. Mohire and A. V. Yadav (2010) Chitosan-based polyherbal toothpaste: as novel oral hygiene product. *Indian J Dent Res*, **21**, 380-384.

24. M. J. Verkaik, H. J. Busscher, D. Jager, A. M. Slomp, F. Abbas and H. C. van der Mei (2011) Efficacy of natural antimicrobials in toothpaste formulations against oral biofilms in vitro. *J Dent*, **39**, 218-224.

25. A. Bernkop-Schnurch, A. Weithaler, K. Albrecht and A. Greimel (2006) Thiomers: preparation and in vitro evaluation of a mucoadhesive nanoparticulate drug delivery system. *Int J Pharm*, **317**, 76-81.

26. R. Gmür and B. Guggenheim (1983) Antigenic heterogeneity of Bacteroides intermedius as recognized by monoclonal antibodies. *Infect Immun*, **42**, 459-470.

27. C. E. Kast and A. Bernkop-Schnurch (2001) Thiolated polymers--thiomers: development and in vitro evaluation of chitosan-thioglycolic acid conjugates. *Biomaterials*, **22**, 2345-2352.

28. M. Lüthi, E. Besic Gyenge, M. Engström, M. Bredell, K. Grätz, H. Walt, R. Gmür and C. Maake (2009) Hypericin- and mTHPC-mediated photodynamic therapy for the treatment of cariogenic bacteria. *Medical Laser Application* **24**, 227-236.

29. M. Kong, X. G. Chen, K. Xing and H. J. Park (2010) Antimicrobial properties of chitosan and mode of action: a state of the art review. *Int J Food Microbiol*, **144**, 51-63.

30. N. M. Alves and J. F. Mano (2008) Chitosan derivatives obtained by chemical modifications for biomedical and environmental applications. *Int J Biol Macromol*, **43**, 401-414.

31. N. V. Ballal, M. Kundabala, K. S. Bhat, S. Acharya, M. Ballal, R. Kumar and P. Y. Prakash (2009) Susceptibility of Candida albicans and Enterococcus faecalis to Chitosan, Chlorhexidine gluconate and their combination in vitro. *Aust Endod J*, **35**, 29-33.

32. I. M. Helander, E. L. Nurmiaho-Lassila, R. Ahvenainen, J. Rhoades and S. Roller (2001) Chitosan disrupts the barrier properties of the outer membrane of gram-negative bacteria. *Int J Food Microbiol*, **71**, 235-244.

33. H. Liu, Y. Du, X. Wang and L. Sun (2004) Chitosan kills bacteria through cell membrane damage. *Int J Food Microbiol*, **95**, 147-155.

34. J. Y. Je and S. K. Kim (2006) Chitosan derivatives killed bacteria by disrupting the outer and inner membrane. *J Agric Food Chem*, **54**, 6629-6633.

35. Y. C. Chung and C. Y. Chen (2008) Antibacterial characteristics and activity of acid-soluble chitosan. *Bioresour Technol*, **99**, 2806-2814.

36. R. Martien, B. Loretz, A. M. Sandbichler and A. B. Schnurch (2008) Thiolated chitosan nanoparticles: transfection study in the Caco-2 differentiated cell culture. *Nanotechnology*, **19**, 045101.

37. L. V. Didenko, D. V. Gerasimenko, N. D. Konstantinova, T. A. Silkina, I. D. Avdienko, G. E. Bannikova and V. P. Varlamov (2005) Ultrastructural study of chitosan effects on Klebsiella and staphylococci. *Bull Exp Biol Med*, **140**, 356-360.

38. J. Simunek, G. Tishchenko, B. Hodrova and H. Bartonova (2006) Effect of chitosan on the growth of human colonic bacteria. *Folia Microbiol (Praha)*, **51**, 306-308.

39. D. Raafat, K. von Bargen, A. Haas and H. G. Sahl (2008) Insights into the mode of action of chitosan as an antibacterial compound. *Appl Environ Microbiol*, **74**, 3764-3773.

40. W. F. Liljemark, C. G. Bloomquist and G. R. Germaine (1981) Effect of bacterial aggregation on the adherence of oral streptococci to hydroxyapatite. *Infect Immun*, **31**, 935-941.

41. S. Nimesh, M. M. Thibault, M. Lavertu and M. D. Buschmann (2010) Enhanced gene delivery mediated by low molecular weight chitosan/DNA complexes: effect of pH and serum. *Mol Biotechnol*, **46**, 182-196.

42. J. P. Lyon, L. M. Moreira, P. C. de Moraes, F. V. Dos Santos and M. A. de Resende (2011) Photodynamic therapy for pathogenic fungi. *Mycoses*.

43. C. Cecchini, A. Cresci, M. M. Coman, M. Ricciutelli, G. Sagratini, S. Vittori, D. Lucarini and F. Maggi (2007) Antimicrobial activity of seven hypericum entities from central Italy. *Planta Med*, **73**, 564-566.

44. E. Buytaert, M. Dewaele and P. Agostinis (2007) Molecular effectors of multiple cell death pathways initiated by photodynamic therapy. *Biochim Biophys Acta*, **1776**, 86-107.

45. M. A. D'Hallewin, D. Kochetkov, Y. Viry-Babel, A. Leroux, E. Werkmeister, D. Dumas, S. Grafe, V. Zorin, F. Guillemin and L. Bezdetnaya (2008) Photodynamic therapy with intratumoral administration of Lipid-Based mTHPC in a model of breast cancer recurrence. *Lasers Surg Med*, **40**, 543-549.

46. H. P. Lassalle, M. Wagner, L. Bezdetnaya, F. Guillemin and H. Schneckenburger (2008) Fluorescence imaging of Foscan and Foslip in the plasma membrane and in whole cells. *J Photochem Photobiol B*, **92**, 47-53.

47. C. R. Fontana, D. S. dos Santos, Jr., J. M. Bosco, D. M. Spolidorio and R. A. Chierici Marcantonio (2008) Evaluation of chitosan gel as antibiotic and photosensitizer delivery. *Drug Deliv*, **15**, 417-422.

48. M. S. Rodriguez and L. E. Albertengo (2005) Interaction between chitosan and oil under stomach and duodenal digestive chemical conditions. *Biosci Biotechnol Biochem*, **69**, 2057-2062.

49. M. Werle and A. Bernkop-Schnurch (2008) Thiolated chitosans: useful excipients for oral drug delivery. *J Pharm Pharmacol*, **60**, 273-281.

521

522

523

524

525

526

527

528

529

530

531

532

533

534

535

536

537

538

539

540

541

Figure legends

Fig. 1

Measurements of the zeta potential of chitosan-TGA at pH 7.5.

Fig. 2

Absorption spectra of (a) hypericin (Hyp) and the mixture of hypericin and chitosan-TGA (TGAHyp) and (b) Foslipos (Fos) and the mixture of Foslipos and chitosan-TGA (TGAFos).

Fig. 3

Candida albicans incubated with a combination of hypericin and chitosan-TGA: (a) differential interference contrast microscopy, (b) chitosan-TGA (green), (c) hypericin (red), (d) overlay.

Fig. 4

Survival in *Candida albicans* after treatment with chitosan-TGA (TGA), hypericin (HYP), Foslipos (FOS), a mixture of hypericin and chitosan-TGA (TGA + HYP) or a mixture of Foslipos and chitosan-TGA (TGA + FOS) in % compared to controls (set as 100%).

Fig. 5

Aggregatibacter aphrophilus: (a and b) incubation with hypericin only, differential interference contrast microscopy (a), overlay with hypericin (red, b); (c-f) incubation with a mixture of hypericin and chitosan-TGA, differential interference contrast microscopy (c), chitosan-TGA (green, d), hypericin (red, e), overlay (f).

Fig. 6

Aggregatibacter aphrophilus: (a and b) incubation with Foslipos only, differential interference contrast microscopy (a), overlay with Foslipos (red, b); (c-f) incubation with a mixture of Foslipos and

chitosan-TGA, differential interference contrast microscopy (c), chitosan-TGA (green, d), Foslipos (red, e), overlay, yellow color indicates colocalization of red and green fluorescence signals (f).

Fig. 7

Cell death in *Aggregatibacter aphrophilus* after treatment with chitosan-TGA (TGA), hypericin (HYP), Foslipos (FOS), a mixture of hypericin and chitosan-TGA (TGA + HYP) or a mixture of Foslipos and chitosan-TGA (TGA + FOS) in % compared to controls (set as 0%).

Fig. 8

Capnocytophaga ochracea: (a and b) incubation with hypericin only, differential interference contrast microscopy (a), overlay with hypericin (red, b); (c-f) incubation with a mixture of hypericin and chitosan-TGA, differential interference contrast microscopy (c), chitosan-TGA (green, d), hypericin (red, e), overlay (f).

Fig. 9

Capnocytophaga ochracea: (a and b) incubation with Foslipos only, differential interference contrast microscopy (a), overlay with Foslipos (red, b); (c-f) incubation with a mixture of Foslipos and chitosan-TGA, differential interference contrast microscopy (c), chitosan-TGA (green, d), Foslipos (red, e), overlay, yellow color indicates colocalization of red and green fluorescence signals (f).

Fig. 10

Survival in *Capnocytophaga ochracea* after treatment with chitosan-TGA (TGA), hypericin (HYP), Foslipos (FOS), a mixture of hypericin and chitosan-TGA (TGA + HYP) or a mixture of Foslipos and chitosan-TGA (TGA + FOS) in % compared to controls (set as 100%).

Fig. 11

Streptococcus sobrinus: (a-d) incubation with a mixture of hypericin and chitosan-TGA, differential interference contrast microscopy (a), chitosan-TGA (green, b), hypericin (red, c), overlay (d).

Fig. 12

Streptococcus sobrinus: (a-d) incubation with a mixture of Foslipos and chitosan-TGA, differential interference contrast microscopy (a), chitosan-TGA (green, b), Foslipos (red, c), overlay (d).

Fig. 13

Survival in *Streptococcus sobrinus* after treatment with chitosan-TGA (TGA), hypericin (HYP), Foslipos (FOS), a mixture of hypericin and chitosan-TGA (TGA + HYP) or a mixture of Foslipos and chitosan-TGA (TGA + FOS) in % compared to controls (set as 100%).

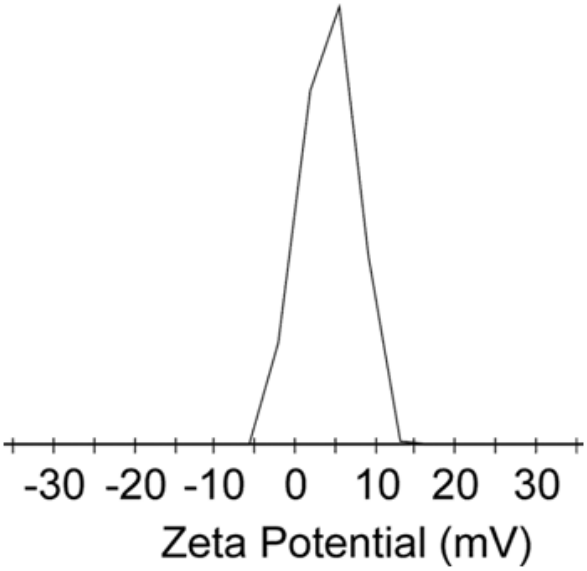

Fig.1

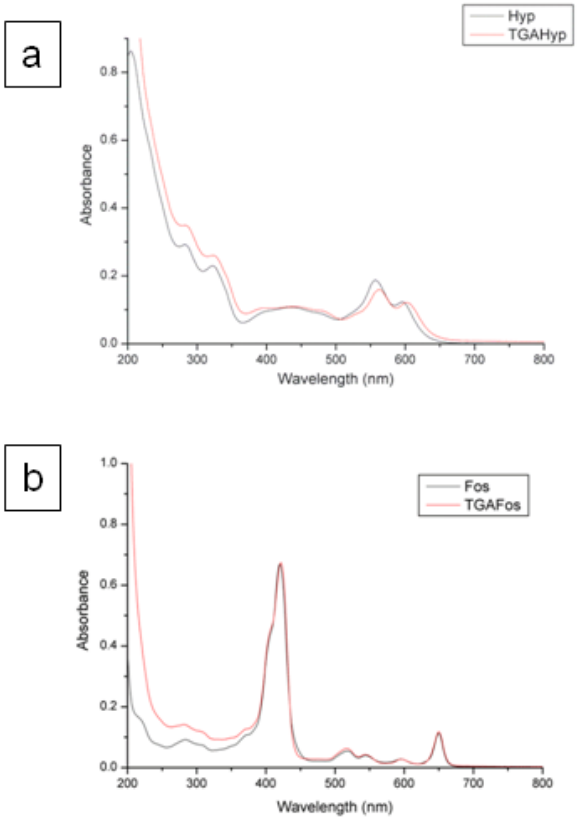
a
Hyp
TGAHyp
Absorbance
Wavelength (nm)
b
Fos
TGAFos
Absorbance
Wavelength (nm)

Fig. 2

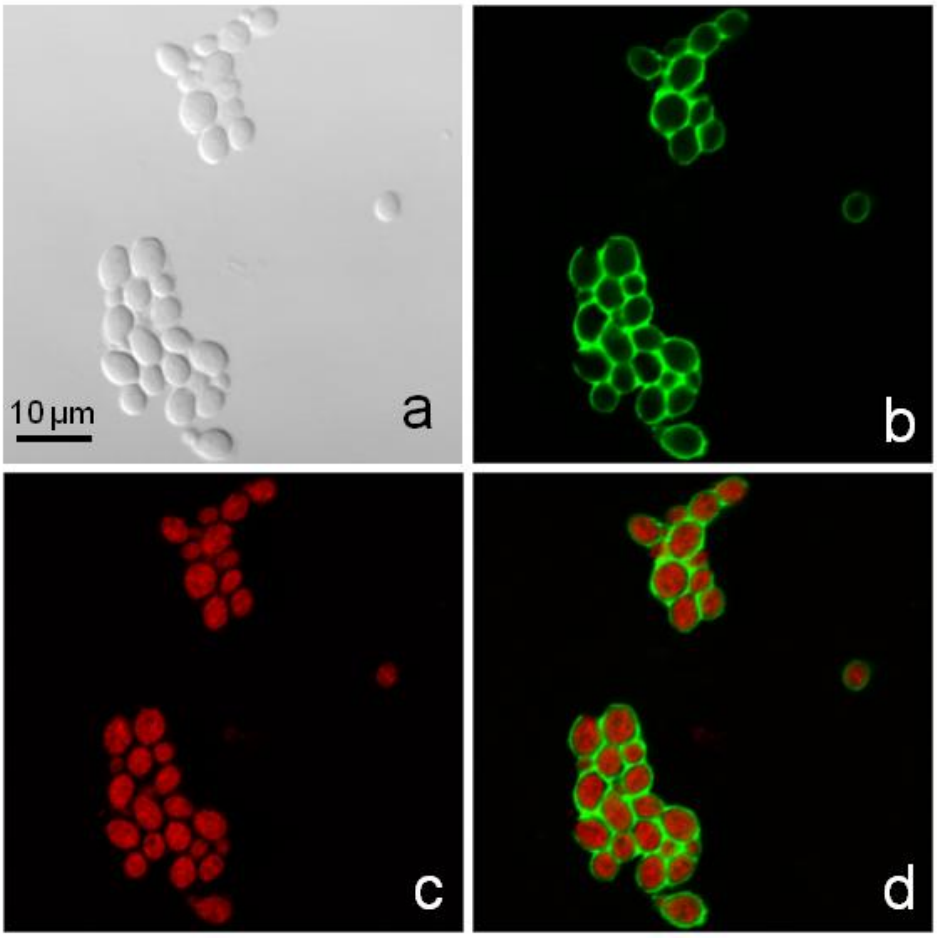

Fig. 3

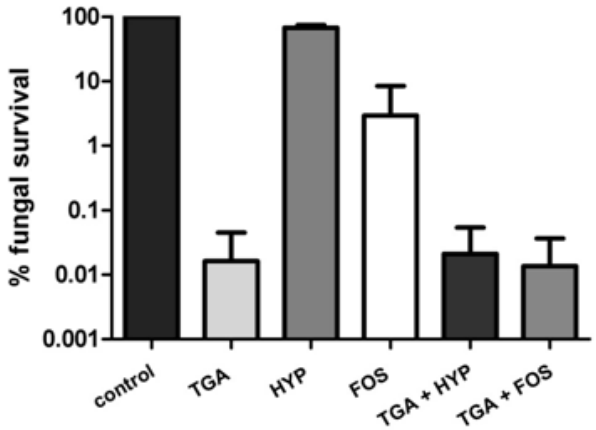
% fungal survival
100
10
1
0.1
0.01
0.001
control
TGA
HYP
FOS
TGA + HYP
TGA + FOS

Fig. 4

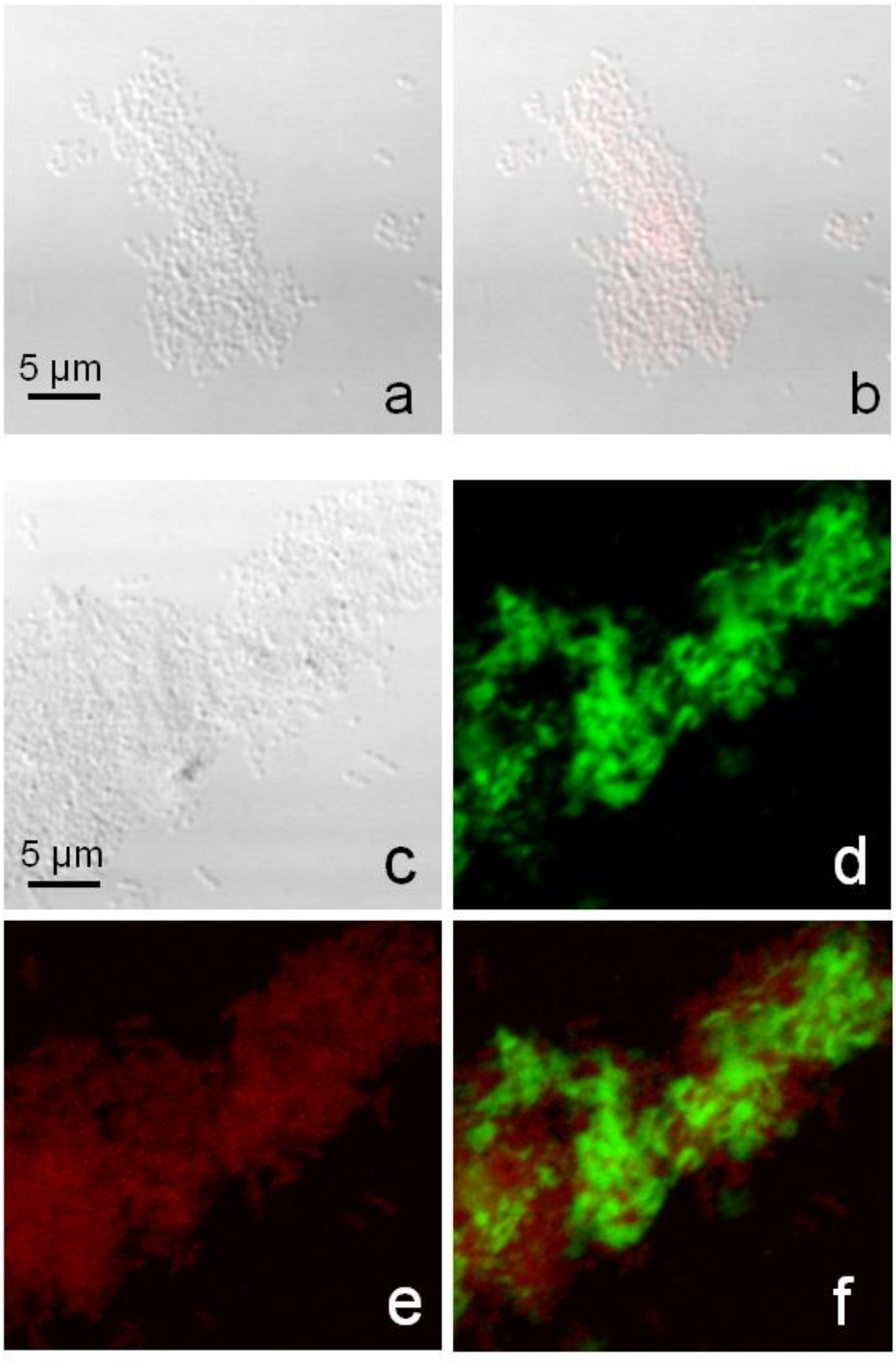

674

675 Fig. 5

676

677

678

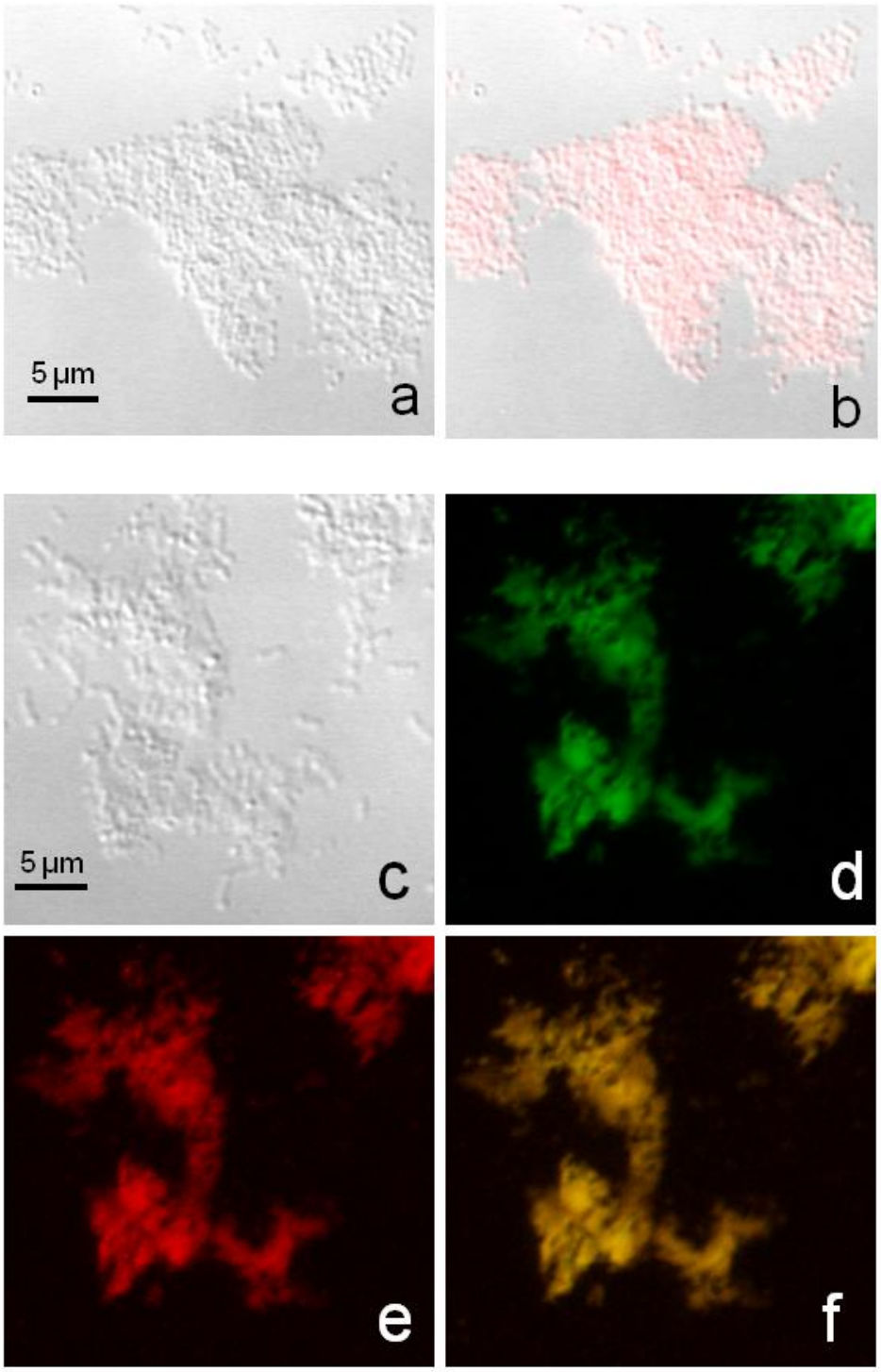

679

680 Fig. 6

681

682

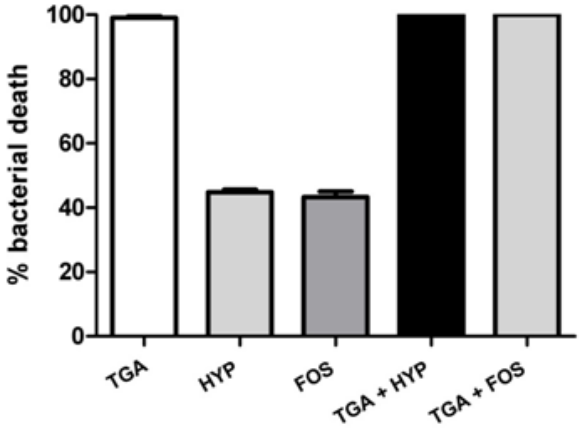

683

684

685 Fig. 7

686

687

688

689

690

691

692

693

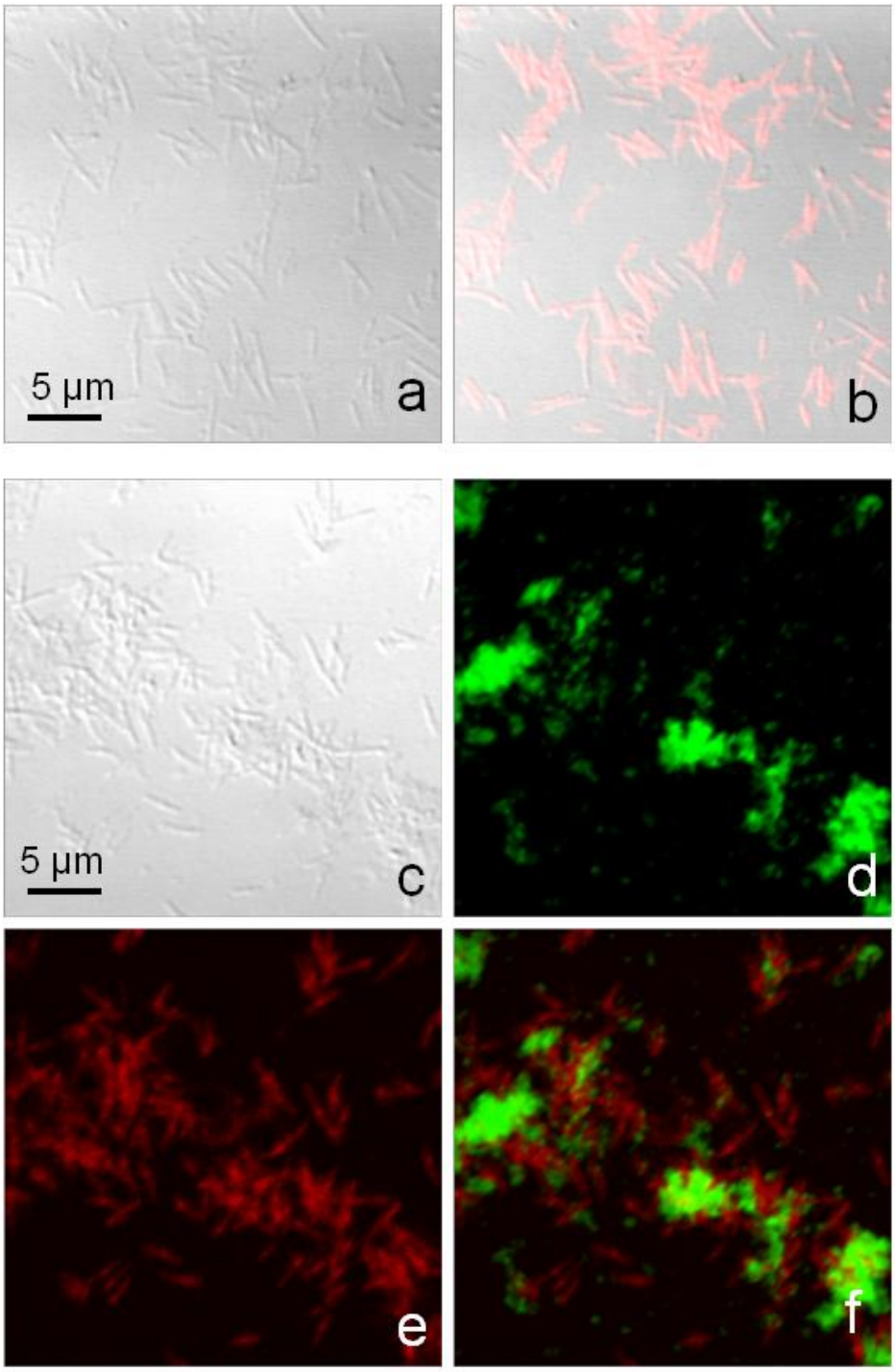

694

695 Fig. 8

696

697

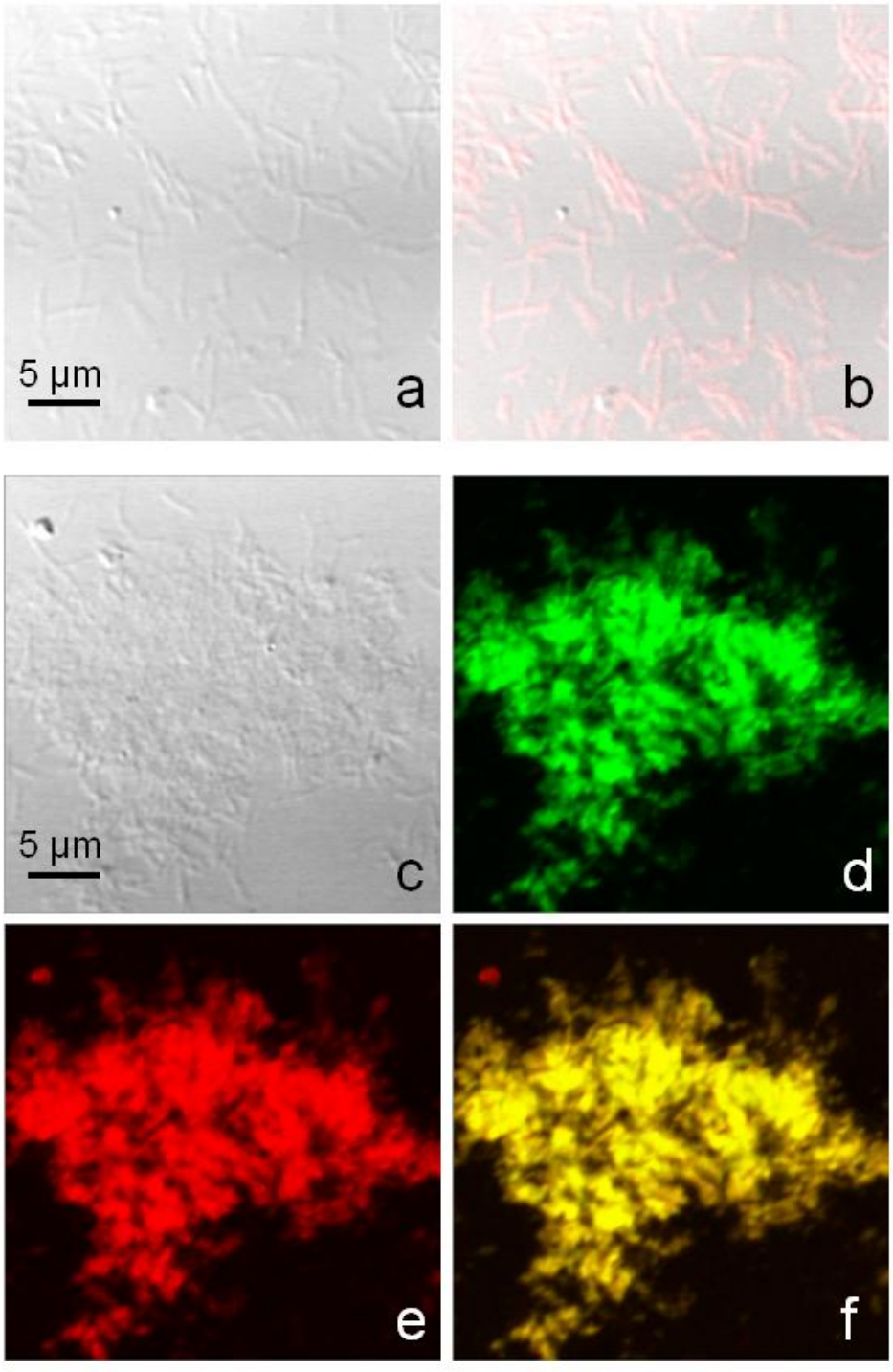

698

699 Fig. 9

700

701

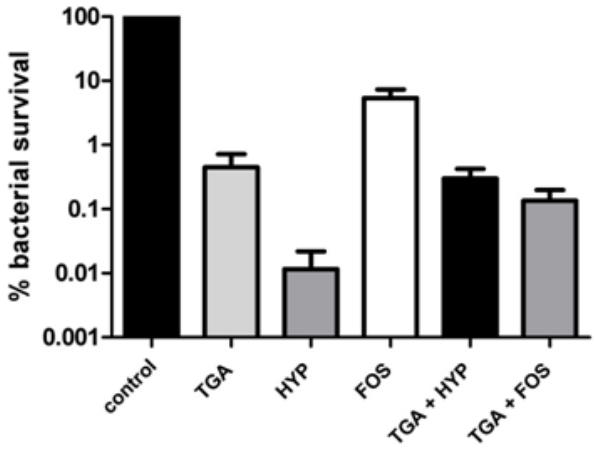
% bacterial survival
100
10
1
0.1
0.01
0.001
control
TGA
HYP
FOS
TGA + HYP
TGA + FOS

Fig. 10

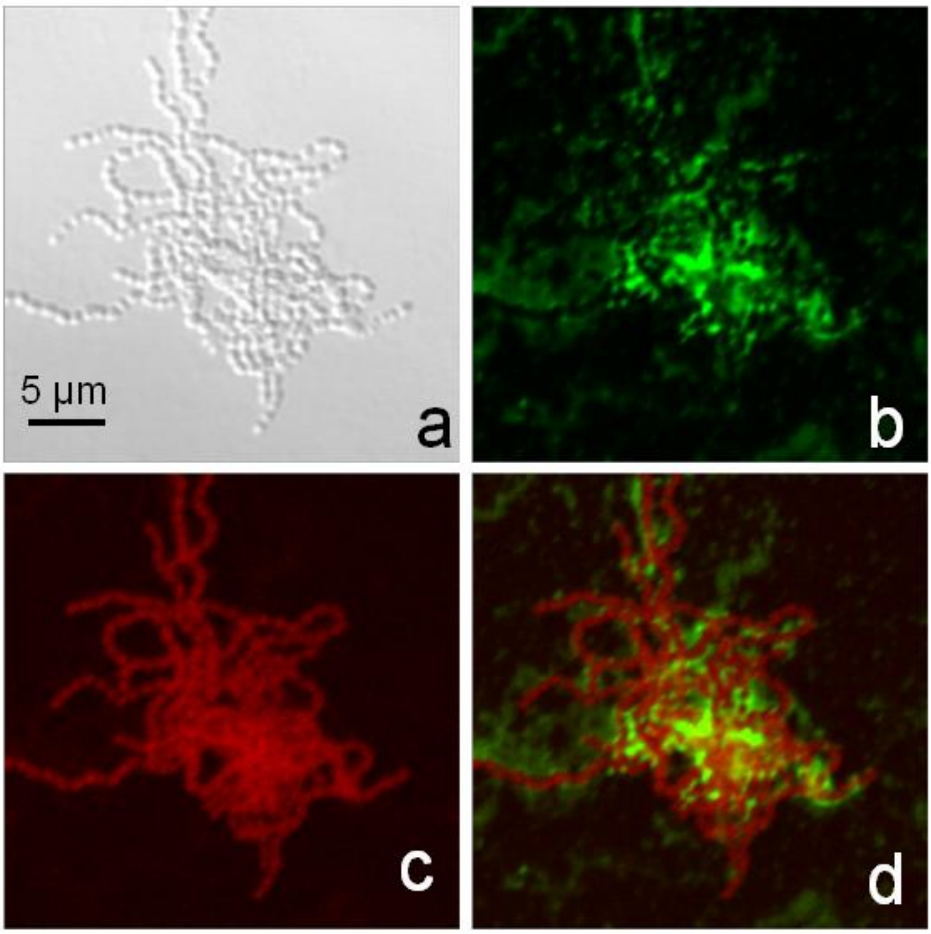

716
717 Fig. 11

718

719

720

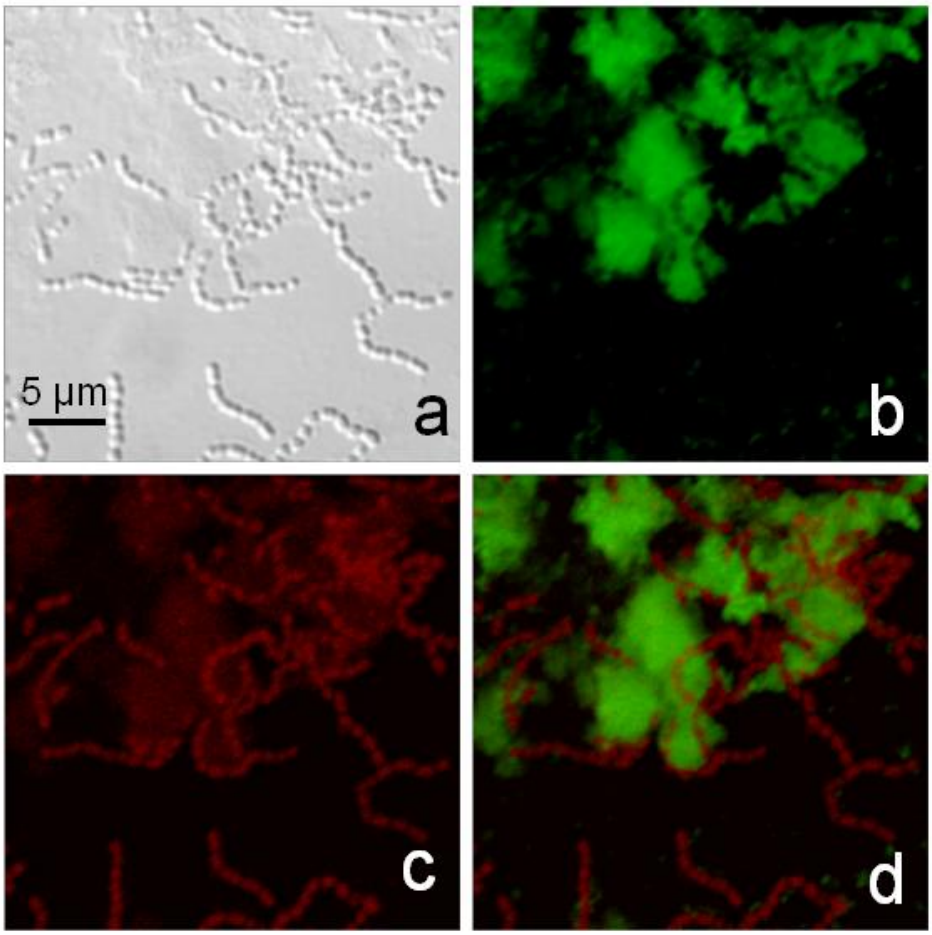

721

722 Fig. 12

723

724

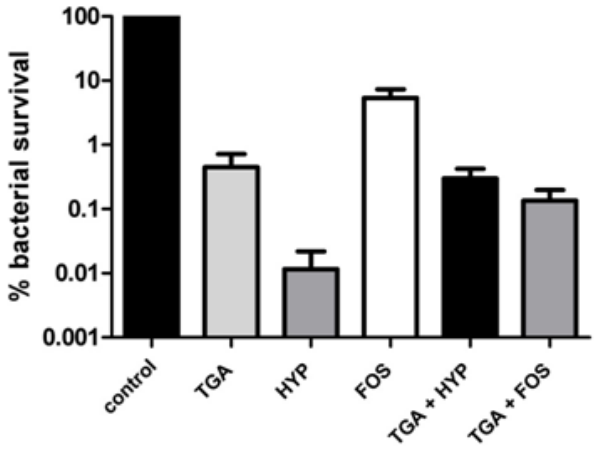

725

726

727 Fig. 13

7.4 The application and Challenges of Clinical PD-PDT in the Head and Neck region; A Short review

The contributions of Emina Besic Gyenge to the study: „The application and challenges of clinical PD-PDT in the Head and Neck region, a short review" were literature research and writing parts of the manuscript.

Journal of Photochemistry and Photobiology B: Biology 101 (2010) 185–190

Contents lists available at ScienceDirect

Journal of Photochemistry and Photobiology B: Biology

journal homepage: www.elsevier.com/locate/jphotobiol

Short Review

The application and challenges of clinical PD–PDT in the head and neck region: A short review

Marius G. Bredell [a,*], Emina Besic [a], Caroline Maake [b], Heinrich Walt [a]

[a] University Hospital Zurich, Department of Cranio-Maxillofacial Surgery, Frauenklinikstrasse 24, CH-8091 Zurich, Switzerland
[b] University of Zurich, Institute of Anatomy, Winterthurerstr. 190, CH-8057 Zurich, Switzerland

ARTICLE INFO

Article history:
Received 29 November 2009
Received in revised form 1 July 2010
Accepted 6 July 2010
Available online 16 July 2010

Keywords:
Photodynamic therapy
Photodiagnosis
Photosensitizer
Head and neck cancer
Laser

ABSTRACT

We review current clinical applications of photodiagnosis (PD) and photodynamic therapy (PDT) in the head and neck field and highlight the actual status, problems, challenges as well as the future of this emerging treatment modality.

In recent years literature presented input from many new developments and their applications. This is due to better awareness and developing knowledge about PD–PDT from the clinical staff, both nurses and doctors. But it is also a result of improved drug and hardware development such as lasers, LEDs and related optical devices. Current photo-medical applications in the head and neck region range from diagnostics, treatment of premalignant and malignant lesions, aesthetic and cosmetic applications to the ever expanding anti-microbial applications.

Although treatment of premalignant and early malignant lesions of the oropharyngeal cavity have long been the favourite lesions to treat with PDT patients with unsalvageable tumors have also been responding remarkably well to PDT, adding significant quality of life.

There is growing interest in anti-microbiological PDT and recent progress has shown that this application is able to significantly reduce the number or even eradicate specific microbial pathogens. During many surgical treatments better control of microbiological activity through PDT may lead to a better outcome.

Despite progressive development in this field a few problems remain: prolonged phototoxicity, limited penetration of the photosensitizer and light, inadequate specificity, PDT-related pain as well as the lack of uniformly accepted protocols both for light application as well as photosensitizers. Recent studies have shown that PDT based pain can be separated from other forms of pain, offering hope that a specific management of pain will be possible. If PDT will become fully accepted by patients and doctors we must care about the negative factors such as pain and prolonged phototoxicity.

Contents

* Corresponding author. Tel.: +41(0)44 2559056; fax: +41(0)44 2554179.
E-mail address: marius.bredell@usz.ch (M.G. Bredell).

1011-1344/$ - see front matter © 2010 Elsevier B.V. All rights reserved.
doi:10.1016/j.jphotobiol.2010.07.002

Nomenclature

PDT	photodynamic therapy	5-ALA	5-aminolevulinic acid
PDD	photodynamic diagnosis	PACT	photodynamic anti-microbial therapy
mTHPC	meta-tetrahydroxy-phenyl chlorine	HpD	hematoporphyrin derivative
PpIX	protoporphyrin IX		

1. Introduction

The application of clinical photodiagnosis and photodynamic therapy (PD and PDT) is constantly growing. Since the earliest reports by von Tappeiner and Jesionek in 1903 and Policard in 1924 [1,2] on the therapeutic use of fluorescent substances, there have been significant developments in the clinical application of more sophisticated treatment modalities within less than a century. The aim of this review is to outline the current spectrum of applications, limitations as well as future of PDT in the head and neck region. The broader acceptance of PDT hinges mainly on the further development of the two basic components namely, the light source as well as the photoactive dye or photosensitizer. A basic advantage of PDT is that there is no lifetime limit to the dose of photosensitizer. Furthermore, the treatment can be repeated as often as needed and, no known interaction exists between current chemo- and radiotherapy protocols and PDT. The excellent functional as well as aesthetic outcomes of PDT treatments may be attributed to the relative limited damage to normal structures like nerves, collagen fibers and large blood vessels, although the microvasculature is affected leading to severe and persistent tumor hypoxia or anoxia [3]. The well known disadvantages are prolonged photosensitivity, possible poor initial selectivity between tumor and normal tissue as well as pain.

Some photosensitizers have a long lag time between initial drug administration and exposure to the therapeutic light source resulting in extended total treatment time. There is a significant drive to modify this. With time the drugs have also been modified to absorb longer wavelengths improving the depth of penetration in tissues [4]. A recent drug, chlorine e6 alone and in combination with the hydrophilic polymer polyvinylpyrrolidone (PVP) have shown promise in animal and human applications regarding phototoxicity [48,49].

Broadly the use of PDD and PDT can be grouped in the following categories for the head and neck area:

– Diagnostic.
– Treatment of premalignant, as well as early malignant lesions in the head and neck area.
– Treatment of secondary or recurrent squamous cell carcinomas of the head and neck.
– Esthetic and cosmetic applications.
– Treatment of bacterial, fungal, parasitic as well as viral infections (photodynamic anti-microbial therapy or for short PACT).

The main limitations in the more generalized clinical application of PDT are firstly the lack of clinical knowledge and especially the lack of established treatment protocols and possibly the perception of the application of a technology still very much in a developmental phase. An expanding array of photosensitizers [50] that could either be administered systemically or as a topical application is available and may in future enhance the choice of the most appropriate drug for the particular situation. Light sources needed for the activation of the photosensitizer may range from pulsed-dye lasers, potassium titanyl phosphate lasers to neodymium:Yttrium–aluminium-garnet (Nd:YAG) lasers. Smaller semiconductor diode lasers have become more popular due to the mobility, price and power advantages [5]. LED lights are becoming more and more powerful, with deeper penetration and thus wider application than just superficial tumors. The use of mobile PDT units may make a considerable difference in the accessibility of PDT services to communities not close to a hospital rendering a PDT service [6]. Although this may be the case, technical equipment (light source) is needed with the necessary technical support to be able to effectively run such a service. When reviewing the literature, there are few standardized protocols to compare results and may lead to confusion by the interested practitioner. Much work is still needed to clearly define treatment protocols and develop affordable and easy to use equipment so that PDT may be used on a daily basis in most centers for a wide variety of clinical applications.

At present the use of PDT has been approved for use in clinical treatment in the USA, EU, Canada, Russia and Japan. The FDA approved the use of PDT in Barreťs esophagitis, obstructive tracheobroncheal carcinoma using the photosensitizer Porfimer sodium (®Photofrin), and the use of 5-aminolevulinic acid, 5-ALA (®Levulan) and 5-ALA in alcohol solution (®Kerastick) for actinic keratosis while verteporfrin (®Visudyne) may be applied for macular degeneration. In addition to the above the EU also approved the use of meta-tetrahydroxy-phenyl chlorine (mTHPC), also known as temoporfrin, (®Foscan) as photosensitizer for the treatment of early and palliative cases of head and neck carcinomas. For squamous- and basal cell carcinomas methyl aminolaevulinat (®Metvix) was approved as photosensitizer prodrug (Biel [8]).

2. Diagnostic: (PDD: photodynamic diagnosis)

Early and accurate detection of oral dysplasia and cancer in patients would lead to an increase in early diagnosis and an improved prognosis of many patients. All cells have a degree of fluorescence when exposed to light which is called auto fluorescence. This fluorescence is a re-emission of light that can be in varying colors and is attributed to the presence of chromophores (fluorophores) within them. By using fluorescence spectroscopy these substances can be detected and are thus representative of biochemical changes within these tissue [7]. Fluorescence can be detected as auto fluorescence when induced by violet light (400 nm) or may be enhanced by the topical or even systemic application of 5-ALA. An increased red and decreased green fluorescence is an accurate predictor of dysplasia and malignancy. This effect is further enhanced by the limited ability of cancerous tissue to metabolize iron and topical application of iron will thus result in an increase of intracellular protophorphyrin IX (PpIX) [7]. Emerging techniques like elastic scattering spectroscopy, Raman spectroscopy as well as the now often applied fluorescence spectroscopy will have to be compared to the proven use of toluidine blue as well as to the gold standard, namely biopsies, to verify their efficacy and accuracy as diagnostic tools in the early detection of cancer.

In recent times the diagnostic use of 5-ALA in bladder, brain and breast tumors has been expanding. The photosensitizer can be taken in orally a few hours before intraoperative localization of the tumor border. There is hope that breast cancer will be investigated more intensely with mini-endoscopes equipped with fluorescence optics, allowing 5-ALA based localization of PpIX within affected

mammary ducts. The potential of further diagnostic applications of orally applied 5-ALA has been demonstrated in the field of breast cancer surgery where both the differentiation of normal from affected tissue could be demonstrated in a clinical setting [46]. Furthermore the use of 5-ALA could be expanded in sentinel node identification [46,47]. The combination of both these techniques could be worth further investigation in the field of head and neck surgery.

The photosensitizer hypericin, which is a component of St. John's Wort, has been identified as a powerful tumor imaging agent that may be able to assist in the definition of tumor margins as well as diagnosis in deeper lying tumors [14].

3. Treatment of premalignant and early malignant head and neck lesions

Under the term head and neck cancer malignant lesions we group lesions of the oral cavity, neck, pharynx, larynx, nasal cavity, sinus cavities, orbit and all other related structures like the skin. The most common of these tumors are squamous cell carcinomas with an incidence ranging from 4% of all malignancies to as high as 30% in some developing countries.

The term head and neck cancer however does not distinguish between the origin of the tumor (epithelial or mesenchymal). It also does not distinguish between the deeper lying tumors for example the infratemporal fossa and the more superficial tumors that may be more accessible to treatment. Of course there are differences in etiology and treatment outcomes of this wide array of tumors. There is more and more evidence to suggest that the prognosis and thus per definition the tumor biology differs from site to site and thus should be defined first before studies are undertaken and results published [52]. This may also hold true for the evaluation of the effectiveness of treatment of PDT in head and neck cancer.

There is a wide array of photosensitizers available on the market. Clear and strict descriptions of clinical applications exist for each drug, although off-label use is common.

Mainly two products namely porfimer sodium (®Photofrin) and haematoporphyrin derivative (HpD/Photofrin) as well as mTHPC (®Foscan) are used for the treatment of head and neck cancer. mTHPC is a second generation synthetic photosensitizing drug. There is a delay of 4 days after injecting the drug before activation with laser which allows accumulation in cancer cells. There may be pain associated with the administration of the drug. Light sensitivity lasts for at least 15 days.

Of late the chlorine e6 derivative (®Photolon) has been gaining literature support as a photosensitizer for superficial and deep lesions in the head and neck area with the benefit of a shorter period of post treatment photosensitivity [55].

Systemically administered photosensitizers like mTHPC are registered for use in premalignant lesions as well as early invasive as well as otherwise untreatable carcinomas of the oropharyngeal region. It is also possible to treat very superficial lesions with 5-ALA that is either topically applied or administered orally [8].

Copper et al. [9] reported on their experience in the treatment of multiple primary tumors in the head and neck. The authors used mTHPC mediated PDT for the treatment of multiple primary mucosal malignancies in the oral cavity and oropharynx. Of the 27 patients with 42 tumors the staging ranged from carcinoma in situ lesions (3 cases), stage I (23 cases), II (15 cases) to stage III (1 case). Most patients were treated for a single tumor, although three patients were treated with multiple synchromatous tumors. In 28 of the 42 tumors (67%) treatment was successful with a cure rate of 85% for stage I or in situ disease versus 38% in the stage II and III group. Most patients had a good functional outcome and recurrent tumors could be treated with conventional single or combined surgical, radio or chemo-therapy protocols. One patient developed more serious light exposure complications. This study highlights the potential benefits as well as the current limitations in treatment of single and multiple primary squamous cell carcinomas of the oropharyngeal carcinomas. Contrary to conventional chemotherapies resistance to PDT has not yet been described [10]. Hopper et al. [21] reported on the Phase II trials with m HTC in 2004 and showed good results for early oropharyngeal squamous cell carcinomas. Understandably better results have been seen with T1 than in T2 lesions [22].

Porfimer sodium (®Photofrin) seems to be highly successful especially in the treatment of T2 and smaller tumors of the larynx [8]. Other anatomical areas of application are the oral cavity and oropharynx [20]. This product is a mixture of several porphyrins from blood and limited absorption of red light with good drug penetration. Light sensitivity for up to six weeks after administration may diminish the quality of life. Another negative aspect is the relatively poor tumor selectivity.

New generation chlorin based photosensitizers are designed to overcome problems of the older photosensitizers like poor selectivity, long administration to exposure time and photosensitivity. A 1:1 mixture comprising of chlorine e6 and polyvinylpyrrolidone (®Fotolon) may also have increasing indications in at least the photodiagnosis and phototreatment applications [23,51]. The mechanism of action seems to be by triggering reactive oxygen species as well as light dependent cell death via necrosis [53]. Adding the hydrophilic polymer polyvinylpyrrolidone (PVP) seems to improve the efficacy of the drug by improving tumor-to-normal tissue ratio. Penetration after superficial application in an in vivo study was significantly improved by this improved formulation [54,55].

The use of a new photosensitizer talaporfin sodium (®Laserphyrin) used with a newly developed ultra mobile semiconductor low energy PD laser with a wavelength of 664 nm has recently been reported by Yoshida et al. [24]. This study clearly demonstrates the importance of adequate intake of the photosensitizer in this case to a level of above 1 μg/g in the tumor tissue to ensure an adequate response. Tumor-to-normal tissue ratios ranged from 0.36:1 to 5.69:1 in 9 of 11 patients. Of the 24 patients treated with T1 and T2 laryngeal, oral and pharyngeal cancer, two presented with recurrences after a median follow-up period of 20 months.

Another possible photosensitizer that has been tested in an in vitro study is hypericin. A tumorcidal effect was reached by exposure times of 5–10 s with a 593 nm laser light and nearly complete squamous cell cancer killing after 120 s of exposure. In vivo tests in mice confirmed the therapeutic effect of hypericin directly injected in the tumor [14]. Infrared pulsed laser emissions may be used to activate the drug and improve tissue penetration of hypericin PDT [19].

Use of 5-ALA is suitable for topical application, but may also be taken in orally resulting in systemic absorption and reasonable selectivity. Use is restricted to very superficial lesions like leukoplakia or skin lesions like acne vulgaris, sebaceous gland hyperplasia, rosacea and hirsutism, but is not to be used for invasive lesions. Commercially 5-ALA is marketed known as ®Levulan®Kerastick or as its methylated esther ®Metvix. After absorbtion, 5-ALA is metabolized to another heme precursor, PpIX, which is the actual active photosensitizer. Peak light absorption is at 635 nm. Normally the photosensitizer can be activated by a light source 3–4 h after oral administration of a dose of 10–60 mg/kg. Local application is possible but technically difficult in the oral area where of carriers in a cream or gel form has been used [20]. Due to the short half-life, photosensitivity is normally resolved after a 24 h period. Since first reports on treatment of premalignant lesions with 5-ALA in 1996 there seems to be consistent favorable results in the literature with 100% response rate to less than 50% [20]. There were marked dif-

ferences in the treatment protocols and that may explain the widely different outcomes. Recent development of a novel 5-ALA patch for skin application has simplified the treatment of skin lesions as no cream or ointment needs to be applied [56,57].

Successful PDT has also been reported in early oesophageal cancer by Maunoury et al. [29]. A response rate of 75% was noted with the use of porfimer sodium as photosensitizer in a group of patients ($n = 24$) with early SCC and ADC (T1 or T2). In a larger study Radu et al. [30] reported their experiences of 101 early squamous cell carcinomas in the oral cavity, pharynx, esophagus as well as in the tracheobronchial tree. These tumors were detected as second primary malignancies in patients with primary head and neck cancer. All patients had carcinoma in situ or T1 lesions with less than 2 mm infiltration. First generation photosensitizer, haematoporphyrin derivative (HpD/Photofrin) and ®Photofrin II was used. Complete response was seen in 85% of patients with 9 of these recurring after 3–34 months. A permanent eradication was thus seen in 77% of the tumors without any mortality. No difference was seen in the response rate of the different treatment sites.

There appears to be a correlation between the fluence rate measured in mW/cm^2 and the type of reaction from tumors. In tumors, pre-existing hypoxia has been clearly recognized as a barrier to other oxygen dependent treatment modalities like radiotherapy. A higher fluence rate as well as higher concentration of photosensitizers often leads to necrosis while a lower fluence rate and photosensitizer dose may lead to more apoptotic cell death as well as a cell mediated response. This may be explained by the improved reoxygenation ability at a lower fluence rate [25,26]. The lower fluence rate thus seems to have a much wider influence than just direct cell destruction as inflammatory cells are more widely distributed in these circumstances leading to wider and not clearly defined tumor injury [27,23]. This antitumor immunogenicity with activation of CD4+ and CD8+ T cell clones with recognition of tumor specific antigens has been recognized as a factor contributing to tumor immunity [4].

Hyperbaric oxygen has been proposed as a method to improve tumor tissue oxygenation and thus improve the response of tumors to PDT [28].

4. Secondary or recurrent squamous cell carcinomas

Major emphasis has been placed on the use of PDT in patients with secondary or recurrent squamous cell carcinomas of the head and neck region. PDT has been employed as a palliative treatment modality where other treatments have failed.

This has been the case in many institutions in countries like Germany. A recent report by Lorenz and Maier [11] highlights the possible beneficial effect of PDT in this group of patients. In the group of 24 patients, 12(50%) reacted favorably with complete remission and partial remission was seen in 9(37.5%) with three patients showing no response. The mean duration of overall survival was 305.7 days and the mean recurrence free survival was 302.7 days. Patients with a complete response had a significantly better mean survival of 414.1 days. In 19% of the patients a significant improvement of quality of life was measured. Important to note is that in this group of patients the presence of lymph node and other distant secondary metastases were excluded before commencement of treatment. The maximal tumor thickness was 1 cm with the average tumor surface area of 6 cm^2.

Debulking of large tumors in a progressive layer by layer approach has also been proposed by using PDT [12,13]. Another use of PDT in large tumors is by interstitial photodynamic therapy (IPDT). In these cases the delivery of light to deeper parts of the tumor is achieved by placing thin optical light diffusers into the tumor mass. There is evidence supporting the increased effectiveness of this therapy due to the improved photo-oxidation and distribution within the tumor bed [14]. Currently this treatment is mostly indicated in cases where no other means of salvage is possible. Lou et al. [15] reported their experience of 45 patients with end stage head and neck cancer unsuitable for any other treatment modality. Significant relief in mass effect was noted in 24 patients with 5 disease free patients after 10–60 months. One patient suffered from a carotid blowout. The use of MR imaging guided interstitial photodynamic laser therapy has been proposed by Jager et al. [16] with the advantage of being able to deliver an accurate, safe and more uniform light delivery in these advanced head and neck tumors [4].

In a large multicentre study [17], 128 patients with advanced, histological confirmed squamous cell carcinoma and deemed to be incurable by an interdisciplinary team was included in the study. Often these patients were extensively pre treated. mTHPC was used as photosensitizer and delivered at a concentration of 0.15 mg/kg and the surface of the tumor was illuminated on the fourth day with 652 nm, 20 J/cm^2 and with an intensity of 100mW/cm^2 resulting in a dose of 20 J/cm^2. In 43% the lesions achieved 100% tumor mass reduction on at least one occasion during follow-up with a median duration of the response of 117 days with 35% completely cleared 1 year after treatment. Two important subgroups with better responses were identified, namely those who had lesions of 10 mm thickness or less and those where illumination of the whole surface could be achieved. Despite the above 29% of tumors thicker than 10 mm achieved an overall tumor response. Median survival in patients having a 100% tumor response was 426 days compared to 212 days in the partial responders group. The cost effectiveness of PDT using mTHPC has been confirmed when compared with four cycles of palliative chemotherapy [18].

5. Cosmetic applications

Cosmetic applications of PDT are rapidly expanding. This especially applies to the use of 5-ALA in a wide range of skin conditions. Besides the FDA approved use for treatment of premalignant and malignant skin conditions off-label uses for photorejuvination, treatment of sebaceous gland hyperplasia, rosacea and hirsutism is now recognized [31]. Use of PDT in the treatment of acne vulgaris has also in recent times attracted much interest. Many protocols have been suggested without one to have been proven to be the best. Use of 5-ALA is clearly effective; however the side effect profile has been excessive [32]. 5-ALA or its derivatives normally comes in a cream base and light can be applied at around 30 min or as late as 4 h after application. Longer time interval allows for increased drug penetration and may be further increased by degreasing the skin with acetone before 5-ALA application. Recently a self-adhesive 5-ALA patch for the treatment of actinic keratoses has been developed [33]. Use of a 532 nm diode laser leads to the possibility to also treat pigmented lesions as lentigines, keratoses and ephelides (freckles) by attacking the underlying abnormal vasculature. Bowen's disease is also shown to react well to treatment [5,34]. Rhinophyma as well as sebaceous gland hyperplasia may also successfully be treated by 5-ALA PDT [5].

When cells rapidly proliferate or have a high metabolic turnover they convert more 5-ALA to PpIX, increasing the effect of PDT in these areas with resultant reduction of skin hyper pigmentation. 5-ALA-PDT has shown to be effective in the treatment of patients with actinic damage and an improvement in overall cosmesis [32].

During and after treatment patients may experience discomfort as well as in some cases even intense pain. Swelling as well as erythema may persist for the period of 24 h after activation. With protocols intended to increase the penetration and effect of the PDT there are obvious increased symptoms involved [35]. Multiple

short incubation time (<1 h) treatments results in improved acne reduction and and decrease in edema, crusting, dyspigmentation and thus improved patient compliance [31].

Recently, it had been shown that different clinicopathologic features of head and neck basal cell carcinoma may also lead to different response rates [36]. In this study the response rate was 100% for ulcerative, 90% for nodular, 62% for superficial, 14% for pigmented forms. This shows the added consideration that has to be taken to improve outcomes in PDT.

6. Treatment of infections in the head and neck region

PACT (Photodynamic anti-microbial chemotherapy) has shown activity against bacteria, fungi, viruses and protozoa. The broad spectrum of action including the efficient inactivation of antibiotic-resistant strains seems to be a major benefit. Resistance seems not to be a major factor as the active singlet oxygen and free radicals may interact with several metabolic pathways [37,38]. HPD, toluidine blue, methylene blue as well as poly-L-lysine-chlorin(e6) conjugate have all been mentioned as promising candidates for use in this potential application [20]. Dental practice biofilms have been shown to be sensitive in varying degrees to PACT. The potential use of this application in the treatment of common periodontitis, peri-implantitis, caries and in the sterilization of the root canal in endodontic treatment is significant. Erythrosine seems to be more effective than others in eradicating Streptococcus mutans [39]. Further potential applications in this field are virtually limitless. However, investigations in our laboratories recently indicated that the sensitivity even of closely related oral bacteria to various photosensitizers and PACT may be quite different (Besic Gyenge et al., submitted for publication). We therefore propose that for the treatment of multispecies pathogen populations the application of photosensitizer combinations for PACT may be useful.

7. Complications

Some of the potential complications of PDT have been discussed already. A recent report by Procianoy et al. [40] highlighted the potential caution one has to take in patients suffering from Xeroderma pigmentosum, a down regulation of DNA repair mechanism disorder. In this case there was clear aggravation of the malignant process after PDT. A potential further suppression of the DNA repair process was postulated as possible explanation of this event. Recent in vitro investigations of our own group using prostate cancer cells as model system also revealed a down regulation of several genes associated with DNA repair mechanisms after mTHPC-mediated PDT (Rossi et al., in preparation). Pain management problems have regularly been reported and remain a challenge. Remifentanil is often used to cover the peri-operative intense treatment pain problems. In opiate tolerant patients clonidine may be a useful adjunct. Specific anaesthetic challenges have been identified, especially regarding the protection of patients against undue light exposure and ensuring a safe anaesthesia to patients requiring such a service [41]. Skin protection by the use of textiles or cream is vitally important in the perioperative period of potential phototoxicity.

8. The future of PDT

Much of the future of PDT depends on the ease of use, cost effectiveness as well as the treatment outcomes and quality of life compared to conventional treatments.

One of the major problems in head and neck surgery is the difficulty in predicting the responders from the non responders. This concerns especially the early carcinomas. One possible reason for the rate of non responders is the under staging of the tumors [30], especially in areas where ultrasound diagnostics may be difficult. Clearly one cannot only rely on the biopsy specimen as it may not be representative of the whole tumor. For oncological safety reasons one would like to include a margin of healthy tissue and this has to be taken into account in the planning phase of PDT, especially regarding the deepest part of tumor infiltration.

Future increased use of PDT can be expected especially with development of photosensitizers with high absorption at longer wavelengths leading to deeper penetration and thus the possibility to treat larger tumor volumes. Selective absorption is another key issue that can still improve considerably along with the problematic post treatment photosensitivity by decreasing the half-life of such developed drugs. Liposomal mTHPC may play such a role in the future. Currently this drug has been limited to the successful use in the treatment of feline squamous cell carcinoma [42].

In dire need is the scientific establishment of treatment protocols. The wide differentiation of photosensitizer concentrations, lighting protocols regarding both total dose as well as fluence rates may lead to a multiple of unsuccessful treatments before a particular unit can establish a clinically proven protocol. One of the emerging fields of application is PDT targeting. Photosensitizers can be locked onto a delivery vehicle for instance a molecule with high affinity for the target. This will lead to more selective treatment of the target area [43].

Of course the reverse may also be possible where photosensitizers can be used to deliver bioactive molecules including genes, into cells [44].

Quantum dots have also recently come to our attention [45]. These products can be used as photosensitizers in PDT. One major potential benefit in the use of quantum dots is their tunable optical properties and surface chemistries resulting in the possible use to sensitize other PDT agents or even molecular oxygen through an energy transfer process.

In a different class of application of photodynamic interaction is the uncaging of drugs or other biologic agents. The encaged structure is internalized by the target cell and upon photo activation, the capsule disrupted and the biologic active agent released [43].

9. Summary

Photodynamic therapy in the head and neck region is still being regarded as an emerging treatment modality. This is probably due to the lack of established treatment protocols as well as the major changes and dynamics in the fields of lighting and photosensitizers which may result in initial poor results. With traditional treatment modalities surgeons regard incomplete response as a treatment failure. Although to a certain extent it also holds true for PDT one mostly still has another opportunity for further retreatment or change to another treatment modality like surgery or radiochemotherapy.

When evaluating the literature many of the problems that have been retarding growth in the PDT field has been or is being addressed by further development of photosensitizers and light sources. On the horizon there is hope for much improved tumor selectivity by the way of attachment of photosensitizers to nano particles with the ability to fix to specific marker molecules.

So it would seem as if PDT in the head and neck field is indeed promising and rapidly expanding to a flexible treatment modality with significant added benefits to our patients.

References

[1] H. von Tappeiner, A. Jesionek, Therapeutische Versuche mit fluoreszierenden Stoffen, Munch. Med. Wochenschr. 47 (1903) 2042–2044.
[2] A. Policard, Etudes sur les aspects offerts par des tumeurs experimentales examinees a la lumiere de Wood, C. R. Soc. Biol. 91 (1924) 1423–1428.

[3] T. Dougherty, C. Gomer, B. Henderson, Photodynamic therapy, J. Natl. Cancer. Inst. 90 (1998) 889–905.
[4] P. Harrod-Kim, Tumor ablation with photodynamic therapy: introduction to mechanism and clinical applications, J. Vasc. Interv. Radiol. 17 (2006) 1441–1448.
[5] K. Zakhary, D.A.F. Ellis, Applications of aminolevulinic acid-based photodynamic therapy in cosmetic facial plastic practices, Facial Plast. Surg. 21 (2005) 110–283.
[6] K. Moghissi, B.A. Dixon, Yorkshire laser centre mobile photodynamic therapy unit: for service to district general hospitals, Photodiagn. Photodynam. Ther. 2 (2005) 169–174.
[7] B. Swinson, W. Jeres, M. El-Maaytah, P. Norris, C. Hopper, Optical techniques in diagnosis of head and neck malignancy, Oral Oncol. 42 (2006) 221–228.
[8] M. Biel, Advances in photodynamic therapy for the treatment of head and neck cancers, Lasers Surg. Med. 38 (2006) 349–355.
[9] M.P. Copper, M. Triesscheijn, I.B. Tan, M.C. Ruevecamp, F.A. Stewart, Photodynamic therapy in the treatment of multiple primary tumors in the head and neck, located to the oral cavity and oropharynx, Clin. Otollaryngol. 32 (2007) 185–189.
[10] R. Naim, Im Fokus: photodynamische therapie mit m-THPC (Foscan), HNO 56 (2008) 490–492.
[11] K.J. Lorenz, H. Maier, Plattenepithelkarzinome im Kopf-Hals-Bereich. Photodynamische therapie mit m-THPC (Foscan), HNO 56 (2008) 402–409.
[12] W. Jeres, U. Tahwinder, C.S. Betz, M. El Maaytah, S. Abbas, S. Wright, C. Hopper, The application of photodynamic therapy in the head and neck, Dent. Update 34 (2007) 478–486.
[13] M.G. Dilkes, E. Benjamin, S. Ovaisi, A.S. Banerjee, Treatment of primary mucosal head and neck squamous cell carcinoma using photodynamic therapy: results after 25 treated cases, J. Laryngol. Otol. 117 (2003) 713–717.
[14] C.S. Head, C.S. Head, L. Quang, J. Sercarz, R. Saxton, Photodynamic therapy and tumor imaging of hypericin-treated squamous cell carcinoma, World J. Surg. Oncol. 4 (2006) 87.
[15] P.J. Lou, H.R. Jager, L. Jones, T. Theodossy, S.G. Brown, C. Hopper, Interstitial photodynamic therapy as salvage treatment of recurrent head and neck cancer, Br. J. Cancer 9 (3) (2004) 441–446.
[16] H.R. Jager, M.N. Taylor, T. Theodossy, C. Hopper, MR Imaging-guided interstitial photodynamic laser therapy for advanced head and neck tumors, AJNR Am. J. Neuroradiol. 26 (5) (2005) 1193–1200.
[17] A. D'Cruz, M.H. Robinson, M.A. Biel, MTHPC-mediated photodynamic therapy in patients with advanced, incurable head and neck cancer: a multicenter study of 128 patients, Head Neck 26 (2004) 232–240.
[18] A. Kübler, C. Niziol, M. Sidhu, A. Dünne, J.A. Werner, Eine Kosten-Effektivitäts-Analyse der photodynamischen Therapie mit Foscan(Foscan-PDT) im Vergleich zu einer palliativen Chemotherapie bei Patienten mit fortgescrittenen Kopf-Halstumoren in Deutchland, Laryngo Rhino Otol. 84 (2005) 725–732.
[19] M. Bublik, C. Head, P. Benharasch, M. Paiva, A. Eshraghi, T. Kim, R. Saxon, Hypericin and pulsed laser therapy of squamous cell cancer in vitro, Photomed. Laser Surg. 24 (2006) 341–347.
[20] K. Kanopka, T. Goslinski, Photodynamic therapy in dentistry, J. Dent. Res. 86 (2007) 694–707.
[21] C. Hopper, A. Kübler, H. Lewis, I.B. Tan, G. Putnam, m-THPC-mediated photodynamic therapy for early oral squamous cell carcinoma, Int. J. Cancer 111 (2004) 138–146.
[22] M.P. Copper, B. Tan, H. Oppelaar, M.C. Ruevekamp, F.A. Stewart, Meta-tetra(hydroxyphenyl)chlorin Photodynamic Therapy in early-stage squamous cell carcinoma of the head and neck, Arch. Otolaryngol. – Head Neck Surg. 129 (2003) 709–711.
[23] S.P. Thong, M. Olivo, K-W. Kho, R. Bhuvaneswari, W.W.L. Chin, K-W. Ong, K.-C. Soo, Immune response against angiosarkoma following lower fluence rate clinical photodynamic therapy, J. Environ. Pathol. Toxicol. Oncol. 27 (2008) 35–42.
[24] T. Yoshida, R. Tokashiki, H. Ito, A. Shimizu, K. Nakamura, H. Hiramatsu, K. Tsukahara, S. Shimizu, D. Takata, I. Okamoto, M. Suzuki, Therapeutic effects of a new photosensitizer for photodynamic therapy of early head and neck cancer in relation to tissue concentration, Auris. Nasus. Larynx. 12 (2008) 15–27, doi:10.1016/j.anl.2007.10.008.
[25] T.M. Sitnik, J.A. Hampton, B.W. Henderson, Reduction of tumor oxygenation during and after photodynamic therapy in vivo: effects of fluence rate, Br. J. Cancer 77 (1998) 1386–1394.
[26] T.M. Busch, Local physiological changes during photodynamic therapy, Lasers Surg. Med. 38 (2006) 494–499.
[27] B.W. Henderson, T.W. Busch, J.W. Snyder, Fluence rate as a modulator of PDT mechanisms, Lasers Surg. Med. 38 (2006) 489–493.
[28] N.S. Al-Walli, G.J. Butler, J. Beale, R.W. Hamilton, B.Y. Lee, P. Lucas, Hyperbaric oxygen and malignancies: a potential role in radiotherapy, chemotherapy, tumor surgery and phototherapy, Med. Sci. Monit. 11 (2005) 279–289.
[29] V. Maunoury, S. Mordon, P. Bulois, X. Mirabel, B. Hecquet, C. Mariette, Photodynamic therapy for early oesophageal cancer, Dig. Liver Dis. 37 (2005) 491–495.
[30] A. Radu, P. Grosjean, Ch. Fontolliet, G. Wagnieres, A. Woodtli, H. Van den Bergh, Ph. Monnier, Photodynamic therapy for 101 early cancers of the upper aerodigestive tract, the esophagus, and the bronchi: a single-institution experience, Diagn. Therapeut. Endosc. 5 (1999) 145–154.
[31] T.S. Alster, S. St Surin-Lord, Photodynamic therapy: practical cosmetic applications, J. Drugs Dermatol. 5 (2006) 764–768.
[32] M.A. MacCormack, Photodynamic therapy in dermatology: an update on applications and outcomes, Sem. Cutaneous Med. Surg. 27 (2008) 52–62.
[33] J-D. Fautec, G. Ackermann, M. Birkel, M. Breuer, A.C.E. Moor, A. Ebeling, C. Ortland, Fluorescence characteristics and pharmacokinetic properties of a novel self-adhesive 5-ALA patch for photodynamic therapy of actinic keratoses, Arch. Dermatol. Res. 300 (2008) 53–60.
[34] R. Bissonette, A. Bergeron, Y. Liu, Large surface photodynamic therapy with aminolevinic acid: treatment of actinic keratoses and beyond, J. Drugs Dermatol. 3 (Suppl. 1) (2004) 26–31.
[35] Q. Peng, T. Warloe, K. Berg, J. Moan, M. Kongshaug, K.E. Giercksky, J.M. Nesland, Clin. Res. Future Challenges Cancer. 79 (1997) 2282–2308.
[36] A. Kavaiani, L. Ataie-Fashtami, M. Fateh, N. Sheikhabahee, M. Ghodsi, N. Zand, E.D. Gholamreza, Photodynamic therapy of head and neck basal cell carcinoma according to different clinicopathologic features, Lasers Surg. Med. 36 (2005) 377–382.
[37] M. Wainwright, K.B. Crossley, Photosensitizing agents – circumventing resistance and breaking down biofilms: a review, Int. Biodeterior. Biodegrad. 53 (2004) 119–126.
[38] G. Jori, C. Fabris, M. Soncin, S. Ferro, O. Coppellotti, D. Dei, L. Fantetti, G. Chitti, G. Roncucci, Photodynamic therapy in the treatment of microbial infections: basic principles and perspective applications, Lasers Surg. Med. 38 (2006) 468–481.
[39] S. Wood, D. Metcalf, D. Devine, C. Robinson, Erythrosine is a potential photosensitizer for the photodynamic therapy of oral plaque films, J. Antimicrob. Chemother. 57 (2006) 680–684.
[40] F. Procianoy, A.A.V. Cruz, A. Baccega, V. Ferraz, F. Chahud, Aggrevation of eyelid and conjunctival malignancies following photodynamic therapy in DeSanctis Cacchione Syndrome, Opthal. Plast. Reconstr. Surg. 22 (6) (2006) 498–499.
[41] T. Thodossy, M. Chapman, V. Mitchell, C. Hopper, Anaesthetic considerations in patients receiving photodynamic therapy in head and neck surgery, Eur. J. Anaesthesiol. 24 (2007) 225–229.
[42] J. Buchholz, B. Kaser-Hotz, C. Rohrer Bley, K. Melzer, R.A. Schwendener, M. Roos, H. Walt, Optimizing photodynamic therapy: in vivo pharmacokinetics of Liposomal meta-(tetrahydroxyphenyl) chlorin in feline squamous cell carcinoma, Clin. Cancer Res. 11 (2005) 7538–7544.
[43] B.C. Wilson, Potential applications of photodynamic therapy in regenerative medicine, J. Craniofacial Surg. 14 (2003) 78–273.
[44] P.K. Selbo, A. Hogset, L. Prasmikaite, et al., Photochemical internalization: a novel drug delivery system, Tumor Biol. 23 (2002) 103–112.
[45] A.C.S. Samia, S. Dayal, C. Burda, Quantum dot-based energy transfer: perspectives and potential for applications in photodynamic therapy, Photochem. Photobiol. 82 (2006) 617–625.
[46] D.P. Ladner, R.A. Steiner, J. Allemann, U. Haller, H. Walt, Photodynamic diagnosis of breast tumors after oral application of aminolevulenic acid, Br. J. Cancer 84 (2001) 33–37.
[47] K.A. Frei, H.M. Bonel, H. Frick, H. Walt, R.A. Steiner, Photodynamic detection of diseased axillary sentinel lymph node after oral application of aminolevulinic acid in patients with breast cancer, Br. J. Cancer 90 (2004) 805–809.
[48] W.W.L. Chin, P.W.S. Heng, P.S.P. Thong, R. Bhuvaneswari, W. Hirt, S. Kreuenzel, K.C. Soo, M. Ollvo, Improved formulation of photosensitizer chlorine e6 polyvinylpyrrolidone for fluorescence diagnostic imaging and photodynamic therapy in human cancer, Eur. J. Pharmaceut. Biopharmaceut. 69 (3) (2008) 1083–1093.
[49] S.V. Scheleg, E.A. Zavrid, T.V. Kochubeev, Y.P. Istomin, V.N. Chalov, I.N. Zhuravkin, Photodynamic therapy with chlorine e6 for skin metastases of melanoma, Photodermatol. Photoimmunol. Photomed. 20 (1) (2004) 21–26.
[50] E. Steenberge, D. Dolphin, Pyrollic photosensitizers, Curr. Med. Chem. 3 (4) (1996) 239–272.
[51] W.W. Chin, P.W. Heng, M. Olivo, Chlorin e6- polyvinylpyrrolidone mediated photosensitization is effective against human non-small cell lung carcinoma compared to small cell lung carcinoma xenografts, BioMed Central Pharmacol. 1 (7) (2007) 15.
[52] J.A. Woolgar, Histopathological prognostic factors in oral and oropharyngeal squamous cell carcinoma, Oral Oncol. 42 (2006) 229–239.
[53] L. Copley, P. van der Watt, K.W. Wirtz, M.I. Parker, V.D. Leaner, Leaner, photolon TM, a chlorine e6 derivative, triggers ROS production and light-dependent cell death via necrosis, Int. J. Biochem. Cell Biol. 40 (2) (2008) 227–235.
[54] Y.P. Istomin, T.P. Lapsevich, S.A. Bizyuk, E.N. Alexandrova, Photodynamic efficacy of topical application of Chlorin e6-polyvinylpyrrolidone complex in tumor bearing rats, Exp. Oncol. 28 (2006) 299–302.
[55] W.W.L. Chin, P.W.S. Heng, P.S.P. Thong, R. Bhuvaneswari, W. Hirt, S. Kuenzel, K.C. Soo, M. Olivo, Improved formulation of photosnsitizer chlorine e6 polyvinylpyrrolidone for fluorescence diagnostic imaging and photodynamic therapy of human cancer, Photochem. Photobiol. 84 (2) (2006) 103–110.
[56] J.-D. Fauteck, G. Ackermann, M. Birkel, M. Breuer, A.C.E. Moor, A. Ebling, C. Ortland, Characteristics and pharmacokinetic properties of a novel self-adhesive 5-ALA patch for photodynamic therapy of actinic keratoses, Arch. Dermatol. Res. 300 (2008) 53–60.
[57] A. Hauschild, G. Popp, E. Stockfleth, K.-G. Meyer, D. Imberger, P. Mohr, G. Itschert, R. Kaufmann, K. Neuber, Y. Frambach, H. Gollnick, M. Brunnert, M. Stocker, C. Ortland, S. Karrer, Effective photodynamic therapy of actinic keratoses on the head and face with a novel, self-adhesive 5-aminolaevulinic acid patch, Exp. Dermatol. 18 (2008) 116–121.

8

CV / PUBLICATION LIST

Emina BEŠIĆ GYENGE, MSc. of Biochemistry

Born: 8th May 1977, Sanski Most, Bosnia
Nationality: Swiss

Adress: University of Zurich, Institute of Anatomy
Winterthurerstrasse 190
8057 Zurich, Switzerland

Phone office: +41 (0)44 635 52 35
E-mail office: emina.besicgyenge@uzh.ch

EDUCATION

June 2007 - June 2012	Ph.D. student, program in cancer research, University of Zurich, Institute of Anatomy, Zurich, Switzerland
Okt. 2002 – Feb. 2007	Biochemistry master program, University of Zurich, Zurich, Switzerland, Degree in Master of Science in Biochemistry, chemistry/biochemistry track, subsidiary subjects in biology and chemistry, University of Zurich, Switzerland
2000 – 2002	Physics master program, Swiss federal Institute of Technology Zurich, Zurich, Switzerland

LANGUAGES

Bosnian:	native speaker
German and English:	fluent
French, Italian	basic

AWARDS

2005	University of Zurich semester price for project: „Ribozyme folding at zero gravity“, Zurich, Switzerland
2009	Best presentation award “Schmutzigerpreis”, annual assembly of Swiss Consortium for maxillo-facial surgery and oral diseases, Brig, Switzerland
2009	Best presentation award, Medical Laser Applications, Munich, Germany

GRANTS

1. **Photodynamic Therapy for the Treatment of Oral Pathogens**, 2009-2012, Société Suisse d’Odonto-stomatolige (SSO)
2. **Combined Photodynamic Therapy with Microwave based Hyperthermia against Cancer: *In vitro* Testing**, 2011, IT’IS foundation

PUBLICATION LIST

A. Original Publications (peer-reviewed)

1. M. Lüthi, **E. Besic Gyenge**, M. Engström, M. Bredell, K. Grätz, H. Walt, R. Gmür, C. Maake; Hypericin- and mTHPC-mediated photodynamic therapy for the treatment of cariogenic bacteria. Medical Laser Applications, 2009; 24 (227-236)
2. **E. Besic Gyenge**, S. Hiestand, S. Graefe, H. Walt, C. Maake; Cellular and molecular effects of the liposomal mTHPC derivative Foslipos in prostate carcinoma cells in vitro. Photodiagnosis and Photodynamic Therapy 2011; 8(2):86-96
3. G. Geisberger, S. Paulus, **E. Besic Gyenge**, C. Maake and G. R. Patzke; Targeted Delivery of Polyoxometalate Nanocomposites. Small 2011; 7(19): 2808–2814
4. **E. Besic Gyenge**; X. Darphin, A. Wirth, U. Pieles, H. Walt, M. Bredell, C. Maake; Uptake and fate of surface modified silica nanoparticles in Head and Neck Squamous Cell Carcinoma. Journal of Nanobiotechnology, 2011, 9:32

B. Submitted articles or in preparation

1. **E. Besic Gyenge**; D. Lüscher, P. Forny, A. Laass, H. Walt, C. Maake; Dark activity of Hypericin and a Chlorine Based Photosensitizer alone or in Combination in Squamous Cell Carcinoma Cells. Submitted in Photodiagnosis and Photodynamic Theapy
2. **E. Besic Gyenge**, P. Forny, M. Antoniol, A. Laass, H. Walt, C. Maake, Photodynamic Mechanisms induced by Hypericin and a Chlorine Based Photosensitizer in Head and Neck Squamous Cell Carcinoma Cells. Submitted in British Journal of Cancer
3. D. Hinger, G. Geisberger, **E. Besic Gyenge**, Tobias Gilomen, Rudolf Gmür , Klaus Grätz, Heinrich Walt, Greta R. Patzke, Caroline Maake; Combining Chitosan and Photodynamic Effects for the Treatment of Oral Microorganisms. Submitted in Journal of Translational Medicine
4. G. Geisberger, **E. Besic Gyenge**, C. Maake, and G. R. Patzke Trimethylchitosan-Polyoxometalate Nanocomposites as Novel Drug Carriers; submitted in Biomacromolecules

C. Reviews and others

1. M. Bredell, **E. Besic**, C. Maake and H. Walt; The application and challenges of clinical PD-PDT in the Head and Neck region, a short review. Journal of Photochemistry and Photobiology. 2010; 101(3):185-90
2. H. Walt, **E. Besic Gyenge**, C. Maake; Photodynamic Medicine and Nanotechnology: Synergy Impossible? Nano, The Magazine for Small Science 2011, November; p. 14-17

D. Participation in scientific events (Abstracts available)

1. **Besic E.**, Wirth A., Maake C., Walt H., Grätz K.; Uptake and distribution of Silica Nanoparticles in Human Cancer Cell for Future Therapy. Union of the Swiss Societies for Experimental Biology (USGEB) - BIOLOGY MEETS ENGINEERING, 2008, Laussanne, Switzerland

2. **Besic E.**, Wirth A., Maake C., Walt H., Grätz K.;Uptake and distribution of Hypericin doped Silica Nanoparticles in Human Cancer Cell for Future Therapy. 1st Conference of the European Platform for Photodynamic Medicine (EPPM-1), Dubrovnik, Croatia, 2008

3. **Besic E**., Maake C., Wirth A., Grätz K., Walt H.; Cellular Uptake of Surface Modified Silica Nanoparticles in Human Cancer Cells for Future Therapy. 7th International Symposium on Photodynamic Therapy, Brixen, Italy, 2008

4. D. Lüscher, P. Forny, N. Schatt, H. Walt, K. Grätz, C. Maake, **E. Besic**; Photodynamic Effects of Hypericin and Foslipos in Head and Neck Squamous Cell Carcinoma *in-vitro*, 8th Day of clinical research, Zurich, Switzerland, 2009

5. **E. Besic**, H. Walt, K. Grätz, C. Maake; Photodynamische Effekte von Hypericin und Foslipos im Kopf- und Halstumorzelllinien und in pathogenen Keimen. annual assembly of Swiss Consortium for maxillo-facial surgery and oral diseases, Brig, Switzerland, 2009

6. a) **E. Besic**, M. Engström, R. Gmür, M. Lüthi, K. Grätz, H. Walt, C. Maake; Photodynamic Therapy for the Treatment of Pathogen Bacteria. Medical Laser Applications, Munich, Germany, 2009

b) **E. Besic**, P. Forny, D. Lüscher, N. Schatt, K. Grätz, H. Walt, C. Maake; Photodynamic Effects of Hypericin and Foslipos in Head and Neck Squamous Cell Carcinoma *in-vitro*. Medical Laser Applications, Munich, Germany, 2009

7. P. Forny, D. Lüscher, H. Walt, K. Grätz, C. Maake, **E. Besic**; Photodynamic Therapy of Hypericin and Foslipos in HNSCC in vitro. USGEB – MEMBRANES IN MOTION, 2009, Interlaken, Switzerland

8. a) **E. Besic Gyenge**, P. Forny, D. Luescher, K. Grätz, H. Walt, C. Maake; Photodynamic Effects of Hypericin and Foslipos in Head and Neck Squamous Cell Carcinoma *in-vitro*. 13th Congress of the European Society for Photobiology, Wroclaw, Poland, 2009,

b) **E. Besic Gyenge,** R. Gmür, K. Grätz, H. Walt, C. Maake; Photodynamic Therapy for the Treatment of Oral Pathogen Bacteria. 13th Congress of the European Society for Photobiology, Wroclaw, Poland, 2009

9.a) **E. Besic Gyenge**, M. Lüthi, M. Engström, R. Gmür, M. Gander, K. Grätz, H. Walt, C. Maake; Antimicrobial Photodynamic Therapy: Diversity in Photodynamic Therapy Outcome for Streptococcus Family. USGEB – FRONTIERS IN HUMAN BIOLOGY, 2010, Lugano, Switzerland

b) **E. Besic Gyenge**, P. Forny, D. Lüscher, N. Schatt, K. Grätz, H. Walt, C. Maake; Molecular Biology behind Photodynamic Therapy in Head and Neck Squamous Cell Carcinoma *in-vitro*. USGEB – FRONTIERS IN HUMAN BIOLOGY, 2010, Lugano, Switzerland

10. **E. Besic Gyenge**, P. Forny, D. Lüscher, A. Laas, H. Walt, C. Maake; The Pathways to Death: Photodynamic Therapy in Head and Neck Squamous Cell Carcinoma in-vitro. 8th International Symposium on Photodynamic Therapy and Photodiagnosis in Clinical Practice, Brixen, Italy, 2010

11. **E. Besic Gyenge**, P. Forny, D. Luescher, N. Schatt, M. Antoniol, S. Kurrer, K. Grätz, H. Walt, C. Maake; Photodynamic Effects of Hypericin and Foslipos in Head and Neck Squamous Cell Carcinoma *in-vitro*. 9th Day of clinical research, Zurich, Switzerland, 2010

12. A. Laass, D. Hinger, H. Walt, C. Maake, **E. Besic Gyenge**; Dark Toxicity DNA Damage on Single Cell Level in Photodynamic Therapy *in vitro*. 11th Day of clinical research, Zurich, Switzerland, 2011